The role of TIGAR in Parkinson´s Disease

Karla Lourdes Robles Lopez

Thesis submitted for Doctor of Philosophy (PhD)

Supervisors: Prof. Oliver Bandmann, Dr. Heather Mortiboys, Dr. Guillaume Hautbergue and Dr. Robin Highley

Sheffield Institute for Translational Neuroscience (SITraN)

Department of Neuroscience, The Medical School

University of Sheffield

Abstract

Parkinson's disease (PD) is the second most common neurodegenerative disease. The pathological hallmark of PD is the loss of dopaminergic neurons in the substantia nigra pars compacta (SNpc). Common identifiable genetic causes of early onset PD (EOPD) are *Parkin* and *PINK1* mutations. *Tigarb*, the orthologue of human *TIGAR* (TP53–Induced Glycolysis and Apoptosis Regulator), up-regulation was demonstrated in a zebrafish *pink1-/-* model along with dopaminergic cell loss and mitochondrial dysfunction (Flinn et al., 2013). *Tigarb* knockdown rescued the dopaminergic neurons and mitochondrial dysfunction. Here, *tigarb* upregulation suggests an involvement in PD neuropathology. Therefore, we investigated whether TIGAR is present in the human brain and elucidate its relationship between TIGAR protein and the Lewy body pathology. TIGAR was found in the Lewy Bodies and Neurites in SNpc of sporadic PD and Dementia with Lewy bodies patients. TIGAR protein was not found in the ubiquitylated inclusions of motor neurone disease or multiple system atrophy, suggesting a degree of disease specificity. TIGAR role was investigated in fibroblasts from PD patients and controls. TIGAR is expressed and translated in human fibroblasts. TIGAR gene expression and protein level between controls and *parkin*-mutant fibroblasts was not significantly different. TIGAR cellular localisation was not affected in *parkin* mutant fibroblasts after rotenone toxic and cellular stress exposure. TIGAR involvement in autophagy was not found in sporadic PD patients. RNAi methods for efficient *TIGAR* and *PINK1* knockdown were designed in using HEK 293T cells as host line, where *TIGAR* and *PINK1* deficiency showed no significant effect in the ATP production and mitochondrial morphology. CRISPR/Cas9 and microRNAs mediated knockdown were investigated to assess gene function and to select the best approach with reproducible and reliable results.

Acknowledgements

I am extremely and deeply grateful with my supervisor Prof. Oliver Bandmann, he was more than a supervisor, but also a friendly and kind guide through my PhD journey. I would also like to deeply thank my helpful, sensible and kind secondary supervisors Dr. Heather Mortiboys, Dr. Guillaume Hautbergue and Dr. Robin Highley, as well as my wonderful personal tutor Dr. Denise Bee. I could not achieve this without their wonderful and excellent guidance.

I wish I could name all my lovely family and all my wonderful friends, that became my family in this country, that help me through the good and bad times. I could not have done it without all of them and I feel extremely grateful with life for putting them in my path.

"Man kann davon überzeugt sein, sich etwas zu wünschen- vielleicht jahrelang - solang man weiß, dass der Wunsch unerfüllbar ist. Steht man plötzlich vor der Möglichkeit, dass der Wunschtraum Wirklichkeit wird, dann wünscht man sich nur eins: Man hätte es sich nie gewünscht." M. Ende

Contents

List of figures

List of tables

List of abreviations

AD	Alzheimer's Disease
ALS	Amyotrophic lateral sclerosis
ATG	Autophagy related genes
ATM	Ataxia-Telangiectasia Mutated
BSA	Bovine serum albumin
Cas9	CRISPR-associated endonuclease 9
CMA	Chaperone-mediated autophagy
CI-V	Complex I-V
CRISPR	Clustered Regularly Interspaced Short Palindromic Repeats
DA	Dopaminergic
DAB	3,3'-Diaminobenzidine
DLB	Dementia with Lewy Bodies
DDR	DNA damage repair
ds	double stranded oligo
dsRNA	double stranded RNA
DSB	double strand breaks
CCCP	Carbonyl cyanide m-chlorophenyl hydrazine
ECAR	Extracelular acidification rate
G-6P	Glucose-6-phosphate
GBA	Glucocerebrosidase
GSH	Glutathione
GWAS	Genome-wide association study
hCG	human chorionic gonadotropin
HDR	Homology Directed DNA Repair
HK-I	Hexokinase I
HK-II	Hexokinase II
iDA	Induced dopaminergic neurons
iN	Induced neurons
iNP	Induced neural precursors
iNS	Induced neural stem cells
iPSC	Induced pluripotent stem cells
LDH	Lactate dehydrogenase
LRRK2	Leucine-rich repeat kinase 2
miR	pre-miRNA
miRNA	micro RNA
MND	Motor Neuron Disease
MRC	Maximal respiratory capacity
MSA	Multiple System Atrophy
MPP+	1-methyl-4-phenylpyridinium
MPTP	1-methyl 4-phenyl, 1, 2, 3, 6 tetrahydropyridine
Muc1	Mucin 1

mTOR	mammalian target of rapamycin
NFT	Neurofibrillary tangles
NHEJ	Non-Homologous End Joining Repair
OCR	Oxygen consumption rate
OGD	Oxygen glucose deprivation
OXPHOS	Oxidative phosphorylation
PARL	Presenilin-associated rhomboid-like protein
PD	Parkinson's Disease
PEI	polyethylenimine
PFA	Paraformaldehyde
PFK1	Phosphofructokinase 1
PFK-2/FBPase-2	6-Phosphofructokinase-2-kinase/fructose-2,6-biphosphatase
PDH	Pyruvate Deshydrogenase complex
Ptet	Tetracycline responsive promoter
RCR	Respiratory cell ratio
RNAi	RNA interference
ROS	Reactive oxygen species
RT	Room temperature
sgRNA	small guide RNA
siRNA	small interfering RNAs
SN	Sustantia Nigra
SNCA	Alpha-synuclein
SNpc	Sustantia Nigra pars compacta
SNP	Single nucleotide polymorphism
SRC	Spare respiratory capacity
SSR	Site-specific recombinase systems
TBS	Tris-Buffered saline
TetO	Tetracycline-operon sequence
TetR	Tetracycline-repressor protein
TGF-β	Transforming growth factor β
TIGAR	TP-53-induced glycolysis and apoptosis regulator
TLR	Toll-like receptors
UCP	Uncoupling protein
UDCA	Ursodeoxycholic acid
UPS	Ubiquitin-proteasome system
VDAC	Voltage dependent anion selective channel 1
VPS35	vacuolar protein sorting 35
WB	Western Blot
WT	wild type

1. General introduction

Parkinson's disease (PD) is a common, progressive neurodegenerative disorder. The pathological hallmark of the disease is loss of dopaminergic neurons in the pars compacta of the substantia nigra (SN), resulting in the typical clinical PD triad of tremor, akinesia and rigidity. The majority of PD cases are sporadic: in most populations only ~5-10% of cases are inherited (Pan and Yue, 2014). The exact mechanisms leading to the loss of dopaminergic neurons remain obscure, but new insights into genetic and molecular pathways will provide us with the required knowledge to design disease-modifying therapy for this and, possibly other neurodegenerative disorders.

1.1 Clinical and pathological features

PD patients usually present with a continuum of motor and non-motor symptoms. The age of onset is usually between 5th and 7th decade of life. Clinical criteria to diagnose PD include bradykinesia, pronounced muscular rigidity, tremor at rest, postural instability and hypomimia (Emre et al., 2007; Palma and Kaufmann, 2014; Poewe and Wenning, 2002).

At presentation, 50-70% of dopaminergic neurons in the *substantia nigra pars compacta* (SNpc) will have already been lost and the remaining neurons may contain Lewy bodies that may be accompanied by thread-like Lewy neurites in the neuropil. Lewy bodies and neurites are cytoplasmic protein aggregates composed predominantly of alpha-synuclein and are a pathological hallmark in PD (Baba et al., 1998; Orth and Schapira, 2001). While these inclusions are predominantly found in the pigmented nuclei of the brainstem, Lewy bodies can be found in multiple subtentorial brain areas and also non-neuronal tissue (Braak et al., 2003) including

the cortex, spinal cord, gastrointestinal tract and endocrine organs (Lee et al., 2017; Palma and Kaufmann, 2014). The precise location in the brain where these inclusions are initially formed remains elusive, both single and multifocal initiation sites have been suggested (Freundt et al., 2012; Visanji et al., 2013).

1.2 Etiology of PD

1.2.1 Genetics of PD

PD is a multifactorial disorder: diverse genetic and environmental factors contribute to the development of the disease. Most cases are sporadic, but the identification of monogenic inherited PD genes has significantly contributed to our understanding of PD (Exner et al., 2012).

Studies of genome-wide linkage analysis in PD families have identified a number of chromosomal location of genes (loci) associated with PD. These PD loci are known as *PARK* loci, and a number is consecutively assigned for each new identified locus (Chung et al., 2011).

1.2.1.1 *Monogenic forms*

Dominant

The *alpha-synuclein* (*SNCA*) gene, encoding the alpha-synuclein protein, was the first gene identified as a cause of PD (*PARK1* and *PARK4*) (Farrer et al., 1999; Polymeropoulos, 1997; Polymeropoulos et al., 1996; Singleton et al., 2003a). However, mutations in this gene are very rare (<1%) (Hoffman-Zacharska et al., 2013; Lohmann and Klein, 2008; Markopoulou et al., 2008). Mutations in the *Leucine-rich repeat kinase 2* (*LRRK2*) gene are the most common genetic cause of PD (*PARK8*) (Paisán-Ruíz et al., 2004; Zimprich et al., 2004). The *Glucocerebrosidase* (*GBA*) gene encodes the β-glucocerebrosidase lysosomal

enzyme, homozygous and compound heterozygous mutations which cause of Gaucher disease (GD). Heterozygous *GBA* mutations have been identified as a strong risk factor for PD (Aharon-Peretz et al., 2004; Lesage et al., 2011; Neumann et al., 2009; Sidransky et al., 2009). The neuropathology from people with PD and mutations in *GBA* is comparable to that of classical, sporadic PD (Aharon-Peretz et al., 2004; Ma et al., 2013; Sidransky et al., 2009).

Recessive

The *Parkin (PARKN)* gene is the most common cause of autosomal recessively inherited PD with early onset PD (EOPD) (Asakawa et al., 2001; Kitada et al., 1998) representing ~50% of mutations occurring in EOPD (Lohmann et al., 2003; Lücking et al., 2000; Pramstaller et al., 2005). The *PTEN-induced putative kinase 1* (*PINK1; PARK6*) gene is the second most common cause (1-7%) of EOPD (Valente et al., 2001, 2004). Mutations in *DJ-1 (PARK7)* are rare and account for <1% of PD cases (Alcalay et al., 2010; Bonifati et al., 2004).

Sporadic

PD etiopathology is mainly sporadic (~90%), where no evidence of familial history can be found. However, there is a 2-14 fold increased risk for PD for first-degree relatives of an affected PD patient compared to the general population. It is a complex disorder where a number of factors interact and contribute to the development of the disease. One of these factors are genetic variations, with ~28 independent risk significant loci identified (Nalls, 2014). The majority of the candidate risk-related genes and loci have been found by linkage analysis and genome wide association studies (GWAS). Some of these candidate genes had been demonstrated to be relevant for the disease across different populations and models. Here, we will focus in the main candidate genes with strong risk association for PD.

Variations within the *SNCA* gene have been established as one of the main susceptibility genes for PD. *SNCA* mutations in familial PD support its role as a risk factor and susceptibility for the disease. More than 800 variations with positive *SNCA* risk association for PD have been reported up to date. Reported *SNCA* variations are: a) single nucleotide polymorphisms (SNP) analysis, which revealed a positive association between SNPs within promoter region (REP1), the 3'UTR region (e.g. rs356165), 3' end (e.g. rs356219) and intronic region (e.g. rs2736990) of the gene and increased risk for PD across different populations; b) locus duplications and triplications and; c) point mutations in the amino-terminal region. The rs256220 SNP is the variation that showed the highest reproducibility across different studies (Redenšek et al., 2017). Some of the SNPs were reported to have a significant impact the *SNCA* levels in blood, serum, plasma and brain samples. The suggested biological effect might be by modifying *SNCA* expression at transcriptional levels and protein aggregation. Few studies investigated the association of SNPs in the clinical phenotype (severity and outcome) with inconclusive results. Increased levels of *SNCA* had been associated with increased risk for PD, whereas decreased levels were described as protective from the disease (Loureiro and Silva, 2017).

In 1-10% of sporadic PD cases, *LRRK2* variations have been associated in different populations. *LRRK2* variants include from rare high penetrant variants to common variants with decreased effect confirmed as a susceptibility gene. The biological effect of the reported variants involved endo-lysosomal pathways, autophagy and mitochondrial function by affecting LRRK2 function, interaction and phosphorylation with binding proteins (Redenšek et al., 2017). The most common

reported variation is p.Gly2019Ser (rs34637584), where LRRK2 increased activity has been associated with increased risk for PD (Wallings et al., 2015).

MAPT, commonly known as tau, is a protein ubiquitously expressed in the neurons and involved in cellular maintenance and organisation. Pathologic aggregations have been described in a number of neurodegenerative disorders, such as Alzheimer's Disease (AD), Pick's disease, and other parkinsonian disorders. Tau pathology has been described in PD cases, mostly with *LRRK2* mutations (Soto-ortolaza et al., 2013). It has been confirmed by different studies as a risk factor for PD, with up to 40 mutations described. However, variants reported have not been replicated. The SNP rs393152 and the inversion locus polymorphism on chromosome 17 (900 kb) including several genes besides MAPT, are the ones consistently reported with associated risk for PD. Two haplotypes of this locus have been described: H1 and H2, where H1 increased *MAPT* transcription and H2 decreases it (Peeraully and Tan, 2012). The biological effect has been suggested to occur alongside SNCA and hyperphosphorylation of the protein, leading to impairment of the microtubule organization, altered cytoskeleton, defective axonal transport and impaired autophagy with protein aggregation (Pascale et al., 2016).

The *GBA* gene was confirmed as a genetic risk factor for PD. Heterozygote mutations have been reported to increase the risk for PD in many populations (Li et al., 2013). The encoded enzyme is located in the lysosomal membrane, where ceramide and glucose are produced after glucocerebrosides had been cleaved. *GBA* mutations decrease the enzymatic activity.

Although the GWAS and statistic analysis reported strong association between the different genes and the risk for PD, their contribution for the disease remains low. The candidate genes and with the highest association are: *SNCA*, *MAPT*, *LRRK2*, *GBA*, *Bone marrow stromal cell antigen 1* (*BST1*), *CCDCC2/HIP1R*, *cyclin G association kinase* (*GAK*), *diacylglycerol kinase theta* (*DGKQ*), *serine threonine kinase 39* (*STK39*) and *synaptotagmin XI* (*SYT11*) (Ferreira and Massano, 2017).

Environmental factors

Some environmental factors have been described as exogenous risk factors for sporadic PD. It is suggested that the complex interplay between these and susceptibility genes might trigger for the disorder. Epidemiological studies showed positive associations between PD and pesticides, including toxins such as paraquat, rotenone, organophosphates and organochlorines. Paraquat is a mitochondrial Complex I (CI) inhibitor, which also promotes cytosolic oxidative stress and apoptosis mediated by caspase-3. Rotenone, also induce mitochondrial dysfunction via CI inhibition. Both reagents have been used to study PD-related mechanisms in cellular and animal models (Fleming, 2017).

Heavy metals have been also associated with PD development and other neurodegenerative disorders. These include iron and manganese as the main culprits. Excessive exposure to pesticides and heavy metals lead to PD symptoms and cognitive impairment, due to accumulation within the basal ganglia and SN mainly (Kwakye et al., 2015; Wang et al., 2016c). Their toxic mechanism remains unknown, but it has been suggested to be secondary to oxidative stress, mitochondrial dysfunction and impaired protein clearance leading to apoptosis.

Currently, the list of suspected environmental factors is growing, however, their role as risk factors remain to be verified. Amongst these are newer pesticides. Protective factors such as, smoking and caffeine, have also been reported. However, the mechanisms underpinning the apparent protective effect remain to be determined (Hernán et al., 2002).

1.3 Pathogenesis in PD

1.3.1 Mitochondrial dysfunction in PD

There is strong evidence that mitochondrial function plays a key role in the disease process. The main mitochondrial functions involved are defects in the respiratory chain complexes. The first evidence was found during the 80's decade in drug users in California. They developed parkinsonian symptoms after self-administration of the synthetic heroin analogue 1 methyl-4-phenyl-1,2,3,6-tetrahydropiridine (MPTP). Post-mortem studies performed in these people revealed dopaminergic neuronal damage within the SN (Langston et al., 1983). Later, it was found that MPTP crosses the blood brain barrier, enter to the astrocytes where is oxidised to 1-methyl 1-4-phenylpyridinium (MPP+). MPP+ was found to be a dopamine receptor substrate. Therefore, when MPP+ is released, it enters the dopaminergic neuron. Mitochondrial dysfunction follows when CI is inhibited, leading to neuronal death (Langston et al., 1984; Ransom et al., 1987). Further evidence was found in the brains of sporadic PD patients, in which CI deficiency was reported in the SN and other brain regions (Mann et al., 1992; Mizuno et al., 1989; Navarro et al., 2009; Parker et al., 2008; Schapira et al., 1989). Furthermore, CI inhibitors, such as MPTP, rotenone and paraquat, recapitulate PD pathology in cells and animal models featuring dopaminergic neuronal loss, as well as clinical signs of PD (Cochemé and Murphy, 2008; Corona et al., 2010; Decressac et al., 2012; Gille et al.,

2004; Irwin and William Langston, 1985; Langston et al., 1984; Qureshi and Paudel, 2011; Sallinen et al., 2010; Sharma and Nehru, 2013; Tanner et al., 2011; Wu et al., 2011; Yong-Kee et al., 2012). CI deficiency has been consistently demonstrated in PD tissue such as human fibroblasts, platelets and lymphoid cells (Krige et al., 1992; Mann et al., 1992; Mortiboys et al., 2008, 2013; Parker et al., 1989; Rh et al., 1995; Yoshino et al., 1992).

CI inhibition leads to increased reactive oxygen species (ROS) mitochondrial production and reduced ATP production, which results in cellular neuronal damage and death. Furthermore, CI deficiency induces Ubiquitin proteasome system (UPS) impairment, followed by accumulation of misfolded proteins (Reeve et al., 2015). Mutant *SNCA* (Braidy et al., 2013; Chinta et al., 2010; Choubey et al., 2011; Hsu et al., 2000; Kamp et al., 2010), *PINK1* (Chung et al., 2016; Exner et al., 2007; Hilker et al., 2012; Lutz et al., 2009; Morais et al., 2014; Park et al., 2006; Priyadarshini et al., 2013; Rakovic et al., 2011) and *Parkin* (Flinn et al., 2009; Grünewald et al., 2010; Haylett et al., 2016; Hoshino et al., 2013; Mortiboys et al., 2008, 2013; Müftüoglu et al., 2004; Palacino et al., 2004; Rakovic et al., 2010; Seibler et al., 2011; Sethi and Kang, 2011; Vergara et al., 2014) deficiency are related to impaired mitochondrial morphology, CI dysfunction, increased ROS production and altered bioenergetics status of the cell. *LRRK2* mutations also lead to increased ROS and oxidative stress, CI, II and IV deficiency, altered mitochondrial morphology and mitochondrial dynamics by affecting the function of uncoupling and mitochondrial fission proteins (Grunewald et al., 2013; Mortiboys et al., 2010a, 2015; Papkovskaia et al., 2012).

1.3.2 Autophagy and mitophagy in PD

Autophagy is the cellular process by which all the damaged/dysfunctional organelles and proteins are cleared from the cell. Autophagy is usually triggered by different cellular stimuli and can be divided into 3 types depending on the structures processed into the lysosomes: macroautophagy, chaperone-mediated autophagy (CMA) and microautophagy. The formation of the autophagic vesicle follows 5 steps: initiation, nucleation, elongation, fusion and degradation. Macroautophagy is the most studied process of all (Yoshii and Mizushima, 2017).

In macroautophagy, the components are sequestered in double-membrane vesicles, forming the autophagosome, which fuses the lysosome for degradation. In microautophagy, lysosomes are in charge of the uptake and degradation of cytoplasmic contents directly without forming the autophagosome. In CMA, the process requires the presence of the KFERQ (LysPheGluArgGln) peptide in the substrate protein. This substrate protein is then recognised by the chaperone heat shock proteins (Hsp70), and brings it to the lysosomal receptor, where it is translocated by LAMP2A. The substrate is unfolded and degraded in the lysosome.

Autophagy is a highly regulated process, where a number of molecules are required upon stimulation (eg. Nutrient starvation and oxidative stress). Specific adaptor proteins p62/SQSTM1 are required for recognition of ubiquilated proteins. The autophagy related genes (ATG) are necessary to form the autophagic vesicles and autophagosomes. The ATG genes are regulated by: a) the mammalian target of rapamycin (mTOR), which inhibits autophagy under physiological conditions; b) beclin complex and; c) LC3 lipidation process. LC3-I (cytosolic protein) conversion to LC3-II (recruited to the autophagosome membrane) is a hallmark marker of

24

autophagy. Mitophagy is the process in which damaged mitochondria are removed and cleared from the cell. This regulated process to maintain the right pool and quality mitochondria upon metabolic stress.

Autophagy and mitophagy have been demonstrated to be one of the main cellular pathways that might be impaired in PD and contribute to neurodegeneration (Redenšek et al., 2017).

1.3.2.1   The PINK/Parkin Pathway

Parkin and *PINK1* have roles in the same mitochondrial pathway (Pickrell and Youle, 2017). Both have been found to be involved in the dynamics and homeostasis of mitochondrial function, energy production (ATP), modulation on proteasome degradation and clearance of damaged mitochondria (Geisler et al., 2010a, 2010b; Ryan et al., 2015; Wild and Dikic, 2010).

It was recently found that PINK1 has a role as an ubiquitin kinase and after the mitochondrial membrane potential is lost, it phosphorylates ubiquitin and the Parkin ubiquitin-like domain on S65. These events were reported to be required for Parkin activation (Aguirre et al., 2017; Schubert et al., 2017). Therefore, when PINK1 is stabilised on the mitochondrial outer membrane (OMM), it enables Parkin translocation to the mitochondria (Wild and Dikic, 2010). In response to mitochondrial depolarisation, PINK1 binds, translocates, phosphorylates and activates E3 ligase Parkin. *PINK1* mutations impede PINK1 importation and stabilisation and thus inhibit Parkin binding and translocation to the mitochondria (Geisler et al., 2010a, 2010b), as well as PINK1/PARL processing.

Following activation and mitochondrial translocation, Parkin polyubiquitinates itself and the outer mitochondrial proteins (mitofusins and VDAC) to recruit the autophagy adaptor p62 and induce the proteasome/phagophore formation by binding Agt8/LC3 to promote autophagy (Geisler et al., 2010a, 2010b). PINK1 is imported to the mitochondria and cleaved in presence of a normal mitochondrial membrane potential; this enables PINK1 to recruit and translocate Parkin to the mitochondria. Activated Parkin can ubiquitinate the proteins of the MOM, voltage dependent anion selective channel 1 (VDAC) and p62, which binds LC3. The autophagophore is formed promoting autophagy (Wild and Dikic, 2010). Recently, Wang et al. 2017, found that LRRK2 is also recruited to the depolarised mitochondria alongside PINK1 and Parkin. They suggested that the three PD proteins remove RHOT1/Miro (an outer mitochondrial membrane protein) to be degraded by the proteasome. This leads to mitophagy after the targeted mitochondria is arrested. (Wang, 2017) (Figure 1.1).
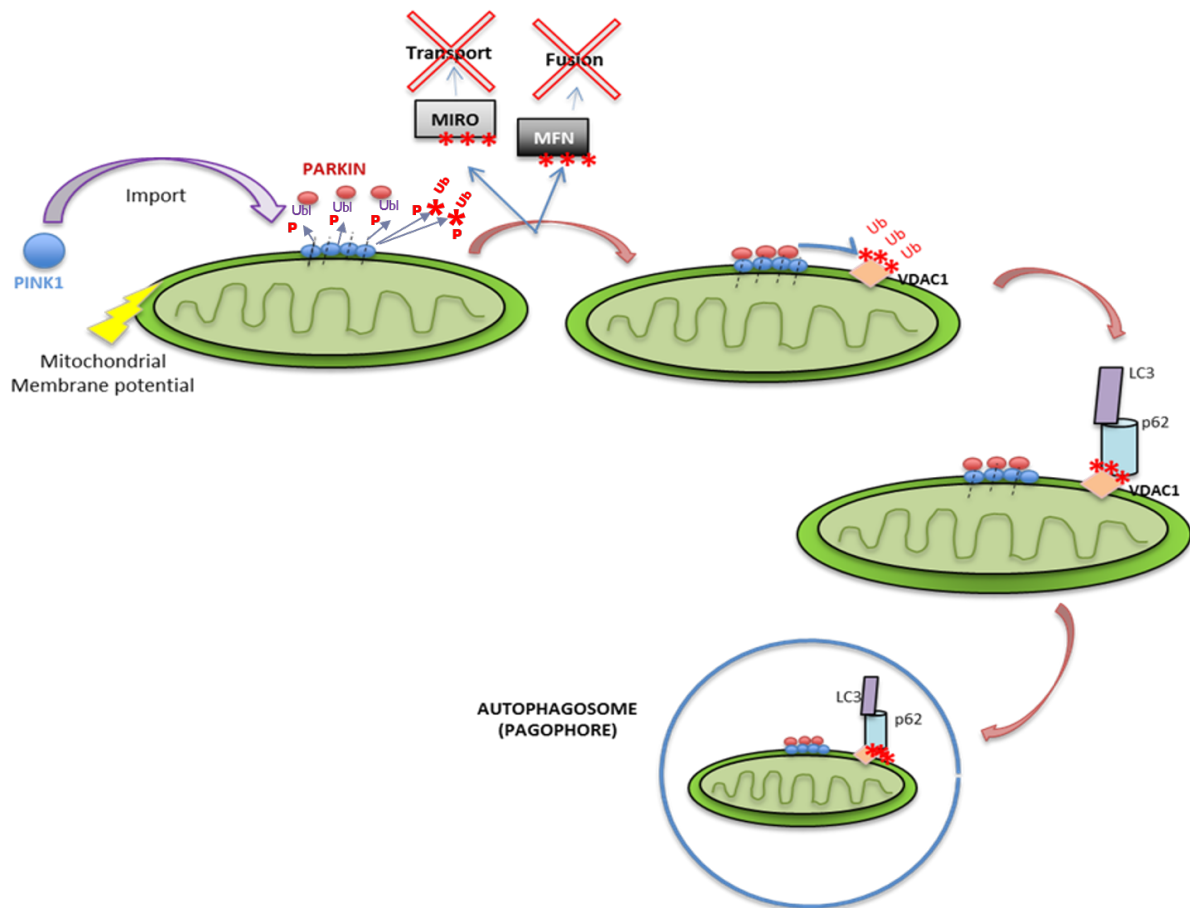
Figure 1.1 Schematic representation of the PINK/Parkin pathway. PINK1 is imported to the mitochondria and cleaved in presence of a normal mitochondrial membrane potential (MMP). PINK1 phosphorylates ubiquitin and Parkin ubiquitin-like (Ubl) domain. This enables PINK1 to recruit and translocate Parkin to the mitochondria. Activated Parkin can ubiquitinate the proteins of the outer membrane (OMM) VDAC and p62, which binds LC3. The autophagophore is formed promoting mitophagy (Aguirre et al., 2017; Schubert et al., 2017; Wild and Dikic, 2010).

Further research has suggested a physical interaction between the *Parkin* RING 1 domain and the *p53* (*TP53*) promoter region. *Parkin* seems to be a *P53* target gene under both stress and non-stress conditions (Alves da Costa and Checler, 2010; da Costa et al., 2009; Zhang et al., 2011). Protein-protein interaction between cytosolic p53 and Parkin inhibits Parkin translocation and mitophagy in cardiac myocytes from mice (Hoshino et al., 2013). Furthermore, *Parkin* may act as

a *p53* target to maintain genome stability by regulating ROS levels (Zhang et al., 2011).

1.3.3 Neuroinflamation

Neuroinflammation is a further characteristic of PD pathology. However, it is unknown whether it is cause or consequence of the disease process. Post-mortem studies of brains of PD cases and animal models have shown that pro-inflammatory factor levels are increased. One of the main mediators involved in inflammation are activated microglia resulting in chronic exposure to ROS and production of cytokines within the brain. Mutant *SNCA* can be recognised as a pathogen by toll-like receptors (i.e. TLR2, TLR4), which triggers inflammation through NF-Kb translocation and cytokine production, activation and expression. The immune response may depend of the conformation of SNCA, where β-sheet conformations showed higher sensitivity. Protein aggregates and misfolded SNCA activate microglia, which also triggers the production of inflammatory cytokines (TNF-α and IL-1β) leading to neurotoxicity and neuronal death (Austin et al., 2011; Béraud et al., 2011). Despite this, recent findings have demonstrated that microglia can also have protective effects by clearing damaged neurons as a result of neurotoxic exposure (Gomez-Nicola and Perry, 2014).

1.3.4 Alpha-synuclein (SNCA) pathology

As mentioned above, *SNCA* was the first gene described as a genetic cause for familial PD. Subsequently, alpha-synuclein was discovered to be the main component of the Lewy bodies and glial cytoplasmic inclusions in PD and related alpha-synucleinopathies. Despite this, how *SNCA* promotes PD pathology and the exact physiological function are still unknown (De Franceschi et al., 2017). Alpha-synuclein is composed of 140 amino acids and expressed in neuronal synaptic

terminals (Sengupta et al., 2015). Alpha-synuclein is important for normal synaptic function, vesicle trafficking, release and recycling, as well as a regulator of dopamine metabolism (release and uptake) (Lautenschläger et al., 2017; Nakata et al., 2012; Pelkonen et al., 2013). Several mechanisms for SNCA PD-related pathology have been reported, mostly related to toxic effects. Duplications, triplication, gene mutations and posttranslational modifications in *SNCA* inducing its overexpression have been related to increased protein aggregation within the neurons in *in vitro* an *in vivo* models (Bezard et al., 2013). Protein aggregates are resistant to degradation due to impaired autophagy, leading to cellular death. Overexpressing *SNCA* (Wild type and mutant) can impair autophagy through different mechanisms: by inhibition of the chaperone-mediated autophagy; compromising the synthesis and clearance of the autophagosome and UPS pathway; attaching to lysosome receptor LAMP2A, preventing its internalisation to the lysosome; and inhibition of lysosomal enzymes, such as GBA (Gan-Or et al., 2015). Mitophagy might be also impaired by mutant *SNCA*, due to increased protein aggregation with increased ROS levels. As a result, increased levels of oxidative stress promote mitochondrial fragmentation and dysfunction, affects MMP and permeability. This entire cascade of events leads to impaired mitophagy and clearance (Redenšek et al., 2017; Wang et al., 2016a).

Others suggested that increased levels of alpha-synuclein might impair the dynamics and recycling of the synaptic vesicles (Mazzulli et al., 2016). They can also impair the interaction with dopamine, induce a conformational change and inhibit the degradation of alpha-synuclein through the CMA (Chinta et al., 2010). Additional toxic mechanisms include impaired Ca2+ homeostasis; tyrosine hydrolase phosphorylation and function. Alpha-synuclein aggregates also lead to increased

neuroinflammation in the microglia induced by proteins of the immune response (i.e. Major histocompatibility complex and TLR) (Gustot et al., 2015; Luth et al., 2014; Venda et al., 2017).

1.4 TIGAR

TIGAR (*T*P53-Induced *G*lycolysis and *A*poptosis *R*egulator; also known as *C12orf5)* was identified by Bensaad, et al. 2006. The *TIGAR* locus is on chromosome 12p13-3. It has 6 coding exons and two p53 binding sites known as BS1 (intron 1) and BS2 (intron 2). It is characterised by a structural and protein similarity to the biphosphatase domain of the enzyme 6-phosphofructose-2-kinase/fructose-2,6-biphophatase (PFK-2/FBPase-2). Both FBPase-2 and TIGAR, decrease Fructose-2,6-Biphosphate (Fru-2,6 P_2) levels. Fru-2,6 P_2 is the substrate of Phosphofructokinase-1 (PFK-1), the key enzyme in the glycolytic pathway. By lowering the Fru-2,6 P_2 levels, TIGAR inhibits the glycolytic pathway and promotes the Pentose Phosphate Pathway (PPP). This, in turn, reduces reactive oxygen species (ROS) by increasing the production of NADPH and reduced glutathione (GSH) (Figure 1.2) (Bensaad et al., 2006).

Li and Jogl (2009) reported that TIGAR protein also has a similarity to the catalytic unit of the Fru-1,6-P_2 and F26BPase enzymes. F26BPase is the key metabolic activator enzyme of glycolysis and Fru-1,6-P_2 is a glycolytic intermediate. Due to the shared homology, TIGAR binds the catalytic unit of the F26BPase enzyme. Following this event, inhibition of glycolysis occurs due to down-regulation of the F26BPase and removal of the Fru-1,6-P_2 enzymes. The closest structural relation exists between TIGAR and the PhoE phoshphatase (PhoEP) enzyme, whose unknown activity might have an additional underlying role in glycolysis (Li and Jogl, 2009).

Furthermore, Gerin et al., 2014; found that the 2,3-Biphosphoglycerate (23BPG), cofactor of the Phosphoglycerate mutase enzyme (PGAM), has a higher affinity (~400-fold) for TIGAR compared to F26BP. This suggests an added action of TIGAR as a phosphatase, on the grounds of a shared distant homology with the histidine phosphatase family (PhoEP) and substrate specificity. However, 23BPG has been reported as present and active only in erythrocytes (where it is important for oxygen binding to haemoglobin) without any other known functional relevance in other cell types (Gerin et al., 2014).
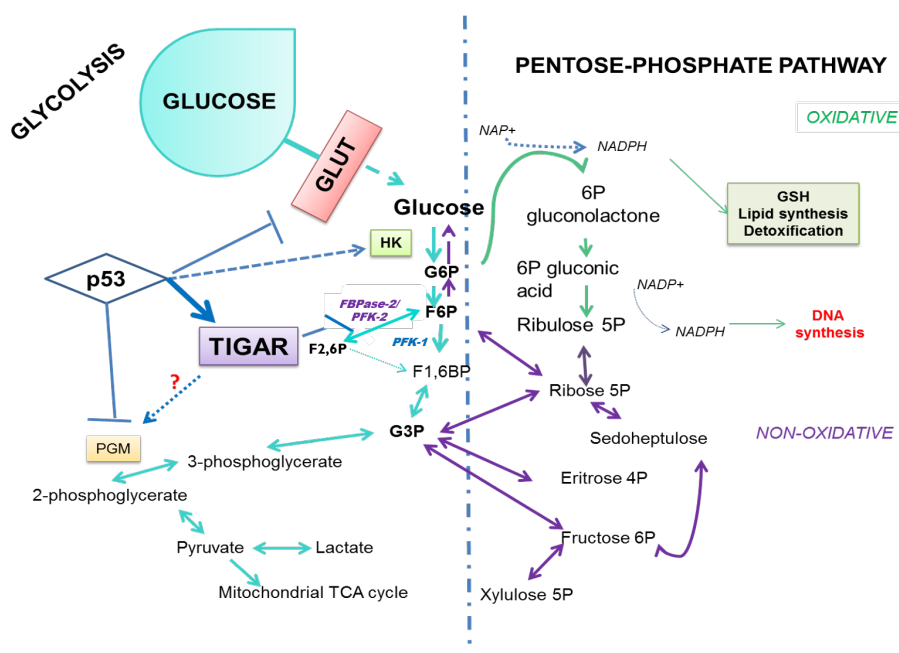
Figure 1.2 *TIGAR* **function in the glycolytic and Pentose Phosphate pathway.** TIGAR has a shared homology to the biphosphatase domain of the PFK-2/FBPase-2 enzyme. Therefore, TIGAR acts by inhibiting the glycolytic enzyme PFK1, lowering the F2,6 P_2 and F1,6 P_2 levels. 3, Phosphoglycerate; G6P (G3P) Glucose-6-phosphate; Gluthathione (GSH); Hexokinase (HK); 6-Phosphofructo-1-kinase (PFK1); Phosphoglycerate Mutase (PGM); Tricarboxylic Acid Cycle (TCA) (Maddocks and Vousden, 2011; Riganti et al., 2012).

1.4.1 TIGAR regulators

The type of TIGAR response (glycolysis and metabolic regulation, ROS scavenging, cellular survival and autophagy) within a cell depends on several different factors, including stress due to ischaemia or hypoxia; as well as the cell type (Bensaad et al., 2009; Cheung et al., 2012; Sun et al., 2015; Zou et al., 2012).

p53. The first identified protein acting as an upstream regulator of TIGAR is p53. P53 is a transcription factor that induces different cellular responses depending on the cellular physiological demand or damage response. Despite the importance of p53-regulation of TIGAR, it is now known that there are several other TIGAR-mediated mechanisms, which are p53-independent. These are important because p53 is not essential to maintain TIGAR basal expression levels (Lee et al., 2015).

p63 and p73. Recent findings have described further molecules that regulate TIGAR levels and activity. These include p63 and p73, two other genes from the same family of transcription factors as p53 and have been suggested to be upstream regulators of TIGAR. A p63- and p73-dependent cellular survival function of TIGAR has been demonstrated in intestinal crypts. However, the full details of these regulatory mechanisms remains unclear and not fully confirmed (Lee et al., 2015). In addition, an inverse correlation has been described between TIGAR expression and both p63 and p73, within thymic lymphomas. This mechanisms probably involves different P63 and P73 isoforms, which would influence the tumour growth rate (Venkatanarayan et al., 2016).

SP-1. SP-1 is a common transcription factor that is responsible for the activation or repression of several different genes, affecting a diversity of cellular

mechanisms, including, cellular metabolism, cellular proliferation and growth, chromatin remodelling and apoptosis (Beishline and Azizkhan-Clifford, 2015; Henson et al., 1992). SP-1 has been described in a diversity of cell types, including neuronal cells, where it provides a role in neuronal modulation and protection in Huntington's Disease (Qiu et al., 2006). SP-1 has also been suggested to play a role in various neurodegenerative diseases, mainly tauopathies: In AD, co-localisation of SP-1 has been seen with tau protein in neurofibrillary tangles (NFT), dystrophic neurites, threads and plaques. Whereas in other tauopathies, such as Pick's disease and progressive supranuclear palsy, SP-1 is present in neurons, astrocytes and oligodendrocytes. Moreover, a negative correlation between Lewy pathology and SP-1 has been found in PD and dementia with lewy bodies (DLB) (Santpere et al., 2006). SP-1-mediated regulatory mechanisms of TIGAR were first demonstrated In cancer liver cells, where SP-1 positively interacts with the TIGAR promoter, where it modulates TIGAR basal transcription (Zou et al., 2012).

CREB. The highly conserved promoter region of TIGAR contains specific sites for many DNA binding-motifs of a variety of transcription factors. Recently, a CREB box within this region has been described (Zou et al., 2013). CREB is a transcription factor from the leucine zipper family. It is responsible for a number of transcriptional responses to different stimuli (e.g. growth hormonal and stress signals); (Wang et al., 2016e). CREB expression levels correlate with, and are indispensable for, TIGAR expression. However, further transcription factors that drive TIGAR expression remain to be elucidated (Zou et al., 2013).

PI3-AKT-mTOR. The PI3-AKT-mTOR pathway also has been described as an upstream regulator of TIGAR in colonic cancer cell lines. This is an important signalling pathway for protein translation by activating eIF4F, an initiation factor that induces protein translation (Ahmad et al., 2017)

NSD2. The nuclear receptor-binding SET domain-containing 2 (NSD2) protein, also known as multiple myeloma SET domain (MMSET) or Wolf-Hirschhorn syndrome candidate 1 (WHSC1), is a H3K36 histone methyltransferase. Some of its main functions are via epigenetic gene regulation, NF-Kb and cytokine modulation as well as driving expression of oestrogen receptor in breast cancer. NSD2 overexpression can lead to tumour resistance via glycolytic enzymes and PPP pathway induction. The proposed mechanism is by direct stimulation of NSD2 recruited in the promoter of the glycolytic genes *TIGAR*, *HK-II* and *G6PD* (Wang et al., 2016b).

ATM. A possible relation between neurodegenerative disease process via upregulation of the ATM-p53-TIGAR pathway has been suggested. The Ataxia-Telagiectasia Mutated gene *(ATM)* encodes a key protein involved in DNA-damage repair (DDR) to double-strand breaks (DSBs). It acts as an upstream regulator by promoting several genes related to cellular proliferation, apoptosis and repair, such as p53. Recently, the up-regulation of the *ATM* gene was found to co-occur with a progressive decrease of TIGAR protein levels in patients with AD (Katsel et al., 2013).

HK-II. HK-II (hexokinase II) is prevalent in tissues with high energy demand, such as skeletal muscle, heart and adipocytes (John et al., 2011). It also has an important role in regulating cellular survival and autophagy under glucose deprivation conditions or type of cellular damage (Tan and Miyamoto, 2015). Overexpression of mitochondrial HK-II may confer neuronal protection and survival in animal and cellular models of PD and neurodegeneration (Corona et al., 2010; Gimenez-Cassina et al., 2009). Under hypoxic conditions, mitochondrial HK-II is important for TIGAR mitochondrial translocation, where both proteins form a complex. This results in HK-II stabilization and enhanced activity and interaction with TIGAR upon presence of glucose and active HIF-1α.

1.4.2 TIGAR mechanisms

Cellular protection and DNA repair. One of the main actions described in the p53-TIGAR pathway, is the PPP, which protects cells from damage and aid survival by reducing levels of reactive oxygen species and providing cells with NADPH and GSH (Bensaad et al., 2006).

In hepatocarcinoma, TIGAR has been suggested as providing cellular protection by promoting DDR via a number of mechanisms: Firstly, the PPP pathway is involved by providing the cell with nucleotide precursors for DNA synthesis, as well as reducing agents (e.g. NADPH and G6PD) to protect against reactive oxygen species (Xie et al., 2014). Secondly, in response to cellular hypoxia, TIGAR induces nuclear translocation of the oxidoreductase enzyme thioredoxin-1 (TRX1), which is important in the DDR pathway (Yu et al., 2015; Zhang et al., 2014). Thirdly, recent evidence demonstrates that TIGAR is a modulator of Cdk-5, which is known to phosphorylate ATM, consequently triggering the pathway for DDR (Yu et al., 2015).

TIGAR role cellular protection during embryogenesis was assessed in mice embryos. TIGAR is widely expressed in mouse brain, mainly in the cerebellum, olfactory bulb and cortex (Li et al., 2014). It has been suggested that TIGAR levels are continuously modified during development from the embryonic stage until adult stage in the mouse brain. TIGAR showed to have the highest expression during the embryonic and young adult stage. The highest expression of TIGAR in the mice brains provided neuroprotection from DNA and cellular damage upon oxidative stress and injury by shunting the metabolism to the PPP pathway (Cao et al., 2015).

Cancer. Under adverse metabolic conditions, such as cancer, p53-TIGAR and the PPP can contribute to cell survival due to its indirect anti-oxidant effect and by providing metabolites, such as ribose-5-phosphate, for DNA biosynthesis and repair (Bensaad et al., 2006; Wanka et al., 2012). The property of TIGAR as a ROS scavenger and induce anabolism by providing metabolites for DNA synthesis and cell growth contribute for the tumour development. TIGAR related mechanisms have been described in different cancer types enlisted in Table 1.1.

Another function of the p53-TIGAR pathway is by the regulation of important cell cycle genes, which is key to involving tumour progression. When there are low levels of cellular stress, p53 induces TIGAR to allow cell repair via the following cascade of events: modulation of cell-cycle progression genes and synthesis inhibition of cyclins lead to de-phosphorylation of RB-protein. As a result, the RB-E21 complex is stabilised delaying entry to the S phase of the cell cycle. Consequently, better combined therapy via TIGAR mediated-cell cycle arrest with anti-proliferative

drugs, can be provided in order to provide a better outcome in some cancers (Madan et al., 2012).

The glycoprotein Mucin 1 (MUC1) is a component of epithelial apical surfaces. MUC1-C (C terminal subunit of MUC1) and TIGAR, both have been shown to be overexpressed in colonic cancer (Al-Khayal et al., 2015; Cheung et al., 2013a; Niv, 2008) and multiple myeloma (Kawano et al., 2008; Yin et al., 2012a). Inhibition of MUC1-C also results in *TIGAR* down regulation. This is due to the role of MUC1-C inhibitors by two mechanisms. First, by preventing AKT phosphorylation and therefore, inactivation of EIF4A. This causes reduced TIGAR translation and thereby impairing cellular growth and survival (Ahmad, R, 2017). Second, TIGAR reduced expression lowers the NADPH and GSH levels, leaving vulnerable the cell to ROS damage and mediated cellular death (Yin et al., 2012a, 2014).

Cells depend on energy supply for their maintenance and the glucose uptake. This depends on the function of key enzymes, such as glycolytic enzymes. The Hexokinase family are enzymes that are responsible for the conversion of glucose to glucose-6-phosphate (G-6P). This is a crucial step in the glycolytic pathway and the PPP. This family contains four different isoforms of the enzyme: HK-I, HK-II, HK-III and HK-IV (also known as glucokinase). HK-I is present in all cellular types, but especially in the cerebral tissue and blood cells. It has been suggested that HK-I specifically shunts the glycolytic pathway (John et al., 2011; Magrì et al., 2016). HK-II stabilization induced the mitochondrial membrane potential and reduced ROS production upon hypoxia, which might promote cellular survival and likely contribute to tumour progression. The HK-I and HK-II are cytoplasmic proteins that have been

previously shown to translocate to the mitochondria through interaction with VDAC (Cheung et al., 2012).

NSD2 overexpression induces HK-II, G6PD and, predominantly, TIGAR. However, p53 expression is unaffected. Taken together, this suggests a p53-independent TIGAR function, where NSD2 acts as the key regulator and coordinator of the enzymes in the PPP pathway. This provides tamoxifen resistance and poor survival rates in some patients with breast cancer (Wang et al., 2016b).

Cancer	TIGAR related mechanisms
MM	MUC1-C (oncoprotein) inhibition led to a p53-independent reduction of TIGAR protein levels, without affecting *TIGAR* mRNA; suggested to be due to a posttranscriptional mechanism (Yin et al., 2012b).
NCC	Inhibition of the apoptotic and cell survival regulator c-Met, a tyrosine kinase, induced cellular death by lowering p53, TIGAR and NADPH levels. Moreover, *TIGAR* overexpression reversed the growth inhibition by c-Met (Lui et al., 2011). Therefore, induced down-regulation of *TIGAR* has a potential antitumour effect (Lui et al., 2010).
CC	Reduced apoptotic rate in U2OS cells with *TIGAR* overexpression, with increased ROS induced apoptosis when *TIGAR* is knocked down (Bensaad et al., 2006). Upregulation of *TIGAR* in colorectal cancer, mainly in advanced stages. This suggest to be a good biomarker of colorectal cancer as well as a therapeutic target (Al-Khayal et al., 2015).
BC	Breast cancer tissue samples of patients with primary invasive breast cancer revealed high expression of *p53* correlated to low expression of *TIGAR, SCO2* and *COX* (Won et al., 2012). Downregulation of Cav-1 promotes the upregulation of *TIGAR* expression in breast cancer cells, resulting in cancer cell proliferation and the suppression of cancer cell apoptosis(Shi et al., 2016)
GB and glioma cells	*TIGAR* overexpression conferred cell survival. TIGAR shared homology with TKTL1 enzyme, which is overexpressed in different neoplasias. TKTL1 inhibition suppressed the antioxidant protective and starvation effect of TIGAR. Under normoxia, a role of TIGAR preventing apoptosis was proposed. Under hypoxia, where ATP production by OXPHOS is limited, suggested to be due to a dual modulation of energy production and antioxidant production (Wanka et al., 2012). In glioblastoma cells, *TIGAR* knockdown caused early cell senescence and inhibitied cell proliferation, followed by increased sensitization to radiation and impaired DNA damage repair (Peña-Rico et al., 2011).
CLL	*TIGAR* expression was related to an increased in cell sensitivity response to the cytotoxic agent Fludarabine, by inducing apoptosis in a caspase-3 dependent manner (López-Guerra et al., 2008).
NSCLC	*TIGAR* expression was correlated with FDG-PET results as a marker for evaluation of clinical outcome in patients with NSCLC. In patients with NSCLC, positive expression of *TIGAR* was correlated with substantially longer survival rate than those with a negative expression (Zhou et al., 2013).

HCC	*TIGAR* expression is increased after treatment with epirubicin (anti-cancer agent). Knock down of *TIGAR* led to epirubicin induced apoptosis. In addition, ROS production is increased. As a result, cancer cells have enhanced chemosensitivity to epirrubicin. A prospective role involving mTOR inhibition has been suggested and remains to be elucidated (Xie et al., 2014).

Table 1.1. TIGAR main mechanisms in cancer. Fluorodeoxyglucose positron emission tomography (FDG-PET); Transketolase-like 1 (TKTL1); Cytochrome C oxidase assembly protein (SCO$_2$); Cytochrome c oxidase (COX); Non-small cell lung carcinoma (NSCLC); Caveolin 1 (Cav-1); Nicotine adenine dinucleotide reduced (NADH); oxidative phosphorylation (OXPHOS); Reactive oxidative species (ROS); Multiple Myeloma (MM); Hepatocarcinoma (HCC); Non-small cell lung carcinoma (NSCLC); Chronic lymphocityc leukemia (CLL) Glioblastoma (GB); Breast cancer (BC), Nasopharyngeal cancer cells (NCC).

Ischemia-reperfusion injury. Hypoxia and ischemic reperfusion injury can result in apoptosis in a number of cell types including cardiac myocytes. Main detrimental effect is by reperfusion with high volume of oxygenated blood, which induce inflammation and oxidative stress. Glycolysis has been described to have a vital role for myocyte survival and it seems that maintenance and homeostasis of this metabolic pathway is regulated by TIGAR and p53. After myocardial infarction, TIGAR and p53 expression were significantly increased. In this context, the activation of the p53-TIGAR pathway inhibited glycolysis and energy metabolism, which result in apoptosis (Kimata et al., 2010).

On the contrary, TIGAR overexpression in the brain leads to protection against brain injury such as ischemia, oxidative stress and oxygen glucose deprivation (OGD). This is achieved via reducing levels of reactive oxygen species and GSH, and increasing levels of NADPH (Cao et al., 2015). SP-1-mediated upregulation of TIGAR is greatly influenced by metabolic hormones that regulate glucose and reactive oxygen species. This modulates the TIGAR response to ischemia/reperfusion injury in brain tissue (Sun et al., 2015). In addition, SP-1 regulation of TIGAR has been linked to so-called cerebral preconditioning when transient changes occur in the brain in response to ischemic or hypoxic injury,

providing tolerance against subsequent lethal ischemic or hypoxic insults. SP-1 and TIGAR contribute to this tolerance by regulation of cellular apoptosis and ROS scavenging (Zhou et al., 2016).

Interestingly, in testicular ischemia reperfusion injury (TIRI) has also been related to TIGAR-p53 pathway activation. TIRI is the considered underlying pathology behind testicular torsion and detorsion, which can lead to impaired spermatogenesis and testicular function, which could translate into infertility. Here, in contrast to the brain, increased expression of the p53-TIGAR pathway promotes cellular apoptosis in germinal cells (Al-Maghrebi and Renno, 2016).

Autophagy/Mitophagy and apoptosis. TIGAR has been implicated in autophagy through diverse range mechanisms. TIGAR can promote apoptosis by inhibiting the glycolytic pathway (Bensaad et al., 2006). Here, a relationship between reduced levels of ROS and autophagy inhibition has been suggested (Bensaad et al., 2009; Ye et al., 2013).

This implies an opposing effect and highlights the complexity of the role of TIGAR in regulating ROS levels in response to cellular stress involving both apoptotic and autophagy pathways (Bensaad et al., 2009). Increased levels of ROS induce p53, which in turn activates transcription of TIGAR, consequently reducing autophagy within the cytoplasm (Cheung et al., 2012). Resveratrol is an anti-cancer agent that acts by a variety of mechanisms. One of these is via induction of ROS-mediated apoptosis in cancer cells. Resveratrol inhibits TIGAR and, subsequently, autophagy increases in a dose-dependent manner (Hsieh et al., 2015; Kumar et al.,

2015). Moreover, *TIGAR* knockdown induced caspase-3 elevation, apoptosis and enhanced mitochondrial ROS production in mouse brain tissue from a model of ischemia/reperfusion injury (Li et al., 2014). Therefore, neuronal protection against DNA and mitochondrial damage has been suggested to be a result of the metabolic shift from glycolytic pathway to PPP and oxidative stress reduction (Cao et al., 2015; Li et al., 2014). However, in contrast to this, while a protective role through Cdk5-ATM and the PPP pathway has been suggested for TIGAR, there is also evidence for TIGAR-mediated toxicity. In glioblastoma, as mentioned above, cells are sensitised by ROS and therefore, made responsive to radiation therapy. As a consequence, inhibition of TIGAR produces high levels of ROS, which promotes DNA damage and cellular death (Yu et al., 2015).

TIGAR modulates autophagy in a p53-independent manner. Upon metabolic stress and nutrient starvation, TIGAR can reduce autophagy, by reducing ROS levels. TIGAR has been proposed as a target of the mammalian rapamycin complex 1 (mTORC1)-related pathway. (Bensaad et al., 2009; Tai et al., 2015; Ye et al., 2013). This was demonstrated when cells were treated with the mTOR inhibitor Rapamycin. Rapamycin result in TIGAR downregulation in the treated cancer cells. Furthermore, in cancer cells treated with epirubicin, TIGAR knockdown promoted autophagy by inhibiting mTOR and increased ROS production. Here, apoptosis was induced by treatment with epirubicin and inhibited autophagy. These findings suggest a dual function of TIGAR only as a pro-survival molecule but also as a pro-apoptotic mediator (Xie et al., 2014). Furthermore, Resveratrol treatment in cancer cells downregulation of TIGAR expression suggested to be a result of mTOR

inhibition (Kumar et al., 2015). However, TIGAR ROS-independent function in mTOR-mediated autophagy remains to be investigated.

Mitophagy plays a crucial role in mitochondrial homeostasis in myocytes. p53/TIGAR is involved in the Bnip3-mitophagy pathway independent of the PINK1/Parkin Pathway. Increased ROS signalling activate Bnip3 which adopts a homodimer form in order to promote autophagy and cellular death under conditions of severe oxidative stress. (Hoshino et al., 2012).

Early development and regeneration. The effect of TIGAR in development was investigated in a mouse model. It was found that development was not affected when TIGAR was deficient in mice. In contrast, regeneration of adult intestinal epithelium requires TIGAR, particularly after induced damage in rapidly proliferating cell types. A lack of TIGAR in damaged intestinal epithelium results in a failure to regenerate, reduced tumour size and progression, which could also be contributing to tumour progression in cancer cells (Cheung et al., 2013).

Other mechanisms. A number of other p53-independent pathways outside glycolysis and the pentose phosphate shunt have been described. These include a role in the regulation of imprinting of genes in the human placenta, possibly related to the implantation process (Hamada, 2016). Further mechanisms involve the Transforming growth factor β (TGF-β) and human chorionic gonadotropin (hCG), which modulate oxidative stress and homeostasis in glioblastoma, one of the most common malignant brain tumours. Both proteins share a structural homology. In cancer tissues, they regulate cellular survival and oxidative stress. TGF-β treatment causes over expression of hCG-β in glioma cells, while inhibition of hCG-β leads to

ROS production, thioredoxin (Trx1) expression and thioredutase activity depletion, resulting in TIGAR inhibition. Treatment with TGF-β alongside hCG-β inhibited TIGAR expression glioma in treated cells. This has been proposed as a new therapeutic target for glioblastoma and related malignancies (Ahmad et al., 2015).

1.4.3 TIGAR and PD

In a study conducted in a *pink1*-deficient zebrafish model, researchers from our group found that *tigarb* (the zebrafish homologue of *TIGAR*) mRNA was upregulated. This zebrafish *pink1* model, contrary to the PD mice models, displayed PD characteristic phenotype with dopaminergic neuronal as well as mitochondrial dysfunction and impaired morphology. Microarray expression analysis performed in the RNA extracted from the *pink1* model showed a 12-fold up-regulation of of *TigarB* mRNA levels. The *TigarB* upregulation was subsequently confirmed by qPCR. Furthermore, in situ hybridization analysis demonstrated a significant increase of TigarB expression in the brains of the *pink1* mutant zebrafish, which was particularly marked in the brain. Moreover, *Tigarb* knock down in the *pink1* deficient model, using the morpholino antisense-mediated approach normalised mitochondrial function, with normalisation of CI and CIII activity resulting in rescue of the dopaminergic neuronal loss (Flinn et al., 2013). These promising results suggested a new mechanism in PD mediated by TIGAR unknown mechanisms. Since this exciting discovery was performed in a zebrafish model, a confirmation of TIGAR mediated mechanisms in PD needed to be undertaken and investigated in a human cellular model and PD brain tissue.

1.5 Aims and objectives

In this study, we aimed to determine TIGAR related mechanisms in three different models: post-mortem tissue from the brains of people with PD, fibroblasts derived from patients with familial and sporadic PD and, a stable inducible cell line with *TIGAR* and *PINK1* knock-down.

- First, we aimed to identify whether TIGAR is present in human dopaminergic neurons in healthy brains as well as in the brains of patients with PD and DLB using immunohistochemistry. We further investigated whether TIGAR upstream and downstream regulators were associated to TIGAR in this context. TIGAR disease specificity was investigated by assessing TIGAR expression in another synucleinopathy, namely multiple system atrophy (MSA), and a further neurodegenerative disease with ubiquitinated inclusions, namely motor neuron disease (MND).

- Second, we aimed to identify if TIGAR was present in human fibroblasts in controls and patients with PD mutations. We then determined whether TIGAR knockdown can rescue the mitochondrial dysfunction and morphology in parkin-mutant fibroblasts. TIGAR role in autophagy was also investigated in fibroblasts from sporadic PD patients. We further investigated if TIGAR translocates to the mitochondria in the parkin-mutant fibroblasts after toxin exposure.

- Third, we aimed to silence *TIGAR* and *PINK1* via RNAi methods using a microRNAs approach. Then, we generated a stable inducible cell line with *TIGAR* and *PINK1* deficiency. We subsequently assessed the effect of *TIGAR* and *PINK1* knockdown on mitochondrial function and morphology in a stable inducible human cellular model with *TIGAR* and *PINK1* deficiency. Finally, we compared gene

silencing efficacy and efficiency by comparing RNAi conventional methods with newer genome editing techniques, namely CRISPR/Cas9.

1.6 Hypothesis

We hypothesised that there would be an increased expression of TIGAR in the SN of post mortem brains of people with PD. Consequently, TIGAR protein will be present in the Lewy bodies. We also hypothesised that up and down stream regulators and targets of TIGAR would be altered in PD in post-mortem brains of people with PD.

Since fibroblasts from PD patients with known PD-gene mutations display mitochondrial dysfunction, we hypothesised that TIGAR expression will be altered, at the gene and protein level. This will confirm the findings in the zebrafish model. Therefore, TIGAR knockdown will rescue the mitochondrial function in PD fibroblasts with known gene mutations. Moreover, TIGAR related mechanisms will be via TIGAR mitochondrial translocation upon toxic exposure in PD fibroblasts with mitochondrial defect. Another TIGAR related mechanisms will be through autophagy impairment in sporadic PD fibroblasts with mitochondrial defect treated with inducers (CCCP) and inhibitors (Bafilomycin) of autophagy. Further confirmation of TIGAR related mechanisms and its implication in PD, will be through studying *TIGAR* knockdown in a stable inducible human cellular model with *PINK1* deficiency. Here the mitochondrial phenotype and function will be rescued. TIGAR might be involved in the disease by decreasing the glycolytic pathway and the energy supply, by affecting the mitochondrial function and the cellular clearance mechanisms.

2. TIGAR neuropathology

2.1 Introduction

The neuropathological hallmark of Parkinson's disease (PD) is the loss of dopaminergic neurones in the substantia nigra (SN). Another characteristic of the disease is the presence of spherical cytoplasmic inclusions in residual neurones called Lewy bodies.

The histological characteristics of classic Lewy bodies in the SN on haematoxylin and eosin staining are an eosinophilic hyaline core with a pale halo surrounding it. Lewy bodies in the cortex are more pale and lack a halo. (Spillantini et al., 1997). Lewy bodies are composed mainly of neurofilaments and ubiquitylated proteins, of which alpha-synuclein has been recognised as the main component. Immunohistochemistry for alpha-synuclein also reveals neuritic deposits called Lewy neurites as well as more diffuse intracellular aggregates, called pale bodies, that lack the classical morphology of Lewy bodies. To date, there are about 300 molecules that have been identified in Lewy bodies (Leverenz et al., 2007; Wakabayashi et al., 2013) .

2.2 Lewy body diseases

Since Lewy bodies were first discovered, it has been shown that there is a spectrum of diseases that also have these inclusions and related alpha-synuclein pathology. These disorders are now called synucleinopathies. They are PD, dementia with Lewy bodies (DLB), multiple system atrophy (MSA) and Lewy body variant of Alzheimer's Disease (LBAD). For PD and DLB most deposits can be found

in neurons, whereas in MSA they are mainly present in glial cells (Ingelsson, 2016; Miraglia et al., 2015).

2.2.1 Dementia with Lewy bodies (DLB)

DLB is the second most common alpha-synucleinopathy. Clinically, DLB presents predominantly with dementia within one year after the onset of motor symptoms (Irwin et al., 2017). However, when dementia and the movement disorder are present at the same time, it can be very difficult to distinguish between PD and DLB. DLB has considerably more cortical amyloid deposits than PD cases (Gomperts et al., 2008; Irwin et al., 2017).

2.2.2 Multiple system atrophy (MSA)

The pathological hallmark of MSA is the presence of alpha-synuclein positive cytoplasmic inclusions in oligodendroglia (McCann et al., 2014). It is a progressive neurodegenerative disease with complex variety of clinical symptoms, such as parkinsonism, autonomic dysfunction, pyramidal symptoms, and cerebellar ataxia. It is a sporadic disorder, which can be associated with other pathological processes, including Alzheimer-type, Lewy pathology and entities with other pathological tau deposits. Consequently, more than one neuropathological disorder can be present in one patient. A neuropathological consensus criteria for a definite MSA diagnosis have been agreed. These require the presence of widespread and numerous CNS alpha-synuclein positive glial cytoplasmic inclusions, accompanied by pathological changes in the striatonigral or olivopontocerebellar regions (Trojanowski and Revesz, 2007).

2.2.3 Incidental Lewy body disease

Lewy bodies occur in about 10% of normal brain of people older than 65 years old (Gibb and Lees, 1988; Klos et al., 2006). This is called "incidental Lewy body disease" and can be associated to a reduction of the neuronal population in the SN. Further, the nigrostriatal pathology is of intermittent severity between that seen in the population with and without PD. There are suggestions that this could be a preclinical stage of either PD or DLB (Caviness et al., 2011; DelleDonne et al., 2008).

2.2.4 Lewy pathology localisation in the brain

While Lewy bodies are initially confined to the brainstem pigmented nuclei, their appearance tends to progress through the brain in a staged manner. This corresponds loosely to the clinical severity of the patient (Braak et al., 2003; Luk and Lee, 2014). Lewy bodies are found in almost all sporadic and familial PD cases, though there are some exceptions, such as some carriers of *Parkin* mutations (Cornejo-Olivas et al., 2015; Farrer et al., 2001; Gouider-Khouja et al., 2003; Pramstaller et al., 2005; Yamamura et al., 1998), *Pink1* and some with mutations in *LRRK2* (Gaig et al., 2007; Kalia et al., 2015; Luk and Lee, 2014).

2.3 *Lewy bodies and PD-related genes neuropathology*

Lewy bodies contain mainly alpha-synuclein. However, a large number of different molecules have been identified within these inclusions. Some of these are proteins link to PD genes, such as *DJ-1, LRRK2, Parkin* and *PINK1*. Alongside these molecules, other protein constituents of Lewy bodies include are known to have roles in: mitochondrial function, the ubiquitin-proteasome system, aggresome formation and autophagy (Velayati et al., 2010; Wakabayashi et al., 2013).

The genes most commonly associated with familial PD are: *Alpha-synuclein (SNCA),* Leucine Rich Kinase 2 *(LRRK2)*, *PTEN* (phosphatase/tensin homolog on chromosome 10)-induced putative kinase 1 (*PINK1), Parkin* and *DJ-1* (Bonifati, 2014). The *glucocerebrosidase* gene (*GBA1*) encodes a lysosomal enzyme. Homozygous mutations of *GBA1* are responsible for the metabolic disorder known as Gaucher disease (GD). It is now known that heterozygous mutations in this gene are one of the main risk factors for developing PD. *GBA1* mutations have also been associated with DLB and MSA (Gámez-Valero et al., 2016; Mitsui et al., 2015). The neuropathology from people with PD and mutations in *GBA1* is comparable to that of classical, sporadic PD (Aharon-Peretz et al., 2004; Ma et al., 2013; Sidransky et al., 2009). The main neuropathological features of individuals with mutations of these genes, is described in Table 2.1.

Gene	Mutation/substitutions	Neuropathological findings
SNCA	A53T	Severe neuronal loss in SN, LC and Widespread and diffuse LB, LN and thread like depositions, rarely GCI and tangles. Rarely, TDP-43-positive inclusions. Occasionally plaques A53T+S167N *PRKN* polymorphism with AGD, FTLD. (Fujishiro et al., 2013; Hoffman-Zacharska et al., 2013; Markopoulou et al., 2008)
	E46K	Widespread LB pathology(Fujioka et al., 2014; Zarranz et al., 2004)
	A29S	LB pathology(Fujioka et al., 2014)
	G51D	LB and tau pathology, TDP-53 pathology(Fujioka et al., 2014)
	A30P	LB, LN, tau pathology and GCI (Fujioka et al., 2014; Seidel et al., 2010)
	H50Q	LB, LN, tau pathology(Fujioka et al., 2014)
	A18T	NA (Hoffman-Zacharska et al., 2013)
	A29S	LB and LN pathology (Hoffman-Zacharska et al., 2013)
	SNCA locus triplication	Widespread LN, some GCI (Singleton et al., 2003b) and tangles (Fujishiro et al., 2013)
	SNCA locus duplication	LB and tau pathology (Fujioka et al., 2014; Konno et al., 2016)
PINK1	N451S het	Brainstem and neocortical LB in SN and neocortex. Diffuse Aβ deposits (Gandhi, 2006).
	Y431H het	Severe neuronal loss in SN. LB in SN and neocortex. Sparse neuritic plaques (Gandhi, 2006)
	A339T het	Severe neuronal loss in SN. LB in SN and neocortex. Diffuse Aβ deposits (Gandhi, 2006)
	C575R het	Severe neuronal loss in SN. LB in SN and neocortex. Moderate neuritic plaques(Gandhi, 2006).
	c.1488+1G>A+delEx7	Severe neuronal loss in SN. LB in SN, brainstem and nucleus basalis of Meynert (Samaranch et al., 2010)

PARKIN	R275W, del 40 bp Exon3	Neuronal loss in SN, LB in SN, LC, nBM, amygdala parahipocampal region (Farrer et al., 2001),
	Hom del Ex 3	Moderate loss of neurons of SN and LC (Sasaki et al., 2004)
	delExon7, del1072T	Severe neuronal loss in SN and LC, few LB in SN and LC (Mori et al., 2003)
	Compound het Ex7 (C924T)	Neuronal loss in SN. LB in SN, LC and nbM (Schlossmacher et al., 2002)
	Compound het (Ex7del+1072del)	SN, locus ceruleus, VNM and NA: Moderete - severe neuronal loss, reactive gliosis, neuritic dystrophy and LB. (Pramstaller et al., 2005)
	Hom del Ex2+del Ex4	LB and LN in SN and LC, amygloid nucleus, VMN, nbM, striatum, anterior cingulate cortex. Tau positive inclusions in ETC
	Compound het: acceptor splice site mutation (IVS5-1G>A) + Ex7del.	Severe neuronal loss in SN. ETC cortex with NFT and neruritis. Negative alpha-synuclein staining and LB no present.(Cornejo-Olivas et al., 2015; Pramstaller et al., 2005)
	Compound het delEx3/del Ex4	Neuronal loss and presence of LB in SN and LC (Sharp et al., 2013)
	Hom delEX3/del Ex 7	Severe neuronal loss in SN, less in LC. No LB and LN (Kitada et al., 1998)
	Hom delEx4	Severe neuronal loss in SN, less in LC. No LB and LN. Tau inclusions and NFT, thorn shaped astrocytes (Hayashi et al., 2000; Mori et al., 2003)
	Compound het delEx3/Ex6 transversion	Severe neuronal loss in SN > LC. No LB and LN. Thorn shaped astrocytes (van de Warrenburg et al., 2001)
	Comp het delEx6/delEx7	Severe neuronal loss in SN > LC. No LB and LN .(Mori, 2003)
	Hom delEx2	Severe neuronal loss in SN > LC. No LB and LN (Gouider-Khouja et al., 2003)
	Het C212Y	PSP, neuronal loss in SN, striatum, GP, nbM, STN and Thalamus. No LB and LN. (Morales et al., 2002)
	Hom delEx3	Neuronal loss in SN and LC. No LB. Lewy-like inclusions in the anterior horn of the SC, asyn and ubiquitin positive (Sasaki et al., 2008)
LRRK2	G2019S	Severe-moderate neuronal loss in SN, LC and SI, ETC and VMN. LB in SN, LC, SI, amygdala, ETC, VMN, hypothalamus, subthalamus, nbM, CG, medulla, BG, transentorhinal and FC. Tau-positive inclusions, aggregates of TDP-43 protein, ubiquitin-only inclusions as well as only dopaminergic neuronal loss without inclusions. Mild neuronal loss in SN. α-synuclein negaive LB and LN. (Dachsel et al., 2007; Gaig et al., 2007, 2008; Giasson et al., 2006; Gilks et al., 2005; Gomez and Ferrer, 2010; Rajput et al., 2006)
	R1441C	Neuronal loss in SN and degeneration. Diffuse or brainstem LB pathology. Tau positive lesions with PSP-like pathology (Wider et al., 2010; Zimprich et al., 2004)
	Y1699C	Degeneration of SN. Ubiquitin positive inclusions in SN. Neuronal loss in SN and LC (Khan et al., 2005; Zimprich et al., 2004)
	R1441G	Neuronal loss in SN and LC, no LB (Marti-Masso et al., 2009)
	R1441R	Neuronal loss in SN and LC (Craig, 2008)
	I1371V	Neuronal loss in SN and LC (Giordana et al., 2007)
	R793M/L1165P	Neuronal loss in SN and LC (Covy et al., 2009)
	N1437H	Neuronal loss in SN and LC, sparse NFT and Tau pathology (Puschmann et al., 2012)
DJ-1	R98Q polymorphism	LB and LN in SN (Bandopadhyay et al., 2004)
	L172Q	Severe neuronal loss in SN, LC, GP and putamen. Diffuse LB pathology. Axonal a-syn positive spheroids and glial inclusions (Taipa et al., 2016).
GBA	L444P, N370S, R463C, D409H, R131C, C193E,	Neural loss in SN and LC. Diffuse LB pathology (Neumann et al., 2009).

	RecNcil, RecA456P	
	N370S hom; N370S het; L444P/D409H+duplication	Neuronal loss in SN. LB and LN in SN and CA2-4 hippocampus. (Tayebi et al., 2003)
	N370S hom, N370S het, D409H/L444P+duplication	Neuronal loss with/without astrogliosis in SN, CA2-4, calcarine layer 4b and cortical layer 5. LB inclusions in SN and CA2-4. Gb-positive LB hippocampal inclusions. (Goker-Alpan et al., 2010; Wong et al., 2004)
	N188S/E326K, T369M, E326K, N370S, L444P	Widespread extensive neocortical LB, AD-stages, PD or pure DLB (Gámez-Valero et al., 2016).

Table 2.1 Neuropathology findings in post-mortem brains with PD-related mutations. Amyloid-beta peptide (Aβ), Alzheimer's Disease (AD); Agyrophilic disease (AGD); alpha-synuclein (asyn); Dementia of Lewy bodies (DLB); Progressive supranuclear palsy (PSP); Frontotemporal lobar degeneration (FTLD); cingulate gyrus (CG); globus palidus (GP); sustantia nigra (SN); locus ceruleus (LC); entorhinal cortex (ETC); subthalamic nucleus (STN); glial cytoplasmic inclusions (GCI); Lewy bodies (LB); Lewy neurites (LN); motor nucleus of the vagus (VMN); basal nucleus of Meynert (nbM); nucleus ambiguous (NA); sustantia innominata (SI); neurofibrillary tangles (NFT); heterozygous (het), homozygous (hom); deletion (del); exon (Ex).

2.4 Lewy bodies and PD-related proteins

More recently, one proteomic study has identified over 300 proteins in cortical Lewy bodies, some which had been previously described. The total number of molecules that constitute the Lewy bodies is not established and continues growing. Functional classification of these proteins showed enrichment of the following processes: apoptosis (34%), cytoskeleton (19%) metabolism (14%), extracellular matrix (10%), protein synthesis and degradation (8%), neurotransmission (2%), immune and inflammation (2%) and unknown function (11%). Fully validation of these processes through functional analysis is yet to be done (Leverenz et al., 2007).

Alpha-synuclein is the main component of the pathological inclusions found in PD and related disorders. It is normally contained in the cytosol and presynaptic terminals of the neurons and its physiological function remains unclear (De Franceschi et al., 2017). The common pathological aggregation of alpha-synuclein in these neurodegenerative disorders classifies them as a group known as "synucleinopathies" (Iwai et al., 1995; Jellinger, 2003). The exact mechanisms leading to toxicity and pathology in PD and other alpha-synucleinopathies remain

elusive. One hypothesis is that different alpha-synuclein isoforms might lead to neuroinflammation and neurotoxicity by affecting the protein-protein interactions and axonal transport (Nakata et al., 2012; Sekigawa et al., 2015). This process has been also suggested to occur alongside the expression different isoforms of parkin and synphilin-1, which might result in impaired substrate degradation, protein aggregation and clearance (Brudek et al., 2016a; Lonskaya et al., 2013a, 2013b).

PD, DLB and MSA have in common pathological lesions containing alpha-synuclein. These lesions tend to affect specific vulnerable brain areas, resulting in common clinical manifestations features. Therefore, the alpha-synucleinopathies are suggested to be part of a single clinicopathological disorder (Galvin et al., 1999; Jellinger et al., 2003; Yang and Yu, 2017). A large number of proteins have been found in the pathological inclusions from patients with these disorders. Some have been suggested to have a functional, cellular and/or structural relation with alpha-synuclein: LRRK2 (Qing et al., 2009; Volpicelli-Daley et al., 2016), Pink1 (Chung et al., 2016), synphilin-1 (Engelender et al., 1999; Xie et al., 2010) and Parkin (Chung et al., 2016; Lonskaya et al., 2013a; Schlossmacher et al., 2002). Thus, all appear to share a common pathologic pathway.

2.4.1 PINK1 neuropathology

PINK1 protein is expressed in the human brain in all cell types mainly in the mitochondrial membrane. PINK1 has been found in post-mortem tissue from people with sporadic PD, DLB and MSA (Murakami et al., 2007), and with familial PD associated to *PINK1* heterozygous mutations (Gandhi, 2006). PINK1 expression was found in neurons (cytoplasm and axonal processes), glial cells (nuclei surrounding rim), endothelial and smooth muscle cells of blood vessels within the SN. PINK1 was

not found in *cortical* Lewy bodies, Lewy Neurites or other alpha-synuclein or tau positive inclusions. In contrast, it was found in a small percentage (5-19%) of Lewy bodies in the brainstem and SN within the halo and in a small proportion in the core of the inclusion. This difference between cortical and brainstem Lewy bodies could be explained by the fact that the antibody used for this study recognises only a portion of the protein, the insoluble fraction. This might reflect the solubility of PINK1 might affect the detection. Given that there are morphological differences between cortical and brainstem Lewy bodies, this could also reflect different protein contents (Gandhi, 2006).

More recent research by Murakami et al. (2007) in contrast, found PINK1 to be present in relatively high levels in neurons within the SN. This work used a more sensitive antibody that fully recognises the full length and whole fraction (soluble and insoluble) of PINK1. This study was also able to show that PINK1 is present in Lewy bodies, neurites and glial cytoplasmic inclusions in the SN. Furthermore, PINK1 was found in the glial cytoplasmic inclusions of patients with MSA. This suggests a role in the development of pathogenic inclusions of both principal alpha-synucleinopathies. How PINK1 could be contributing to the pathological progression remains unclear. One suggestion is that PINK1 aggregates in inclusions after it becomes misfolded and insoluble. Altered PINK1 activity due to misfolding and altered solubility, could also lead to protein aggregation alongside its substrates into the inclusions. This raises the question of whether PINK1 and alpha-synuclein may act in the same pathological pathway and is the subject of further research (Murakami et al., 2007).

2.4.2 Parkin neuropathology

Parkin is expressed in neurones in the human brain under physiological conditions, in the same cytosolic and synaptic terminal compartments as alpha-synuclein (Schlossmacher et al., 2002). It also was found to be expressed in the autophagic vacuoles in the cytoplasm within the astrocytes (Lonskaya et al., 2013b). In the brain of patients with PD, an insoluble form of Parkin accumulates vacuoles in the striatum (caudate nucleus). Parkin has been found to co-localise with Beclin-1, an autophagy-related enzyme, in the SN of the normal human brain. In PD patient brains, the interaction between Parkin and Beclin-1 appears to be significantly reduced. Here, Parkin mutations might affect structural formation, which could lead to protein insolubility and affect Parkin enzymatic and protein interactions (Lonskaya et al., 2013a, 2013b). This suggests a prospective role of Parkin in the neuronal clearance and autophagy through the autophagosomes.

Parkin protein has been identified in the core of Lewy bodies in the SN, entorhinal, brainstem and cingulate cortex in brains from patients with PD and DLB, where Parkin and alpha-synuclein co-localise (Schlossmacher et al., 2002; Wakabayashi et al., 2012). This has lead researchers to suggest a role of Parkin in the initiation of Lewy body development. However, the mechanisms leading to this process still remain unclear and not fully confirmed (Schlossmacher et al., 2002).

2.4.3 LRRK2 neuropathology

In the normal brain, LRRK2 is ubiquitously expressed in neurons especially in the cerebral cortex, in striatum and SN (Higashi et al., 2007). However, it has been found to be expressed in most brain regions and a diversity of cell types (astrocytes and microglia), with a moderate expression in the SN (Miklossy et al., 2006; Vitte et

al., 2010). It was found that LRRK2 expression in surviving neurons within the SN was extremely decreased in post-mortem brains from people with sporadic and familial PD with *LRRK2* mutations (Higashi et al., 2007; Vitte et al., 2010). There are discrepancies between LRRK2 expression in Lewy bodies. LRRK2 presence is controversial; where it is present sometimes in Lewy bodies (but not Lewy neurites), in the halo and core in the cortex, SN and Locus coeruleus; absent in cortical Lewy bodies in PD and DLB brains (Higashi et al., 2007; Miklossy et al., 2006; Vitte et al., 2010). This was more pronounced in brains from PD patients with *LRRK2* mutations (Vitte et al., 2010).

Patients with the G2019S mutation of *LRRK2* have significantly higher levels, compared to sporadic PD patients, of phosphorylated alpha-synuclein at serine 129 (pS129). This difference is principally seen in the dorsal motor nucleus of the vagus. Moreover, alpha-synuclein solubility in G2019S patients was found to be altered in the Basal Ganglia and limbic cortex (Mamais et al., 2013).

Increased levels of LRRK2 directly correlate with increases in total and phosphorylated alpha-synuclein levels in the brains of PD patients. Furthermore, LRRK2 protein was found to co-localise with total and phosphorylated alpha-synuclein in Lewy Bodies and neurons. This co-localisation occurred mainly in the cortical regions and in a lesser extent in the brainstem (Guerreiro et al., 2013). How LRRK2 interaction with alpha-synuclein leads to pathology remains unclear.

2.4.4 DJ-1 neuropathology

DJ-1 is expressed in numerous tissues, including the brain and is localised in both the nucleus and the cytoplasm. It is highly expressed in the glia, mainly in

astrocytes. It has been found at very low levels if at all in neurons of the frontal cortex and SN. It is occasionally present in the halo of Lewy bodies and rarely in Lewy neurites within the SN and absent in the Lewy bodies within the frontal cortex (Bandopadhyay et al., 2004; Taipa et al., 2016).

2.5 TIGAR neuropathology

TIGAR (TP53-induced glycolysis and apoptosis regulator) has been widely studied in oncology (Lee et al., 2014a), but very little is known about its role in neurodegeneration. It has been suggested that TIGAR is involved in AD (Katsel et al., 2013): TIGAR protein levels were significantly reduced in patients with severe dementia with greater levels of cognitive impairment. However, TIGAR protein levels were not found to be related to conventional Braak neuropathology stage or neuritic plaque density measurements. Therefore, they suggest that the main role of TIGAR here is mainly in the neurobiology of AD and the cognitive impairment. Furthermore, in severe dementia and AD neuropathology, ATM (Ataxia-Telangiectasia mutated) expression was found to be increased along with some of its downstream genes. This, suggests that the regulation of TIGAR might involve the ATM-p53 pathway, which responds to stress and damage (see Introduction). TIGAR protein functions to provide cellular protection from ROS and to improve cell survival. Consequently, low levels of TIGAR hinders these mechanisms and leads to cell death. Interestingly, p53 protein levels did not differ between controls and patients, suggesting that post translational mechanisms that modify the action of p53, and as result TIGAR levels, are involved. This suggests that ATM up-regulation and TIGAR down regulation might be characteristic of the development and progression of dementia in AD (Katsel et al., 2013).

In a study conducted in a *pink1*-deficient zebrafish model, researchers from our group found that *tigarb* (the zebrafish homologue of *TIGAR*) mRNA was overexpressed compared to controls. This was associated with the loss of dopaminergic neurones and mitochondrial dysfunction. Furthermore, *TigarB* knock down normalised mitochondrial function and rescued the dopaminergic neuronal loss (Flinn et al., 2013). Both mitochondrial dysfunction and neuronal loss have been reported in tissue from patients with PD (Abramov et al., 2011; Ando et al., 2017; Chung et al., 2016; Gandhi, 2006; Manzoni et al., 2013a; Murakami et al., 2007; Rakovic et al., 2010, 2013; Schapira et al., 1989), as well as cellular models and *in vivo* models that are PINK1 deficient (Anichtchik et al., 2008; Flinn et al., 2013; Sallinen et al., 2010).

Several lines of investigation have suggested further PINK1- and TIGAR-related cellular mechanisms, including oxidative stress and mitophagy may be involved in PD pathogenesis. However, to our knowledge, there are no reported publications showing the involvement of TIGAR in human PD pathology. Therefore, we aimed to identify whether TIGAR is present in human dopaminergic neurons in controls as well as patients with PD and DLB using immunohistochemistry. Unpublished pilot data from our laboratory suggested that TIGAR protein may be present in Lewy bodies: Immunohistochemistry for TIGAR appeared to be positive in Lewy bodies when using an antibody to the C-terminus (Abcam ab129333) but not when using an antibody to the central portion of the protein (Millipore #AB10545). This may have been due to aberrant cross reactivity by the first antibody, or the fact that there is only antigen availability of the C terminus region in Lewy bodies.

2.6 Aims and objectives

The discovery of TIGAR up regulation in the *Pink1*-deficient zebrafish model of Parkinson's disease suggested a role for TIGAR in PD pathogenesis. Therefore, we aimed to determine:

a) If TIGAR is present in the human SN and,

b) Whether TIGAR protein is indeed present in Lewy bodies

c) Elucidate the relationship between TIGAR protein levels and PD.

To assess this, we used immunohistochemistry to examine the expression levels and localization of TIGAR protein in the post mortem brains from people with PD, DLB, MSA and controls. While we concentrated on the SN, we also studied the hippocampus, a forebrain region that is also affected by alpha-synuclein pathology. On finding TIGAR in Lewy bodies, we studied motor neuron disease (MND), another disease with ubiquitylated proteinaceous inclusions, to investigate whether TIGAR was specific for Lewy bodies or could be seen in other conditions with proteinaceous inclusions.

2.7 Hypothesis:

We hypothesised that there would be:

- An overexpression of TIGAR in the SN of post-mortem brains of people with PD.

- TIGAR protein in Lewy bodies detectable using antisera to the C-terminal region of the protein.

- Altered expression of regulators, such as p53 and HK-II, and targets of TIGAR in PD.

2.8   Materials and methods

2.8.1   Human brain tissue

2.8.1.1   Patients and controls

Sheffield Brain Bank

Post mortem human brain tissue was obtained from people who donated their brains, after obtaining permission from the next of kin. The acquisition of the brain tissue by the Sheffield Brain Tissue Bank (SBTB) was performed with ethics committee approval by the Scotland A Research Ethics Committee (ref 08/MRE00/103). Details of the cases are given in Table 2.2 below.

ID	Gender	Diagnosis	Age at death (y)	Duration of Disease	Cause of death	PMD
LP0079/06	M	DLB	78	N/A	Intraventricular haemorrhage	N/A
LP112/06	M	DLB	86	N/A	N/A	N/A
LP003/04	F	DLB	66	N/A	N/A	N/A
LP016/05	M	DLB	72	2y	Broncopneumonia	N/A
LP097/09	F	sPD	84	N/A	N/A	N/A
LP052/09	M	sPD	76	N/A	N/A	N/A
LP015/03	F	sPD	74	3 m	N/A	>100 hrs
LP087/03	M	sPD	71	9 y	N/A	N/A
LP073/09	M	MSA	69	3 y	N/A	34 hrs
LP120/04	F	MSA	63	N/A	Broncopneumonia	N/A
LP129/01	M	MSA	62	N/A	N/A	N/A
LP014/11	M	sMND	51	2.3 y	N/A	N/A
LP059/09	F	sMND	80	8.6 y	N/A	50 hrs
LP072/05	M	sMND	66	10 m	N/A	8 hrs
LP094/06	M	sMND	71	9 m	N/A	53 hrs
R1208/90	M	sMND	48	13 m	N/A	8hrs
LP085/07	F	Control	59	-	Atypical pneumonia	5hrs
LP005/07	M	Control	63	-	N/A	N/A
LP098/07	M	Control	67	-	Hepatocellular carcinoma	60 hrs
NA188/96	F	Control	82	-	N/A	N/A
LP056/90	M	Control	51	-	Mesothelioma	25 hrs
LP309/90	M	Control	82	-	Carcinomatosis, thoracic cord compresion	36 hrs
LP335/90	F	Control	29	-	Acute intermittent porfiria	20 hrs

Table 2.2. Sheffield Brain Bank Tissue used in this study. Female (F); male (M); sporadic Motor neuron disease (MND); Multiple system atrophy (MSA); sporadic Parkinson´s Disease (sPD); Dementia of Lewy Bodies (DLB); Post mortem delay (PMD); Not available (N/A); months (m), years (y).

Tissue acquired within the Ethics committee approval Tissue Bank, Queen Square Brain Bank for Neurological Disorders (QSBB) and NeuroResource REC Ref. 08/H0718/54+5. Details of the cases are given in Table 2.3 below.

ID	Gender	Diagnosis	Age (years)	Duration of disease	Cause of death	PMD (hrs)
P2/10	F	sPD	82	25y	Chest infection	56
P54/11	M	sPD	80	16y	Pneumonia	67.30
P89/10	M	sPD	77	16y	Ischaemic heart disease	42.55
P21/12	M	sPD	83	6y	Heart failure	44.55
P33/12	M	sPD	74	13y	Pneumonia	43.10
P22/12	M	sPD	85	10y	Urinary tract infection	32.45
P11/11	M	DLB	60	8y	Pneumonia	26
P34/07	M	DLB	80	10y	Gradual deterioration	45.10
P28/11	F	DLB	86	17y	Chest infection	78.40
P68/10	M	DLB	73	12y	Chest infection	42.30
P48/03	F	DLB	74	5y	DLB	47.45
P80/10	M	DLB	67	7y	DLB	40.55
P72/07	M	Control	85	-	Multiple system failure	76.50
P47/11	F	Control	79	-	Pancreatic carcinoma	78.50
P75/10	F	Control	83	-	Squamous cell carcinoma	39.45
P64/11	F	Control	80	-	Pancreatic carcinoma	49.10
P82/10	F	Control	87	-	Colon carcinoma	84.15
P78/06	F	Control	68	-	Breast carcinoma	44.55

Table 2.3. Queen Square Brain Bank Tissue used in this study. Female (F); male (M); sporadic Parkinson´s Disease (sPD); Dementia of Lewy Bodies (DLB); Post mortem delay (PMD); Not available (N/A); years (y).

2.8.2   Immunohistochemistry

Immunohistochemical analysis was performed on paraffin-embedded tissue from midbrain, hippocampal sections of four cases of sporadic PD, four DLB and four matched control cases from the SBTB. Midbrain sections of six sporadic PD, six DLB and six matched controls cases from the QSBB were also analysed. Spinal cord sections from four MND patients and four controls were also analysed.

Paraffin embedded sections of SN, hippocampus and spinal cord tissue were used for antibody optimisation. Heat-mediated antigen retrieval of sections was carried out using a pressure cooker. Antigen retrieval was performed in either Access Citrate (pH6) buffer solution or Access Super (pH8) buffer solution (IntelliPATH FLX Detection Kit, Menarini Diagnostics) 20psi for 40s. at 120°C. Following antigen retrieval, sections were washed with distilled water and Tris-Buffered saline (TBS) and incubated for 5 min. with MenaPath Peroxidase Block (IntelliPATH FLX Detection Kit, Menarini Diagnostics) to prevent all endogenous peroxidase activity. Afterwards, sections were incubated with MenaPath Casein Background Blocker (IntelliPATH FLX Detection Kit, Menarini Diagnostics) for 10 min. and rinsed with TBS. Sections were then incubated with primary antibody for 1 hr. at RT. Following primary antibody incubation, sections were incubated with Universal Probe (IntelliPATH FLX Detection Kit, Menarini Diagnostics) for 10 min., washed again and incubated with HRP-Polymer (IntelliPATH FLX Detection Kit, Menarini Diagnostics) for 15 min. Sections were washed again with TBS and incubated with DAB chromogen for 5 min. The slides were then rinsed in deionized water and counter stained with haematoxylin. Sections were dehydrated through increased concentrations of ethanol (70%, 95%, 100%), cleared in xylene and mounted with Dibutyl Phthalate and Xylene (DPX) mountant (Leica).

2.8.3 Antibody optimisation

We first attempted to replicate the pilot finding using the antibody recognising the C- terminal region of TIGAR. The first aim was to find the best antibody to label TIGAR and optimise it to investigate TIGAR protein in the midbrain region. Optimisation of the antibody was initially performed in SN, using different concentrations of primary antibody (ranging from 1:50 to 1:1000) with antigen

61

retrieval by using a Pressure cooker at pH9 and pH6. A pathologist assessed staining and helped to identify the optimal antibody condition for our area of interest. From this, rabbit antibody against TIGAR (Thermo Scientific) at a concentration of 1:400 and a pH 9 was chosen as the best conditions to assess TIGAR presence in midbrain sections from the PD and DLB cases and controls.

Antibody	Region	Antigen retrieval	Dilution/time
Anti-TIGAR antibody. Millipore (AB10545) Polyclonal (R)	KLH-conjugated linear peptide that lies in the central region of the protein	PC, pH9	1:400 / 30 min
Anti-TIGAR antibody. ABCAM (ab62533) Polyclonal (R)	Synthetic peptide (Human) of 19 amino acids from a region near the centre of TIGAR	PC, pH9	1:800 / 30 min
Anti-TIGAR antibody. ABCAM (ab129333) Polyclonal (R)	Synthetic peptide corresponding to a region within C terminal amino acids 220-270 of Human TIGAR	PC, pH9	1:750/ 30 min
TIGAR Polyclonal antibody Thermo Scientific (PA5-29152) Polyclonal (R)		PC, pH9	1:400 / 1 hr
Anti-TIGAR Antibody LS-C286858 (LifeSpan Biosciences) Polyclonal (R)		PC, pH6	1:50 / 1 hr
Anti alpha-synuclein antibody (NCL-L-ASYN) Molyclonal (M)	Prokaryotic recombinant protein corresponding to the majority of the full length alpha-synuclein molecule	PC, pH9*	1:1000 / 1hr
Anti-HK-I [4D7]. ABCAM (ab105213) Molyclonal (M)	Recombinant full length protein, corresponding to amino acids 1-917.	PC, pH9	1:2000 / 1 hr
Anti-HK-II. Thermo Fisher (MA5-14849) Molyclonal (R)	Synthetic peptide corresponding to the sequence of human HK-II	PC, pH6	1:50 / 1 hr
Anti-p53 (Bp53-12) sc-263 Molyclonal (M)	Antibody raised against recombinant p53 of human origin, with epitope mapping to the N-terminus part	PC, pH8	1:200 / 1 hr
Anti-p53 Dako GA616 Molyclonal (M)	Recombinant human wild-type p53 protein.	High pH Target Retrieval Solution	NA+ / 20 min

Table 2.4 Antibodies tested and optimised for immunohistochemistry in Human brain tissue. Hexokinase I (HK-I); Hexokinase II (HK-II); Mouse (M), Rabbit (R); Monoclonal (Mono); Polyclonal (Poly); Non applicable (NA) Pressure cooker (PC). * Pre-treatment for 1 hr with formic acid followed by antigen retrieval. +Anti-p53 antibody Ready to Use (prediluted).

2.8.4   Co-localisation with alpha-synuclein

2.8.4.1   Double staining: Immunofluorescence
Fluorescent immunostaining against TIGAR in the midbrain was optimised to allow double staining to investigate colocalisation with alpha-synuclein. Paraffin embedded sections were dewaxed in two washes with xylene, followed by

rehydration, starting with two washes with absolute ethanol, then 95% and 70% serially each for 5 min. The tissue was then incubated for 20 minutes in 3% H_2O_2 in fresh methanol. Sections were washed with running tap water. Heat-mediated antigen retrieval of sections was carried out using a Pressure cooker in pH8 buffer solution (IntelliPATH FLX Detection Kit) for 40 minutes at 120°C. Following antigen retrieval, sections were washed with distilled water and Tris-Buffered saline (TBS). Subsequently, they were incubated for 15 min in 0.2% glycine and washed three times with TBS for 5 min each. The sections were then incubated with rabbit (TIGAR) or mouse (alpha-synuclein) blocking serum for 30 min. The excess was removed after the 30 min. Sections were then incubated with avidin block for 15 min. and rinsed with TBS, then incubated for further 15 min with biotin block and rinsed with TBS. They were incubated with primary antibody overnight at 4ºC. After incubation, the slides were rinsed three times with TBS for 5 min each and then incubated with secondary biotinylated antibody for 30 min. Slides were then rinsed with TBS and incubated with secondary fluorescent antibody Alexa Fluor 488 or 555 for 1 hr. at RT in the dark. Then slides were rinsed with TBS and incubated in Sudan Black (filtered, 0.3% sudan black/ 70% alcohol) for 5 min. Slides were then washed with tap water and stained with Hoeschst (1:1000) for 10 min and mounted with DPX mountant.

2.8.4.2   Double staining: DAB immunofluorescence

Double staining with DAB and immunofluorescence was combined. Firstly, all slides were processed for DAB staining as described above, counterstaining with haematoxylin and washed for 5 min in Scott's Tap Water. After this, slides were incubated with the appropriate goat serum blocking buffer for 30 min and then thoroughly washed and sequentially incubated with avidin and biotin block for 15 min each. This was followed by three washes with TBS buffer and incubated with primary antibody (TIGAR or alpha-synuclein) at 4º C overnight. After this time, slides were

thoroughly washed with TBS and incubated with secondary antibody at RT for 30 min, followed by three washes with TBS. Then, slides were incubated in the dark with secondary fluorescent antibody Alexa Fluor 488 or 555 (1:1000) at RT for 1 hr. Slides were then washed three times with TBS and incubated with Hoeschst (1:1000) for 10 min. Finally, slides were rinsed with TBS and mounted with DPX mountant.

2.8.4.3   Serial sections: DAB staining

Co-localisation of TIGAR with alpha-synuclein was also assessed in four PD cases from the Sheffield cohort. This was performed by cutting serial sections from the midbrain. Staining was performed alternatively for TIGAR (1:400) and alpha-synuclein (1:1000). Slides were stained using the IntelliPATH FLX™ Automated Slide Stainer. The IntelliPATH FLX Detection Kit was used for detection. DAB was used for detection and sections counterstained with haematoxylin.

2.8.5   p53 Immunohistochemistry

Midbrains from the four PD and four control cases from the Sheffield cohort were immunostained with anti-p53 (Bp53-12) sc-263. However, due to heavy neuromelanin cross-reactivity with this antibody, an alternative method for immunohistochemistry was sought. We are grateful to Mrs Helen Crowle of the Department of Cellular Pathology, Hull and East Yorkshire NHS Trust for performing the immunohistochemistry for p53.

Briefly, the slides were stained on the Dako Omnis Automated Slide Stainer using the Dako Envision Flex High pH (GV80011) kit. Target retrieval was performed by using a high pH Target Retrieval Solution for 30 mins. The p53 is a ready-to-use antibody (Dako GA616) and incubation time was 20 mins. Peroxide blocking was

done for 3 mins, in secondary labelled polymer for 20 mins and substrate chromogen for 5 mins.

2.8.6   Hexokinase I and II immunohistochemistry

For HKI and HKII study we stained the four PD midbrain cases and four midbrain controls slides from the Sheffield Brain Tissue Bank with Anti-HKI (1:2000) and Anti-HKII (1:50). All were stained with a Menarini IntelliPATH automated slide stainer using the IntelliPATH FLX Detection Kit. DAB was used for detection and haematoxylin was the counterstain.

2.8.7   Image aquisition

Whole slide images were captured using a Hamamatsu NanoZoomer XR.

2.8.8   Quantitative histopathology evaluation

The neuronal and neuritic load of TIGAR labelling was assessed separately. For the neuronal load, the digitised whole slide images were scrutinised by two pathologists. The total number of neurones that were positive and negative for TIGAR were counted and the percentage of neurones that were positive were calculated.

To quantify neuritic pathology, regions of interest were captured from the whole slide images at 20x magnification (405 x 721µm). Six regions of interest per case were randomly selected by a pathologist from the SN, entorhinal cortex and cortex of the occipitotemporal gyrus. Intensely stained neurites were counted by two observers who were blind to case identity and diagnosisand the mean count per case calculated.

HK-I was quantified using image analysis. A total of 6 fields per case were captured from the SN at 40x objective and were analysed with Image J. Each field was divided into 100 equal squares and subjected to colour deconvolution to separate DAB staining (brown) from haematoxylin staining (blue; Figure 2.1 b). The Shanbhag threshold (Shanbhag, 1994) was applied to the DAB-only images. Then, the stained area fraction was measured in the pictures submitted to the threshold (Figure 2.1 c). The percentage of each image that was positive for DAB staining was assessed. The mean of the 10 values across the 6 fields was calculated for each case and used in the statistical analysis for each case.
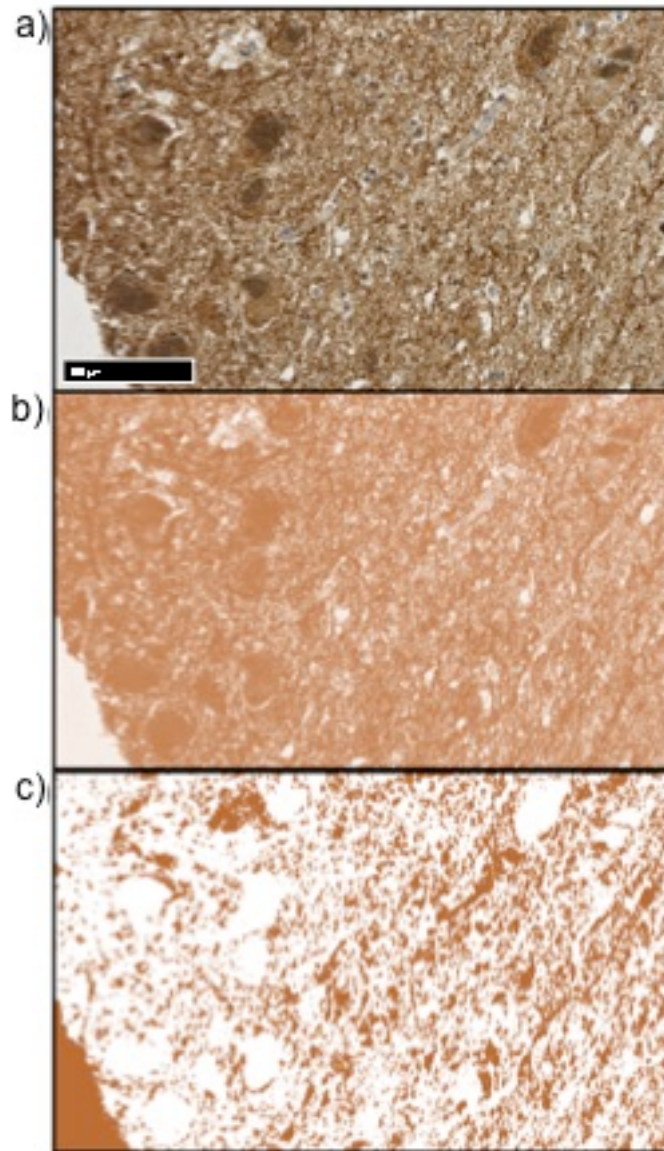
Figure 2.1. Image processing method for quantification of HK-I and TIGAR. Representative images showing original picture (a) processed with ImageJ. ImageJ color deconvolution plug-in was used to obtain the DAB-only images (b). a Shanbhag threshold was applied to the DAB only images, after which unlabelled areas appear in brown (not quantified) and labelled areas appear in white (quantified). Scale bar 100μm.

2.8.9 Statistical analysis

Statistical analysis used for TIGAR included t-Test, Kolmogorov-Smirnov test, Mann U-Withney and Levene's test on Microsoft Excel and SPSS (IBM).

2.9   Results

2.9.1   TIGAR immunohistochemistry in Sustantia nigra

2.9.1.1   Antibody optimistation

Antibodies that recognise the central or near the central region of TIGAR protein.

Every run included positive and negative controls, as well as an isotype control that matched the species and the concentration of the antibody. The positive showed positive labelling, whereas any signal was detected with the negative and isotype controls. *Anti-TIGAR antibody (ab62533)* (Figure 2.2a, b) and *anti-TIGAR antibody (ab10545)* (Figure 2.2c, d) showed some cytoplasmic neuronal labelling, but with significant cross-reactivity to neuromelanin (Figure 2.2). There was significant background staining with minimal differentiation between cell and tissue types. There was no difference between one PD case (Figure 2.2 b-d) and the two controls (Figure 2.2a-c) and no labelling of Lewy bodies (Figure 2.2d).
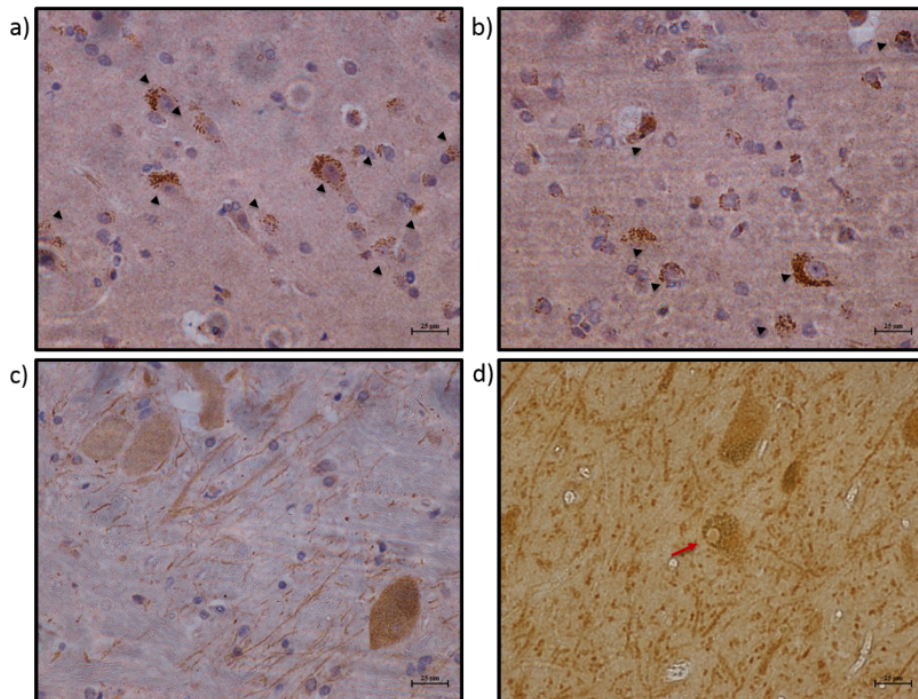
Figure 2.2 Antibodies central or near central region of the protein. Representative images of TIGAR staining in SN. Anti-TIGAR ab62533 one control (a) and one patient (b) and ab10545 in one control (c) and one patient (d). Images Showed no difference between controls and patients, granular staining (dark arrow heads) and negative Lewy bodies (red arrow). Bar 50μm

Consequently, these antibodies were not used for further experiments due to the lack of clear immunostaining of TIGAR and poor quality of the stained samples. These antibodies were directed against the central portion of the protein, in contrast to the antibody used in pilot work, which was directed against the C-terminal region. Therefore, we turned to other antibodies that recognised this a specific portion of the protein.

2.9.2 Antibodies that recognise the C-terminal region of TIGAR protein

*Anti-TIGAR antibodies ab129333 (*Figure 2.3 *a, d), LS-C286858* (Figure 2.3 b, e) *and PA5-29152* (Figure 2.3 c, f)*.* Trial staining on SN showed a positive neuronal labelling, in the cytoplasm and nuclei, as well as a strong labelling of some neurites. The three antibodies that label the C-terminus showed positive staining for TIGAR in the SN from the controls group.

Positive Lewy body staining was confirmed with three different antibodies to the C-terminus. This immunolabelling was interpreted as verification that TIGAR is genuinely present in Lewy bodies (Figure 2.3 a-c) and not a result of an artefactual cross-reaction of the antibody. There was good quality with minimal background staining with lower neuromelanin staining the *PA5-29152* antibody (Figure 2.3 c, f). This antibody showed homogenous results across all the samples and avoid non-specific staining, by reducing the concentration of the antibody. Thus, PA5-29152 antibody was chosen for further experiments.
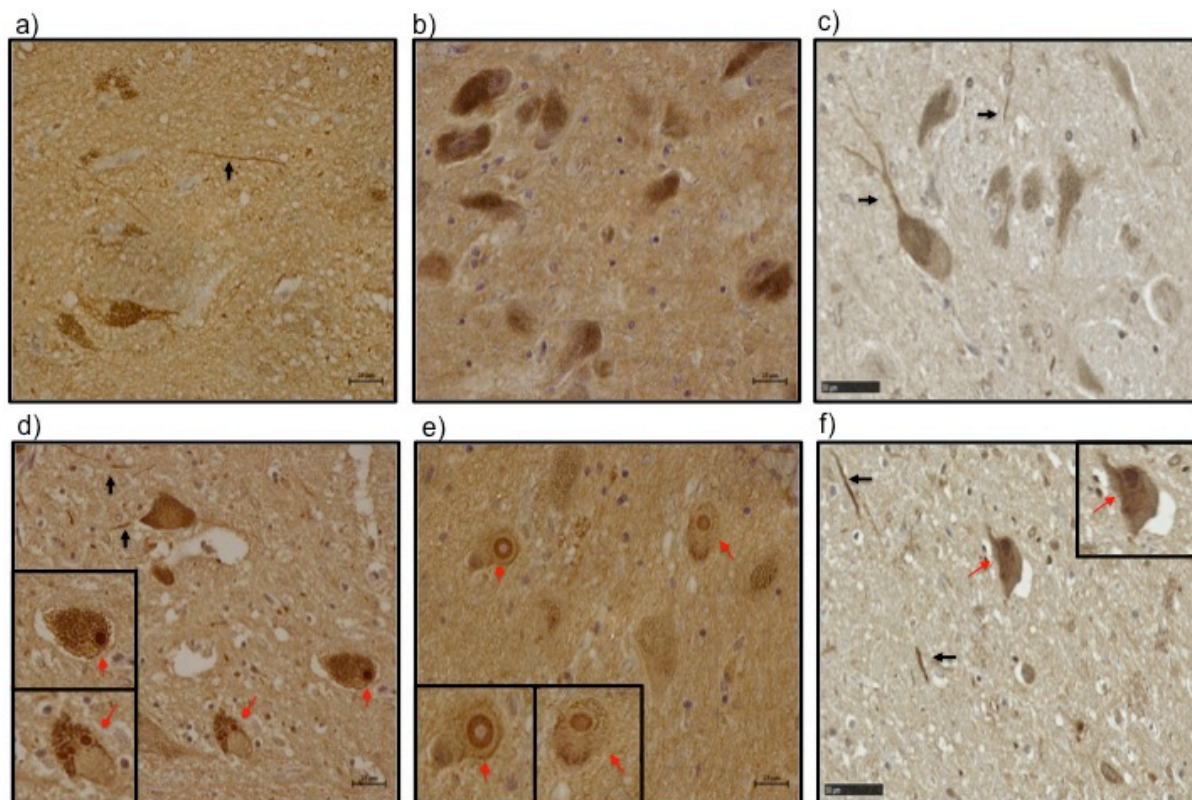
Figure 2.3. Antibodies that recognise the C-terminal region of the protein. Representative images of TIGAR staining in SN. Representative images of the controls (a-c) and patients (d-f) stained with Anti-TIGAR antibody *LS-C286858* (control-a and patient -d); *ab129333* (*control-b* and *patient-e*) and Thermo Scientific *PA5-29152* (*control-c* and *patient-f*). There was positive TIGAR labelling in the Lewy bodies (red arrow) in the PD cases (a-c) with some neurite staining (black arrow) in controls (a and c) and patients (d and f). Bar 50μm.

2.9.3   TIGAR expression in the SN

2.9.3.1   TIGAR immunohistochemistry in SN: Sheffield Brain bank cohort

Neurons from controls and patients showed variable levels of cytoplasmic labelling: some had pale staining, while others had stronger cytoplasmic labelling (Figure 2.4). TIGAR-positive neurites were also seen in the SN from controls and patients. TIGAR was present in the Lewy bodies in both PD (Figure 2.4 b) and DLB cases (Figure 2.4 c). No Lewy bodies were found in the control group (Figure 2.4 a).

As noted above, TIGAR expression was seen in Lewy bodies of PD and DLB cases.
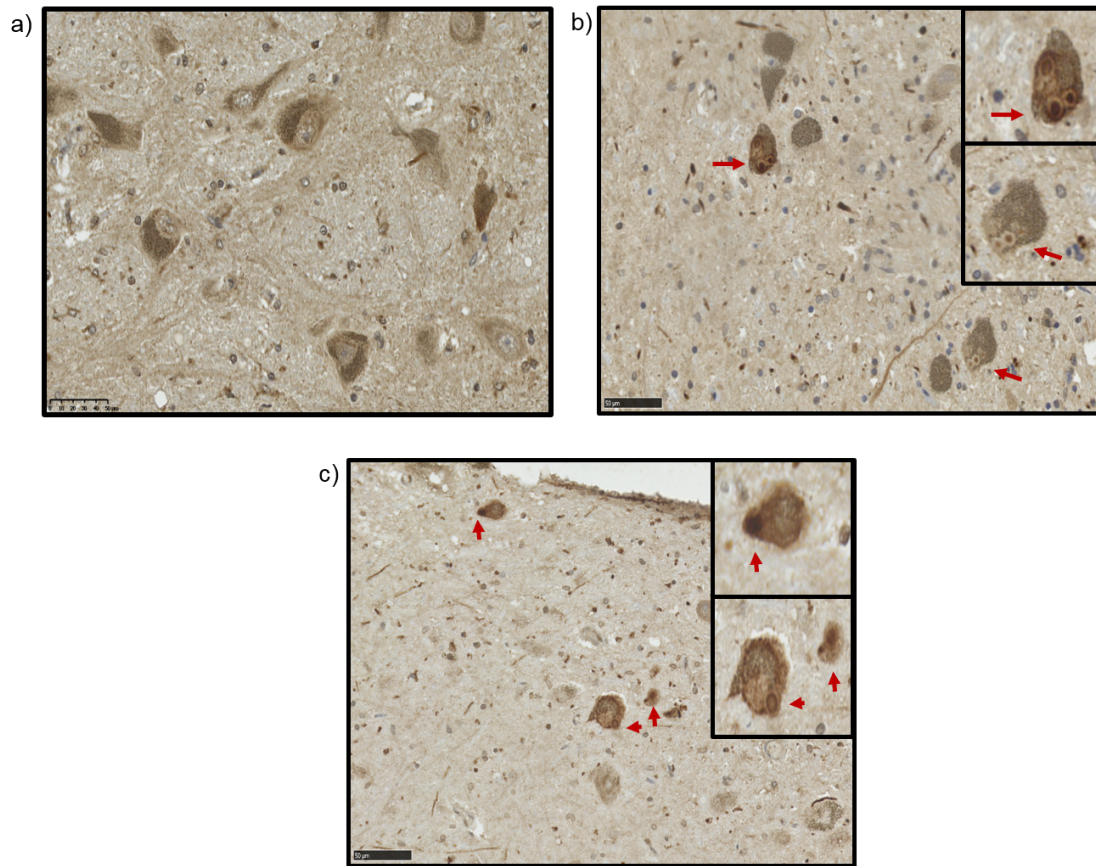
Figure 2.4. Pathological features in the Sustantia Nigra. Representative pictures of TIGAR-positive Lewy Bodies (red arrows) in PD (b) and DLB (c) cases. Lewy bodies are absent in the controls (a). Bar 50µm.

2.9.4   Double staining immunohistochemistry

2.9.4.1   Double staining immunohistochemistry

TIGAR fluorescence

Firstly, the stained fluorescent slides were analysed to confirm that the antibody worked for fluorescent detection of TIGAR. Neuronal bodies, neurites and cytoplasmic inclusions in the PD and DLB cases were present and positive (Figure 2.5).
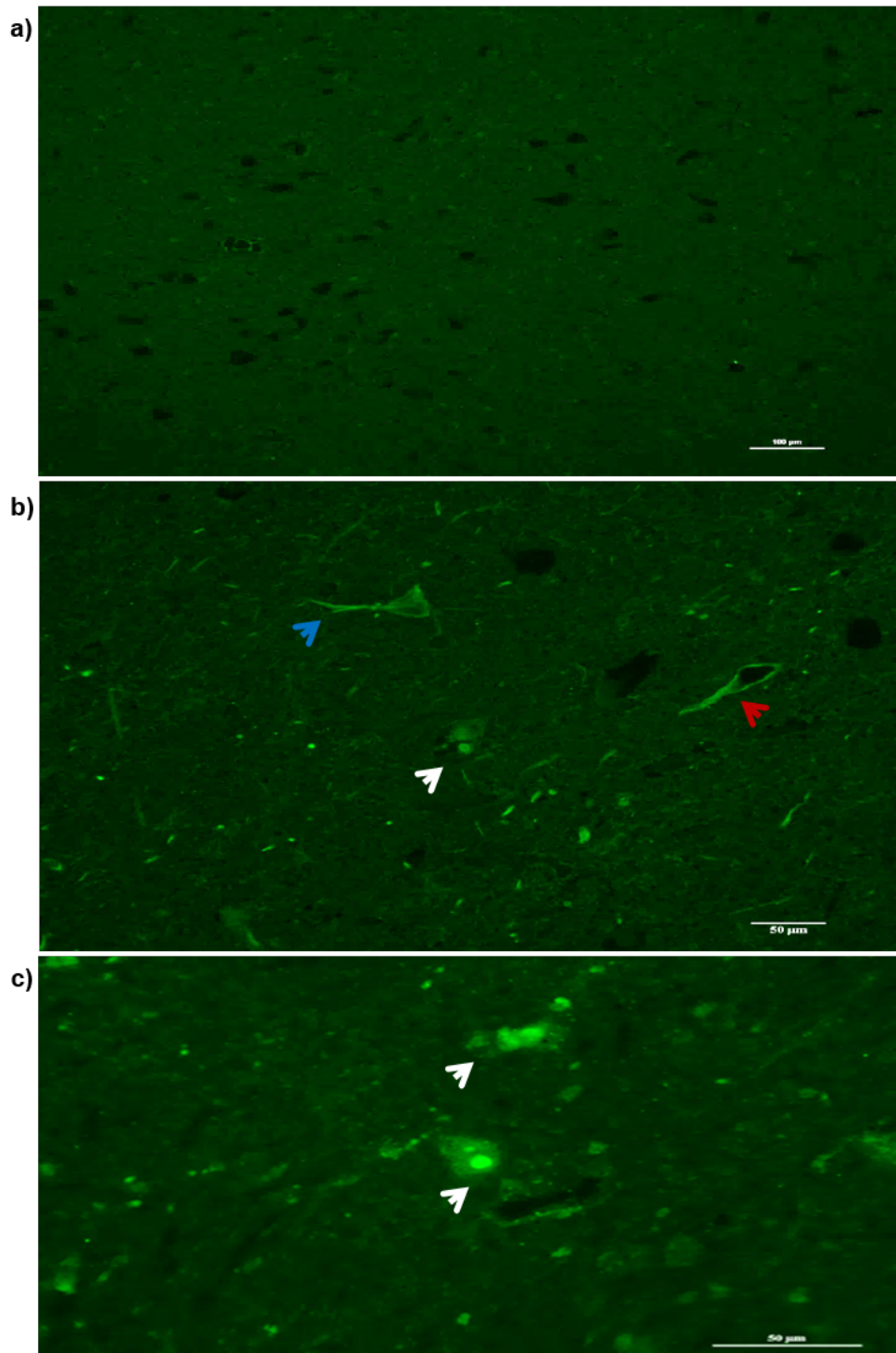
Figure 2.5. TIGAR fluorescence in Sustantia Nigra. Representative images of TIGAR fluorescence staining in the SN in a control (a), PD (b and DLB (c) cases, showing the presence of TIGAR in Lewy bodies (white arrows), neurons (red arrow) and neurites (blue arrow). Bar 50µm.

2.9.5 Colocalisation with alpha-synuclein

2.9.5.1 Double STAINING: DAB/Fluorescence and double fluorescence

Double staining with: DAB for TIGAR (Figure 2.6 a, c) and fluorescent alpha-synuclein (red) (Figure 2.6 b, d); and fluorescent images acquired for TIGAR (green) (Figure 2.7 a) and alpha-synuclein (red) (Figure 2.7 b) revealed the colocalisation between the two proteins in Lewy bodies and some neurites (Figure 2.6; and Figure 2.7 d).
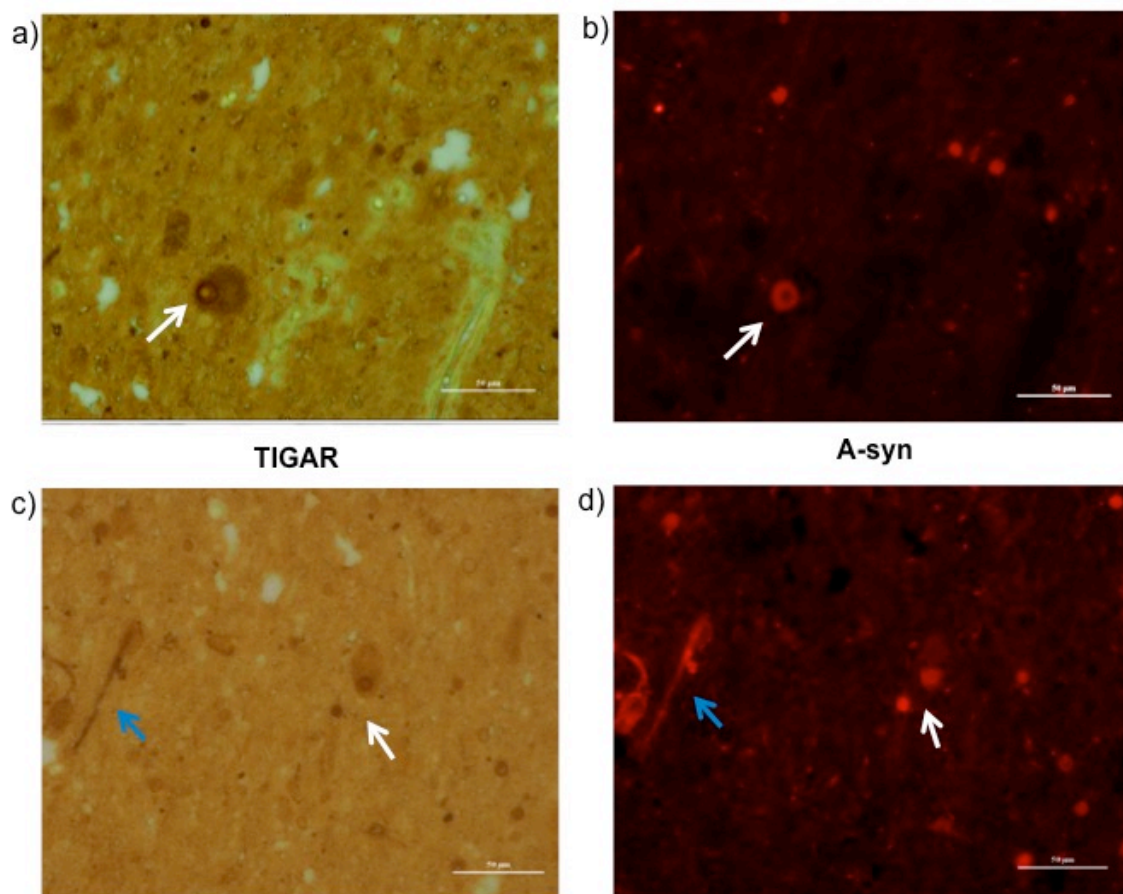
Figure 2.6. Double staining in SN: DAB/Fluorescence. Microscopic analysis of DAB staining showing TIGAR (a and c) and immunofluorescence staining showing alpha-synuclein with AlexaFluor 555 (red) (b and d), from a PD (a and b) and DLB (c and d) cases. Acquired images reveal the co-localization of TIGAR and alpha-synuclein in the Lewy bodies (white arrow) and neurite (blue arrow). Bar 50µm.
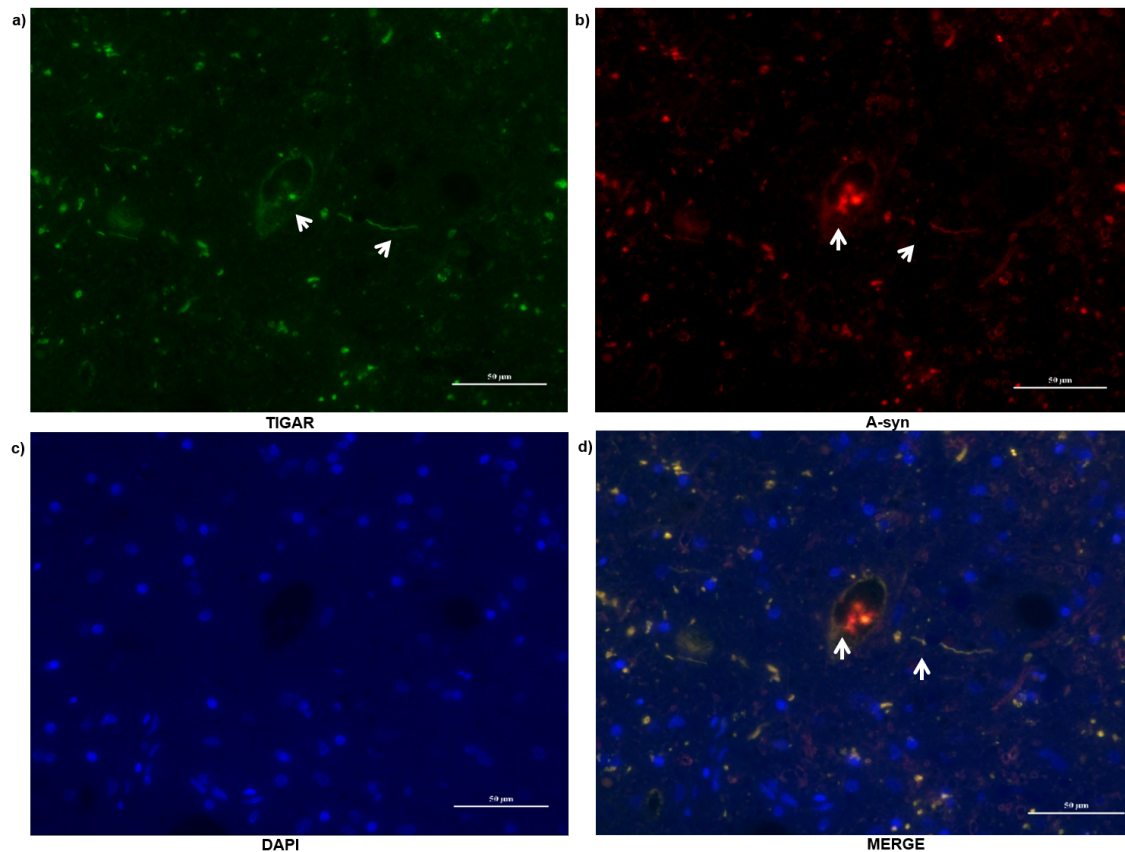
Figure 2.7. Double fluorescence staining in Sustantia Nigra. Microscopic analysis of immunofluorescence staining showing TIGAR conjugated with AlexaFluor 488 (green) and alpha-synuclein with AlexaFluor 555 (red) and, nuclear staining DAPI (blue). Merge image reveals the co-localisation of TIGAR and alpha-synuclein in the Lewy bodies and neurites. Original magnification at 40x.

2.9.5.2   Co-localisation: serial sections

Using the three different detection methods (double fluorescence, fluorescence and DAB and DAB in adjacent sections), we confirmed that TIGAR is co-localised with alpha-synuclein. Mainly in the Lewy bodies in the SN.

74
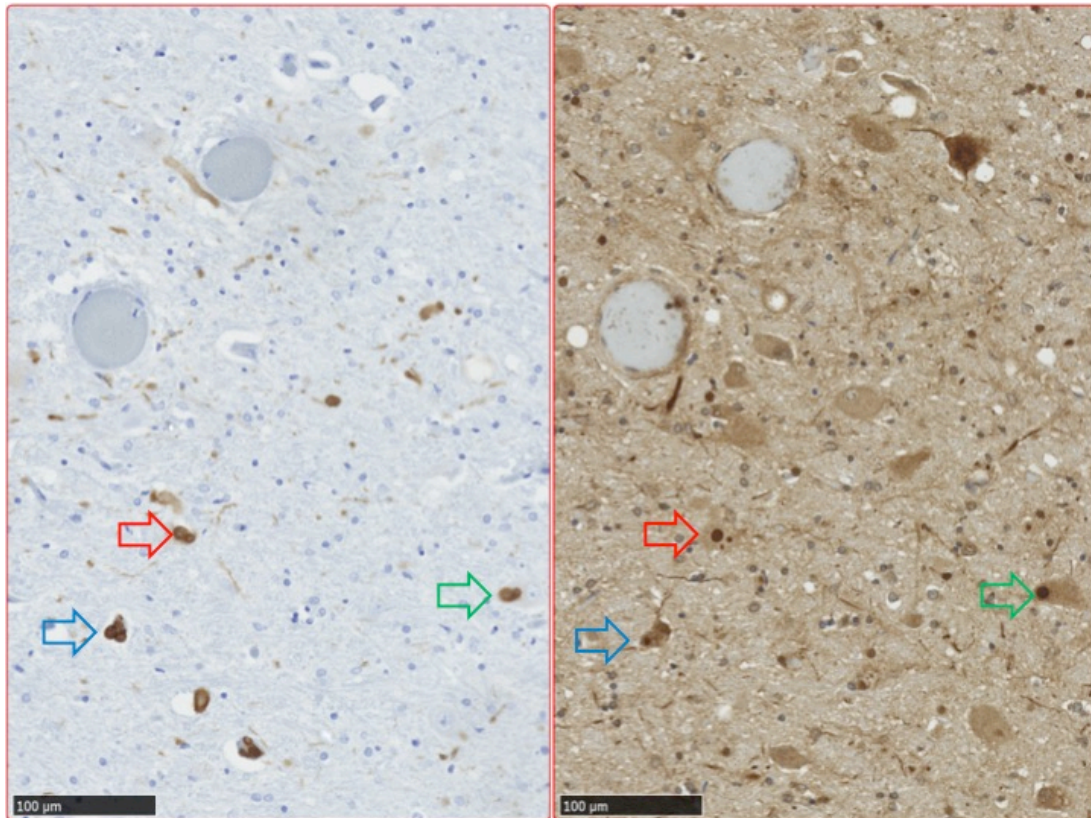
Figure 2.8. Aligned adjacent sections in the Sustantia Nigra. Representative images of DAB immunohistochemistry for alpha-synuclein (left panel) and TIGAR (right panel) in the SN of a PD case, showing the presence of TIGAR in Lewy bodies (red, blue and purple arrows). Bar 100µm.

2.9.6 Quantification of TIGAR in dopaminergic neurons

TIGAR quantification in the dopaminergic neurons was carried out by two pathologists (JS and RH). This was performed first to assess the inter-rater reliability, in which the percentage of neurones that were intensely stained was counted to assess TIGAR expression. There was a 90% inter-rater agreement between the two observers. Only data obtained from the blinded pathologist was taken for the group comparison. A total number of four controls, four PD and four DLB cases were analysed. High levels of neuronal intensity were quantified in the controls (mean=34.25 (5.24%), SD=3.04), PD (mean=51.75 (17.52%), SD=5.8) and DLB cases (mean=62.75 (15.89%), SD=15.08; Figure 2.9). Neurones of the SN varied in their intensity of TIGAR expression across the three groups, but there were a

significantly greater proportion of neurones with strong TIGAR expression in PD than controls (2-way ANOVA, P=0.2350). The DLB cases showed greater variance and no statistical difference compared to the control group (2-way ANOVA, P=0.3166, t=1.384, d.f. 6).
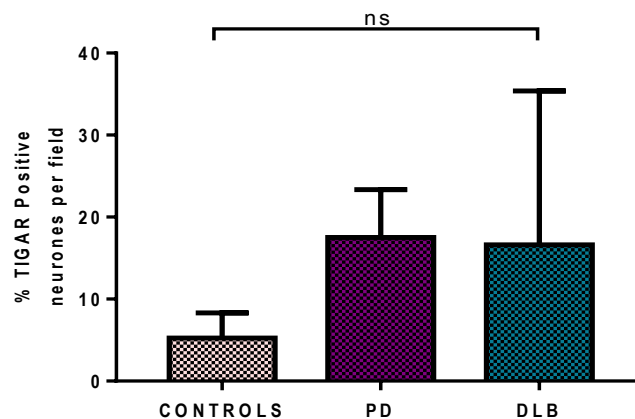
Figure 2.9. Neuronal TIGAR expression in PD, DLB cases and controls. Bar graph represents the percentage of SN neurones that stain intensely positive for TIGAR in each group. There was a higher TIGAR expression in neurones PD (P=0.2350) and DLB (P=0.3166) cases compared to controls, however they did not reach statistical significance (2-way ANOVA, Tukey´s test).

After neuronal expression was quantified, we then assessed the density of TIGAR positive neurites in the SN from the same group of controls and patients. This was carried out by two blinded researchers (LT and KR). Inter-rater reliability 99.8% showed agreement between the observers. Thus, the mean of both observer's counts was used for the group comparison as both observers were blind. The same group of controls and patients was used to assess the total number of TIGAR positive neurites for the controls (mean=4.833, SD=4.771); PD (mean=18.375, SD=0.9648) and DLB cases (mean=312.41, SD=61.076). There were also markedly more TIGAR positive neurites in both PD (t-test, ***P<0.0005, t=8.277, d.f. 6) and DLB (t-test, **P=0.002, t=10.041, d.f. 3.037) cases compared to controls (Figure 2.10).

These quantitative differences suggested that there is a greater neuronal cytoplasmic expression and a greater neuritic pathology in PD and DLB cases in the SBTB cohort.
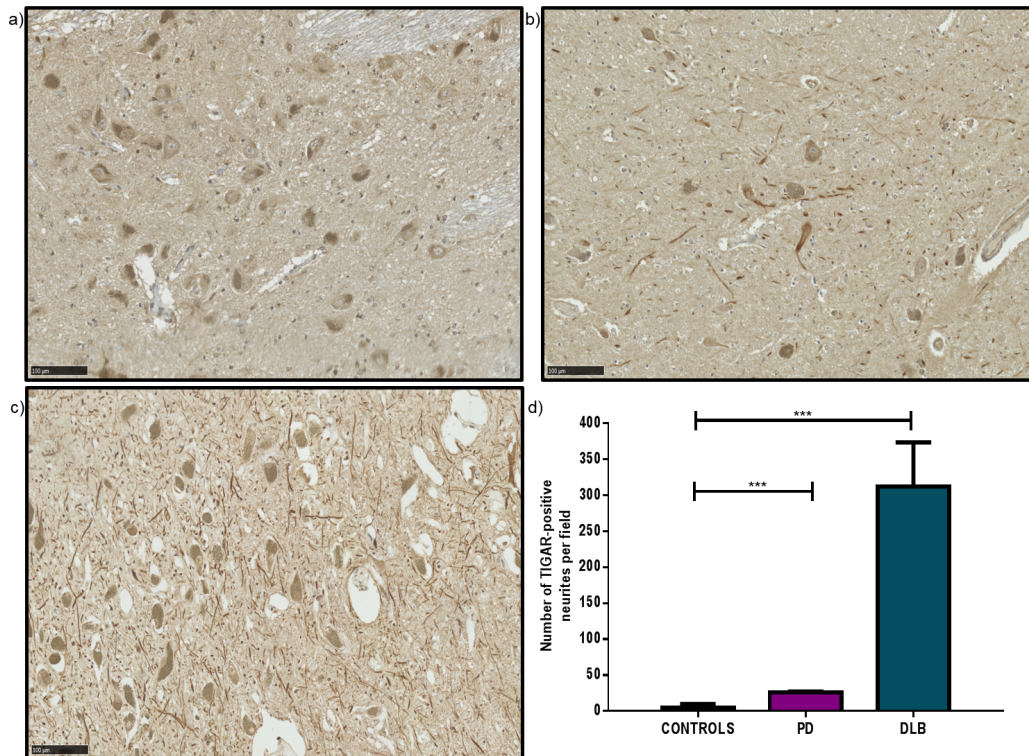
Figure 2.10. TIGAR positive staining in neurites in the Sustantia Nigra of the PD, DLB and control cases. Immunoreactivity in representative control (a), PD (b) and DLB (c) cases. The percentage of SN neurites that stain intensely positive for TIGAR is significantly higher in DB cases (t-test, ***$p<0.0005$) and slightly higher in PD cases (t-test, **$P=0.002$) compared to controls.

2.9.7 TIGAR immunohistochemistry in SN: Queen Square Brain Bank Cohort

We then aimed to expand our patient cohort and further characterise TIGAR in PD and DLB cases from another source, the Queen Square Brain Bank (QSBB) in an attempt to validate these findings. Again, we found TIGAR-positive Lewy bodies and neurites in the six PD and six DLB cases (Figure 2.11). Neurones and neurites from the controls, PD and DLB cases varied in the intensity of the staining.

Therefore, we next proceeded to examine the TIGAR expression in this group.
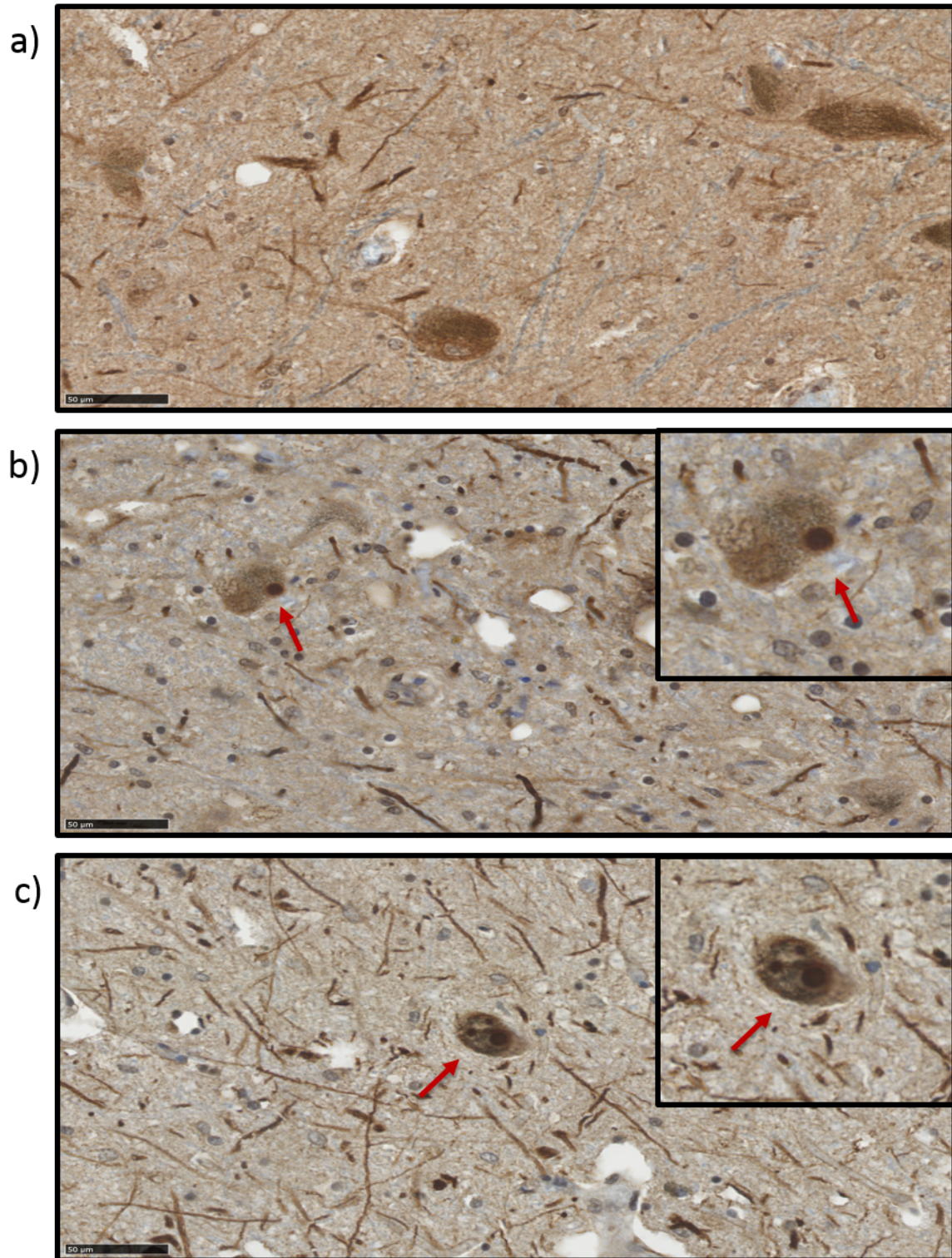
Figure 2.11, Immunohistochemical staining in Sustantia Nigra. Immunostaining for TIGAR by peroxidase substrate DAB counterstained with haematoxylin (a-c). Representative picture of a control (a), PD (b) and DLB (c) cases from QSBB, cases confirming the presence of TIGAR in Lewy bodies (red arrow) and neurites. Bar=50μm.

2.9.8 Quantification of TIGAR expression in SN

TIGAR neuronal staining protocols were performed by the same researchers using the same methods as with the SBTB cases. The percentage of neurones that were intensely TIGAR-positive was assessed by one blinded pathologist (JS) in six controls (mean=360.8 (52.37%), SD=31.71), six PD (mean=115.5 (29.38%), SD=17.74) and six DLB (mean=198.5 (49.04%), SD=27.29) cases (Figure 2.12)

The neurones of the SN varied in their intensity of TIGAR expression, but there were not significantly difference regarding the proportion of neurones with strong TIGAR expression between PD (t-test, P=0.160, t=1.55, d.f. 7.851) and DLB (t-test, P=0.849, t=0.195, d.f.10) patients when compared to controls.
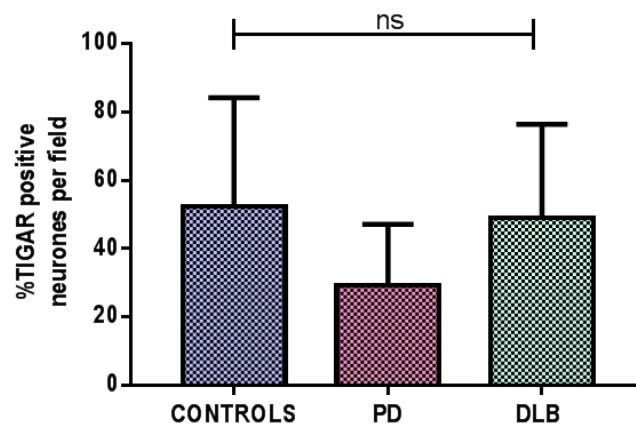
Figure 2.12. TIGAR positive staining in neurones and neurites in the SN of the PD, DLB and control cases from QSBB. The percentage of neurons in entire SN (a) positive for TIGAR relative to total number of neurons per field. The analysis showed no difference between the PD (t-test, P=0.160) and DLB (t-test, P=0.849) cases compared to controls.

We then quantified the number of TIGAR positive neurites in the SN from the same group of controls and patients. The Inter-run sections used for comparing both cohorts were the same control sections. Quantification of TIGAR positive neurites was carried out by one blinded researcher in controls (mean=90.88, SD=82.55), PD

(mean=27.833, SD=26.16) and DLB cases (mean=63.833, SD=32.31). This also

showed no difference between both PD (t-test, P=0.125, t=1.784, d.f. 5.99) and DLB

(t-test, P=0.481, t=0.748, d.f. 6.49) cases compared to controls (Figure 2.13).
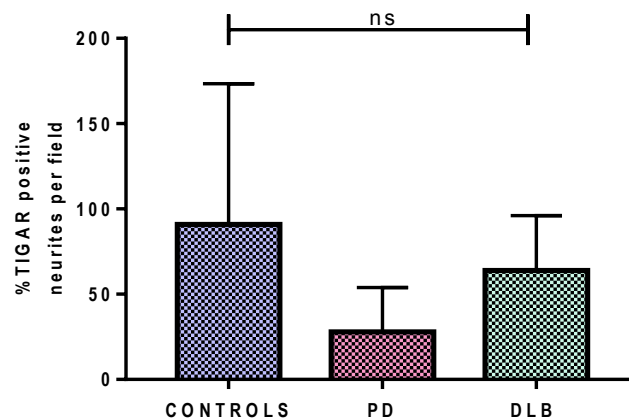
Figure 2.13. TIGAR positive staining in neurites in the SN of the PD, DLB and control cases. Bar graphs representing the percentage of TIGAR positive neurites in the controls and diseases cases. No significant difference was found in PD (t-test, P=0.125) and DLB (t-test, *P*=0.481) cases compared to controls.

We found that TIGAR was present in the Lewy bodies in the SN in the PD and

DLB cases, and absent in the control group from the QSBB. This corroborates with

the previous results obtained with the SBTB. However, we did not find TIGAR

quantitative differences between controls and PD and DLB cases from the QSBB as

we did we the SBTB.

2.9.9 p53 in SN

To elucidate the mechanism in which TIGAR might be involved in PD

pathogenesis, we wanted to know if any other proteins that are upstream or

downstream of TIGAR might be dysregulated in PD brains. For this reason, we

proceeded to determine p53 localization in the SN in four PD, one DLB cases and

four controls from the Sheffield Brain Tissue Bank. Initial staining with the Anti-p53 sc-263 antibody heavily stained melanin and failed to get a good staining (data not shown). Therefore, p53 staining was performed in the Department of Cellular Pathology, Hull and East Yorkshire NHS Trust.

The positive control showed positive labelling of cell bodies (neoplastic tissue). There was no p53 expression in either the control (Figure 2.14 a) or the PD (Figure 2.14 b) and DLB (Figure 2.14 c) disease group, suggesting no up regulation in the expression of the p53 protein in the SN. Moreover, Lewy bodies were negative for p53 (Figure 2.14 b, c). In this study and with our methods, we did not find p53 involvement.
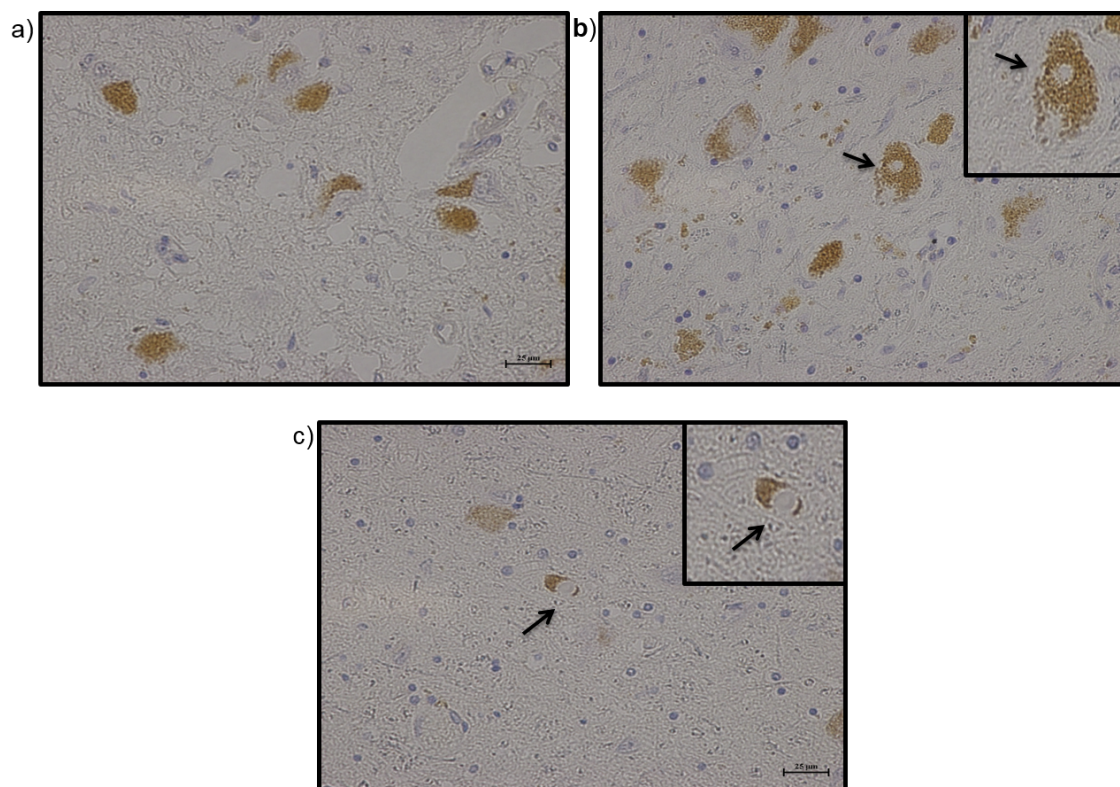
Figure 2.14. p53 staining in the Sustantia Nigra. Immunoreactivity in representative control (a), PD (b) and DLB (c) cases showing negative p53 expression within neurons and absence in Lewy bodies (arrows) from PD (b) and DLB (c) cases. NB the brown pigment shown is neuromelanin-not DAB-labelled TIGAR Bar=25μm.

2.9.10 Hexokinase I and II in SN

In addition to p53, Hexokinase I (HK-I) and II (HK-II) are well known to be regulators of TIGAR. Therefore, we wanted to investigate if there was an association with TIGAR expression in the SN. We assessed HK-I and HK-II expression in four controls and four Parkinson's disease cases. HK-II, which is more abundant in muscle and liver, was not found or was found in very low levels. Moreover, we had to use high antibody concentration, which gave a considerable amount of non-specific background staining (Figure 2.15). HK-II was not found in the Lewy bodies in the patient group (Figure 2.15 b-c).
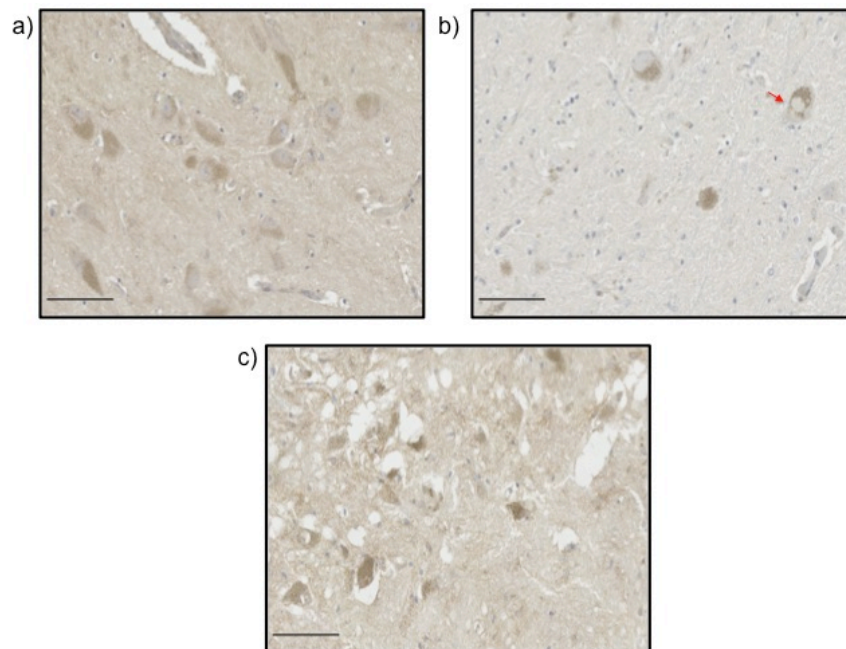
Figure 2.15. HK-II immunohistochemistry in Sustantia Nigra. Representative images of HKII DAB staining in SN in a control (a), PD (b) and DLB (c) cases showing non-specific labelling. There was no difference between cases and controls. HKII was not found in Lewy bodies (red arrow). Bar=100μm.

We could only find positive expression of one of the hexokinase isoforms, HK-I, which is well known to be abundant in the brain (Aleshin et al., 1998). HK-I staining showed a strong cytoplasmic expression in granular pattern in neurons and glia (Figure 2.16). This pattern varied within controls (Figure 2.16 a) and disease cases

(Figure 2.16 b-c). HK-I was not found in the Lewy bodies of the disease cases (Figure 2.16 b-c).
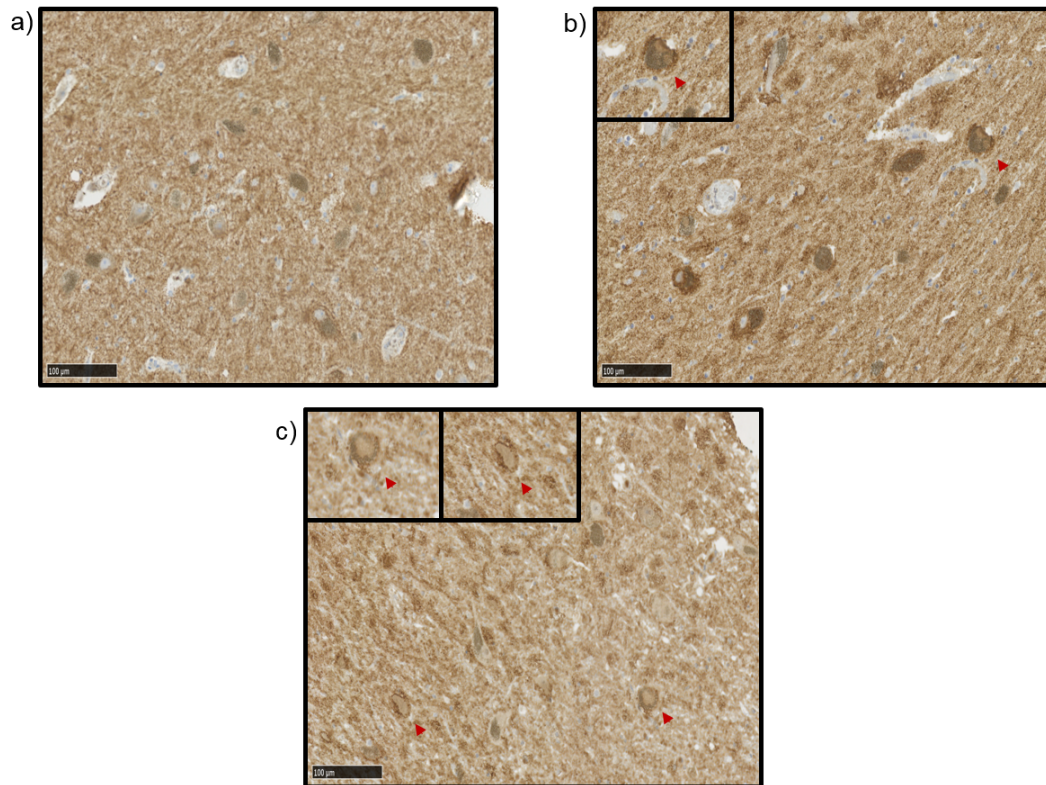
Figure 2.16. HK-I immunohistochemistry in SN. Immunoreactivity in representative control (a), PD (b) and DLB cases (c). Images show varied neuronal cytoplasmic staining with slightly higher expression in the PD cases (b). Bar = 100μm.

Each captured imaged from the SN from four controls and 4 PD cases was analysed with ImageJ. The DAB-only images, which were subjected to the threshold, gave the stained area fraction and measured. Overall, a total number of HK-I positive neurones were quantified for the controls (mean=61.99, SD=1.73); PD cases (mean=67.85, SD=1.03). Neuron intensity of ten fields from ten regions of the SN revealed a slightly increased HK-I expression in the PD cases compared to the controls (t-test, *P=0.0259, t=2.942, d.f. 6) (Figure 2.17).
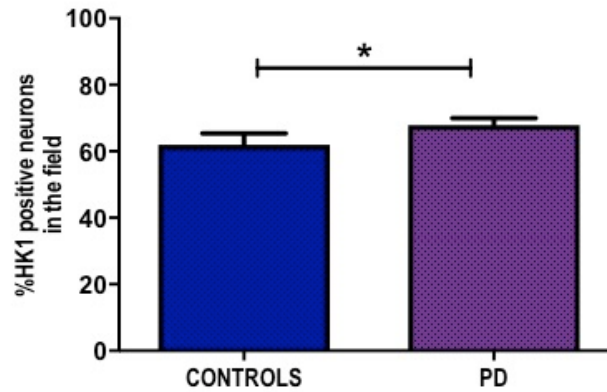
Figure 2.17. HK-I positive staining in neurones in the SN of the PD and control cases. Bar graphs represent the percentage of neurons that stain positive for HK-I. HK-I showed slightly higher expression in PD cases (t-test, *P*=0.0259) compared to controls.

2.9.11 TIGAR expression in mesial temporal lobe

Alpha-synuclein pathology has been found in the hippocampus in PD and DLB cases (Galvin et al., 1999). Thus, we aimed to look for TIGAR expression in the cohort of controls, PD and DLB cases in hippocampal tissue, both anterior and posterior, from the SBTB. Since we previously found TIGAR presence in the Lewy bodies in the SN in the PD and DLB cases, we wanted to determine whether TIGAR colocalization in Lewy bodies was also present in the hippocampus in the patient group. The presence of alpha-synuclein pathology had been confirmed previously in these cases and the paraffin-embedded tissue blocks were already available.

TIGAR showed variable neuronal expression in the hippocampus in the controls and diseases cases (Figure 2.18 b-c). Some showed strong labelling in the region of the perforant processes pathway in the CA2 (Figure 2.18 c).

84
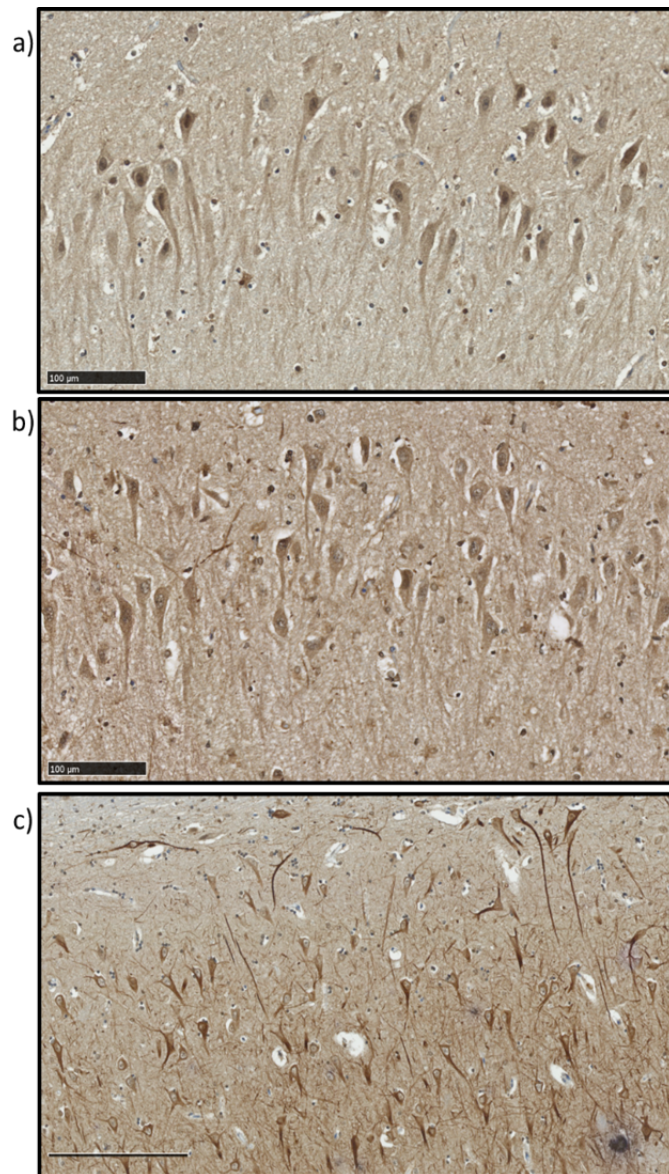
Figure 2.18. TIGAR staining in Hippocampus. Representative image of TIGAR presence in hippocampal regions CA2 in a control (a), PD (b) and DLB case (c). TIGAR expression showed to be variable in the pyramidal cells in controls (a) and disease cases (b-c). There was also some intense labelling in the performant pathway in some cases (c). Bar=100μm

TIGAR labelling in pyramidal neurons from the entorhinal and occipitotemporal regions appeared to have slightly higher expression in the disease group (Figure 2.19 c-f) when compared to the controls (Figure 2.19 a-b). However, not every cell showed to be affected, some showed higher expression, others do not. Therefore, we next proceeded to quantify TIGAR positive neurons in these regions.
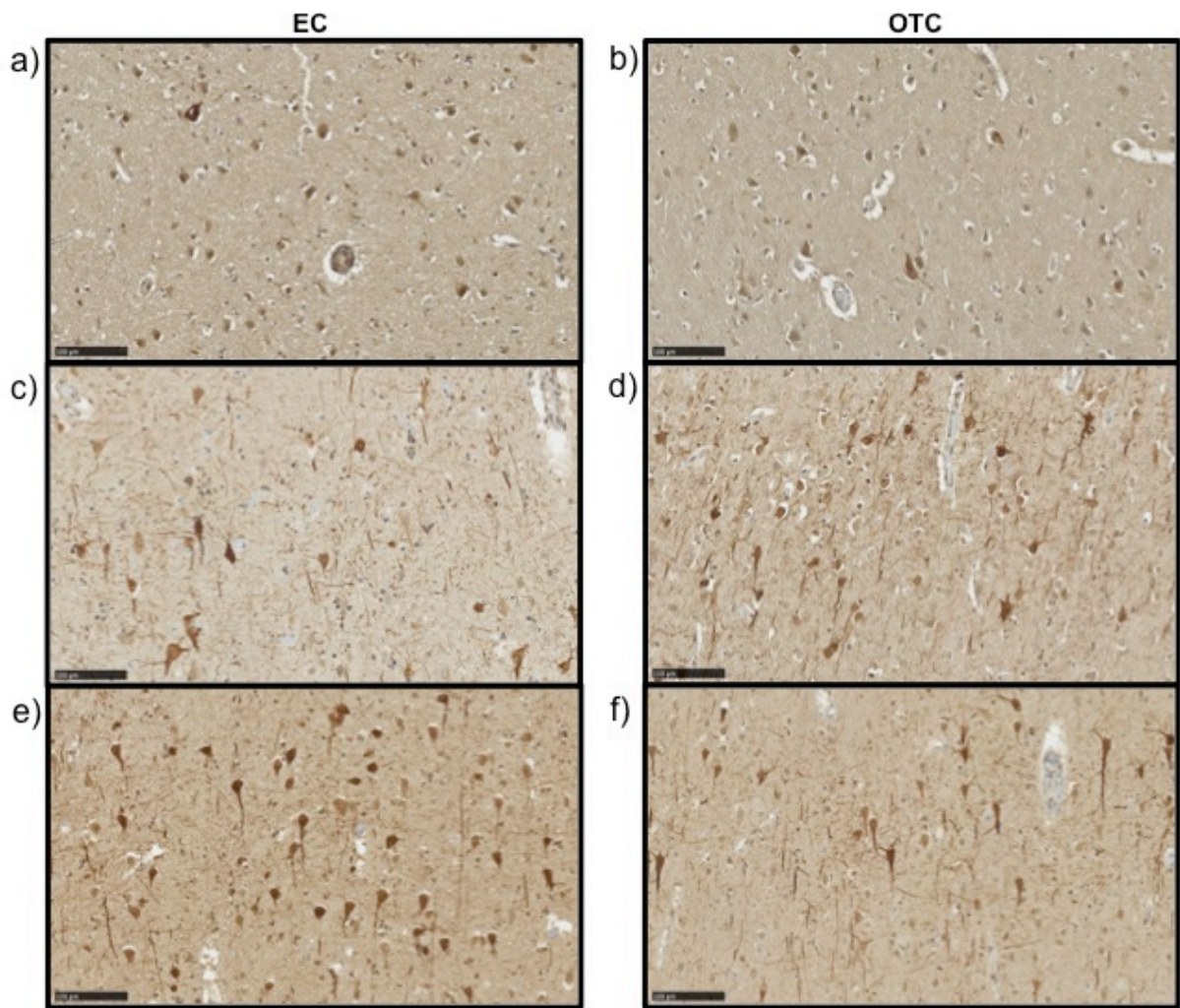
Figure 2.19. TIGAR staining in entorhinal and occipitotemporal cortex. Representative image of neurones of the entorhinal (left panel: a, c, e) and occipitotemporal cortex (right panel: b, d, e) in mid layers from controls (a, b), PD (c, d) and DLB (e, f) cases. Images showed variable TIGAR neuronal expression in controls (a-b) and disease cases (c-f) in both regions. Some cells and processes appeared to have higher TIGAR expression in the disease cases (c-f) compared to the controls (a-b). Bar 100µm.

2.9.12 Quantification of TIGAR staining in occipitotemporal cortex and entorhinal cortex.

Three regions of interest were captured at 20x from the occipitotemporal and three from the entorhinal cortices from digitised whole slide images of sections at the level of the posterior hippocampus from one control, one PD one DLB cases were assessed. Two blinded researchers counted the number of TIGAR-positive neurons

and neurites. There was no correlation between the two independent researchers (occipitotemporal cortex count correlation=63.3%; entorhinal cortex count correlation=21.22%) (Figure 2.20 a, b); therefore this assessment method was aborted.

As an alternative, image analysis was used to assess, based on the proportion of the image that was positive for TIGAR was performed by ImageJ analysis. This did not detect any statistical difference (Mann U-Whitney, P=0.800) between the control (mean=44.28; SD=7.47), PD (mean=50.41; SD=16.74) and DLB cases (mean=50.40; SD=13.96) (Figure 2.20 c, d).

Thus, we found that TIGAR was not involved in PD pathology in other areas different outside the SN. These suggest a specific role of TIGAR in PD and DLB disease process in the SN. There was no labelling of neocortical or hippocampal bodies.
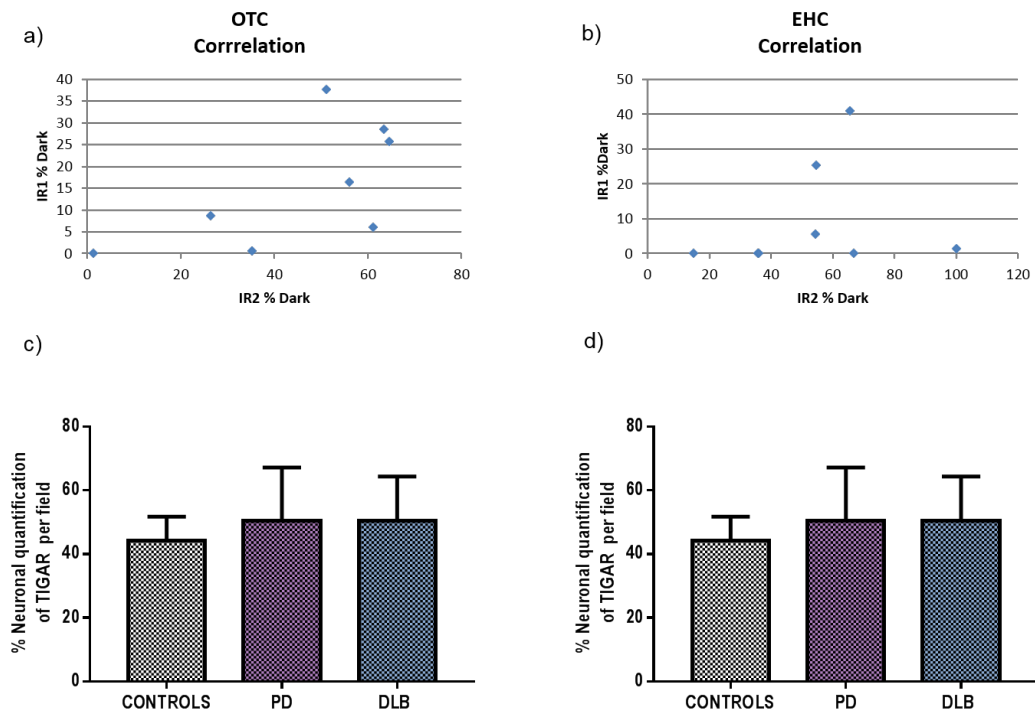
Figure 2.20. Quantification of TIGAR in hippocampus. Scatter charts showed no correlation between the two independent researchers in counts from the occipitotemporal cortex (OTC) (63.3% correlation) (a) and the entorhinal cortex (EHC) (21.22% correlation) (b). Bar graphs represent the percentage of TIGAR positive neurons processed and quantified by Image J for the OTC (c) and the EHC (d); no statistical difference was found between controls and patients (Mann U-Whitney, *P*=0.800).

2.9.13 TIGAR in MSA

We then assessed TIGAR expression in another synucleinopathy, namely MSA. We wanted to determine whether TIGAR had a disease specificity for PD or whether it was also present in other synucleinopathies. In the SN, many neurons showed apparent intense neuronal cytoplasmic and neurite staining. TIGAR-positive glial cytoplasmic inclusions were not seen (Figure 2.21 a-b).

2.9.13.1 Quantification of TIGAR in MSA

We then analysed the variability of TIGAR expression in neurones and neurites between controls and MSA cases (Figure 2.21 a-b). We assessed the levels of these by using the same methods as for the PD and DLB cases above. The proportion of TIGAR positive neurones was quantified for controls (mean=52.37, SD=31.71) and MSA cases (mean=29.42, SD=4.42). TIGAR positive neurites were

also quantified in controls (mean=90.88, SD=82.55) and MSA cases (mean=43.77, SD=24.01). We found no significant difference in TIGAR expression in neurones (t-test, *P*=0.138, t=1.73, d.f. 5.377) and neurites (t-test, *P*=0.241, t=1.29, d.f. 6.37) between the controls and the MSA patients (Figure 2.21 c-d).

There was no other significance evidence between the control and patient group, likewise we did investigate further regions involved in its pathology.
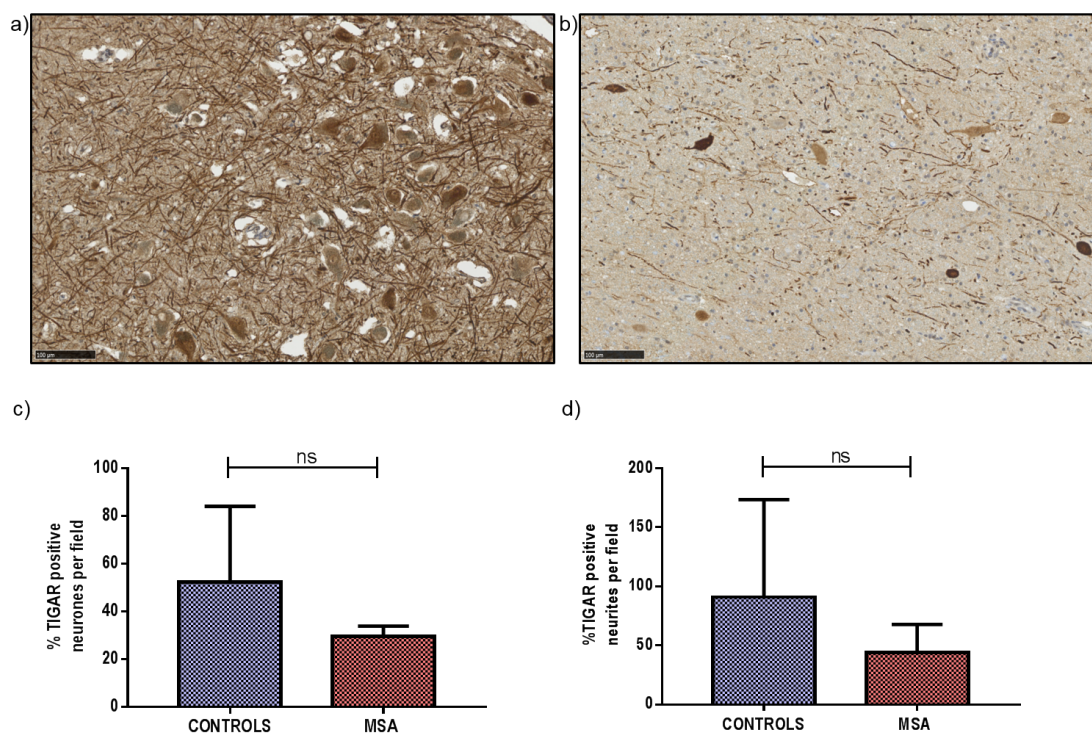
Figure 2.21. TIGAR staining in SN from MSA cases. Immunostaining for TIGAR by peroxidase substrate DAB counterstained with haematoxylin in control (a) and MSA cases (b). Images showed variability in TIGAR expression between the controls (a) and patients (b). Controls and patients showed a diverse range of immunoreactivity within the SN. Bar graphs represent the proportion of TIGAR positive neurones (c) and TIGAR positive neurites (d) between controls and patients. No statistical difference was found in neurones (c) (t-test, *P*=0.138) and neurites (d) (t-test, *P*=0.241) expression between the controls and patients. Bar 100 μm

2.9.14 TIGAR in spinal cord: Motor Neurone Disease

We proceeded to assess the presence of TIGAR in the ubiquitylated inclusions in neurones of another neurodegenerative disorder: The lower motor neurons of motor neurone disease (MND).

In contrast to its presence in Lewy bodies, TIGAR protein was not found in the TDP-43 positive cytoplasmic inclusions typical of MND. However, TIGAR immunostaining in spinal cord showed that TIGAR is present in motor neurons and neurites (Figure 2.22 b). Thus, results suggest TIGAR disease specificity for brainstem neuronal Lewy pathology of PD and DLB.
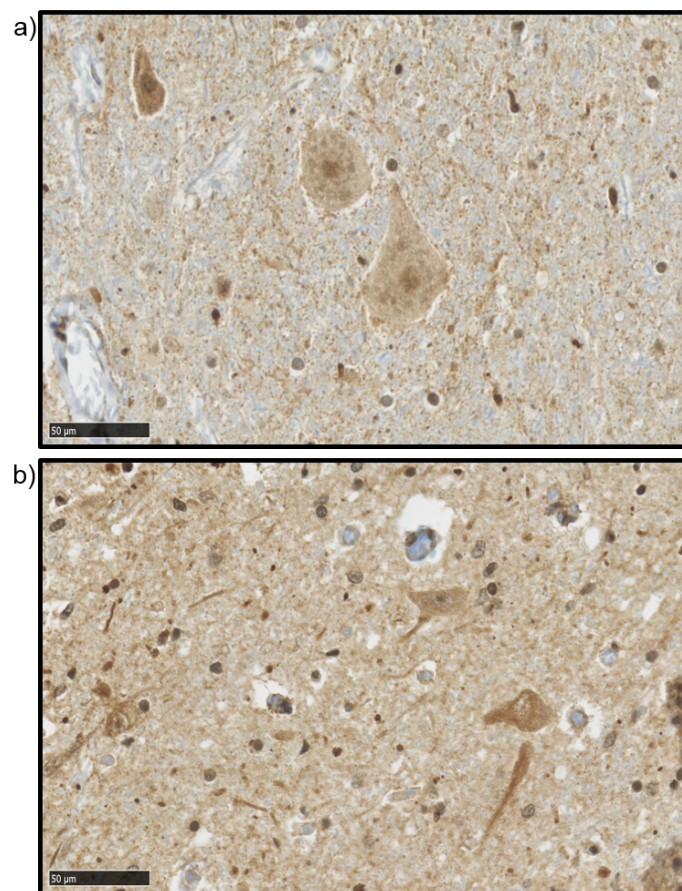
Figure 2.22. TIGAR presence in Spinal cord. Microscopic analysis of TIGAR immunoreactivity in Spinal cord from a control (a) and ALS patient (b). TIGAR was not found in the TDP-43 positive inclusions of MND cases. A variable pattern of TIGAR positive immunoreactivity was observed in the nuclei and neuronal bodies in both controls and patients. Bar 50µm.

2.9.15 Quantification of TIGAR in spinal cord in MND

We investigated TIGAR expression in a different neurodegenerative disease with ubiquitinated inclusions, such as MND, to assess TIGAR disease specificity. It was noted that motor neurons from the spinal cord varied in their intensity of TIGAR

expression in both the control and patient groups. Therefore, we decided to assess the proportion of TIGAR positive and negative motor neurons in controls and MND cases by using the same methods as above.

Quantification of TIGAR positive neurones was carried out by one blinded researcher. The percentage of TIGAR positive neurites was obtained for controls (mean=37.55, SD=26.04) and MND cases (mean=22.04, SD=20.07). However, there was no significant difference between the proportion of neurons with strong TIGAR expression in controls and MND cases (t-test, P=0.354, t=1.01, d.f. 7) (Figure 2.23 a-c). Thus, results suggest a TIGAR specific role for PD and DLB.
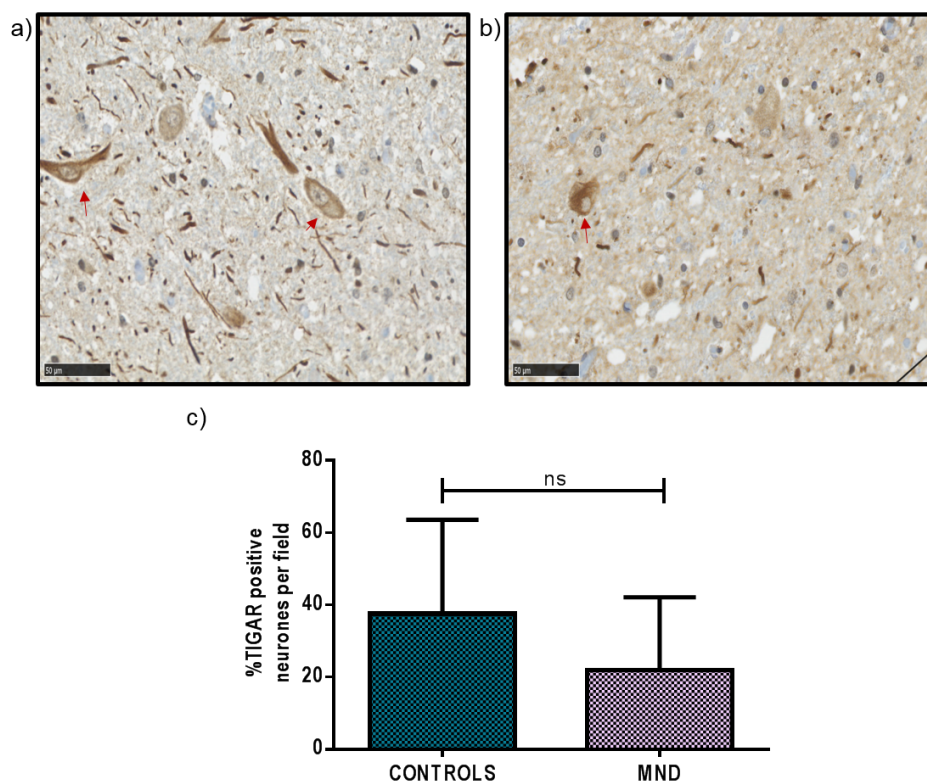
Figure 2.23. TIGAR-positive neurons in the spinal cord of controls and MND cases. Immunoreactivity in representative control (a), and MND cases (b). The percentage of neurons in the spinal cord that stain intensely positive for TIGAR (red arrows) was not significantly different in the MND cases compared to the controls. (t-test, P=0.354). Bar=50µm.

Therefore, we then assessed TIGAR positive neurites in the same groups. This was carried out by two blinded researchers. Inter-rater reliability 99.6% showed agreement between the observers. Thus, the mean from both observer's counts was used for the group comparison. A total number of TIGAR positive neurites were quantified for the controls (mean=64.27, SD=71.81) and MND cases (mean=4.83, SD=2.92). There was also no difference of TIGAR-positive neurites between controls and MND cases (t-test, P=0.196, t=1.654, d.f. 3.008) (Figure 2.24 a-c).
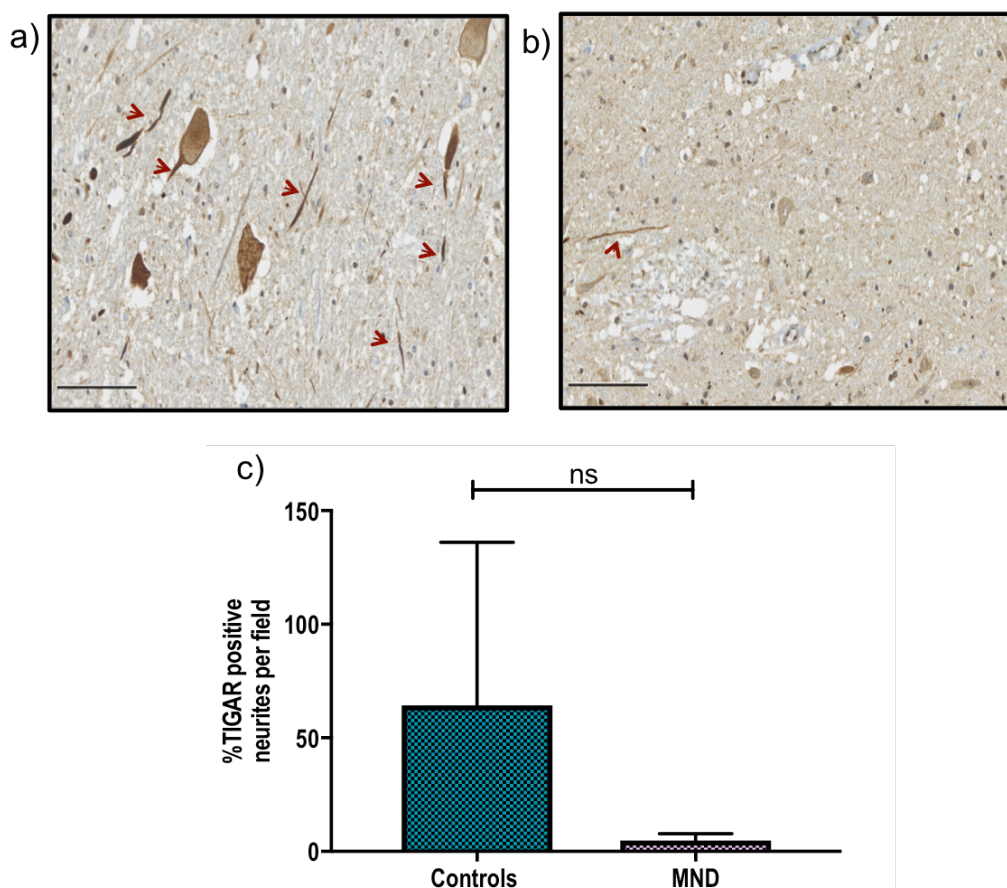
Figure 2.24. TIGAR positive staining in neurites in the Spinal cord of the MND and control cases. Immunoreactivity in representative control (a), and MND cases (b). The percentage of neurites in the Spinal cord that stain intensely positive for TIGAR (red arrows) was not significantly different in the MND cases compared to controls. (t-test, *P*=0.196). Bar 100µm.

2.10 Discussion

2.10.1 Antibody confirmation

The present study addressed the normal and pathological TIGAR-related characteristics in the human brain in PD and related disorders. Although TIGAR expression has been characterised before by Western blot, Immunohistochemistry and microarray analysis in the superior temporal gyrus in normal brain and in patients with Alzheimer's Disease (AD). Here, TIGAR gene and protein expression was reduced in patients with severe dementia (Katsel et al., 2013). Therefore, we wanted to assess it in the PD and related disorders DLB and MSA cohort. We also wanted to look in another neurodegenerative disorder characterised by pathological inclusions, such as MND, to determine if TIGAR was also present in other disease with ubitiquinated inclusions. Here, we demonstrated the presence of TIGAR in neurons in the normal and pathological brain. We could confirm that the obtained findings were true and reproducible by using three different antibodies that showed the similar result across the stained brains.

2.10.2 TIGAR presence in human brain

There was TIGAR widespread expression in the midbrain and hippocampus, as well as the spinal cord. This result suggests that TIGAR function is important for the normal cellular metabolism across different regions of the CNS and cellular types. This could be due to its role in the Pentose Phosphate Pathway (PPP), which provides antioxidant defence against ROS, cellular stress and hypoxia, as well as providing the nucleotides for DNA synthesis (Bensaad et al., 2006). In neurons, the PPP has been suggested to be essential for glucose metabolism and for antioxidant function via glycolysis inhibition (Herrero-Mendez et al., 2009). Neurons seem to be susceptible to continued damage from oxidative stress (Herrero-Mendez et al., 2009).

Therefore, TIGAR function by lowering ROS production, maintaining NADPH and glutathione could be indispensable for the maintenance and antioxidant protection of the neurons preventing permanent damage (Bolaños and Heales, 2010).

NADPH is produced in high levels in response to stress and is an important reducing cofactor that counters oxidative stress. It is produced from the metabolised glucose from the PPP and generated by the enzyme glucose-6-phosphate dehydrogenase (G6PD). Glutathione (GSH) is an anti-oxidant and cofactor alongside NADPH, which combats oxidative stress after it is converted into its reduced form by the glutathione reductase (Zuo and Motherwell, 2013). A recent study by Dunn et al., 2013; characterised the activity of the PPP across different regions of the brain in Alzheimer's disease (AD), PD and normal control tissue by measuring levels of NADPH in post-mortem brain tissue. In the cerebral cortex and putamen of AD and severe and moderate PD groups NADPH and G6PD were increased; whereas in the mild PD group there was a decrease in G6PD. The mild group was related to be an early stage of PD, whereas the moderate/severe group was related to later stages of the disease. This evidence showed that an impairment of glucose metabolism and PPP inhibition leaves neurons vulnerable and exposed oxidative stress, which has been suggested to be a feature of an earlier stage in the development of PD (Dunn et al., 2013). Furthermore, oxidative stress has been suggested to have a role in the formation of Lewy bodies at early stages of the disease (Dias et al., 2013).

NAPDH is produced through the PPP and utilised by glutathione in the redox cycle to decrease ROS levels (Ramos-Martinez, 2017). It has been reported that neurons have been reported to be deficient in the SN from brain tissue of patients

with PD (Fitzmaurice et al., 2003; Perry et al., 1982; Sofic et al., 1992). Therefore, it is important to produce glutathione through the recycling via the PPP and NADPH to prevent damage from oxidative stress insult. In this study NADPH levels were reduced in the putamen and cortex of early stage PD patient, suggesting a defect in the sensing or inhibitory mechanisms that prevent NADPH production and inability to recycle glutathione. A number of studies have suggested a dysregulation of the PPP pathway and glucose metabolism is one of the earliest events occurring in the pathogenesis of neurodegeneration (Bouzier-Sore and Bolaños, 2015; Dunn et al., 2013; Hilker et al., 2012).

2.10.3 TIGAR expression in the SN in PD, DLB and MSA

In a previous study performed in post-mortem tissue, studying TIGAR mRNA and protein levels in the superior temporal gyrus from brains of AD patient group and compared to controls. Microarray data and protein levels obtained by western blotting showed reduced levels of TIGAR in the AD patient group compared to controls. However, no difference was found between patients and controls tissue expression performed in the superior temporal gyrus, one of the most affected brain areas in AD. This suggested that TIGAR was probably involved in the functional cognitive process rather than the neuropathology seen in the later stages of the disease (Katsel et al., 2013). Initially in our study, TIGAR expression was moderate-high in the PD and DLB group compared to the control group from the first cohort studied (Sheffield Brain Tissue Bank). This initially suggested TIGAR upregulation in the SN of the disease cases groups, and a possible role in dopaminergic cell degeneration leading to disease development. However, when we attempted to replicate this with a second cohort (from the Queen Square Brain Bank) no significant difference was found. These can be due to the fact that

immunohistochemistry is a method in which specific subtle changes of proteins might not be detected.

In immunohistochemistry, there are several critical factors that influence the outcome of the results of the protein of interest. These include: uncontrollable variables from the patient (disease duration and severity, case-case variation, diet, age, treatments and surgery, comorbidities, cause of death), quality of tissue, how the tissue was obtained, handled (post-mortem delay, ambient temperature, storage, mode of inactivation), fixed, processed (storage medium and conditions) and interpreted (observer variability and subjectivity). In our study, tissue was obtained from two different sources, which might have had an impact on the quantification. For example, paraffin processing at very high temperatures, could have an impact in the tissue adhesion and result in loss or impaired antigenicity. Immunohistochemistry, as a quantitative measure, DAB-based immunohistochemistry is generally not ideal, due to the amplification steps involved. Therefore, more accurate quantitation methods, such as Enzyme Linked Immunosorbent Assay (ELISA), are required to fully assess TIGAR protein levels in the brains from controls and disease patients. Therefore, TIGAR suspected neuronal upregulation in PD can be further assessed.

TIGAR role in PD was initially suggested by findings from our group in a zebrafish *pink1*-deficient model (Flinn et al., 2013). TIGAR up-regulation may be a feature of PINK1-related disease only and not sporadic disease. In sporadic cases the combination of different environmental and genetic factors may have a considerable influence. Then, TIGAR expression might be altered only in a subset of cases. This is also true for some of the different genes described in sporadic PD.

Post-mortem studies in PD patients with *PINK1* mutations are rare and difficult to obtain. However, it would be interesting to see if what was reported in the zebrafish brain can be confirmed in the human brain with Pink1 mutations.

Alpha-synuclein aggregates are different in MSA when compared with PD and DLB (Yang and Yu, 2017). The main pathologic features of MSA is the presence of glial cytoplasmic inclusions alongside striatal and olivopontocerebellar degeneration (Miraglia et al., 2015). In this study we characterised TIGAR presence in the SN of MSA patients. We did not find TIGAR-positive glial cytoplasmic inclusions or differences in TIGAR expression. However, our cohort was relatively small (3 patients).

A recent study in MSA showed that neuronal loss, gliosis and glial cytoplasmic inclusions are mainly found in the motor, supplementary motor cortex, postcentral somatosensory cortex and temporal lobe neocortex (Salvesen et al., 2015). Here, significant neuronal loss as a consequence of changes in cell density rather than cortical tissue volume, was found in the parietal and temporal neocortex. In addition, they found that glial cells were more abundant in these regions, which compensated for loss of neurones resulting in a normal cortical volume (Salvesen et al., 2015). If there is a TIGAR-related pathologic mechanism in MSA, the main affected regions, such as neocortex, need to be evaluated. Furthermore, double staining immunohistochemistry for TIGAR and alpha-synuclein should be performed in order to assess more robustly for co localisation in glial cytoplasmic inclusions. TIGAR-related pathology in MSA remains inconclusive following our study. In order to assess in a more robust method, such as immunoelectron microscopy or laser

capture microdissection (LCM), and a larger cohort should be assessed, not only looking at the SN, but other affected regions of the brain.

2.10.4 TIGAR and alpha-synuclein: co-localisation in Lewy Bodies

Alpha synucleinopathies are a group of disorders that share many neuropathological characteristics, principally the aggregation of alpha-synuclein. In the normal human brain alpha-synuclein is present in presynaptic terminals of the neurons (Galvin et al., 1999; Iwai et al., 1995; Murphy et al., 2000; Wang et al., 2014). Although the synucleins have different isoforms, only the alpha isoform has been found to be accumulated in the synaptic terminal and involved in the formation of pathological oligomeric aggregates in the SN (Dimant et al., 2013). Many theories have suggested different mechanisms for this including: increased levels of alpha-synuclein and toxic gain-of-function; protein misfolding leading to aggregation and neurotoxicity; mitochondrial dysfunction; impaired vesicle dynamics; defective synapsis and impaired intracellular trafficking. Moreover, two clearance mechanisms, the lysosomal autophagy system (LAS) and the ubiquitin-proteosome system (UPS), are also suggested to be impaired in PD (Bang et al., 2016; Beilina and Cookson, 2015; Xilouri et al., 2016). This would impede the degradation of abnormal aggegates.

TIGAR localisation in the regions studied in the brains of people with PD showed no difference from normal human brain. Interestingly, we found that TIGAR is present in Lewy bodies in the SN in PD and DLB, which was not found in the controls. We found co-localisation of TIGAR with alpha-synuclein in Lewy bodies. This result reinforces the suggested association of TIGAR with PD pathology. To our

knowledge, this association has never been reported before in humans. It is still to be elucidated if TIGAR has a role in the formation of Lewy bodies.

PD-related proteins such as LRRK2, PINK1 and Parkin; have also been found in Lewy bodies. Their role in Lewy body formation is still elusive. Interestingly, TIGAR was first linked to PD in a zebrafish *pink1* deficient model, and both proteins were found to be in the Lewy bodies in the SN. Therefore, the suggested shared distribution within the brain and pathological inclusion would suggests that there may be a common involvement of both PINK1 and TIGAR in the development of Lewy pathology.

Lewy body pathology could be the result of a cellular self-defence mechanism that disposes of and restricts cytotoxic proteins (Fecchio et al., 2013) Thus, the inclusion of TIGAR in Lewy bodies could be the result of the same cellular mechanism. This suggests an acquired cytotoxic property of TIGAR.

Both, TIGAR and alpha-synuclein, have been described to have a role in autophagy impairment, so it is possible that both proteins, when produced in excess, impair autophagy and therefore promote protein aggregation. Alternatively, alpha-synuclein overexpression and aggregation, might be promoting TIGAR sequestration and subsequent aggregation. There is already evidence for the capacity of alpha-synuclein to sequester proteins: Alpha-synuclein aggregates interact with mitochondrial complex I, promoting mitochondrial dysfunction and alpha-synuclein tends to aggregate in the mitochondria in the SN and basal ganglia of post-mortem tissue (Devi et al., 2008).

As noted above, TIGAR promotes apoptosis by inhibiting glycolysis in some models. A correlation between ROS level reduction and autophagy inhibition has been suggested (Bensaad et al., 2009; Ye et al., 2013). This implies that TIGAR opposes autophagy (Bensaad et al., 2009).

2.10.5 TIGAR, p53 and the Hexokinases

To elucidate the mechanism that might be implicated in the TIGAR-related pathology, we looked at p53 expression in the SN of the PD patients compared to the normal controls: p53 is a good candidate as is an upstream regulator of TIGAR and has it's a suggested role in neurodegeneration.

Our results demonstrate p53-independent expression of TIGAR in the pathologic inclusions in the SN from brains of patients with PD and DLB. If there is a direct relationship between p53 and TIGAR, it is possible that this was not evident in our work due to the changes affecting p53 structure and function, before and after the cellular insult. There is also a possibility that p53 structural and functional changes are transient and no longer evident at autopsy. Wild type alpha-synuclein promotes p53 down regulation (Alves et al., 2016; Duplan et al., 2016). Therefore, as alpha-synuclein is altered in PD, MSA and DLB this may have reduced p53 expression such that no changes could be seen in the present study. Very low levels of expression p53 in normal aged brain has been reported previously, where significantly increased p53 expression was detected in brains from AD patients (de la Monte et al., 1997). Previously, transcriptional regulation of p53 by parkin in familial PD was demonstrated and suggesting a potential involvement of p53 in PD pathology. Here, brains from patients with parkin mutations showed significantly high

p53 mRNA and protein levels in the striatum. However, the study was carried only in two patients with familial PD (Du et al., 2009). Therefore, p53 levels in the SN might be difficult to assess and it only could be detected when it is overexpressed and in particular conditions. Such very low levels of p53 expression suggest that related mechanisms and pathways need further evidence and might not have a pathological relevance.

Another possibility is that p53-independent pathways are involved in the pathogenesis of PD. In order to further characterise other possible TIGAR regulators, we looked at hexokinase I (HK-I) and hexokinase II (HK-II) expression in the SN of the PD cases and controls. Our results showed no difference in HK-II expression between normal controls and PD patients in the SN. This is likely to be due to low levels of HK-II normally expressed in the human brain (John et al., 2011).

HK-I is structurally similar to HK-II, but, in contrast, is expressed principally in the brain. Like HK-II, HK-I is important for promoting the glycolytic pathway shunt (John et al., 2011; Magrì et al., 2016). Our results revealed only a very slight increase in HK-I expression in the SN in PD compared to our controls.

2.10.6 TIGAR in hippocampus
The hippocampus and mesial temporal lobe is one of the brain areas that can be affected and susceptible to Lewy body pathology (Fujishiro et al., 2013; Jellinger et al., 2003). There is a diversity of pathological changes in this area. More frequent findings are hippocampal atrophy, Lewy bodies and Lewy neurites, senile plaques and phospho-tau pathology. Less frequent findings are the presence of glial cytoplasmic and nuclei inclusions, neuronal loss and Pick body-like inclusions (Dalfó

et al., 2005; Gaig et al., 2007; Galvin et al., 1999; Klos et al., 2006; Rohan et al., 2015; Yang and Yu, 2017). The relationship of hippocampal pathology with dementia and severe cognitive decline is controversial (Elder et al., 2017; Tanner et al., 2017). Lewy pathology is mainly found in the entorhinal cortex, amygdala and CA2/CA3 regions of the hippocampus. The CA1 region, fusiform gyrus and dentate gyrus are only rarely affected. In DLB a correlation between hippocampal atrophy and impaired cognition has been reported (Elder et al., 2017; Foo et al., 2016; Gazzina et al., 2016). This finding is not consistent, however: other studies have not found a correlation between cognitive decline and Lewy pathology. This could be explained by the different approach from the different studies; where the investigation was undertaken in post-mortem tissue and reports (retrospective study), MRI and ongoing prospective studies in patients with PD only, MSA only or PD, DLB and AD as a group. Moreover, the disease duration varied amongst the different populations study, as well as the neuropsychological assessment (Koga et al., 2016; Tam et al., 2005; Tanner et al., 2017). TIGAR expression in the entorhinal and occipitotemporal cortices as well as the hippocampus, did not showed any difference between controls and PD and DLB patients. We also did not find TIGAR-positive Lewy bodies. Overall, TIGAR pathology involvement in the neuronal alpha synucleinopathies seems to be confined to the SN. The limitation of the current study is the small number of patients studied. Further research need to be conducted including patients that developed dementia.

2.10.7 TIGAR and MND

One of the main pathological characteristics of MND is the presence of proteinaceous cytoplasmic inclusions in affected motor neurones, which are positive for antibodies to the transactive response DNA binding protein-43 (TDP-43) and

ubiquitin(Arai et al., 2006; Ciryam et al., 2017). Given that both PD and ALS are both neurodegenerative diseases and have intracellular neuronal inclusions, it is possible that these two diseases share some neuropathological processes. Therefore, it was important to determine whether the inclusions of both diseases were positive for TIGAR. Previous gene chip analysis of mRNA expression of TIGAR in our laboratory (Highley et al., 2014) has suggested a 1.65 fold reduction in TIGAR mRNA in motor neurones in ALS (P=0.0008). However, we found that while TIGAR is present in the neurones of the spinal cord, there was no significant difference between controls and patients.

In this study we looked for TIGAR at the protein level, compared to Highley et al. 2014, that looked at the mRNA levels. The discrepancy between the results could be due to the fact that immunochemistry is not a good method for quantitation, therefore more sensible and specific techniques (ELISA, LCM, western blotting, etc.) are required to confirm the results. Post-transcriptional modifications and regulatory processes occur at any time during the protein lifetime in response to cellular activity demands. Therefore, these modifications offer an alternative explanation for the discrepancy between the mRNA and protein TIGAR levels obtained and affect the function of the protein. These modifications could be transient or permanent, which can affect the expression of the protein in situ. Post-transcriptional modifications have been suggested to have a role in PD pathology and related diseases, affecting related proteins such as alpha-synuclein (Guhathakurta et al., 2017) and potentially TIGAR. If the latter is true, future research needs to address this issue by studying the proteomics by specific techniques such as, mass spectrometry or proteomic arrays, in situ. Another explanation could be that the data obtained by Highley et. al,

2014; were false-positive results due to variability of the platforms and procedures used. Validation studies, such as qRT-PCR or enzyme-linked assays, which is a useful technique frequently used to confirm the possible biological relevance obtained by microarrays.

As consequence, it was concluded TIGAR-positivity in ubiquitylated inclusions in PD and DLB but not in ALS inclusions, seems to have a disease-specificity for pathology occurring in neuronal PD and DLB in the SN. This is in contrast to p62, ubiquitin and many other proteins that are present in the inclusions of other diseases. The related proteins, p53 and HK-II, did not show altered expression on immunohistochemistry in our study. However, further studies are needed to elucidate the suspected role of TIGAR in the human brain pathology. Specifically, it is necessary to assess whether its localisation in pathologic inclusions are merely due to recruitment or the result of other events involved in PD and DLB development.

2.11 Conclusion

We have found that TIGAR is present in Lewy bodies in the SN of PD and DLB patients where it co localises with alpha-synuclein. This suggests a potential role of TIGAR in the formation of Lewy bodies and neurodegeneration more generally. The TIGAR-positive pathological inclusions were only found in the SN and thus seemed to be restricted to this area. No TIGAR-positive inclusion was found in the spinal cords of patients with MND, or in the glial cytoplasmic inclusions of cases of MSA. This suggests specificity for Lewy-type pathology and no involvement in other neurodegenerative diseases. There was no difference of p53 localization and expression when comparing the PD cases to controls. Further cellular and post-

mortem tissue studies need to be conducted to elucidate the TIGAR-related pathological mechanisms and pathways leading to neurodegeneration.

3 TIGAR in PD cellular model

3.1 Introduction

3.1.1 Cellular models for Parkinson's research

Different cellular models have successfully reproduced neuronal degeneration occurring in PD. Important disruptions and alteration in cellular biochemical pathways have been found in these models and suggested as part of the etiopathology. Cellular models have been widely used to study mainly protein aggregation and the mechanisms of cellular death leading to neuronal loss of the dopaminergic cells in the SN pars compacta (SNpc). In this study we focused on the utility of human fibroblasts from patients with familial and sporadic PD.

3.1.2 Mitochondrial dysfunction in Parkinson's disease from patient skin tissue

Mitochondrial dysfunction linked to Complex I (CI) deficiency has been reported in several tissues from patients with PD and has a key role in the pathogenesis. Several compounds have been described as neurotoxins, acting by inhibiting CI activity and the mitochondrial respiratory chain. 1-methyl 4-phenyl, 1, 2, 3, 6 tetrahydropyridine (MPTP), the 1-methyl 4-phenyl pyridium ion (MPP$^+$), and rotenone are some of the widely used toxins to create PD cell models (Gerlach and Riederer, 1996; Tanner et al., 2011). MPTP is recognised as a toxin that induces cell death specifically in the SN and causes PD symptoms in humans and animal models. Oxidative stress and ROS production have also been linked to PD pathogenesis, the oxidative stress inducer Paraquat, another CI mitochondrial inhibitor is also used in current models of PD (Cochemé and Murphy, 2008; Tanner et al., 2011). One of the difficulties for studying neurodegenerative diseases, such as PD, is the

inaccessibility to the affected areas in patients to study the different biological mechanisms and processes.

3.1.3 Skin fibroblasts

Skin fibroblasts derived from biopsies taken from a diagnosed PD patient have been widely used in PD research as a non-neuronal cell model, as well as in a wide range of systemic diseases. They are a representation of primary human cell culture, reflecting the influence of the individual genetic background and environment in the disease process. This model offers the advantages of robustness, easy storage, transport and availability.

The 2mm punch biopsies are taken from the skin usually from the forearm, set up for culture from which fibroblasts can be isolated. Initially it is a culture containing keratinocytes and fibroblasts, which can be then be purely separated after the third passage. Since these cells come from the skin, they can be easily contaminated with *Mycoplasma*, for which they need to be regularly tested to prevent any deleterious effect due to the infection. Subsequent fibroblasts cultures will be consisting of a diverse population of mitotic and post-mitotic cells (Bayreuther et al., 1991). There are numerous cell repositories and laboratories from which skin fibroblasts, from patients with sporadic PD and with mutations in PD related genes, can be obtained: Coriell Institute (https://www.coriell.org) and The NINDS human cell and data repository (https://nindsgenetics.org) (Wray et al., 2012). Fibroblasts express PARK genes at endogenous levels. Furthermore, they display the important similar cellular contact interaction, comparable to neurons and response to trophic signals. Unlike tumour cell lines, glycolysis does not occur at maximal glycolysis. They also reflect additive cellular damage according to the patient age (Auburger et al., 2012).

Notably, they can be converted to induced pluripotent stem (iPS), induced neurons (iN), induced dopaminergic neurons (iDA), induced neural progenitors (iNP) and/or induced neural stem (iNS) cells by reprogramming and applying differentiation methods (Badger et al., 2014; Gopalakrishnan et al., 2017; Momcilovic et al., 2016; Xu et al., 2017).

3.1.4 Skin fibroblasts from patients with PARK gene mutations

3.1.4.1 Alpha-synuclein

Alpha-synuclein is the main component of the pathological hallmark of PD, the Lewy Body. This was the first identified gene in familial cases of PD, the function of which remains unknown. Several studies have suggested that it is expressed in peripheral tissues from living patients, such as skin, stomach and colon. Post-mortem studies have reported its expression in peripheral ganglia, plexus, glands, etc. (Tolosa and Vilas, 2015). Healthy fibroblasts can take up recombinant *alpha-synuclein*, which aggregates and potentially forms inclusions in these cells. It occurs in a time dependent manner and is linked to an enhancement of the cellular oxygen consumption and apoptosis (Braidy et al., 2013). However, endogenous levels of *alpha-synuclein* expression in these fibroblasts have been repeatedly reported to be undetectable (Ambrosi et al., 2014; Braidy et al., 2013; Sanchez-Martinez et al., 2016).

3.1.4.2 LRRK2

Skin fibroblasts from patients with *LRRK2* mutations have mitochondrial dysfunction (Grunewald et al., 2014; Mortiboys et al., 2010a, 2013, 2015; Papkovskaia et al., 2012) and more specifically complex III (CIII) and IV (CIV) defect in fibroblasts with *LRRK2^{G2019S}* mutations (Mortiboys et al., 2015). *LRRK2^{G2019S}* fibroblasts from PD patients displayed increased autophagy, where pharmacological inhibition in the MEK/ERK pathway induced a reduction in autophagy (Bravo-San

Pedro et al., 2012, 2013; Yakhine-Diop et al., 2014). In fibroblasts, LRRK2 protein levels was not affected by the *G2019S* mutation, but the LRRK2 kinase activity was increased (Bravo-San Pedro et al., 2013). Mortiboys et al., 2015; demonstrated that mitochondrial function is rescued after *LRRK2* siRNA mediated knockdown, which suggest that the mitochondrial defect is secondary to the mutation rather than due *LRRK2* haploinsufficiency or a nonspecific downstream effect (Mortiboys et al., 2015). Altered lysosomal morphology has been also documented in *LRRK2^G2019S* fibroblasts (Manzoni et al., 2013b). The Two-pore channel 2 (TPC2) proteins, which regulate the Ca2+ signalling dynamics and trafficking, were linked to altered mitochondrial morphology in *LRRK2^G2019S* fibroblasts (Hockey et al., 2015). Co-immunoprecipitation of LRRK2 and TCP2 was demonstrated and suggested that LRRK2 possibly acts by phosphorylation of TCP2. TPC2 in *LRRK2*-PD related mutations are suggested to be due to interaction and modulation of autophagy in this cells (Hockey et al., 2015). *LRRK2^G2019S* mutation fibroblasts were reported to display excessive fission due to constant phosphorylation and activation of Drp-1, a fission protein, by LRRK2 (Mortiboys et al, 2010; Su and Qi, 2013). Increased mitochondrial uncoupling proteins (UCP2 and UCP4) expression lead to an enhancement of the mitochondrial proton leak, linked to LRRK2 kinase activity in patient fibroblasts (Grunewald et al., 2013; Papkovskaia et al., 2012).

Our group also assessed mitochondrial function and morphology in *G2019S* manifesting (M) and nonmanifesting (NM) carriers. Similar defects in the mitochondrial function, basal mitochondrial oxygen consumption and maximal respiration and a CIV defect in both groups were found. Coupled respiration and CIII were both lower in both groups, but more markedly in the *G2019S-M* than in the

G2019S-NM. (Mortiboys et al., 2015). Ursodeoxycholic acid (UDCA) rescues mitochondrial function in people with *LRRK2^{G2019S}* mutations (*M* and *NM*). This cell model provided a new reliable platform for drug testing. (Mortiboys et al., 2013, 2015).

LRRK2 fibroblasts with different pathogenic mutations within the kinase and ROC domains demonstrated that the cytoskeleton, and cellular adhesion remain unaffected after the kinase activity is inhibited (Garcia-Miralles et al., 2015). However, another study by Caesar, et al. 2015, demonstrated that *LRRK2^{G2019S}* fibroblasts harbour cytoskeletal alterations due to a direct effect in actin dynamics and depolymerisation (Caesar et al., 2015). Fibroblasts harbouring mutations within the core portion of the LRRK2 protein (*R1441G*, *Y1699C* and *G2019S*), located in the ROC, COR and kinase functional domains, showed impaired autophagic response, mTORC1 independent, upon starvation. Here, impairment of the autophagy/lysosomal pathway was suggested as one of the leading disease mechanisms and highlights the importance of studying a variety of disease related mutations (Manzoni et al., 2013a). Moreover, fibroblasts from patients with *LRRK2 R1441C* and *G2019S* mutations, displayed enhanced basal mitophagy and autophagy (Smith et al., 2016; Su and Qi, 2013; Yakhine-Diop et al., 2014). Increased autophagy with mitochondrial dysfunction in the *G2019S* fibroblasts has been suggested to be activated via increased mitochondrial recruitment of dynamin-related (Drp-1), a protein involved in the mitochondrial fission (Su and Qi, 2013).

3.1.4.3   PARKIN
Fibroblasts from patients with *parkin* mutations have been widely used as a PD cellular model investigating the biochemical, functional and physiological mechanisms implied in the development of the disease (Grünewald et al., 2010; Haylett et al., 2016; Lobasso et al., 2017; Mortiboys et al., 2008, 2013, Rakovic et al.,

2010, 2011; Vergara et al., 2014; Zanellati et al., 2015). Parkin belongs to the Ubiquitin E3 ligases family of proteins involved in the mitochondrial fusion and fission. As an E3 Ubiquitin ligase, Parkin acts in a diversity of cellular functions by modifying substrates and proteins, which leads to protein stability, regulation, modification, localisation and functionality (Panicker et al., 2017).

Defective cytoskeletal proteins in *parkin*-mutant fibroblasts, cause irregular cellular shape and impaired elasticity, via actin regulation (Vergara et al., 2014). *Parkin* mutations impair the cellular bioenergetics status, mitochondrial function, respiration and morphology (Grünewald et al., 2010; Mortiboys et al., 2008; Pacelli et al., 2011) alongside biomechanical and molecular alterations as some of the principal causes of PD (Pacelli et al., 2011; Vergara et al., 2014). *Parkin*-mutant fibroblasts have a CI defect (Mortiboys et al., 2008; Pacelli et al., 2011), defective CI biogenesis and lower ATP production (Grünewald et al., 2010; Mortiboys et al., 2008). However, CI deficiency was inconsistent in other *parkin*-mutant cell lines, where activity remained similar between controls and patients (Grünewald et al., 2009; van der Merwe et al., 2014). Reduced CIV and citrate synthase enzyme were found in *parkin*-mutant fibroblasts (Pacelli et al., 2011). Oxidative stress may also be present in *Parkin* mutant fibroblasts (Grünewald et al., 2010; van der Merwe et al., 2014; Mortiboys et al., 2008, 2013; Pacelli et al., 2011). These defects were present in fibroblasts with *parkin* knockdown, which support reports that the effect is due to *parkin* deficiency (Mortiboys et al., 2008). The peroxisome proliferator-activated receptor gamma coactivator 1 alpha (PGC-1α), a protein with several functions, pathway is dysregulated in *Parkin* deficient fibroblasts. This protein play a role in PD pathology by protecting the cells against oxidative stress and promoting

mitochondrial biogenesis (Pacelli et al., 2011). Resveratrol treatment rescues CI activity, where the rescue effect was suggested to be a mediated-mechanism via CI mitochondrial biogenesis or/and post-transcriptional modifications (Ferretta et al., 2014).

Drug screens performed by Mortiboys et al, 2013, showed that the natural compound ursolic acid, and the licensed drug ursodeoxycholic acid, rescued mitochondrial dysfunction in *parkin*-mutant fibroblasts. Here, enhanced Akt phosphorylation followed by the activation of the glucocorticoid receptor is crucial for the rescue effect (Mortiboys et al., 2013).

Mitofusins (Mitofusin 1 and 2), located in the OMM, maintain the balance between mitochondrial fission and fusion (Schrepfer and Scorrano, 2016). *Parkin*-deficient fibroblasts showed impaired Mitofusin 2 ubiquitination, which was rescued in by overexpressing *Parkin* (Rakovic et al., 2011). Impaired mitochondrial fusion and fission in *parkin*-deficient fibroblasts, but not in partially deficient cells, result upon cellular stress (Mortiboys et al., 2008). Impaired mitophagy has been related to *parkin* loss of function, which alters the PINK1/Parkin mitophagy pathway. Parkin mediated ubiquitination and mitophagy was impeded by ubiquitin-specific protease 15 (USP15), a deubiquitinating enzyme. *USP15* knock-down in *parkin* deficient fibroblasts rescued the mitophagy pathway, suggesting USP15 as new therapeutic target for PD (Cornelissen et al., 2014).

Further research investigated the lipidome profile of *parkin*-deficient fibroblasts. Results showed a reduced phospholipid and glycosphingolipid content

and proportion; whereas high levels of phosphatidylinositol, phosphatidylserine and gangliosides were detected (Lobasso et al., 2017). These results suggested an unknown connection leading to inflammation, defective autophagy, mitochondrial function and morphology.

3.1.4.4 PINK1

After mitochondrial depolarization in *PINK1*-mutant fibroblasts with missense and nonsense mutations, PINK1 accumulates in the mitochondrial membrane and is effective but not essential to induce Parkin mitochondrial translocation upon stress, polarizing and non-depolarizing (Rakovic et al., 2010). Specific mutations alter PINK1 function at different stages. Different mutations can affect in a different manner the mitochondrial membrane potential (MMP) and biochemical properties, where missense mutations appear to be more deleterious (Grünewald et al., 2009). *PINK1* expression and mitochondrial accumulation, but impaired stabilization in the outer mitochondrial membrane (OMM), were found in *PINK1* mutant fibroblasts with missense mutations (See general introduction).

PINK1 deficient fibroblasts displayed reduced *parkin* expression; in addition to a high susceptibility to proteasomal stress upon caspase activation (Klinkenberg et al., 2010). *LRRK2* was found to be dysregulated in *PINK1* mutant fibroblasts and corroborated in iPSC-derived neurons lines with *PINK1* mutations. *PINK1* overexpression in control and mutant cell lines led to *LRRK2* down-regulation; whereas in mutant tissue only, its dysregulation increased *LRRK2* protein levels. It has been suggested that *PINK1* might be inhibiting *LRRK2* at the transcriptional level (Azkona et al., 2016).

A loss of PINK1 kinase activity, possibly secondary to ATP-binding site alteration, leads to proteasomal inhibition and Parkin translocation impairment (Ando et al., 2017; Exner et al., 2007; Siuda et al., 2014). *PINK1* p.G411S heterozygote mutation was described as a variant of risk for PD. Fibroblasts harbouring the mutation showed a partial dominant-negative effect, where mutant PINK1 heterodimerizes with wild-type PINK1, leading to impaired function and reduced kinase activity (Puschmann et al., 2016). Enzymatic kinase activity of PINK1 is important for Ubiquitin phosphorylation in the S65 residue (p-S65-Ub), which was not found in fibroblasts with *PINK1* mutations. Nevertheless, the physiological relevance and pathology remain unknown (Fiesel et al., 2015). Increased glycolysis, mitochondrial function and bioenergetics status, decrease levels of CI and CIV and enzyme activities of the respiratory chain were reported to be inconsistent in fibroblasts with *PINK1* mutations and suggested to be mutation-dependant (Abramov et al., 2011; Azkona et al., 2016; Exner et al., 2007; Grünewald et al., 2009; Lopez-Fabuel et al., 2017; Siuda et al., 2014). Mitochondrial morphology was reported altered in fibroblasts with missense mutations (Grünewald et al., 2009) and in *PINK1* deficient fibroblasts and rescued when wild-type *PINK1* and *Parkin* are transfected, where a protective mechanism against stress has been suggested (Exner et al., 2007).

Ubiquitination of mitofusins was altered in *Parkin* and *PINK1* mutationt fibroblasts, where the suspected leading mechanism is the degradation of the Mitofusins by the Ubiquitin Proteasome System (UPS) (Rakovic et al., 2011).

3.1.4.5 Sporadic PD

Ambrosi et al. reported that the proteasome catalytic subunit 20S and the polyubiquitinated proteins were higher in fibroblasts from sporadic PD patients.

Parkin protein levels were increased in sporadic PD fibroblasts and demonstrated to be the result of proteasomal impairment (Ambrosi et al., 2014). Sporadic PD fibroblasts also showed increased sensitivity to rotenone exposure, enhancing the proteasome mechanisms in response, rather than activate autophagy. Also, basal mitochondrial respiration may be reduced in the sporadic PD patients (Ambrosi et al., 2014; Winkler-Stuck et al., 2004) and after rotenone exposure (Ambrosi et al., 2014; WIEDEMANN et al., 1999).

3.2   Aims and objectiives

TIGAR PD-related mechanisms have yet to be determined in a human cellular model. Pink1 and Parkin share common pathways in mitochondrial function and mitophagy.

In this study, we aimed to determine TIGAR related mechanisms in fibroblasts from sporadic and familial PD patients. By knocking down TIGAR in this model we wanted to assess whether TIGAR knockdown can rescue the mitochondrial dysfunction.

- Characterize *TIGAR* gene expression and protein level in human fibroblasts to determine differences between controls and patients.

- Correlate TIGAR and Parkin protein levels in fibroblasts from controls and patients with *parkin* mutations.

- Optimise effective and efficient transfection in human fibroblasts.

- Achieve effective *TIGAR* knockdown in fibroblasts and assess the effect in mitochondrial function and bioenergetics status in controls and patients with PD mutations.

- Assess TIGAR cellular localisation in fibroblasts from controls and patients with *Parkin* mutations under normal conditions and upon toxin exposure

- Determine whether TIGAR is involved in autophagy in fibroblasts from controls and patients with sporadic PD, which were previously identified to have mitochondrial defect.

3.3   Materials and methods

3.3.1   Cell tissue culture

3.3.1.1   Fibroblasts

Fibroblast cell lines were obtained from two sources; from punch skin biopsies from control healthy individuals, patients with compound heterozygous or homozygous mutations in the *parkin* gene, one *LRRK2*^{G2019S} and two sporadic PD; and Coriell Cell Repositories (Camden, NJ) (Table 3.1). All biochemical and morphological experiments were performed in fibroblasts from passage 7-12.

Patients

Case ID		Mutations		Gender	AB (y)
Parkin patients	P1	202_203delAG (X2)	Del X4	F	48
	P2	202_203delAG (X2)	Del X2	F	38
	P3	202_203delAG (X2)	202_203delAG (X2)	F	39
	ND31618 (P4)	ARG42PROhet	--	F	63
	ND30171 (P5)	ARG42PRO	Del X3	M	54
	ND37731 (P6)	Del X3 40bp	Del X3-X4	F	64
LRRK2 patients	NPF-008(Pt-1)	G2019S manifesting		M	65
Sporadic patients	OB137 (Pt-a)	Sporadic		M	50
	OB194 (Pt-b)	Sporadic		M	61

Table 3.1. *Parkin, LRRK2* mutant and sporadic fibroblasts from patient biopsies. AB, Age at biopsy; y, years; X, exon; Del, deletion; het, heterozygote; hom, homozygous; M, male; F, Female.

Controls		
Case ID	Gender	AB (y)
GM08400	F	37
GM02153	F	40
GM00730	F	45
GM02189	M	63
GM23967	M	52
GM07924	M	63
ND29510	F	55
OB183	M	50
OB153	M	61

Table 3.2. Fibroblasts from healthy controls biopsies. AB, Age at biopsy; y, years; M, male; Female**.**

3.3.1.2   Cell culture

Skin fibroblasts

Primary fibroblasts cells were maintained in T75 cell culture flasks and incubated in a humidified atmosphere with 5% CO2 at 37ºC. Skin fibroblasts from *parkin*, *LRRK2*-mutant patients and matched controls, were grown in Minimum Essential Medium with 10% Biosera Fetal Bovine Serum (FBS), 5 ml (1%) of Penicillin/Streptomycin, 0.1mM non-essential amino acids, 1mM Sodium Pyruvate, 50ug/mL uridine and 1x MEM vitamins. Sporadic PD patients and matched controls, were grown in DMEM (Invitrogen) with 10% FBS (Sigma), 5 ml (1%) of Penicillin/Streptomycin, 1mM Sodium Pyruvate and 50ug/mL uridine. Media was stored at 4ºC and warmed to RT before use for cell culture and experiments. Cell passaging was performed when cells were $\geq$80% confluent. Fibroblasts were sub-cultured at a ratio of 1:3.

Other cell lines

HEK, HeLa and SH-SY5Y cells were grown in DMEM (Invitrogen) supplemented with 10% FBS (Sigma) and 5ml of Penicillin/Streptomycin. Media was stored at 4ºC and warmed to RT before use for cell culture and future experiments.

3.3.2 TIGAR characterisation in human fibroblasts
3.3.2.1 Sample preparation

Cells were pelleted and lysed to obtain proteins without cell debris. At 70-80% confluency, cells were trypsinised and centrifuged at 400rcf for 4 min. The supernatant was discarded and the cell pellet was washed twice with 5mL of PBS. After the washes, the pellet was left to dry for 5 min and stored at -80ºC for future experiments.

3.3.2.2 TIGAR gene expression

To evaluate the TIGAR gene expression, Real-Time qPCR was performed in fibroblasts from healthy age-matched controls and *parkin*-mutant patients. Total RNA was extracted from cell pellets, using QIAGEN RNeasy kit (Qiagen) and cDNA was synthesised using SuperScript III cDNA first strand-synthesis Kit (Invitrogen), following the manufacturer's instructions. Reaction mixtures were prepared at 20nM in a 20μl mix using 10μM of each primer forward and reverse, 10μl 2 X Brilliant III Ultra Fast SYBR master mix (Agilent), DNASe-RNase free water and 1 μl of cDNA added to a well in a 96 well PCR plate (Biorad), sealed with plastic caps. DNA amplification was performed by thermal cycling: initial denaturation at 95ºC for 10 min, followed by 40 cycles of 95ºC for 30 sec and 60ºC for 1 min, then 60ºC for 1 min in a PCR detection system (CFX96 Real-Time System, Biorad). Target gene expression level was normalised using *GAPDH* and *β-actin* as reference genes. Primer sequences are given in Table 3.3.

The gene quantitation was done relative to the reference genes by subtracting the cycle threshold (Ct) of either *β-Actin* or *GAPDH*, from the Ct of *TIGAR* ($\Delta\Delta$Ct=ΔCt gene of interest-ΔCt reference gene). The resulting value of Ct (ΔCt) was then normalised to control, then the exponent of the base 2 ($2^{-\Delta\Delta Ct}$) was calculated to obtain the fold change. This was represented as the fold difference of template for the genes (Table 3.3). Five 5-fold serial dilutions of cDNA template were prepared and their threshold cycle value was determined. The threshold value versus the dilution factor was plotted in a base10 semi-logarithmic graph to obtain a straight line. The correlation coefficient (R^2) was 0.999. Efficiency of the qPCR reactions of all gene primers were calculated based on the slope of the standard curve, where the closer slope to 100% is -3.32. The efficiency of all the qPCR reactions was 95-99%. For the knockdown expression, the normalised relative *TIGAR* gene expression was first calculated for each condition and then normalised against the untreated control. The knockdown percentage was calculated by subtracting the normalised $\Delta\Delta$Ct expression of the control and multiplying by 100. The following formula was used in Excel for the calculation: $(Power(10,-((\Delta Ct_{target}-\Delta Ct_{reference})/3.333)))*100$.

Gene		Sense	Sequence 5'-3'
TIGAR	A[1]	F	CGGCATGGAGAAACAAGATT
		R	TCCTTTCCCGAAGTCTTGAG
	B[2]	F	CCAAAGCAGCCAGGGAAGAGTG
		R	CCGCTTCTTTCAGGATTAGTTGAC
	C[3]	F	CTCCAGTGATCTCATGAGGACA
		R	TGACTCAAGACTTCGGGAAAG
β-Actin		F	GATGCAGAAGGAGATCACTGC
		R	ACTCTGCTGGAAGGTGGAC
GAPDH		F	CTGACTTCAACAGCGACACC
		R	ATGAGGTCCACCACCCTGT

Table 3.3. Primers used for TIGAR characterisation. All primers were used for *TIGAR* gene expression by qPCR [1](Bensaad et al., 2006). Glyceraldehide 3-phosphate deshydrogenase (*GAPDH*); Primer forward (F); Primer reverse (R).

3.3.2.3   Western blotting

TIGAR and Parkin protein determination

Western Blots were performed to compare the levels of TIGAR protein between controls and *parkin*-mutant fibroblasts, and determine whether the different attempts to knock *TIGAR* down using the siRNA antisense strategy had the desired effect. We also looked if there was a correlation between the protein levels of TIGAR and Parkin, involving the pathologic process in PD. The fibroblast cell pellet was re-suspended in Lysis Buffer containing RIPA (Radio-Immunoprecipitation Assay) buffer (Sigma Aldrich, USA) and diluted phosphatase inhibitors (1% v/v) (Sigma Aldrich, USA) and phosphatase inhibitors cocktail (1% v/v) (PIC). Cell lysates were incubated on ice for 30 min and centrifuged at 15871 g at 4°C. Supernatant was collected and total protein concentration was measured using the Bradford assay to select the appropriate amount of protein.

The Bradford assay is a colorimetric assay, which enables the determination of the protein concentration from the cell lysates. A standard curve was obtained by preparing various protein concentrations of Bovine serum albumin (BSA) as standards. BSA concentrations (µg/ml) of the standards used were: 100, 125, 250, 500, 750, 1000, 1200 and 1500. The same volume of three serial dilutions of the samples and standards were loaded in a 96 well plate in triplicate and 250 µl of Coomassie Blue reagent (Biorad) was added to each well. The absorbance was measured immediately at 595 nm and the standard curve was prepared. The protein concentration was calculated using the linear equation (Figure 3.1).
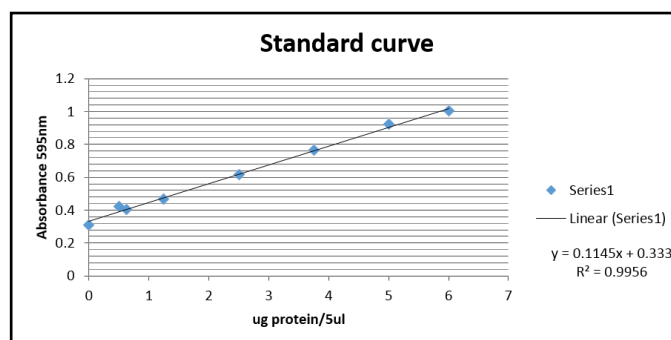
Figure 3.1. BSA standard curve. The absorbance obtained for each standard was plotted in a linear regression graph, where each measurement is theoretical to its concentration. A straight line is obtained and expressed in the equation "y=mx+b"; where y = absorbance (595nm) and x=protein concentration. Each sample represents the average of three replicates. Protein concentration was calculated after the measured absorbance for each sample was obtained

The volume of cell lysate was determined and mixed with 2x Laemmli buffer (4% SDS, 20% glycerol, 10% 2-mercaptoethanol, 0.004% bromophenol blue and 0.125 M Tris HCl). Samples were heated for 3 min at 100°C and centrifuged for 1min at 2347 g. The same amount of protein from each sample was loaded on a 12% polyacrylamide gel (SDS-PAGE) (Table 3.4).

Resolving gel 12%		Stacking gel 5%	
Reagent	Vol	Reagent	Vol
30% Bis/Acrylamide	4 mL	30% Bis/Acrylamide	1.7mL
1.5M Tris HCL / 13.9 mM SDS / pH 8.8	2.5 mL	0.5M Tris HCL pH6.8/ 13.9 mM SDS / pH 6.8	2.5 mL
dH2O	3.5 mL	dH$_2$O	2 mL
10% Ammonium Persulfate (APS)	100 µL	10% Ammonium Persulfate (APS)	50 µL
N, N, N', N -Tetramethyl-ethylenediamine (TEMED)	10 µL	N, N, N', N -Tetramethyl-ethylenediamine (TEMED)	20 µL

Table 3.4. Composition of resolving and stacking polyacrylamide gels.

Gels were assembled in a Mini-PROTEAN Tetra Vertical Electrophoresis cell (Biorad). The pre-stained protein marker (Precision Protein Dual Colour Standard (Biorad)) was loaded, followed by samples into each well. Stacking (separating) gels were run at low voltage (50 V) and running gel at a higher voltage (120 V) in a running buffer (Table 3.5). The process was complete when the dye front ran off the

bottom of the gel. Proteins were transferred applying a wet electrophoretic transfer (Table 3.5) to a PVDF membrane for 1.5 hours at 250 mA.

Buffer	Reagents	Buffer	Reagents	Buffer	Reagents
Running buffer	25 mM Tris	**Transfer buffer**	25 mM Tris	**TBS-T pH 7.6**	150 mM NaCl
	190 mM Glycine		192 mM Glycine		20 mM Tris
	0.1% SDS		20% v/v Methanol		0.1% Tween-20

Table 3.5. Solution and Reagents used for Western Blotting.

The membranes were blocked with 5% non-fat dried milk (Mavel) diluted in TBS-T (Table 3.5), after which, membranes were incubated overnight at 4°C with primary antibodies against TIGAR (Santa Cruz) and Parkin (Cell Signaling) (Table 3.6). Then, membranes were incubated with secondary antibody horseradish peroxidase (HRP) (Table 3.6). Membranes were washed three times in TBS-T at RT for 15 min. Then, membranes were incubated with enhanced chemiluminescence (ECL) in a 1:1 ratio of solution 1 (Luminol Enhancer) and solution 2 (Peroxide solution) for 1 min before imaging. Bands were detected using a G-Box (Syngene). Actin and α-Tubulin were used as loading controls. Quantification was done by densitometry analysis using G-Box Syngene Image software.

Antibodies	Catalogue number	Company	Dilution	Molecular weight (kDa)	Host
Primary antibodies					
Anti-Actin antibody ACTN05 (C4)	ab3280	Abcam	1:1000	42	R
TIGAR antibody TIGAR(G2)	sc-74577	Santa Cruz Biotechnology	1:1000	30	M
Monoclonal anti-α-Tubulin	T9026	Sigma	1:10000	50	M
Monoclonal Parkin antibody	CST-4230*	Cell signaling Technology	1:1000	52	M
Monoclonal Parkin antibody(Prk8)	CST-4211	Cell-signaling Technology	1:1000	50	M
Secondary antibodies					
Anti-rabbit HRP IgG	1706515	Biorad	1:5000	-	G
Anti-mouse HRP IgG	1706516	Biorad	1:10000	-	G

Table 3.6. Antibodies used for TIGAR characterisation and Parkin detection. Goat (G), Mouse (R); Rabbit (R), *discontinued.

3.3.3 Comparison with other common cell lines in research

For future assays in a suitable and different cellular model system, we characterized TIGAR and Parkin protein levels in HEK, HeLa, SHSY-5Y and LUHMES (Lund human mesencephalic). LUHMES cell lysates were provided by Prof. Stephen Wharton's group (SITraN). All cell pellets were prepared as mentioned in sample preparation.

3.3.4 TIGAR immunofluorescence

Immunofluorescence was performed to assess the effects on TIGAR localization and expression after inducing cellular stress. First, we tested different TIGAR antibodies (Table 3.7). Fibroblasts were seeded at 1.3 x 10^4 cells/well in a 24-well plate containing a glass coverslip and grown for 48 hrs. Wells were rinsed with PBS and fixed with 4% paraformaldehyde (PFA) for 10 min. Cells were then rinsed with PBS and permeabilised using 0.3% Triton-X. Followed by incubation with 5% BSA in PBS (Blocking buffer) for 1 hr at RT to block non-specific binding. Cells were then rinsed with PBS and diluted primary antibody (Table 3.7) in blocking buffer was applied to all the wells and incubated overnight at 4ºC. Cells were rinsed with PBS and incubated with fluorescent secondary antibody (Table 3.7) diluted in blocking buffer for 1 hr in the dark at RT.

Antibody	Company	Dilution	Region	Host
Primary antibodies				
Anti-TIGAR antibody. (AB10545) Polyclonal	Millipore	1:500	KLH-conjugated linear peptide that lies in the central region of the protein	R
Anti-TIGAR antibody. (ab 129333) Polyclonal	ABCAM	1:800	Synthetic peptide raised against the 19 aas from a region near the central region of the protein	R
TIGAR Polyclonal antibody (PA5-29152) Polyclonal	Thermo Scientific	1:1500	Synthetic peptide corresponding to a region within C terminal amino acids 220-270 of the protein	R
Anti-TIGAR Antibody (LS-C286858)	LifeSpan Biosciences	1:500		R

Polyclonal				
Anti-TIGAR antibody[1] Monoclonal	(Bensaad et al., 2006)	1:300	Antibody raised against peptide corresponding to aas. 256-270 in exon 6-encoding region of the protein.	M
Anti-TOM20 (FL-145) Monoclonal	Santa Cruz Biotechnology	1:500	Antibody raised against aas 1-145 representing the full length of the protein.	R
Anti-TOM20 Monoclonal	BD Biosciences	1:1000	Antibody raised against aas. 47-145	M
Secondary antibodies				
Alexa Fluor 555[a]	Invitrogen	1:1000	γ-IgG H and L	R
Alexa Fluor 488[b]	Invitrogen	1:1000	γ-IgG H and L	M

Table 3.7. Antibodies used for TIGAR immunofluorescence. Mouse (M); Rabbit (R); aa., aminoacids; gamma immunoglobulins (γIgG). Antibody donation from Dr. Karen Vousden (Bensaad et al., 2006).

3.3.5   RNAi mediated TIGAR knockdown: siRNA transfection

3.3.5.1   Transfection efficiency

Transfection reagents

For transient *TIGAR* siRNA knockdown, we first assessed the transfection efficiency using different reagents and cellular densities in order to achieve the best knockdown effect. Lipofectamine 2000 (Invitrogen) is a cationic liposome formulation, which permits the introduction of the genetic material by cell membrane electrostatic repulsion. EndoFectin™ Max (GeneCopoeia) and DharmaFECT 1 and 3 (Dharmacon, GE) are both cationic lipid-based transfection reagents. These transfections reagents form complexes with nucleic acids and facilitate their delivery into a wide range of commonly used mammalian and primary cell lines.

Transfection procedure

Initially, a suitable dose and concentration was assessed in a 96-well plate format in order to obtain the highest efficiency and least toxicity. After fibroblasts were 70% confluent, one day prior to transfection, cells were seeded at $2\text{-}5\times10^3$ cells/well in 100 µl antibiotic-free media in a 96 well plate.

On the day, transfection complexes were prepared using Opti-MEM® I to dilute transfection reagent, and FITC labelled scramble siRNA (Ambion) control separately. Each mixture was incubated for 5 min at RT. The diluted amounts for each reagent are detailed in the (Table 3.8). Then, mixtures were gently mixed and incubated for 10 min at RT. Opti-MEM was added to the mix for a final volume of 100µl of transfection medium. Cell culture medium was removed from the plates and replaced with transfection medium for each transfection reagent/siRNA complex.

Transfection reagent (TR)	Tube 1: diluted TR		Tube 2: diluted siRNA	
	Volume of TR	Opti-MEM®	Volume of 20µM siRNA[a]	Opti-MEM®
Lipofectamine 2000	0.1, 0.2, 0.5, 0.75 µl	9.5 µl	0.3 µl	9.5 µl
DharmaFECT 1	0.1, 0.3, 0.5 µl	9.5 µl		9.5 µl
DharmaFECT 3	0.1, 0.3, 0.5 µl			
Endofectin™ Max	0.2, 0.35, 0.5 µl	5 µl		5 µl

Table 3.8. Conditions for transfection of fibroblasts for each Transfection Reagent. Reagents tested at different concentrations for cell toxicity and transfection efficiency. *Final concentration 30nM in 200µl of serum-free media

Media was replaced 6 hrs after transfection to avoid cell toxicity and obtain the best transfection efficiency, except for Endofectin.

Self-transfecting Accell siRNA

Dharmacon Accell siRNA® transfection system (Dharmacon, GE) is a new method designed for delivery into cells difficult to transfect. The system uses a naked and chemically modified siRNA, without requiring the use of transfection reagents, virus or any other instrument used in standard RNAi methods. Therefore, lower toxicity without secondary viral effects can be achieved. In the present study, we tested this new method and compare it with conventional RNAi methods here assessed.

126

Accell siRNA transfection in fibroblasts, was optimised by assessing the effect in human fibroblasts treated with positive and negative controls. Negative controls (Table 3.9) are non-sequence-specific siRNAs with minimal targeting of known genes in human cells and should not have a specific cellular response. Negative controls are useful for siRNA delivery assessment and to determine the effect with siRNA-treated samples. Positive siRNA controls (Table 3.9) target highly expressed and non-essential cellular genes; therefore, viability is not affected when they are knocked-down. Positive controls are useful to optimise experimental conditions.

Accell siRNA preparation

Accell siRNAs work at 1µM, which is a higher concentration compared to standard siRNA. First, 5x siRNA buffer (Dharmacon, GE) was diluted in 4 volumes of RNase-fee water to obtain 1x siRNA buffer. All siRNAs (Table 3.9) were then diluted and prepared at 100µM in the 1x siRNA buffer, pipetted then 3-5 times up and down avoiding bubbles. Finally, the solution was placed in a shaker for 90 min at 37ºC, centrifuged, collected, aliquoted and stored at -20ºC for future experiments.

Controls	Company / catalogue number	Unit size	Description
Accell Non-targeting siRNA #1	Dharmacon / D-001910-01-05	5 nmol	Specific negative control, without targeting any gene product.
Accell cyclophilin B	Dharmacon / D-001920-01-05		Specific positive control for silencing.usually known to achieve high levels of knockdown
Accell GAPD siRNA	Dharmacon / D-001930-01-05		
Accell red Non-targeting siRNA (Dy-547-labelled)	Dharmacon / D-001960-01-05		Assessment of siRNA uptake by fluorescent microscopy to dye-labelled siRNA. Filter Cy3 (Rhodamine)

Table 3.9. Accell siRNA controls.

Accell siRNA delivery

Briefly, control fibroblasts were seeded at different densities from 2.5-4 x 10^3 cells/well in 100µl Accell Delivery Media and incubated overnight at 37ºC with 5% CO_2. Then, 24 hrs after plating, growth media was removed and replaced with 100µl

Accell Delivery media containing with or without 1μM siRNA for each control (Table 3.9). Cells were incubated then for 48hrs; after which, medium was replaced with glucose-free galactose medium and further incubated to assess ATP at 96 and 72hrs. mRNA and protein knockdown were assessed at 72hrs.

Cytotoxicity was assessed for all the RNAi methods. First, with ATP assays measurements (See Section 3.3.6.1) at ~70% confluency and viability for: a) each transfection reagent alone; b) with Accell siRNA treated positive and negative controls. A comparison of each condition was performed by testing a range of cellular densities. Efficiency was then assessed by using either FITC scramble siRNA or Accell Red Non-targeting siRNA (Dharmacon, GE Healthcare) then imaged using the InCell Analyzer 2000 (GE Healthcare) and analysed with the InCell Developer Toolbox 1.9.2 Software. The image analysis was performed by image segmention to find nuclei and siRNA fluorescent signal according to intensity, shape and size per cell.

Culture Vessel	Surf. Area (cm^2)	Cell seeding density	Vol. of plating medium	Dilution medium of transfection	siRNA 20 μM	Lipofectamine 2000
96-well plate	0.32	3.5×10^3	200 μl	2 x 100 μl	0.2 μl	0.1-0.75 μl
6-well plate	10	1.6×10^5	2.5 ml	2 x 500 μl	1.5 μl	3.5 μl
T25 flask	60	3×10^6	4 ml	2 x 1 ml	6 μl	20-30 μl

Table 3.10. Scaling up and down transfections. Example of vary amounts of transfection reagents, medium, cells and nucleic acids required in different tissue culture formats.

3.3.5.2 TIGAR siRNA sequences

TIGAR expression was inhibited by transfection with small interfering RNAs (siRNAs) against *TIGAR* from 3 sources: TIGAR siRNA (h) (Santa Cruz); ON-

TARGETplus Human C12orf5 siRNA SMARTpool (Dharmacon, GE Healthcare) and SMARTpool from Accell siRNA (Dharmacon, GE Healthcare) (Table 3.11).

To knock down *TIGAR* expression and avoid off-target effects, transfection conditions were modified to assess increasing concentrations of siRNAs. We first tested the siRNA pool targeting the exon 6 within the 3'UTR region to check *TIGAR* know-down efficiency.

siRNA against TIGAR	Target specific sequence
Santa cruz biotechnolology TIGAR siRNA (h)	
sc-76662A	Sense: CCACUUGCUUCUUAUCUAAtt Antisense: UUAGAUAAGAAGCAAGUGGtt
sc-76662B	Sense: GGAAGCACAUAAAGUAAGAtt Antisense: UCUUACUUUAUGUGCUUCCtt
sc-76662C	Sense: CCAUCAAUUUGGAAGUACAtt Antisense: UGUACUUCCAAAUUGAUGGtt
Dharmacon ON-TARGETplus Human C12orf5 siRNA - SMARTpool	
siRNA J-020597-09	GUAGAAGGCAAAGCGCUAA
siRNA J-020597-10	GUUAAUUCAGACAGCGGUA
siRNA J-020597-11	GCAUGGAAUUUUGGAGAGA
siRNA J-020597-12	GUAUGAACCUACAGGAUCA
Dharmacon Accell SMARTpool siRNAC12orf5	
siRNA A-020597-13	CUAACAUGUUUUACGUAUA
siRNA A-020597-14	GUAUGAACCUACAGGAUCA
siRNA A-020597-15	UCUUAUUAUUUUAUGGUUA
siRNA A-020597-16	GUAUAUCCCUGCAAUUUUA

Table 3.11. TIGAR siRNA pool sequences. The complete target sequences from each of the siRNA contained in each pool from the 2 different sources used in this study.
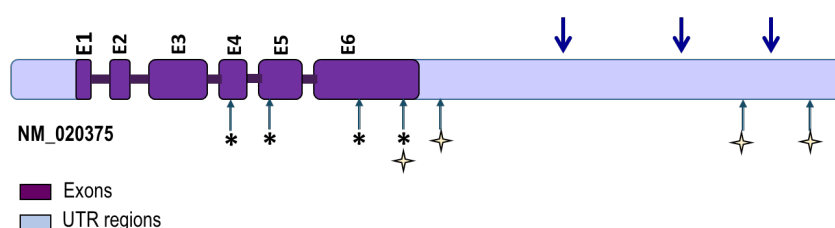
Figure 3.2. *TIGAR* gene schematic representation. The 6 predicted exons of *TIGAR* gene are in represented in purple and the UTR regions are represented in violet. The targeted regions from the first siRNApool against *TIGAR* (Santa Cruz) act are in the 3' UTR region of exon 6 (arrows). The second SMARTpool siRNA against *TIGAR* (Dharmacon) act within the exons 4, 5 and 6 (asterisks). The third Accell SMARTpool siRNA against *TIGAR* (Dharmacon) act within the exon 6 and its 3' UTR region (stars).

Levels of *TIGAR* mRNA were quantified and normalised to β-actin and GAPDH. For western blots, cells were collected from 10 cm petri dishes, after 48hrs of transfection. We then check whether the second siRNA SMARTpool, targeting the exons 4, 5 and 6, had the desired knock-down effect in human fibroblasts. Western blots were performed after 48 hrs of transfection from T25 flask.

3.3.6 Mitochondrial function assessment

3.3.6.1 ATP assays

Cultured fibroblasts typically generate their ATP through glycolysis if grown in glucose-rich medium. When the medium is changed to galactose, they rely on the oxidative phosphorylation pathway to produce ATP (Mortiboys et al., 2008). The ATP assays were performed over 3 consecutive passages as biological triplicates. Galactose media components: DMEM without glucose (Invitrogen) suplemented with 0.9 mg/ml galactose, 10% FBS (Sigma), 5 ml (1%) of Penicillin/Streptomycin, 1mM Sodium Pyruvate, 1X MEM vitamins and 50ug/mL uridine. After reaching 70-80% of confluency, cells were trypsinised and re-suspended with 1 mL of media. Cells were counted by taking 10 µl of cell suspension and using a haemocytometer. Cells were resuspended in 200 µl of normal glucose or galactose media and seeded at a density of $2.5-5x10^3$ per well into 96-well plates according to the assay. ATP cellular level was measured using the ATPlite^{TM} Luminescence Assay System (Perkin Elmer Inc).

ATP production was assessed under different conditions. 24 hrs after of plating, media was exchanged for glucose-free galactose media. Cells were further incubated for 24 or 48 hrs. Reagents were warmed to RT before starting the assay. Lyophilised substrate was reconstituted with 25 mL of substrate buffer solution and gently agitation. Cells were removed from the incubator and media aspirated. In

order to remove any remaining media, 2 washes with 100 µl of PBS were performed, after which 100µl of PBS was added with 50 µl of mammalian cell lysis solution per well and the plate was placed on a plate shaker at 700 rpm for 5 min. This allows cells to lyse fully and to stabilise ATP levels. Then, 50 µl of substrate solution was added and plate was shaken for further 5 min at 700 rpm. The plate was then left to adapt to the dark for 10 min. and assessed using a FLUOstar Omega microplate reader (BMG LABTECH) at 520 nm, Gain 3600 5% adjustment on luminescence mode.

3.3.6.2   CyQUANT measurement

Cell density was measured with CyQUANT Cell Proliferation Assay Kit (Life technologies, USA). To prepare the HBSS buffer 1x, the 5x HBSS buffer was diluted with deionised water. The 1x dye binding solution was prepared by adding CYQUANT dye reagent (1:500 dilution of stock reagent provided) to the 1x HBSS buffer. After ATP was measured, 50 µl of prepared dye solution were added per well and incubated for 1 hr at 37ºC. The fluorescence was measured at 480/530 nm Ex/Em using a FLUOstar Omega plate reader. The normalised data was obtained when the total ATP was divided by the CyQUANT measurement per well in triplicate. Averages from controls were taken as a 100% and the ratio corresponding to patients was calculated.

3.3.6.3   Seahorse assays: Oxygen consumption (OCR) and extracellular acidification rates (ECA) measurements.

PD-mutant fibroblasts and controls

The Seahorse XF24 Analyzer (Seahorse Bioscience) was used to assess the intact cellular endogenous respiration rates and glycolysis at the same time. Mitochondrial respiration was measured as the rate of oxygen consumption (OCR) and glycolysis by the extracellular acidification (ECAR). Basal OCR and ECAR were measured under basal conditions and upon sequential administration of

mitochondrial inhibitors: oligomycin, Carbonyl cyanide m-chlorophenyl hydrazine (CCCP), rotenone and antimycin A (Table 3.12). ATP-linked respiration was obtained from the difference between OCR at baseline and respiration after oligomycin injection. Mitochondrial OCR is measured by the difference of OCR after antimycin A addition and basal OCR. Oxygen consumption due to proton leak was obtained from the difference between antimycin A and oligomycin. Maximal OCR is the measurement resulting from OCR after CCCP administration, subtraction from OCR induced by CCCP. Spare respiratory capacity is obtained by the difference between maximal OCR and basal OCR. The obtained difference OCR after rotenone and antimycin A administration was measured as Non-complex I. Coupling efficiency was obtained from the fraction of ATP synthesis OCR divided by basal mitochondrial OCR. The respiratory cell ratio (RCR) was calculated by dividing maximal OCR by oligomycin-insensitive OCR.

The seahorse assays represent two sets of experiments. First, mitochondrial respiration OCR and ECAR were assessed in two controls and two *parkin*-mutant fibroblasts in triplicate. Second, TIGAR knockdown effect was performed in one control and one *LRRK2*^{G20192}-mutant fibroblasts.

Seeding cells in XF24 Cell Culture Microplates

Seahorse culture plates were prepared by coating with gelatine 48 hrs before plating, covered and stored at 4° C overnight. Seahorse plates were set up 24 hrs previous the assay. Gelatine was removed from all the wells and then rinsed with sterile dH$_2$0. All liquid was removed carefully from the plate and left to dry. Cells were seeded at 3.5 x 10^4 cells/well in 200 µl of galactose media in a 24-well Seahorse culture plate. Cells were placed in the incubator for 1-2 hrs, to let cells to

attach to the plate. Once cells were attached, 300 μl of galactose media was added. Plate was incubated at 37° C overnight.

XF assay media preparation

XF assay media was prepared 24 hrs before assay. 48.5μl of XF DMEM media was aliquoted and heated to 37° C; followed by addition of 0.5 ml of 0.1g/ml of glucose, 0.5 mL of 2-mM glutamine and 0.5 μl of 1-mM Sodium Pyruvate. XF DMEM Media pH was adjusted to 7.4 by diluting NaOH, passed through a sterile filter and stored at 4°C overnight.

Sensor cartridge hydration

The sensor cartridge contains a set of probes, which are important to detect pH and O_2 changes. The day before the assay, XF Flux plate was prepared by: 1) removing the sensor cartridge from the utility plate, 2) 1 ml of calibrant solution was added to each well of the utility plate and, 3) return sensor cartridge onto the utility plate and sensors submerged in XF calibrant solution. Plate was incubated without CO_2 at 37° C overnight.

Running XF assay

On the day, the XF assay media was warmed up to 37° C. Media from the blank wells was removed and replaced with 100μl assay media, which served as guidance. Media contained in wells with cells was removed leaving only 100μl by using guides in blank wells. This was followed by 900μl of XF assay media careful administration to the top of each well, without disturbing the cellular layer. Finally, 900 μl of media was again removed and replaced with 575 μl of fresh XF assay media. Seahorse culture plates were then placed at 37ºC without CO_2 for 1 hr to allow temperature and O_2 calibration.

Loading the XF24 Cartridge plate with compounds

During Seahorse culture plate incubation, the XF24 Cartridge plates were set up with the mitochondrial inhibitors drugs listed in Table 3.12. The drugs were injected sequentially in the injection ports (A-D) to determine the OXPHOS function. The XF24 Cartridge plates were carefully transferred to the Seahorse XF24 flux analyser to allow calibration before the assay. XF24 Cartridge plates were then replaced with XF24 Cell culture plates to run the assay. Each OCR measurement consisted of: 3 min mixing; 2 min wait time and 3 min of continuous measuring of O_2 levels. Basal OCR and ECAR were obtained previous to the addition of Oligomycin, CCCP, Rotenone and Antimycin A. The effect on the mitochondrial respiration and ECAR was measured for 3 min for each component.

Cellular normalisation

For normalisation after cells had been analysed in the Seahorse, Cyquant reagent (1:500) was added to the wells and incubated without CO2 for 30 min. Normalization was performed by nuclear count after imaging fluorescent nuclei using the Incell Analyzer 2000 (GE Healthcare) and analysed with the InCell Developer Toolbox 1.9.2 Software.

Injection	Compound	Action	Assay Conc (µM)	Injection Conc (µM)	Stock Conc (mM)	Dilution Factor	Vol into 3mLs (µL)
A	Oligomycin	Inhibit CV	0.5	5	10	1:2000	1.5
B	CCCP	Uncoupler	2.5	25	10	1:250	7.5
C	Rotenone	Inhibit CI	0.5	5	2	1:250	7.5
D	Antimycin	Inhibit CIII	0.5	5	2.5	1:200	6

Table 3.12. Mitochondrial inhibitors used in this study. Carbonyl cyanide 3-chlorophenylhydrazone (CCCP); complex I (CI); complex III (CIII); complex V (CV); Concentration (Conc). All compounds were diluted in XF Assay media before being loaded in the sensor cartridge.

3.3.7 *TIGAR* knockdown effect in fibroblasts

Transfection conditions and efficiency of RNAi mediated *TIGAR* knockdown were optimised and assessed in control fibroblasts. Cells were transfected with either 30nM siRNA *TIGAR* or Scramble siRNA using Lipofectamine 2000. Mitochondrial respiration and glycolysis was assessed in the knockdowns after 48 hrs using the Seahorse XF24 Analyzer to measure the OCR and ECAR in the derived fibroblasts from one control and one *LRRK2^{G2019S}* patient. Normalisation was done by nuclei count.

3.3.8 Cellular stress: Rotenone toxic exposure

One hypothesis of the causes leading to neuronal cell death in PD suggests an inhibition of the mitochondrial CI activity. One of the important inhibitors of mitochondrial CI, currently used in PD research, is rotenone. In order to assess the effect on TIGAR expression and cellular localisation upon cellular stress, cells from controls and *parkin*-mutant fibroblasts were treated with 25nM rotenone. We assessed four different conditions: 1) glucose only, 2) glucose with rotenone, 3) galactose only and, 4) galactose with rotenone. Cells were seeded at 1.2×10^4 cells/well in a 24-well plate containing a glass coverslip. Media was removed from wells and replaced with: normal MEM glucose media, normal MEM media with 25nM rotenone, galactose media and galactose media with 25nM Rotenone. Cells were exposed for 48 hrs and fixed with 4% PFA as described earlier (*TIGAR immunofluorescence*) for immunofluorescence. We used two different TIGAR antibodies and compared the results. Primary visualization was performed using a Leica SP5 confocal microscope system with a x40/1.3 oil immersion objective lens. TIGAR (Leica/566) and TOM20 (Leica/488), within a high resolution (246.27 x 246.27 microns per image, 1024 x 1024 pixels) z-stack made up of images 0.5 µm

intervals. Then, images were captured in a wide-field system using a Nikon inverted T1 microscope with dual camera. Eight Images per field per condition per patient were captured and deconvolution software was used to improve stacked images (Z-sectioning). This avoided the need of lasers usually employed in confocal imaging. The quantitative colocalisation analysis of TIGAR and Tom20 signals was assessed with ImageJ and JACoP plug-in (BOLTE and CORDELIÈRES, 2006) to determine:

a) *Pearson's coefficient*; which measures dependency of pixels in dual-channels and plotting two images values in grey against each other. It estimated the approximation between the signals. It ranges from 1 (complete positive colocalisation) to -1 (no colocalisation)

b) *Mander's coefficients;* which is based on Pearson's correlation coefficient where intensity average is taken out of the mathematical expression. It ranges from 0 (no overlap) to 1 (complete positive colocalisation).

Both coefficients are used to measure the linear correlation of two variables (Pearson´s) and the proportion of intensity coming from fluorescent pixel colocalising signals coming from different colour channels (Mander´s) (Dunn et al., 2011). Since both coefficients were good indicator of concurring signals; TIGAR and Tom20 signals were used to assess colocalisation.

3.3.9 TIGAR and autophagy

We then investigated whether TIGAR is implicated in autophagy and/or mitophagy. Current treatments for mitophagy activation use high doses of carbonyl cyanide *m*-chlorophenylhydrazone (CCCP), which is a mitochondrial uncoupler. CCCP promotes the dissipation of the mitochondrial membrane potential, which promotes mitochondrial PINK1 accumulation with subsequent Parkin recruitment. Finally, it is believed the process promotes mitochondrial clearance by mitophagy.

Bafilomycin in a lysosomal inhibitor, which acts by inhibiting the vacuolar type H(+)-ATPase and prevents lysosomal acidification. Here, we assessed the effect in fibroblasts from two controls and two patients with sporadic PD.

Each treated cell lysates were provided by MSc Rebecca Burger. Shortly, provided cell lysates were from four different pre-treatment conditions for 4 hours: a) untreated, b) 100nM bafilomycin, c) 10µM CCCP and, c) CCCP with bafilomycin. All cell pellets were then assessed by WB for TIGAR protein levels as described earlier (*TIGAR and Parkin protein determination*) and compared between controls and patients.

3.3.10 Statistical Analysis

Unless specifically stated otherwise, experiments were done in triplicate and values were expressed as means and Standard Deviations (SD). The data was analysed using the software GraphPad Prism 7. Statistical test included: unpaired t-test and non-parametric tests with Bonferroni correction (Mann-Whitney U), and ANOVA with multiple comparisons. For TIGAR colocalisation analysis, Image J software and JaCoP plug-in were used for Pearson's and Manders coefficients.

3.4 Results

3.4.1 TIGAR gene expression

First we investigated *TIGAR* gene expression in primary fibroblasts of the two groups. *TIGAR* mRNA levels were compared between the six patients with *parkin* mutations (P1-P6) and six matched healthy controls (C1-C6). Overall, there was no significant difference, with *TIGAR* expression being similar in the *parkin*-mutant patient fibroblasts and controls (Figure 3.3). *TIGAR* mRNA levels were slightly higher in the patients (mean=1.217, SD=0.1) compared to the controls (mean=1.067, SD=0.81), but this did not reach statistical difference (Mann-Whitney U, *P*=0.3095) (Figure 3.3).
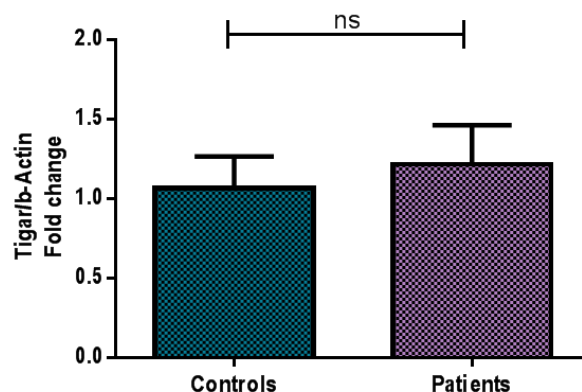
Figure 3.3. *TIGAR* gene expression in fibroblasts from controls and patient fibroblasts with *Parkin* mutations. Bar graphs represent the fold change of TIGAR expression between controls (mean=1.067, SD=0.81, n=6) and patients (mean=1.217, SD=0.1, n=6). Analysis showed no statistical difference between controls and patients (Mann-Whitney U, *P*=0.3095). Results are expressed as the mean +SD of samples from 3 independent experiments.

3.4.2 TIGAR and Parkin protein level

We then investigated TIGAR protein expression in primary fibroblasts from controls and *parkin*-mutant patients. Initially, controls were used to optimise the protein amount and antibody concentration for the group comparison. Next, we investigated whether TIGAR protein levels were different between controls (mean=0.7483, SD=0.1552, n=6) and *parkin*-mutant patients (mean=0.8386,

138

SD=0.297, n=6). No significant difference was found between controls and patients when a group comparison was undertaken (Mann-Whitney U, *P*=0.8182). However, one *parkin*-mutant fibroblast cell line (P1) had an almost 2-fold overexpression (Figure 3.4 b) compared to the controls and the other *parkin*-mutant patient lines (Figure 3.4 a-b). Therefore, we decided to investigate whether Parkin protein levels were correlated to TIGAR protein levels in the fibroblast lines.
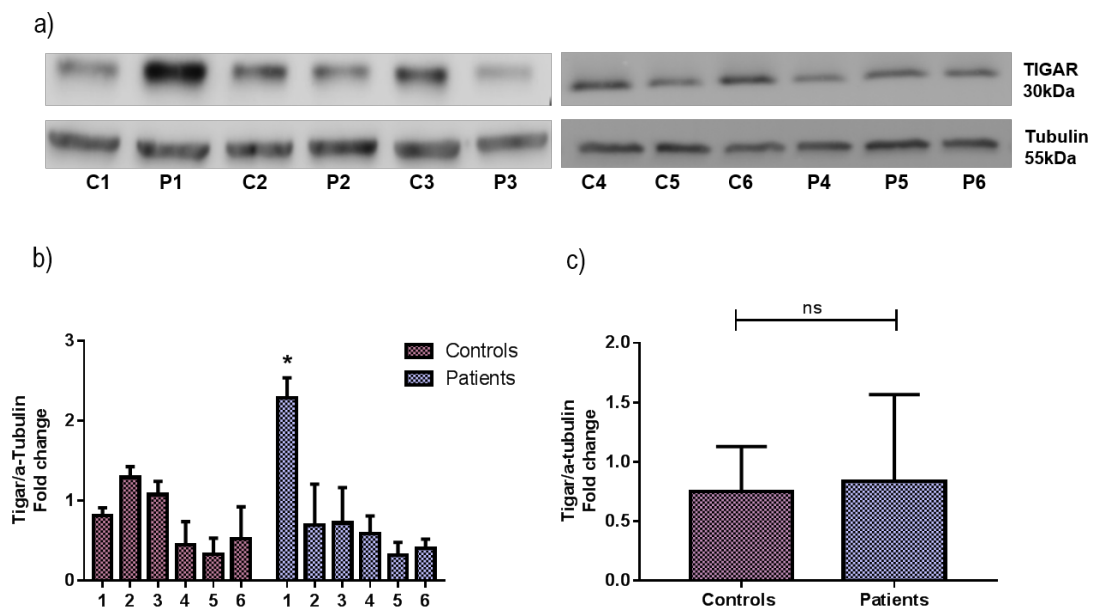
Figure 3.4. TIGAR protein levels in fibroblasts from controls and patients with *Parkin* mutations. WB image (a) and densitometry analysis (b, c) using Tubulin as loading control. b) One *patient*-mutant patient line showed almost a 2-fold increased TIGAR protein levels compared to the controls and other *parkin*-mutant patient lines (2-way ANOVA, *P*=0.0334). c) However, group analysis showed no difference between controls (n=6) and patients (n=6) (Mann-Whitney U, *P*=0.8182). Bars represent the mean values ±SD, from three independent experiments.

Parkin protein levels were quantified in primary fibroblast cell lines from the six controls and six patients with *parkin* mutations by performing WB. As shown in (Figure 3.5), Parkin and b-actin protein levels were determined and quantified by densitometry. WB analysis demonstrated that Parkin was significantly decreased in one patient (P1) (Figure 3.5 a-b), compared with the rest of controls and patients,

where Parkin protein levels remained similar between them (Figure 3.5 a-b). However, when analysed all the controls (mean=0.5922, SD=0.1912, n=6) and patients (mean=0.5018, SD=0.179, n=6), there was no statistical significance (Mann-Whitney U, *P*=0.9372) (Figure 3.5 c).
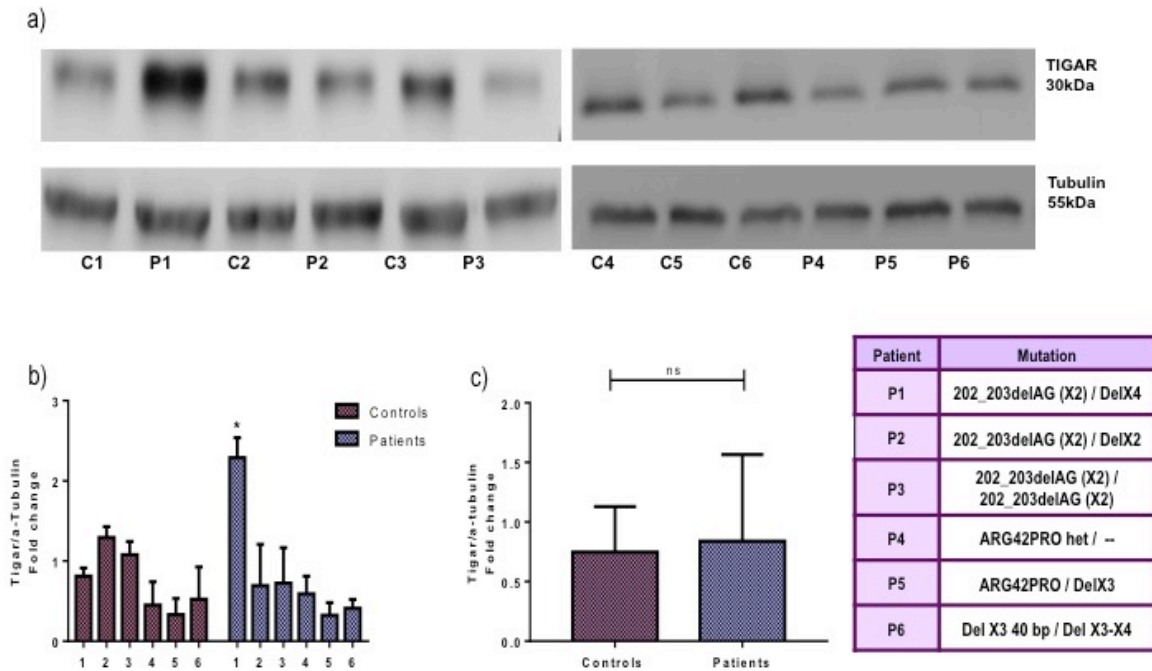
Figure 3.5. Parkin protein in fibroblasts from controls and patients with *parkin* mutations (right bottom panel). WB image (a) and densitometry analysis (b) using b-actin as loading control. b) Parkin protein levels between controls (mean=0.5922, SD=0.1922, n=6) and patients (mean=0.5018, SD=0.179, n=6) were variable. c) No statistical difference was found between *parkin*-mutant patients and controls (Mann-Whitney U, *P*=0.8182). Bars represent the mean values +SD, from three independent experiments.

Only one patient (P1) showed increased levels of TIGAR protein correlated with reduction of Parkin levels. Since controls and fibroblasts have low similar Parkin levels, only TIGAR increase in P1 remained significant. In order to assess whether TIGAR high levels have a pathological effect in parkin deficiency, further functional analysis remain to be performed in this patient. Due to the limited availability of the tissue, these assays could not be performed in the present study.

	TIGAR	PARKIN	TIGAR/PARKIN
C1	0.8124	1.1715	0.6935
C2	1.29344	1.0726	1.2059
C3	1.07753	0.7559	1.4254
C4	0.4512	0.2003	2.2521
C5	0.33022	0.1309	2.522
C6	0.52485	0.2216	2.368
*P1	2.28872	0.2377	9.6291
P2	0.69352	1.2688	0.5466
P3	0.72406	0.6095	1.1879
P4	0.59001	0.6209	0.9502
P5	0.32303	0.0614	5.2599
P6	0.41231	0.2121	1.9436
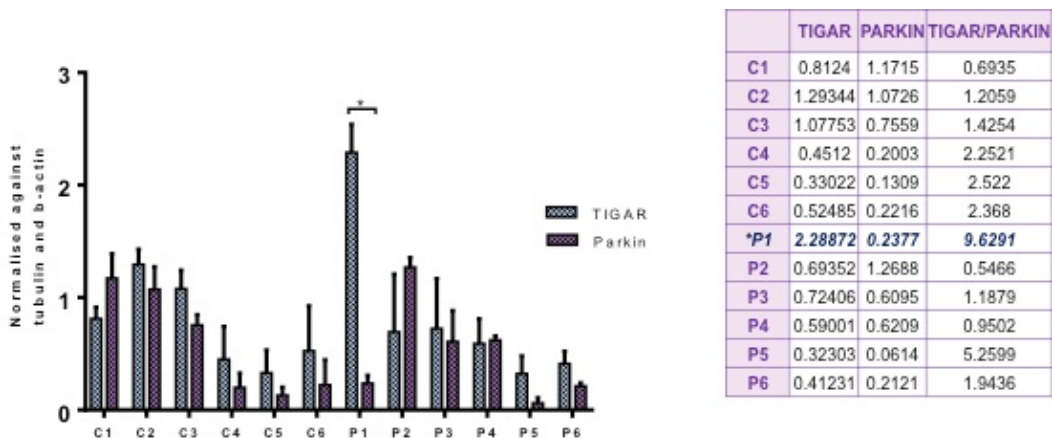
Figure 3.6. TIGAR and Parkin protein levels in fibroblasts from controls and parkin-mutant patients. Correlation of TIGAR and Parkin protein levels in controls and parkin-mutant patient lines. Only one patient demonstrated TIGAR protein increased levels correlated with reduced Parkin levels (2-way ANOVA, ****$p<0.0001$). The ratio of TIGAR and Parkin protein levels is highlighted in the right panel. Bars represent the mean$\pm$SD from three independent experiments.

3.4.3   Assessment of mitochondrial function in Fibroblasts

3.4.3.1   ATP assays

First, total cellular ATP levels were assessed in fibroblast cell lines from six controls and six parkin-mutant patient lines. Transfection optimisations were performed in two control and two *parkin*-mutant cell lines. Then, we assessed *TIGAR* knockdown effect in the mitochondrial function in one *LRRK2^{G2019S}* mutant fibroblasts and matched control.

ATP levels were assessed in four controls and four *parkin*-mutant cell lines. Reduction of ATP cellular levels was seen in four patients: P1 (48%, **P=0.007), P4 (33%, P=0.108), P5 (48%, **P=0.009) and P6 (37%, *P=0.0279) compared to matched controls. Overall, a significant decrease in the ATP production was seen in the *parkin*-mutant fibroblast group by ~41.5% (Mann-Whitney U, *P=0.0286) (Figure 3.7). We then determined whether the ATP defect was associated to a defect in the bioenergetics status. The assays were then performed in two of the six *parkin*-mutant patient lines (P4-P6) due to the limited availability of the other cell lines.

141
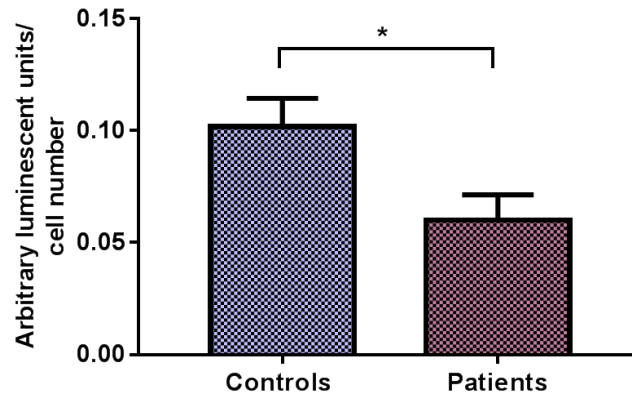
Figure 3.7. ATP assays in controls and *parkin* patients. ATP cellular levels were compared between four controls and four patients. Cellular ATP levels are reduced by ~41.5 % in parkin-mutant patient lines compared to controls (Mann-Whitney U, *P=0.0286). Bars represent the mean and $\pm$SD from three independent experiments.

3.4.3.2 Mitochondrial respiration. Seahorse assays

Controls and patients

Parkin-mutant patients

A great proportion of cellular ATP is produced by mitochondrial oxidative phosphorylation, which plays an important role in cellular survival. To assess the mitochondrial bioenergetics in *parkin*-related PD, we measured the mitochondrial respiration (OCR) and acidification (ECAR) using the Seahorse XF24 Analyzer.

Bioenergetic parameters were calculated in two controls (C4-C5) and two *parkin*-mutant patient lines (P4-P5). Previous basal ATP assays from both patients showed a significant reduction, thus we assessed if it was related to a defect in the bioenergetics status, mainly in the respiration committed to ATP synthesis. The obtained respiratory measurements were normalised to cell number and are illustrated individually (Figure 3.8). Individual data showed a similar trend in controls and patients in all the measurements (Figure 3.8).

	CONTROLS	PATIENTS	*P* value
NORMALISED COMPONENTS OCR			
Baseline	C4=0.032 $\pm$ 0.003	P4=0.0294 $\pm$ 0.001	0.928
	C5=0.042 $\pm$ 0.008	P5=0.035 $\pm$ 0.004	0.547
Mitochondrial OCR	C4=0.023 $\pm$ 0.003	P4=0.022 $\pm$ 0.003	0.997
	C5=0.034 $\pm$ 0.006	P5=0.027 $\pm$ 0.004	0.586
Proton leak	C4=0.006 $\pm$ 0.0007	P4=0.005 $\pm$ 0.002	0.995
	C5=0.009 $\pm$ 0.002	P5=0.010 $\pm$ 0.005	0.995
ATP-linked	C4=0.016 C4 $\pm$ 0.003	P4=0.017 $\pm$ 0.001	>0.999
	C5=0.024 $\pm$ 0.004	P5=0.017 $\pm$ 0.004	0.440
MRC	*C4=0.120 $\pm$ 004*	*P4=0.046 $\pm$ 0.006*	****<0.0001*
	C5=0.071 $\pm$ 0.015	P5=0.083 $\pm$ 0.014	0.058
SRC	*C4=0.088 $\pm$ 0.001*	*P4=0.017 $\pm$ 0.004*	****<0.0001*
	C5=0.029 $\pm$ 0.0009	*P5=0.047 $\pm$0.010*	***0.001*
Non-Complex I	C4=0.001 $\pm$ 0.0004	P4=-0.0002 $\pm$ 0.0007	0.975
	C5=0.002 $\pm$ 0.0009	P5=0.002 $\pm$ 0.0005	>0.999
Coupling efficiency	C4=0.726 $\pm$ 0.015	P4=0.777 $\pm$ 0.089	0.931
	C5=0.726 $\pm$ 0.02	P5=0.626 $\pm$ 0.173	0.674
RCR	*C4=27.111 $\pm$ 6.117*	*P4=10.081 $\pm$ 3.822*	*0.022*
	C5=9.844 $\pm$ 3.823	P5=14.599 $\pm$ 9.190	0.668
NORMALISED COMPONENT ECAR			
Baseline	*C4=0.001 $\pm$ 0.0004*	*P4=0.003 $\pm$ 0.0003*	*0.0165*
	C5=0.004 $\pm$ 0.0008	*P5=0.002 $\pm$ 0.0006*	***0.004*
MC	*C4=0.002 $\pm$ 0.0009*	*P4=0.005 $\pm$ 0.0002*	****<0.0001*
	C5=0.007 $\pm$ 0.001	*P5=0.002 $\pm$ 0.0006*	****<0.0001*
SC	C4=0.0005 $\pm$ 0.0004	P4=0.002 $\pm$ 0.0004	0.059
	C5=0.003 $\pm$ 0.0006	*P5=0.001 $\pm$ 0.0003*	***0.001*

Table 3.13. Bioenergetics parameters from two parkin-mutant cell lines and two matched controls. Maximun respiratory capacity (MRC); Spare respiratory capacity (SRC); Maximum capacity (MC); Spare capacity (SC) Values measured are expressed as mean $\pm$ SD from three independent experiments. 2-way ANOVA.

Overall, data showed a reduction in the basal, mitochondrial OCR, ATP-synthesis, mitochondrial maximal capacity, spare capacity, coupling efficiency and respiratory cell ratio in *parkin*-patients (Figure 3.8 a, d). Statistical analysis showed apparent significant difference only between patient and matching control, however it did not when taken as a grouped data (Table 3.13). Glycolytic function was assessed by the ECAR measurements (Table 3.13). The ECAR measured under basal conditions in individual cases showed a huge variability between individuals (Figure 3.8 e) and overall, grouped data showed no significance between controls and patients (Table 3.13). Therefore, respiratory bioenergetics status needs to be assessed in more patients with *parkin* mutations.
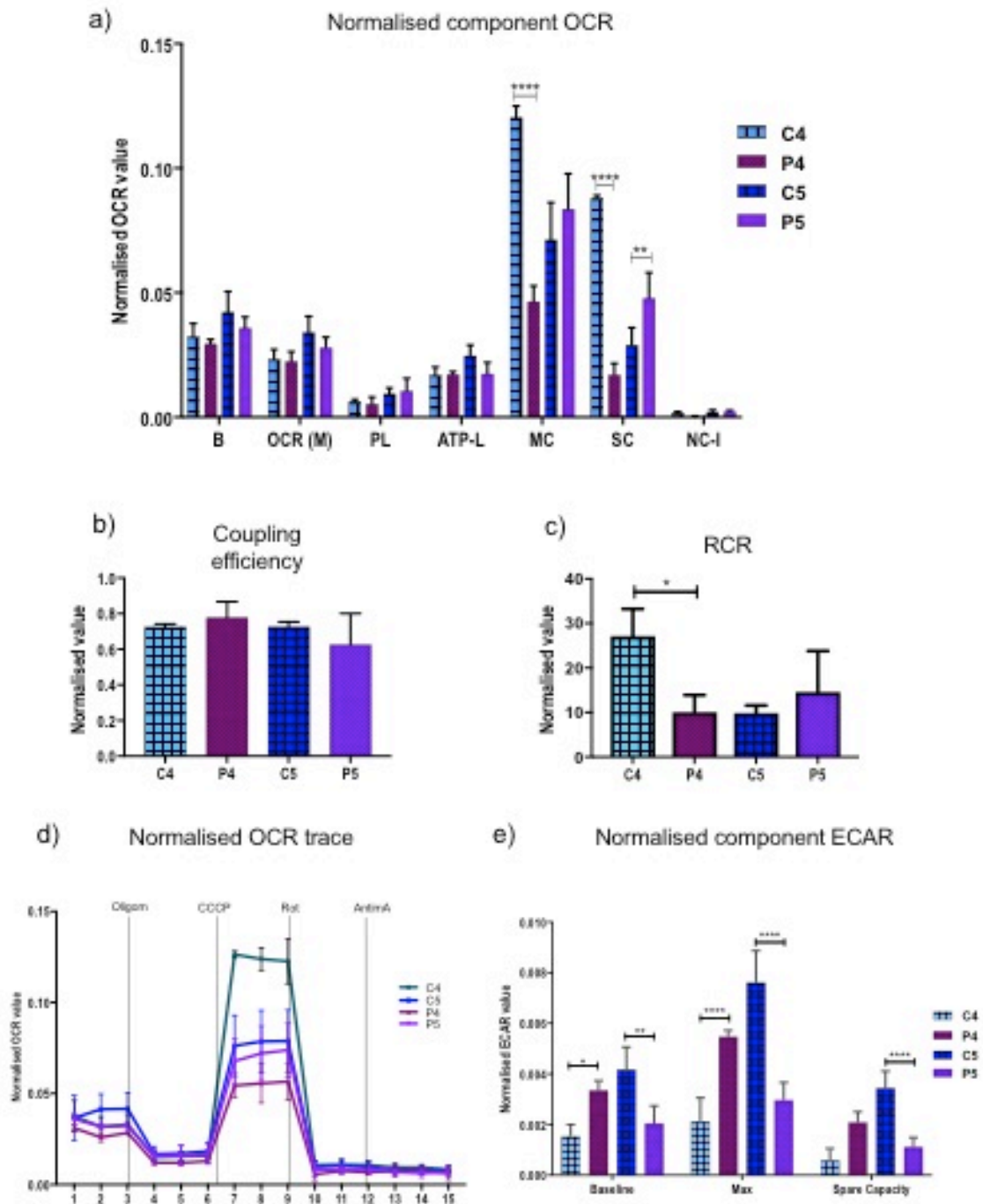
Figure 3.8. Mitochondrial respiration and glycolysis in individual controls and *parkin*-mutant patients. Representation of the measurement of a) Normalised component oxygen consumption rate (OCR), b) Coupling efficiency, d) Cell Respiratory Ratio (CRR), e) Normalised OCR trace and e) Normalised component ECAR representative of glycolysis. OCR rate was measured in XF medium under basal conditions followed by sequential injections of Oligomycin, CCCP, rotenone and Antimycin A. Baseline (B), Mitochondrial (M), Proton Leak (PL), ATP-linked (ATP-L), Maximum Capacity (MC), Spare Capacity (SC), Non-Complex I (NC-I). Data represent the mean+SD from three independent experiments.

3.4.4 TIGAR RNAi mediated knockdown optimisation

3.4.4.1 Transfection optimisation in fibroblasts. Lipofectamine 2000

TIGAR knockdown was first aimed at specific siRNA transfection in three fibroblasts control cell lines. Transfection efficiency was initially evaluated by using Lipofectamine 2000 and FAM-labelled negative control siRNA. We found a transfection efficiency of 62%, 77% and 84% using the 0.1, 0.25 and 0.5 µl of Lipofectamine respectively (Figure 3.9 a). At the 48 hrs post-transfection, cellular toxicity was assessed visually by checking cells under the microscope. Toxicity ranged from 10% with the lowest amount of Lipofectamine and 20% with the highest (data not shown). Therefore, we found that 0.25 µl of Lipofectamine was the lowest amount with the highest transfection efficiency and the lowest toxicity. Secondly, to avoid off-target effect and select the best time course and correct siRNA TIGAR concentration, transfections at three different time points and increased siRNA TIGAR concentrations were assessed. Thirdly, for protein expression, cell pellets and lysates were collected and studied after 48 hrs post-transfection.
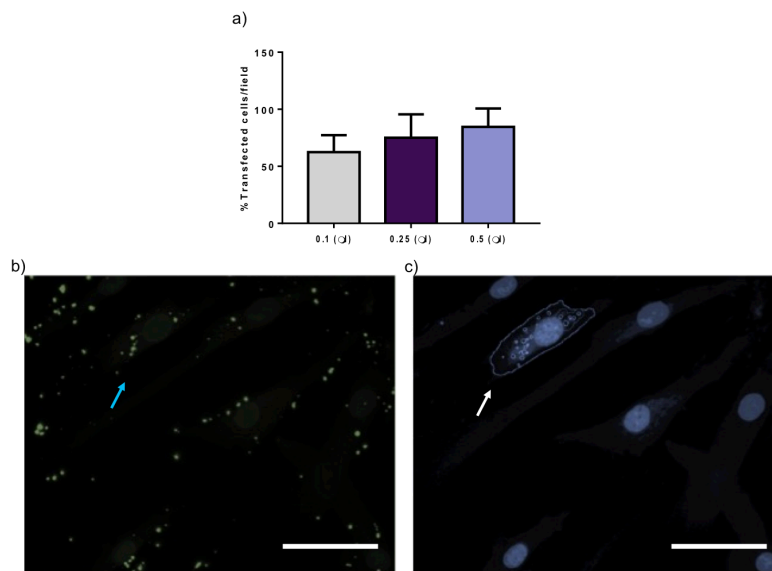
Figure 3.9. Transfection optimisation with Lipofectamine 2000. a) Transfection efficiency at three different concentrations. b) Representative images of Scramble siRNA transfection captured and analysed. c) Image representation of transfection efficiency per field using 0.25µl Lipofectamine. Transfected cells were analysed and counted individually (blue and white arrows). Scale bar 50 µM.

TIGAR expression was measured after 24, 48 and 72 hrs post-transfection in three different control cell lines. Results from the real-time qPCR data showed decreased and increased *TIGAR* expression in the three different experiments. Moreover, the expression was different when normalised to the two reference genes (Figure 3.10). At the same time point, when normalised against B-*Actin*, *TIGAR* mRNA appeared increased, but down regulated when normalised against *GAPDH* (Figure 3.10).
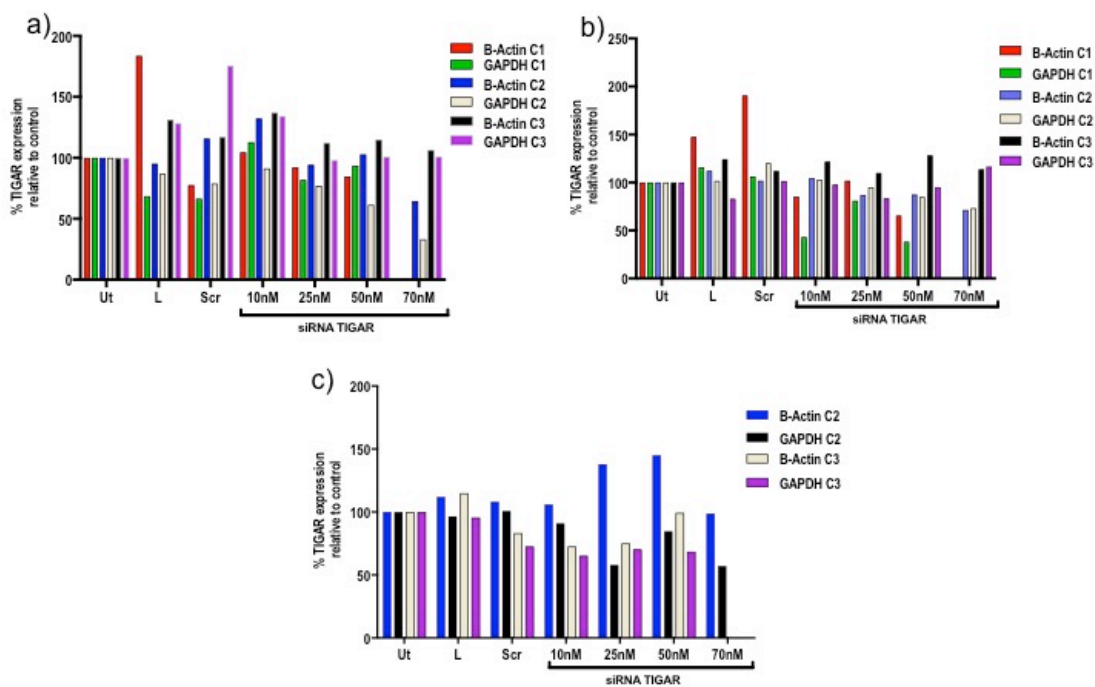
Figure 3.10. siRNA against TIGAR 24, 48 and 72 hrs. Real-Time qPCR data obtained from: a) three fibroblast control cell lines (C1, C2, and C3) transfected with either Scramble siRNA or siRNA against TIGAR (siRNA 10nM, 25nM, 50nM and 70nM) for 24 hrs. siRNA against TIGAR at 70nM was used only in two control cell lines; b) three fibroblast control cell lines (C1, C2, and C3) transfected with either Scramble siRNA or siRNA against TIGAR (siRNA 10nM, 25nM, 50nM and 70nM) for 48 hrs. siRNA against TIGAR at 70nM was used only in two control cell lines and; c) from two fibroblast control cell lines (C2 and C3) transfected with either Scramble siRNA or siRNA TIGAR (siRNA 10nM, 25nM, 50nM and 70nM) for 72 hrs. siRNA against TIGAR at 70nM was used only in one control cell line. Untreated (UT), Lipofectamine only (L), scramble siRNA (Scr). Results using both reference genes are expressed as the percentage mean of *TIGAR* expression normalised against the untreated control of one experiment for each cell line.

Due to the inconsistent results of the qPCR experiments, we decided to assess the effect of the chosen siRNAs against TIGAR at protein level using a different house-keeping control.

3.3.4.3   siRNA against TIGAR optimisation assessment. WB

WB were performed 48 hrs post-transfection using siRNA against TIGAR at a concentration of 50nM. Despite several attempts in different control cell lines, *TIGAR* knockdown was unsuccessful. Furthermore, TIGAR protein levels in the condition with only Lipofectamine, were consistently affected (Figure 3.11, a).
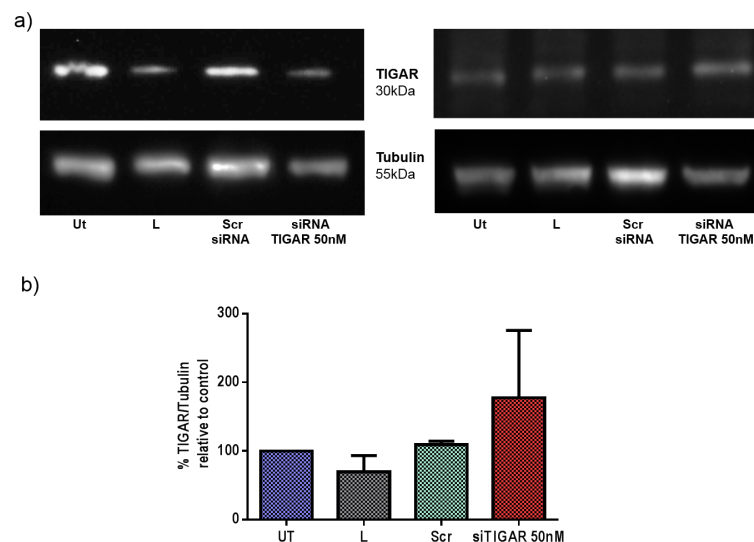
Figure 3.11. WB siRNA against TIGAR. a) After 48 hrs scramble siRNA and siRNA TIGAR treatments, protein extracts from cell lysates were used for WB using Tubulin as loading control. b) Densitometry quantification of TIGAR Proteins levels, normalised against Tubulin and presented as percentage relative to untreated (UT) control. Results are expressed as the mean $\pm$SD of samples from three different experiments.

As the knockdown experiments with siRNA continued to have inconsistent results we decided to stop the experiments and tested new siRNAs for *TIGAR* knockdown.

A different pool of siRNA against TIGAR, which targeted 4 coding regions of the last 2 exons of the *TIGAR* gene (Figure 3.2) was tested. Shortly, one control and

one *parkin*-mutant fibroblasts were transfected to compare efficacy between different cell lines. Due to previous inconsistency assessing gene knockdown with qPCR, we decided to check knock-down efficacy at the protein level. WB were performed 48 hrs post-transfection using 30nM of siRNA against TIGAR. At the 48hrs, ~70% of TIGAR knockdown was successfully achieved with transient transfection mediated by siRNA against TIGAR. This siRNA-mediated knockdown was consistent in the control and the parkin-mutant fibroblasts (Figure 3.12).
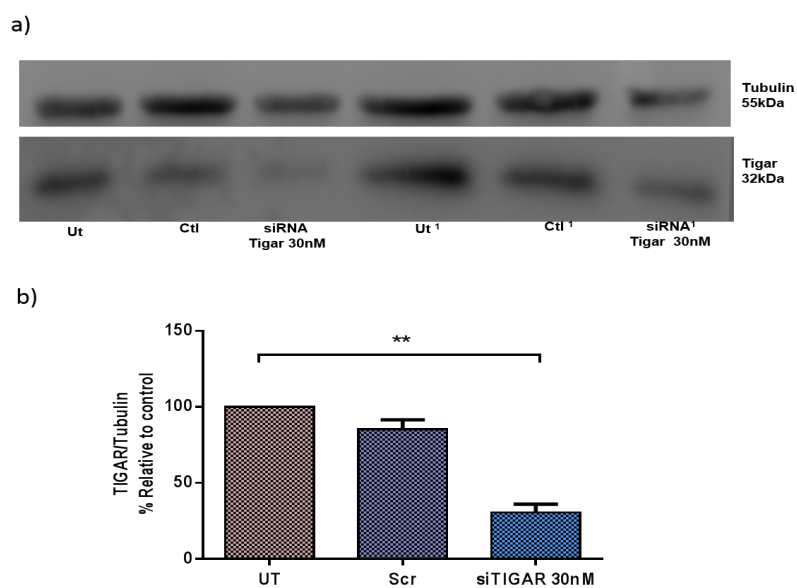
Figure 3.12. WB siRNA against TIGAR. a) After 48 hrs scramble siRNA (Scr) and siRNA TIGAR (siTIGAR) treatments, protein extracts from cell lysates, from a control (left side) and a *parkin*-patient cell lines (right side[1]) were used for WB using Tubulin as loading control. b) Protein levels of TIGAR were normalised to Tubulin, quantified by densitometry and presented as percentage relative to untreated (UT) control. Overall, a knockdown effect of ~70% was achieved in both cell lines. Results are expressed as the mean $\pm$ SD of samples from three different experiments (ANOVA, **P=0.0036)

Due to the successful *TIGAR* knockdown, we then decided to assess if it rescues the mitochondrial function in patient cell lines with a known defect in this.

3.4.5   RNAi mediated knockdown mitochondrial function

Parkin-mutant patient cell lines were unavailable when this study was performed, thus *TIGAR* knockdown effect in the mitochondrial function in PD patient

tissue with a known mitochondrial defect was assessed in the *LRRK2^{G2019S}* patient cell line available. This was investigated by performing ATP and Seahorse assays.

3.4.5.1 ATP assays

TIGAR knockdown in *LRRK2*-mutant fibroblasts

We undertook mitochondrial ATP production assays to determine whether TIGAR knockdown had a rescue effect in the mitochondrial function in the *LRRK2*-mutant patient fibroblasts when compared to a matched control. Basal cellular ATP levels were decreased in the patient by ~30% compared to the matched control.

ATP levels of the transfected fibroblasts were assessed at the 48 hrs and compared with the untreated and the control conditions. Data showed no difference between control and transfected cell lines in both, control and patient. ATP levels were consistently increased with both conditions. The transfection reagent had a marked effect alone, which made difficult to assess the effect of *TIGAR* knockdown (Figure 3.13).

We concluded that since the ATP assays performed in knockdown experiments with siRNA continued to have inconsistent results we decided to stop the experiments and tested other method to evaluate the mitochondrial function.
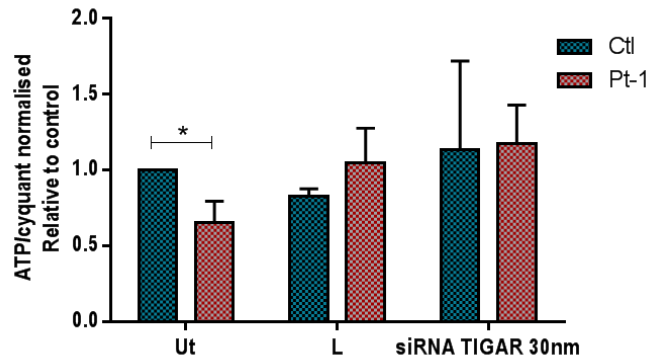
Figure 3.13. Mitochondrial ATP production in _LRRK2_ mutant fibroblasts. Basal mitochondrial ATP production is decreased in the _LRRK2^{G2019S}_ mutant fibroblasts. Mitochondrial ATP production was increased in the control and the patient cell line after treatment with Lipofectamine alone and in the _TIGAR_ knock-downs. Results are expressed as the mean $\pm$ SD of samples from three different experiments (2-way ANOVA, *p<0.05).

3.4.5.2 Seahorse assays: mitochondrial respiration

TIGAR knockdown in _LRRK2_ fibroblasts.

An ATP defect and mitochondrial OCR, maximum and coupled respiration were reported previously and present in this patient (Mortiboys et al., 2015). Therefore, we assessed the effect of _TIGAR_-knockdown in the bioenergetic status in the _LRRK2^{G2019S}_ mutant patient and control cell line. We hypothesised that TIGAR might be implicated in PD pathology, and when silenced, it can rescue the mitochondrial function in cells with the underlying pathology.

Decreased basal (38.5%), mitochondrial (43.9%), ATP-linked OCR (54.7%) and coupling efficiency (55.6%) was observed in the patient (Table 3.14. When TIGAR was knocked down, all these parameters showed an increase, which was less pronounced the lipofectamine treatment was observed (Figure 3.14 a). Due to high variability between treatments, this results where no significant.

		CONTROL	PATIENT
NORMALISED COMPONENTS OCR			
	UT	[a] *1+ 0.0*	[a] *0.615 + 0.370*
Baseline	L	0.994 + 0.11	0.782 + 0.3642
	siTIGAR 30nM	0.875 + 0.045	[a] *0.978 + 0.137*
	UT	[a] *1 + 0.0*	[a] *0.561 + 0.428*
OCR (M)	L	1.079 + 0.124	0.788 + 0.486
	siTIGAR 30nM	1.212 + 0.219	[a] *1.015 + 0.264*
	UT	[a] *1+ 0.0*	0.927 + 0.178
Proton leak	L	1.045 + 0.113	1.002 + 0.219
	siTIGAR 30nM	[a] *1.312 + 0.073*	1.083 + 0.179
	UT	1 + 0.0	[a] *0.435 + 0.522*
ATP-L	L	1.098 + 0.142	0.706 + 0.547
	siTIGAR 30nM	1.182 + 0.270	[a] *1.017 + 0.250*
	UT	[a] *1 + 0.0*	[a] *1.061 + 0.296*
MRC	L	1.183 + 0.149	0.907 + 0.727
	siTIGAR 30nM	[a] *1.484 + 0.261*	[a] *1.590 + 0.304*
	UT	*1 + 0.0*	*1.928 + 0.389*
SC	L	*1.342 + 0.225*	*1.035 + 1.262*
	siTIGAR 30nM	*2.015 + 0.328*	*2.411 + 0.575*
	UT	1 + 0.0	1.219 + 0.159
Non-Complex I	L	1.231 + 0.256	0.859 + 0.064
	siTIGAR 30nM	1.401 + 0.466	0.975 + 0.621
	UT	1 + 0.0	*0.444 + 0.514*
Coupling efficiency	L	1.007 + 0.033	0.724 + 0.416
	siTIGAR 30nM	0.829 + 0.252	*0.997 + 0.015*
	UT	1 + 0.0	*0.667 + 0.747*
RCR	L	1.179 + 0.129	0.810 + 0.673
	siTIGAR 30nM	1.059 + 0.627	*1.74 + 0.298*
NORMALISED COMPONENTS ECAR			
	UT	*1 + 0.0*	*1.78 + 0.626*
Baseline	L	*0.973 + 0.128*	*1.66 + 0.367*
	siTIGAR 30nM	*1.120 + 0.105*	*1.25 + 0.184*
	UT	1 + 0.0	1.261 + 0.199
Max	L	0.854 + 0.0792	1.203 + 0.0348
	siTIGAR 30nM	0.793 + 0.030	0.946 + 0.120
	UT	1 + 0.0	0.581 + 0.304
SC	L	0.660 + 0.174	0.426 + 0.594
	siTIGAR 30nM	*0.271 + 0.132*	0.455 + 0.103

Table 3.14. Bioenergetic parameters in a control and LRRK2 patient fibroblasts. Oxygen consumption rate (OCR), Mitochondrial (M); ATP-L (ATP-linked); Maximum respiratory capacity (MRC); Spare Capacity (SC); Respiratory Cell Ratio (RCR); Untreated (UT); Lipofectamine only (L); siRNA TIGAR (siTIGAR). *Measurements with statistical difference between control, patient and siRNA treatment. [a]Measurements where a difference between control and patient were obtained under basal conditions and where siRNA treatment showed an effect. Values measured are expressed as mean + SD, normalised to control (UT) from three independent experiments.

Maximal respiratory capacity (MRC) showed increased levels when *TIGAR* was knocked down, in both control (2-way ANOVA, *P*=0.569) and patient (2-way ANOVA, *P*=0.471); however, apparent statistical difference was not significant due to inconsistency between the different treatments and huge variability in the patient (Figure 3.14 a). Spare respiratory capacity (SRC) OCR from the patient showed a

significant increase under basal conditions (2-way ANOVA, *P=0.261) and when TIGAR is knocked down when compared to the control under basal conditions (2-way ANOVA, ****P<0.0001). Here, Lipofectamine had the opposite effect in the patient, where it showed reduced levels (Figure 3.14 a). Lipofectamine seemed to continue displaying a slight effect in the control (2-way ANOVA, P=0.852), but not the patient, where it showed significant reduction (2-way ANOVA, P=0.523) (Figure 3.14 a).

Spare respiratory capacity (SRC) relies on glucose and fatty acids as its main source, suggesting that OCR and SRC are modulated by distinctive metabolic regulators. After knocking down TIGAR in the LRKK2^{G2019S} mutant-patient glycolysis is enhanced. This correlates with glycolysis measured by ECAR (Figure 3.14 e), with a significant increase in levels under basal conditions in the patient (2-way ANOVA, **P=0.007); which decreased when treated with Lipofectamine (2-way, ANOVA, P=0.992) and TIGAR knockdown (2-way ANOVA, P=0.139). The spare capacity (SC) in the control was notably reduced when TIGAR is knocked down (2-way ANOVA, *P=0.014).

Overall, we found some differences in the LRRK2-mutant patient. However, these assays were performed in only one patient of one genotype, where a different gene from a different pathway and particular mutations are involved, which influence the overall result. Further assays need to be conducted in a larger group of patients to investigate the potential role involving the PD related genes.
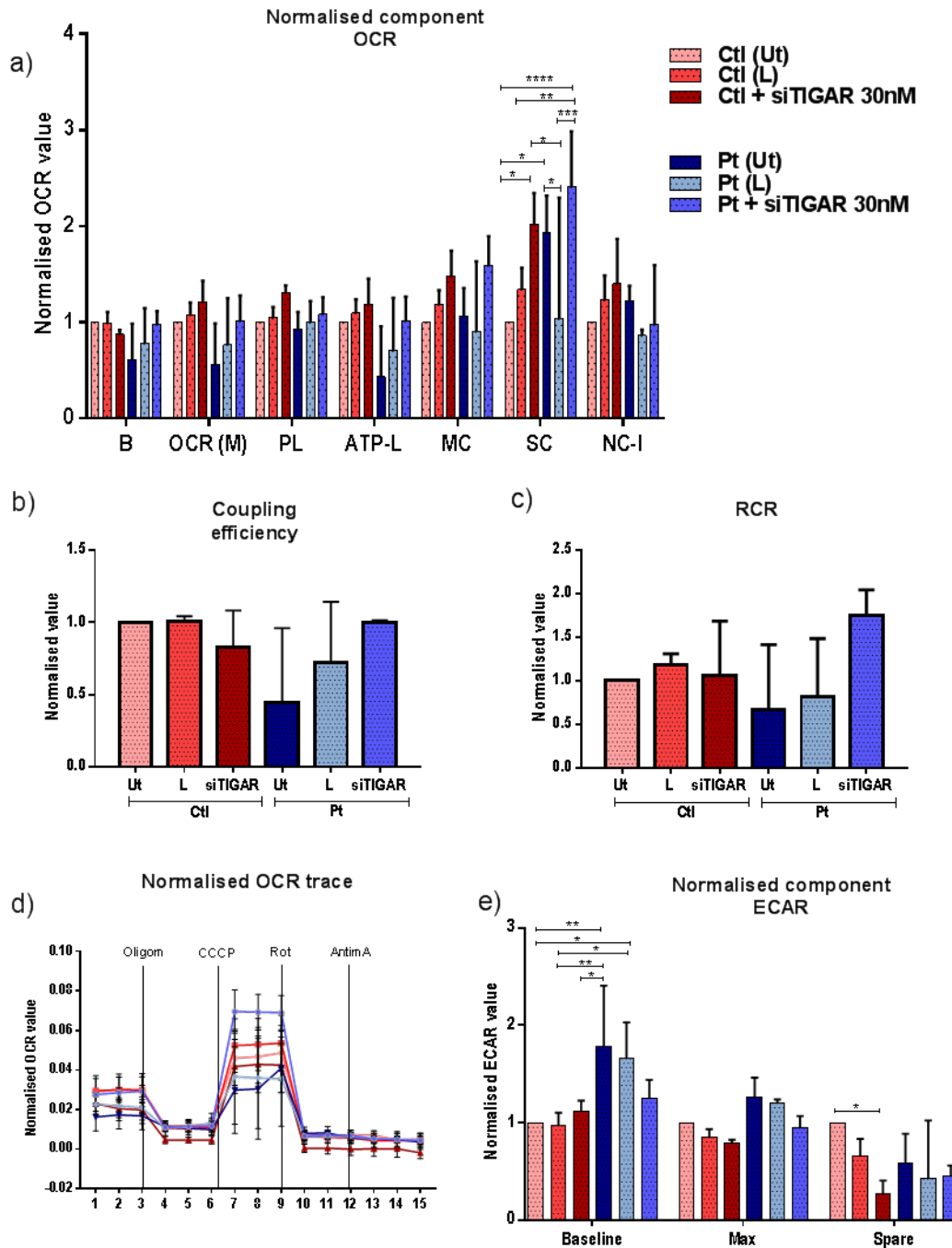
Figure 3.14. TIGAR knockdown effect in a control and a *LRRK2* mutant fibroblast. Mitochondrial respiration (OCR) and glycolysis (ECAR). Representation of the measurement of a) Normalised component oxygen consumption rate (OCR) b) Coupling efficiency, c) Respiratory Cell Ratio (RCR), d) Normalised OCR trace and e) Normalised component ECAR representative of glycolysis. OCR rate was measured in XF medium under basal conditions followed by sequential injections of Oligomycin, CCCP, rotenone and Antimycin A. Oxygen consumption rate (OCR), Mitochondrial (M); ATP-L (ATP-linked); Maximum capacity (Max); Spare Capacity (SC); Respiratory Cell Ratio (RCR); Untreated (UT); Lipofectamine only (L); siRNA TIGAR (siTIGAR); Control (Ctl); Patient (Pt). Data represent the mean $\pm$ SD, normalised to control from three independent experiments *(*2-way ANOVA, **p<0.005*; *p*<0.05*).*

3.4.6 Transfection reagents optimisation

To assess the effect of *TIGAR* knockdown in fibroblasts, without being masked by the effect from the transfection reagent in cells, we further optimised different transfection reagents by measuring ATP levels upon different conditions. For this, we tested a control and a patient cell line. First, the different concentrations of transfection reagents at the 48 hrs (Figure 3.15 b) showed to be more stable compared to the 24 hrs (Figure 3.15 a). Alongside ATP assays, transfection efficiency was assessed with transfected cells with Scramble fluorescent siRNA plated alongside ATP assays under the same conditions. Cells were visualised using the InCell Analyzer 2000 and analysed with the InCell Developer Toolbox 1.9.2 Software. All the compared transfection reagents showed an efficiency of between 60-80%, where the 48hrs showed the best results and more comparable with the untreated condition between the two cell lines. From these experiments, we chose the lowest concentrations for each transfection reagent and continued optimisation assessing different cellular densities at the 48hrs.
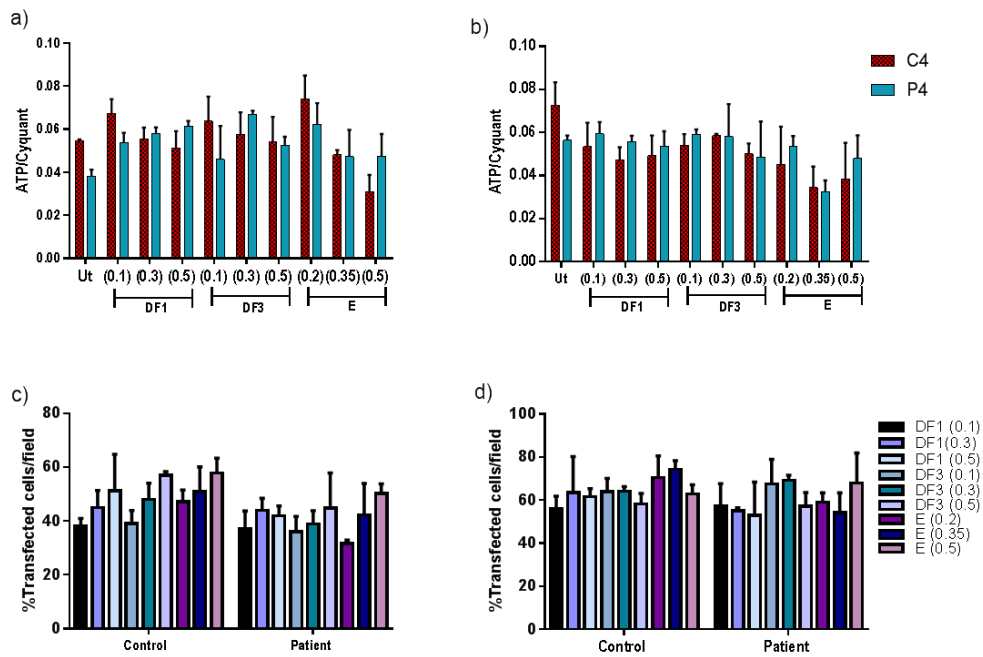
Figure 3.15. Transfection reagents optimisation in fibroblasts. ATP levels at different concentrations of transfection reagent in a control (C4) and a *parkin* patient (P4) at the 24 (a) and 48hrs (b). Transfection efficiency in both cell lines with the different concentrations of transfection reagent using scramble siRNA 30nM at the 24 (c) and 48 (d) hrs. Untreated (Ut); DarmaFECT (DF); Endofectin (E) Data represent the mean $\pm$SD from one independent experiment.

Four different cellular densities were assessed at the 48 hrs in one control fibroblast line. The lowest (2,000 cells/well) and the highest (4,500 cells/well) cellular densities showed the highest variability in the ATP level with all the transfection reagents. ATP levels seemed steadier between the 2,500-3,5000 cells/well in all the conditions (Figure 3.16). Since patient fibroblasts showed to have a higher variability of ATP levels when it is transfected, we decided to test the transfection reagents in two patient fibroblasts cell lines.
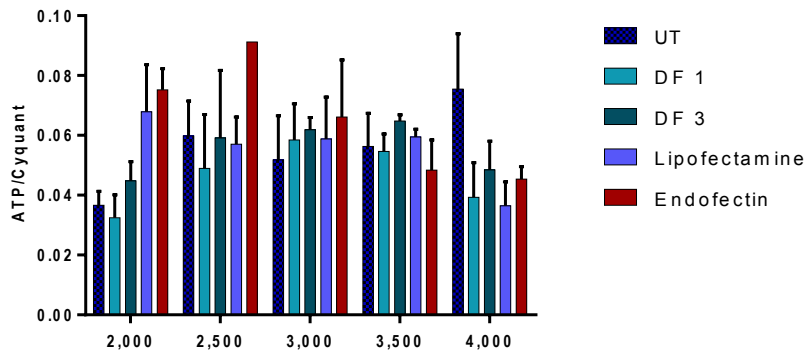
Figure 3.16. Transfection reagents in one control fibroblast. ATP levels in a control fibroblast at four different cellular densities using 0.1µl DharmaFECT 1 (DF1), 0.1 µl DharmaFECT 3 (DF3), 0.2µl Lipofectamine and 0.2 µl Endofectin.

Experiments were performed in the two patient cell lines at the 48 hrs, assessing cellular densities ranging from 2,500-3,500 cells/well. The patient 4 (P4) showed steadier ATP levels between the three different cellular densities (Figure 3.17 a), whereas patient 5 (P5) showed a high variability within the three different cellular densities (Figure 3.17 b). However, in both cell lines, 3,000 cells/well, showed a minimal variability between them and within the different transfection reagents. Therefore, we decided to test it further to see if this remained when both cell lines were compared with matched controls with the same conditions.
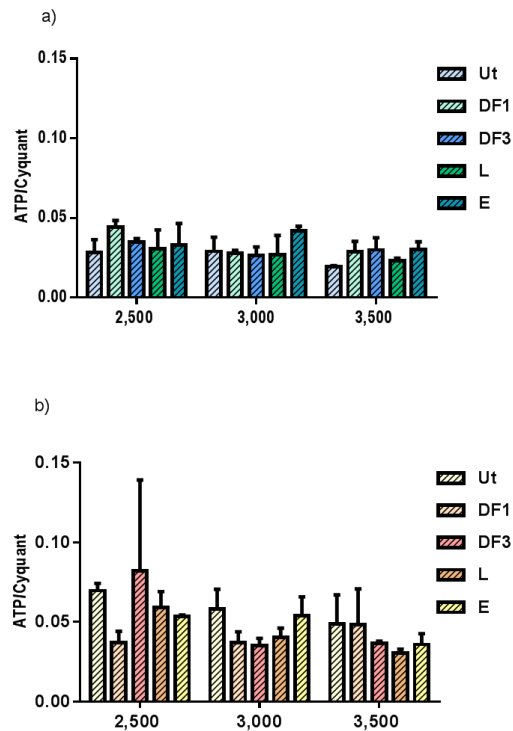
Figure 3.17. Transfection reagents in *parkin*-mutant fibroblasts. ATP levels in two *parkin*-mutant fibroblasts, P4 (a) and P5 (b). Three different cellular densities were assessed using 0.1μl DharmaFECT 1 (DF1), 0.1 μl DharmaFECT 3 (DF3), 0.2μl Lipofectamine (L) and 0.2 μl Endofectin (E) and compared with the untreated (Ut) condition at 48hrs.

Finally, we decided to test one control (C4) and one *parkin* patient (P4) fibroblasts alongside transfection efficiency in the control and the patient and see whether transfection remained efficient at a higher passage. At 2,500 and 3,500 cells/well, C4 and P4 (Figure 3.18) showed slight reduction of ATP levels, except from Endofectin, were the levels were significantly lower than the untreated condition. C4 (Figure 3.18, a) showed comparable levels to the untreated condition across all the samples, whereas P4 (Figure 3.18, b) showed a tendency to an increase in all of them. Transfection remained effective with an overall reduction of $\leq 10\%$, where Endofectin efficiency remained comparable to previous results (Figure 3.18 c, d, e). However, basal ATP levels from the P4 started to be similar to the control cell line, which reflected that both cell lines were probably affected due to higher passage and constant stress. Since after a numerous failed attempts to optimise the transfection

using conventional RNAi methods, we decided to stop this experiments. A new method of RNAi delivery was approached and tested, where the need of a transfection reagent was avoided.
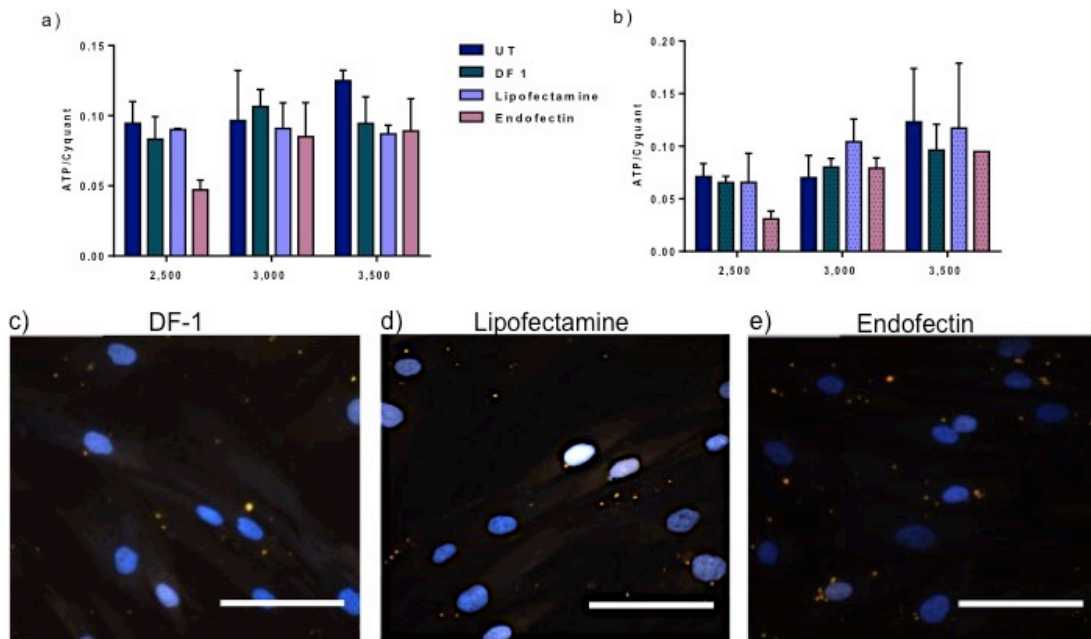
Figure 3.18. Transfection ATP levels and efficiency in one control (C4) and one patient (P4) fibroblasts. ATP levels in a C4 (a) and patient (P4) fibroblasts after 48hrs of transfection. Control (C4) cell line showed less variability between 3,000 cells/ well, P4 (b) showed increased levels at 3,000 cells/ well with all the transfection reagents. c), d) and e) Representation of the different transfection efficiencies obtained at the 48hrs, where Endofectin showed the highest efficiency. Scale bar 50μM

3.4.7   Accell siRNA transfection

Conventional RNAi methods used knockdown *TIGAR* failed to assess its effect in human fibroblasts due to the interfering effect of the transfection reagent, leading to a detectable metabolic response. Thus, self-transfecting Accell siRNAs were tested in human fibroblasts by measuring transfection efficiency and effect in ATP levels. Since they avoid the use of a chemical or mechanical error, we expected a lower effect in the metabolic response of the cells.

First, a control fibroblasts line was used to optimise this new method following the protocol from the provider. Three cellular densities, 2.5-3.5 x 10^3 cells/well were

selected. ATP levels were initially tested at the recommended 96 hrs after transfection (Figure 3.19 a). Cells were transfected with either scramble siRNA (red), GAPDH or Cyclophilin B positive controls and Non-targeting negative control. ATP levels within the three cellular densities with the different controls showed similar comparable ATP levels to the untreated condition (Figure 3.19, a). However, ATP levels seemed to be very sensitive to very high and very low cellular densities, that could result at the 96 hrs.

Next set of experiments was assessed at the 72 hrs, changing the medium to galactose at the 48hrs of transfection (Figure 3.19, b). ATP levels were different within the three densities, where 2,500 cells/well showed only slight changes compared to the untreated condition, and the 3,000 cell/well showed a significantly increase with all the controls. Since an acute effect of the change of the media and lower time of the siRNA in the medium was suspected, we decided to assess at the effect at 96 hrs in the patient. (P4) line, which previously showed the highest variability, then tested. Similar results to the control (Figure 3.19 a) were obtained after media change to galactose at the 48 hrs of transfection and assessed at the 96hrs (Figure 3.19 c). Since transfection efficiency and knockdown efficacy has not been tested previously in fibroblasts, knockdown percentage was assessed.
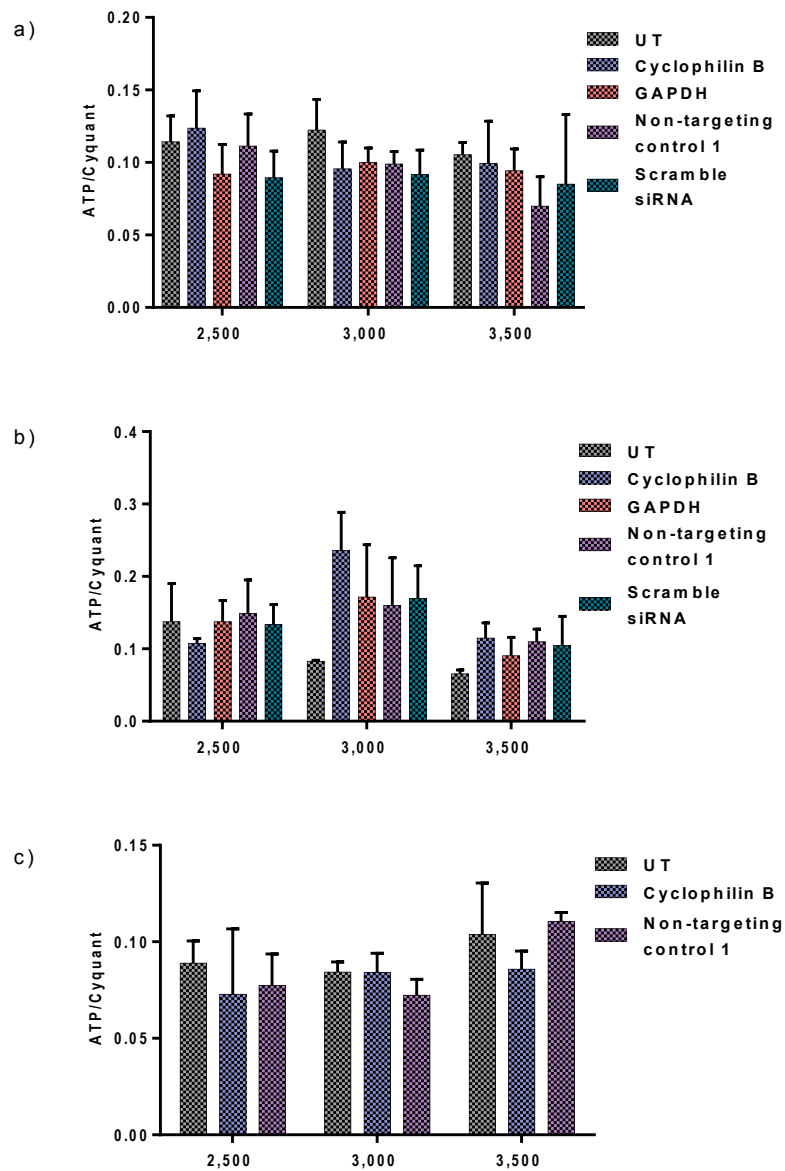
Figure 3.19. Accell siRNA Optimisation in fibroblasts. ATP levels in transfected fibroblasts at 1µM of each siRNA positive target genes (Cyclophilin B, GAPDH), negative (Non-targeting control 1) and Scramble siRNA controls after 96hrs in a control fibroblast (a), 72 hrs (b) and 96 hrs (c) in a *parkin* mutant fibroblasts.

Transfection efficiency and knock down assays were performed in a control fibroblast. Transfection efficiency was assessed by imaging Scramble Accell siRNA (Figure 3.20 c) showing ~60% transfection efficiency at the 72 hrs. mRNA knockdown resulted in ~65% knockdown (Figure 3.20 a) and only 15% at the protein level (Figure 3.20 b-c).

Accell siRNA requires high concentrations of the reagent and more experiment were needed to finally optimise the assays and obtain a higher knockdown effect. In addition, fibroblasts cell line availability was becoming limited due to the fact of its utility in other projects, therefore we decided to stop this experiments and change approach to focus investigating the cellular localisation of TIGAR upon cellular stress and its role in PD.
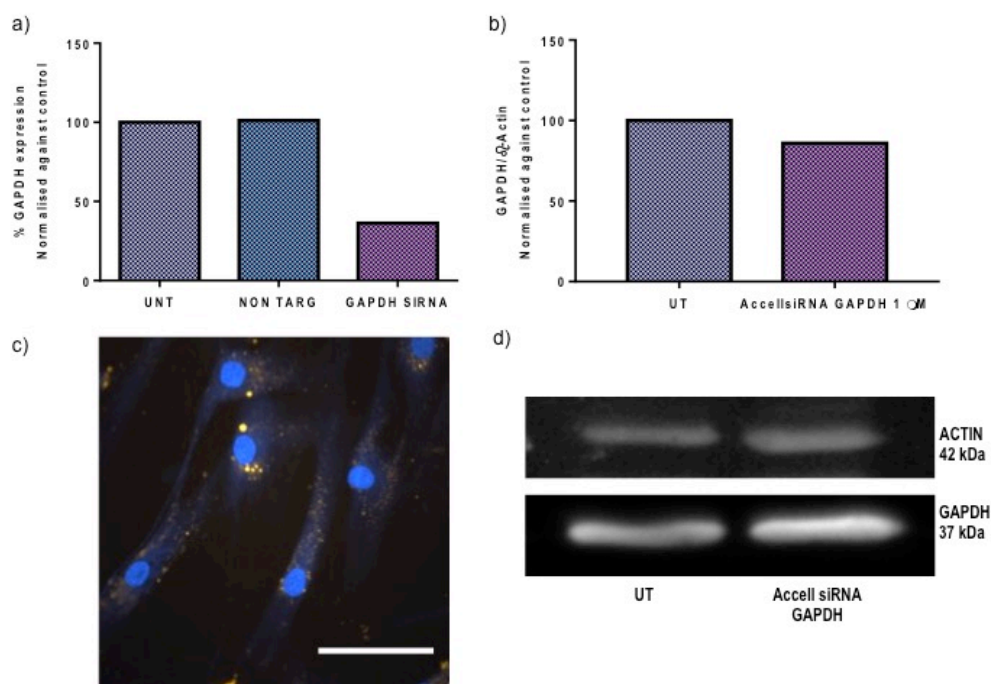
Figure 3.20. Accell siRNA in a control fibroblasts. Transfection in one control fibroblasts. Optimisation with positive and non-tagenting and measure mRNA percentage levels by qPCR (a), GAPDH protein levels by densitometry analysis(b) and WB image (d) compared to control untreated condition. Representative image of transfection efficiency using a scramble Accell siRNA**.** Scale bar 50μM.

3.4.8   TIGAR cellular localisation

3.4.8.1   Antibody optimisation

For future cellular localisation assays, optimisation for TIGAR immunofluorescence was undertaken using different antibodies in human fibroblasts and HeLa cell line as a control cell line.   Different concentrations and blocking methods were assessed. From all the results, only two of the antibodies against

TIGAR (ab12933 and PA5-29152) showed consistent staining signal. However, ab 12933 antibody had an intense perinuclear signal across the different treatments. In order to assess their specificity, we tested by knocking down *TIGAR* in the control fibroblasts.
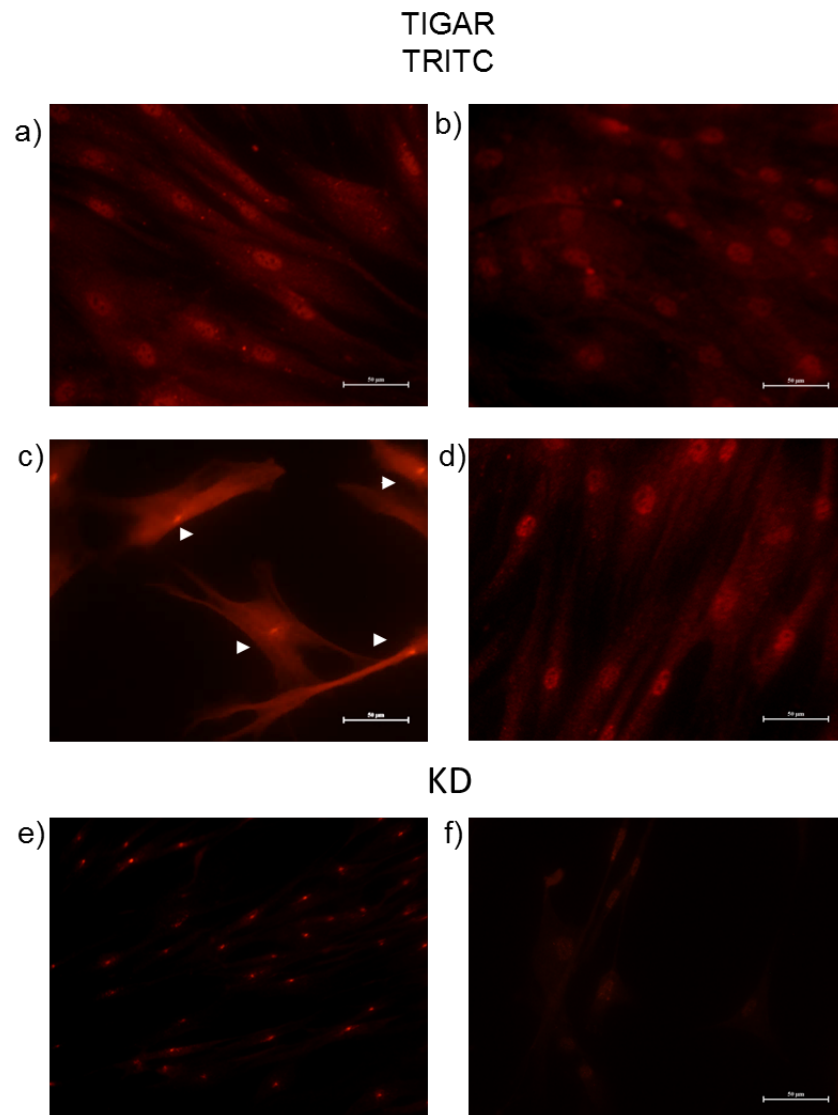
Figure 3.21. TIGAR immunofluorescence in fibroblasts optimisation. Representative images of the different staining using Anti-TIGAR antibodies: a) LCS-C286858 (1:100); b) AB10545 (1:250) c) ABCAM 129333 (1:800); d) (1:500). Antibody against TIGAR in fibroblasts where TIGAR was knockdown for 48 hrs, fixed and labelled with ab1239333 (e) and PA5-29152 (f). Control cellular morphology in figure c was different due to lower confluency. Scale bar 50μM.

From these results, only the PA-29152 antibody had a reduced expression without any other nonspecific signal, whereas ab129333 continued to show an intense perinuclear labelling in all the samples tested (Figure 3.21). Then, we verified and optimised in HeLa cell lines different treatments and rotenone toxic exposure. TIGAR labelling across the different treatments and experiments were consistent (Figure 3.22).
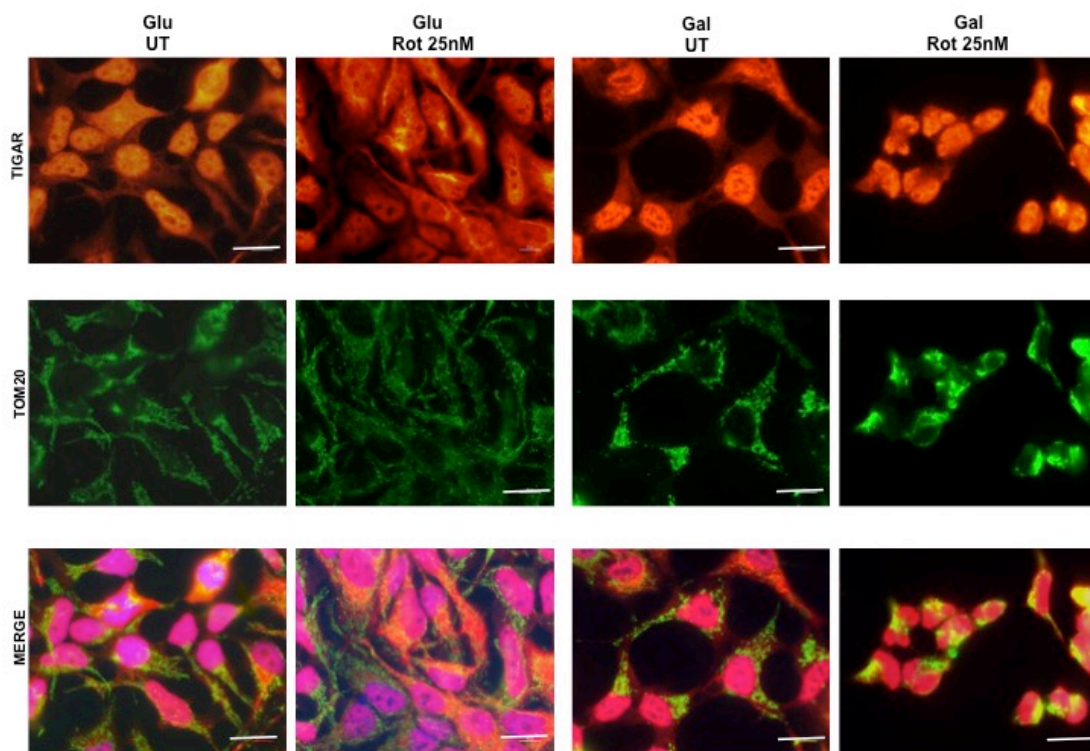
Figure 3.22. Anti-TIGAR antibody PA5-29152 immunofluorescence in HeLa cells. Representative images of labelling of TIGAR (red) and TOM20 (green) to visualize the mitochondria in HeLa cells. Cells were treated with 25nM Rotenone for 48hrs and visualize under the fluorescent microscope. Images showed an intense nuclear staining in some cells under the different conditions. Cytoplasm intensity was lower in most of the cells. Upon rotenone treatment, TIGAR showed a partial mitochondrial translocation in some cells. This event occurred as well in the untreated condition in less proportion. Glucose (Glu); Galactose (Gal); Rotenone (Rot); Untreated (UT). Scale bar 50µM

Notably, TIGAR localisation in fibroblasts in glucose (Figure 3.21 d) seemed to be mainly in the nuclei, whereas in HeLa had a cytoplasmic localisation. However, this changed upon galactose treatment, where intense TIGAR nuclei localisation was remarkable. TIGAR showed a partial mitochondrial co-localisation upon rotenone

toxic exposure. Since there are no previous reports of TIGAR characterisation in human fibroblasts and the effect when stressed with rotenone might induce mitochondrial localisation we performed these experiments in three *parkin*-mutant patients and matching controls cell lines.

3.4.9 Rotenone toxic exposure

We assessed whether TIGAR could be recruited or translocated to the damaged mitochondria in cells with impaired *Parkin* expression. The first set of experiments were performed in three controls (C4-C6) and three *parkin*-mutant (P4-P6) fibroblasts from the second group using Antibody against TIGAR PA5-29152 and the mitochondrial marker TOM20. After treating cell lines in glucose and galactose media for 48hrs after rotenone toxic exposure no evident effect on the overall TIGAR expression could be seen in either controls or patients (Figure 3.23). However, an intense nuclear staining was obtained across all the samples. Previous reports in different cell lines showed TIGAR cytoplasmic localisation.

To confirm this, a monoclonal mouse antibody, courtesy of Dr. Karen Vousden, was tested. Since monoclonal antibodies have shown higher specificity and this was the group that described TIGAR initially (Bensaad et al., 2006), we were confident of the specificity of the antibody. Both antibodies recognise an epitope in exon 6 within the same region; however, PA5-192 comprises 50 aminoacids (220-270), whereas the monoclonal antibody targets only 14 aminoacids (256-270) (Table 3.7).
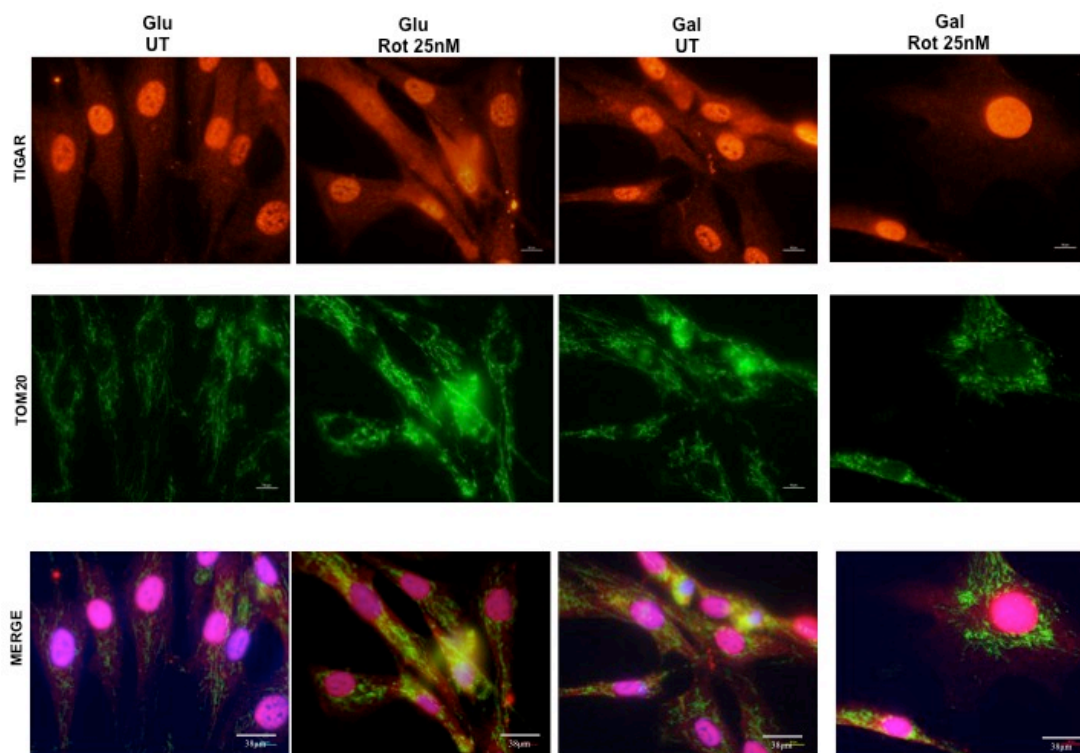
Figure 3.23. Anti-TIGAR antibody PA5-29152 immunofluorescence in control fibroblasts exposed to Rotenone at the 48hrs. Representative images of a control fibroblast cell line. Cells were fixed and stained with antibody against TIGAR PA5-29152 (red) and Anti-TOM20 (green), to visualize cellular localisation and mitochondria. Experiments were performed after 48 hrs of rotenone toxic exposure in glucose and galactose media. Cells were visualized under a confocal microscope. Glucose (Glu); Galactose (Gal); Rotenone (Rot); Untreated (UT). Scale bar 50μM.

Then, the new antibody was tested in HeLa cells under the same treatment conditions (Figure 3.24) and compared the results obtained with the antibody anti-TIGAR PA5-29152 tested in HeLa cells (Figure 3.22) and fibroblasts (Figure 3.23).

TIGAR PA5-29152 showed intense nuclear staining with moderate cytoplasmic staining (Figure 3.23); whereas TIGAR monoclonal antibody showed a more intense cytoplasmic and a less evident nuclear staining (Figure 3.24). Between the untreated conditions in glucose and galactose, there was no difference in TIGAR expression. When rotenone treatment was added to cells led to mitochondrial fragmentation, mainly in galactose treatment, where TIGAR showed an apparent

mitochondrial co-localisation (Figure 3.24). Since these showed a higher antibody specificity and suggested TIGAR mitochondrial co-localisation upon rotenone toxic exposure, we conducted the same experiment and conditions in a control fibroblast cell line using the monoclonal antibody and compared the previous results obtained with PA5-29152 (Figure 3.23).
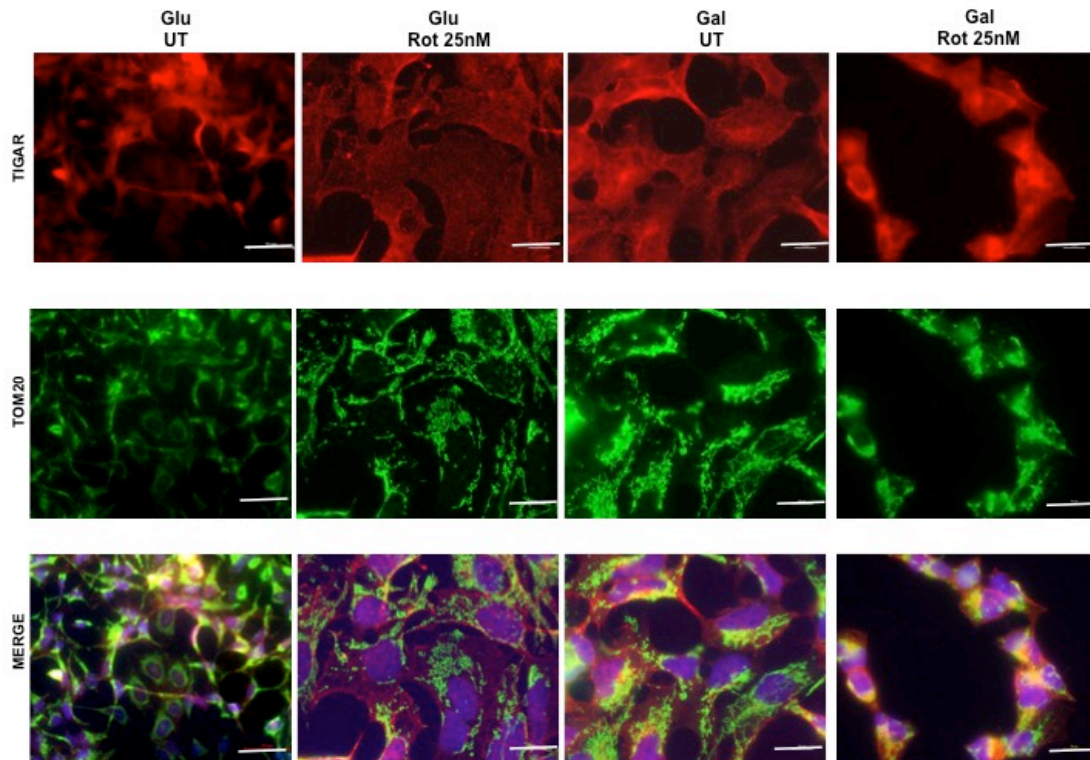
Figure 3.24. Anti-TIGAR monoclonal mouse antibody immunofluorescence in HeLa cells. Representative images of labelling of TIGAR (red) and TOM20 (green) to visualize the mitochondria in HeLa cells. Cells were treated with 25nM rotenone in glucose or galactose for 48hrs and visualized under confocal microscope. Glucose (Glu); Galactose (Gal); Rotenone (Rot); Untreated (UT). Scale bar 50µM.

TIGAR cellular localisation in control fibroblasts was investigated upon glucose and galactose treatment conditions, as well as to the exposure to rotenone (Figure 3.25). An evident TIGAR cytoplasmic localisation was obtained, however, there was no difference in TIGAR expression under the different treatments. Rotenone showed shortened mitochondria (TOM20), which was a reflection of mitochondrial fragmentation, mainly in cells grown in galactose. Mitochondrial

measurements (form factor (branching) and aspect ratio (length)) were not performed. However, TIGAR mitochondrial localisation was not evident. Intense small doted punctae were detected in specific cellular areas near the nuclei.
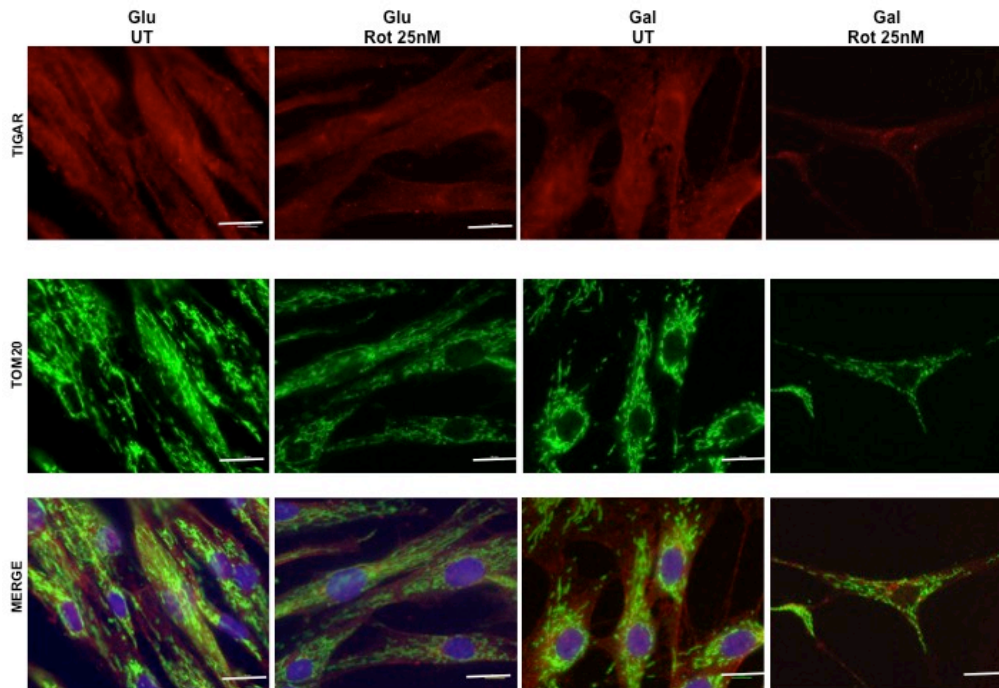
Figure 3.25. Anti-TIGAR monoclonal mouse antibody immunofluorescence in a control fibroblast. Representative images of labelling of TIGAR (red) and TOM20 (green) to visualize the mitochondria in HeLa cells. Cells were treated with 25nM Rotenone in glucose or galactose for 48hrs and visualized under inverted microscope. Glucose (Glu); galactose (Gal); rotenone (Rot); untreated (UT). Scale bar 50µM.

TIGAR mitochondrial localisation was then investigated. These experiments were performed in only one control (C4) and one *parkin*-mutant (P4) fibroblasts.

Co-localisation analysis was performed by inverted microscopy analysis of cells labelled in single images acquired and the correlation between TIGAR and mitochondrial marker TOM20 was calculated (Figure 3.26). TIGAR expression between control (Figure 3.26, a) and patient (Figure 3.26, b), as well as within the different treatments, showed no difference. Mitochondria upon rotenone toxic

167

exposure showed fragmentation in both control and patient fibroblasts and in few regions the presence here of small puncta suggested a possible partial mitochondrial co-localisation.
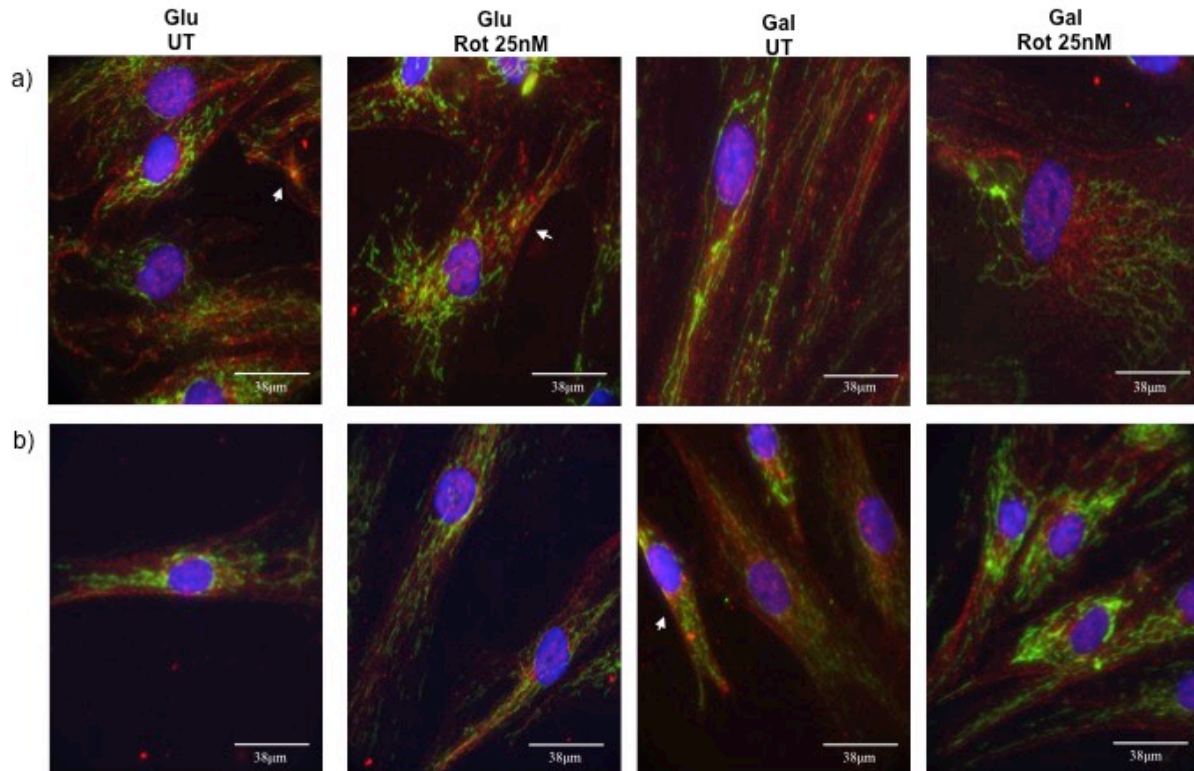
Figure 3.26. TIGAR localisation in fibroblasts from one control and one *parkin*-mutant patient. Representative images of fixed and stained cells with antibodies against TIGAR (red) and TOM20 (green) to visualize the mitochondria in a control (a) and a *parkin*-mutant (b) fibroblasts (P4, ARG42PRO het). Cells were treated with 25nM Rotenone in glucose or galactose for 48hrs and visualized under an inverted microscope. Glucose (Glu); galactose (Gal); rotenone (Rot); untreated (UT). Scale bar 50µM.

Pearson's analysis obtained from both, C4 and P4, showed partial colocalisation (0.4-0.6) with all the conditions (Figure 3.27). However, this coefficient is difficult to interpret and it is only reliable with high correlation. Pearson's coefficient can easily be affected by additional non colocalising signals and a lack of perspective of both channels. Mander's coefficients are easier to interpret and not sensitive to overlapping pixels (Dunn et al., 2011). Therefore, we decided to further analyse with Mander's coefficients to determine the proportion coming from both channels and how they overlap with each other Mander's coefficients (m1 and m2)

were both low in the control and patient in all the conditions. A minimal increase in the Mander's coefficient for the green channel (m2, TOM20 over TIGAR) in fibroblasts was detected (Figure 3.27), showing that the high contribution is coming from the mitochondria rather than the actual presence of TIGAR within it.
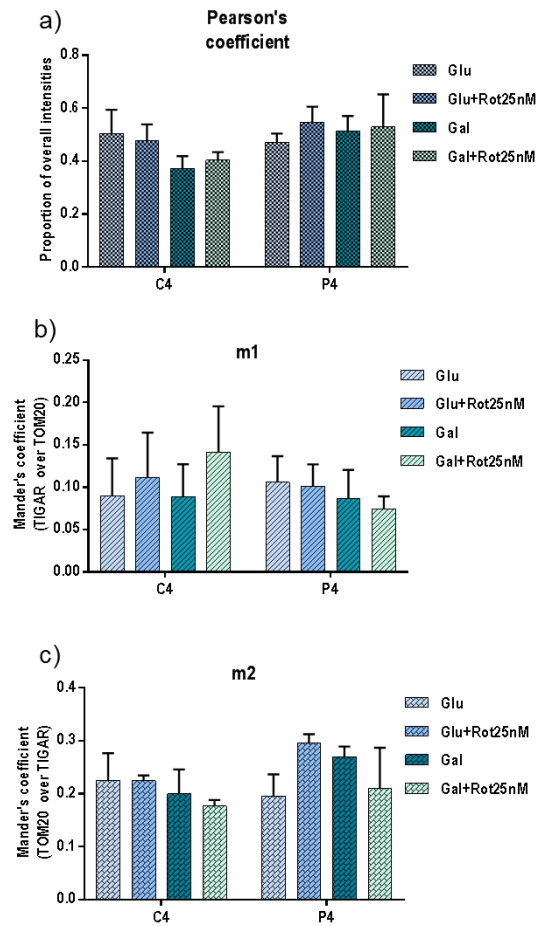
Figure 3.27. Colocalisation coefficients. Colocalisation analysis of TIGAR with TOM20 in a control (C4) and a *parkin*-mutant (P4) fibroblasts. a) Pearson's coefficient; b) Mander's 1 (m1) coefficient and c) Mander's 2 coefficient (m2) from each condition from C4 and P4. Overall, there was no difference between the control and patient in any of the treatments. Results are expressed as the mean $\pm$SD of samples from 3 different experiments

Overall, these findings suggest that TIGAR do not co-localise in the mitochondria upon mitochondrial damage when CI is inhibited.

3.4.10 TIGAR and autophagy

The role of TIGAR role in autophagy was investigated in patients with sporadic PD with mitochondrial defect. We investigated the effect on TIGAR after cells were treated with bafilomycin (autophagy inhibitor) and CCCP (mitophagy inducer). TIGAR protein levels were determined in cell lines from two controls and two sporadic patient fibroblasts.

There was no evident difference in TIGAR protein level amongst patients and controls (Figure 3.28). Results from these experiments showed a great variability in both controls and patients, which is reflected by the high SD obtained. This is perhaps a reflection of the variation occurring between the differences from the patients here tested.
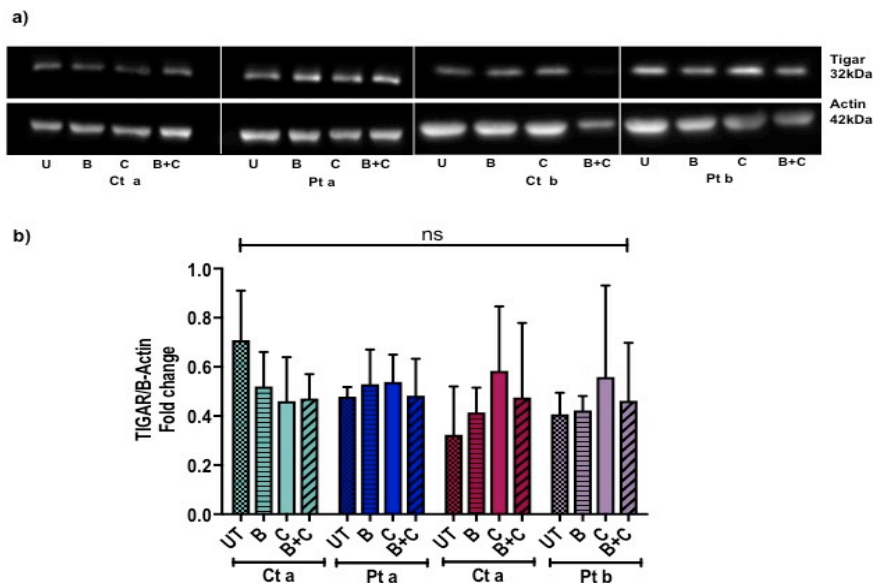
Figure 3.28. Western blot analysis effect on TIGAR after bafilomycin and CCCP treatment in fibroblasts from controls and sporadic PD patient cell lines. a) Representative blots probed in controls (Ct a; Ct b) and sporadic PD patient (Pt a; Pt b) cell lines with antibody against TIGAR. b) Densitometry analysis from each pre-treament conditions (4hrs) in both controls and patients: Untreated (UT), Bafilomycin (B), CCCP (C) and Bafilomycin + CCCP (B+C). There was no statistical difference between controls and patients in any of the treatments. Results are expressed as the mean±SD of samples from three different experiments (2-way ANOVA, $P>0.05$).

3.4.11 TIGAR in other cellular models

Previously, we showed that TIGAR protein is present in human fibroblasts in order to assess its suspected function in this cell model system. In order to continue investigating TIGAR function and its role in PD, we then investigated the protein level in other cellular models that are commonly used in PD research for future experiments. Five different cell lines were assessed by WB under basal conditions and compared to each other. Endogenous TIGAR protein levels are similar between fibroblasts, HeLa and Luhmes, slightly higher in HeLa and significantly increased in HEK293 (Figure 3.29). Therefore, for future experiments, we decided to investigate TIGAR function in HEK293 cell model system.
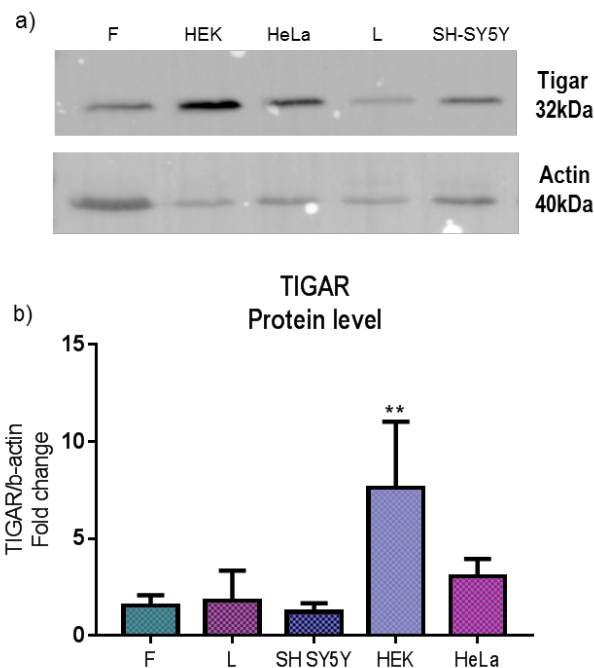
Figure 3.29. TIGAR protein levels in 5 different cell lines. WB image (a) and densitrometry analysis (b) using b-actin as a loading control. TIGAR protein levels showed to be similar between fibroblasts (F), Luhmes (L), SH SY5y and HeLa, whereas HEK cells showed a significant increase of TIGAR protein level when compared to the other cell lines. Bars represent the mean values $\pm$SD, from 3 independent experiments. (ANOVA, **$p<0.005$).

3.5　Discussion

3.5.1　TIGAR in human fibroblasts

As with every cellular model, there are few limitations when using this cellular model. Infrequently, a mixture of cells in proliferation or post-mitotic state can be found. Mycoplasma infection can occur, like in every cell culture, however regular testing and available treatments prevent further infection. As cells are from different individuals, growth rates, seeding density and confluency between individual cell lines, from controls and patients, is variable, but highly valuable to understand the mechanisms of the disease. Unlike neurons, fibroblasts have a different response to trophic factors and signals (Auburger et al., 2012).

Comparison of *TIGAR* mRNA expression levels in the controls and patients with *Parkin* mutations, showed no difference. However, the assessment was performed only in a small sample cohort and the conclusions in the present study are limited by this factor.

No significant difference was seen in TIGAR protein levels either when a group comparison of data obtained from *parkin*-mutant fibroblasts were compared with controls. However, in one patient the TIGAR protein level was increased by ~2.0 fold, whereas in the remaining patients it was slightly decreased by ~0.5 fold. We therefore wanted to establish whether the protein level of TIGAR correlated with the level of Parkin in these fibroblasts cells lines. Notably, in the same patient in whom the level of TIGAR was the highest the Parkin remained the lowest, suggesting that there may be a correlation. Parkin protein level amongst controls and patients showed a variable amount of Parkin, except for P1, that interestingly has the highest

TIGAR protein level. Due to the shared PD related *PINK1/Parkin* pathway, these results might be related to the effect seen in the *pink1-/-* zebrafish, where a *TIGAR* overexpression correlation was demonstrated (Flinn et al., 2013). However, the small number of samples limits the validity of any conclusions, therefore increasing our cohort of controls and patients with *Parkin* and/or *PINK1* mutations, may help to confirm these results.

3.5.2 Mitochondrial function and bioenergetics status in *parkin*-mutant fibroblasts

In previous research performed from our group, fibroblasts from patients with known *parkin* mutations have been shown to have mitochondrial dysfunction with ATP deficient production linked to CI. ATP assays assessed the proliferative and cytotoxicity response of cells, from PD patient tissue, to drug exposure or other biological compounds and/or conditions. Therefore, ATP assays are valuable, sensitive and effective method to investigate the underlying suspected energetic mechanisms involved in PD (Mortiboys et al., 2008, 2010b).

ATP linked-complex I production is facilitated by changing the media growth conditions, since fibroblasts in culture produce their ATP through glycolysis. When media is changed from glucose to galactose, fibroblasts rely on the mitochondrial oxidative phosphorylation (OXPHOS) pathway to produce their energy. One of the patients had to be removed from the overall analysis (P3). ATP assays were performed according to the availability of the tissue. Current results show an ATP reduction of ~41.5% when comparing the group of controls with the patients with *Parkin* mutations, although not as pronounced as previously observed (Mortiboys et

al., 2008). This demonstrated an overall decrease of ATP production linked to a similar defect amongst the five *parkin*-mutant fibroblasts cell lines reported (Mortiboys et al., 2008).

Although fibroblasts are a reliable, robust and useful model of research to study PD in patient tissue, PD is a disease that primarily affects the CNS. In vivo models, such as rodents, have been useful to investigate disease mechanisms, assess toxin exposure (i.e., rotenone, paraquat, herbicides) and to test newer treatments. They offer a great advantage by assessing their effect in motor symptoms and the SN after inducing neurotoxicity and genetic manipulation. Rodent models have shown Dopaminergic neuronal loss. Moreover, they have shown to be useful to study non-motor PD symptoms (i.e. sleep, cognition). However, they do not fully and consistently recapitulate human PD (Blesa et al., 2016; Campos et al., 2013). An alternative approach will be to study TIGAR by reprogramming fibroblasts from patients with PD-related mutations, via induced pluripotent stem cells (iPSC), direct lineage of induced neural stem (iNS), induced neural precursor (iNP), induced neurons (iN), or dopaminergic neurons (iDA). iPSC with PD-related mutations can be differentiated into neurons, which have shown the pathological mechanisms already described in PD (Playne and Connor, 2017; Xu et al., 2017). Direct reprogramming from somatic cells to a specific type of neurons offers a new alternative method for cell modelling avoiding pluripotent state. The direct conversion offers many advantages: functional neurons can be obtained faster (within weeks); the risk of having pluripotent cells left is avoided; it promises to be an efficient and feasible model. However, there are also many disadvantages: less efficiency with scarce or no Tyrosine Hydroxylase positive (TH+) cells, it could still produce longer culture

174

periods for maturation and immature and non-functional neurons, cells are post mitotic and with limited availability. These new methods are still under optimisation, for which different reprogramming protocols have been assessed. Indeed, the effect of TIGAR have been shown to be cell dependent, with complex and somehow contrary and arbitrary functions depending on the metabolic context of a specific cellular type (Bensaad et al., 2006, 2009; Madan et al., 2012). For this reason, any observations in *parkin*- or *PINK1*-mutant fibroblasts would need to be confirmed in further cellular, neuronal model systems or in PD brain tissue.

3.5.3   Tigar RNAi mediated knockdown

Initial transfections using siRNAs (Santa Cruz) against TIGAR were unsuccessful in achieving a satisfactory knockdown in controls. Several potential reasons should be considered for this. For instance, particular cell types can be more difficult to transfect, and this is well established for fibroblasts. Also, the growth and quality variability (i.e., cell confluency, density, passage, etc.) amongst the different fibroblast cell lines used, could affect the transfection process. However, even when transfections assays were performed at the same time with the same methodology, variation cannot be avoided due to cell culture behaviour. This variation in the results could also be caused by the fact that the reference genes are not stably expressed. Also, the factor of the transfection done under serum free media for six hours, might affect the expression of the genes when serum is added hours after the transfection. In Figure 3.10 b-c, the knockdown effect was seen to be reliable between β-actin and GAPDH, whereas at 24 hours (Figure 3.10 a) the knockdown effect showed the highest inconsistency of them all.

The siRNAs against *TIGAR* we used were also only targeting the 3'UTR region of the gene (Figure 3.2). Furthermore, it has been reported that siRNA mediated gene knockdown is generally less effective when targeting only the 3' UTR. A better silencing effect is achieved when targeting the interior region of the mRNA, we therefore used a new SMARTpool of 4 siRNA against TIGAR (Dharmacon) avoiding 50 nucleotides (nt) upstream and downstream region and within the exon 4, 5 and 6 regions of the gene. Successful knockdowns of ~70% were achieved consistently across the different experiments within different cell lines (Figure 3.12), therefore we decided to assess its effect in the mitochondrial function in one *LRRK2*-patient, which displayed a mitochondrial defect previously reported and was available. We wanted to see if the effect of *TIGAR* knockdown was robust and could be applied in PD tissue regardless the genotype.

3.5.4 TIGAR knockdown in mitochondrial function

Transfection with either Lipofectamine only or siRNA against *TIGAR*, showed a significant increase of ATP levels in both treatments in the control and the patient. This means that the ATP increase is the result of the transfection treatment in the cell, therefore any effect of *TIGAR* knockdown is masked by the transfection. Seahorse assays showed the same problem, where Lipofectamine transfection is already affecting the results and having similar comparable readings with the cells where *TIGAR* is knockdown in both, control and patient. Therefore, further transfection reagents and methods were tested and optimized in order to assess *TIGAR* knockdown effect in mitochondrial function in fibroblasts from patients with PD.

3.5.5 Transfection reagents effect in ATP

Transfection experiments in primary cell lines have been shown to be a good method to investigate cellular function, physiology, genomics and drug treatments. Current RNAi methods use physical and chemical reagents in order to deliver the gene or product into the cell. Chemical reagents are some of the most popular methods, they are commonly cationic lipids or polymers, that interact with the negatively charged nucleic acids, allowing their entrance to the cell via endocytosis and prevention to be degraded (Kaestner et al., 2015). In this study, all reagents belonging to this group were used for the transfections, were Lipofectamine 2000 was used for initial transfections and knockdowns. Although fibroblasts are known to be a cell line difficult to transfect, we achieved good transfection efficiency (~77%) and gene knockdown (~69%), as previously seen by others (Mortiboys et al., 2008, 2015; Rakovic et al., 2010). Despite the successful knockdown achieved, the effect of TIGAR silencing in the patient cell lines could not be assessed due to the overlapping effect of the transfection reagent per se. Although different transfection reagents, cellular densities and timings were modified, within the different cell lines; ATP levels continued to be affected by it. This can be explained by a combination of several factors, from the cells and the transfection procedure. With transfections, it is difficult to preserve cellular functionality when cells required to be transfected under serum-free conditions and the need to replace the media. Cells that are also effectively transfected, require to be in division (S or M phase), no overgrown and therefore metabolically active (Hsu and Uludağ, 2012). Consequently, metabolic activity would be affected and visualised in current metabolic measurements here used, such as ATP levels and mitochondrial respiration. Moreover, the growing rate of the cell, passage number and the overall health status and membrane trafficking processes might be another interfering factor, which contributed for the high

variability between the different densities and across the experiments, mainly in the patient cell line, since the mutation by itself might be conferring them an energetic and metabolic defect.

New RNAi methods include Accell siRNA, which has the advantage of be a "self-delivery" method, where no transfection reagent is required. Thus, lower cytotoxicity with good transfection efficiency can be achieved. In this study, the pilot optimisation studies showed indeed that ATP production is less affected at the 96hrs, where the media was changed at the 48hrs after transfection, in the control and the patient, within the different siRNAs, negative and positive controls, same as with the scramble siRNA. Further tests and optimisations are needed for this new promising method. However, due to the fact that fibroblasts cell lines were limited, Accell siRNA reagents needed at higher concentrations and with high price value, we decided to stop this experiments. We then decided to assess TIGAR in different cell lines and further related mechanisms in fibroblasts, such as response to toxic exposure and autophagy. *TIGAR* RNAi methods were further conducted in a stable inducible cellular model, namely HEK293 Flp In cells (see Chapter 4).

3.5.6   Rotenone toxic exposure

Mitochondrial dysfunction, oxidative stress and defective bioenergetics status of the cells can all be triggered by rotenone. The aim of these experiments was to determine the effect of CI inhibition in TIGAR cellular localisation and expression when *parkin* is deficient. TIGAR cellular localisation and expression under the different conditions, glucose and galactose, with or without the rotenone treatment showed no difference in either the control or the *parkin* patient (Figure 3.26 and Figure 3.27). Despite the lack of TIGAR translocation, it does not mean that it is not

implicated in the pathological process. TIGAR mitochondrial translocation has been reported to be dependent on Hexokinase-II (HK-II) expression and presence in the mitochondria, which is highly dependent when glucose is available. Furthermore, TIGAR is affected in different ways by different stressors. Mitochondrial translocation occurs only when O2 levels are $\leq$0.1%, but not with moderate hypoxia or normoxia. Furthermore, the effect was seen in HeLa cells and several cancer cell lines, where metabolic and energetic demands are very different when compared to human fibroblasts. Moreover, TIGAR mitochondrial translocation was linked to cellular survival by protecting cells from ROS damage and regulation of mitochondrial membrane potential.

3.5.7 Tigar and autophagy

Autophagy has been suggested to be implicated in PD and TIGAR pathology. We therefore aimed to assess TIGAR role in treated fibroblasts from patients with sporadic PD with CCCP and bafilomycin. We found no difference between the controls and the patients in any of the conditions. This is in keeping with what results from our group reported in these cell lines, where no significant evidence was found. Many factors could explain this outcome.

To date, altered autophagy remains as a prospective cause in sporadic PD. It remains unclear whether a lack of autophagic response and loss of UPS function or an abnormal accumulation of autophagosomes and lysosomes are behind the pathologic process. Both mechanisms have been shown to produce detrimental effects and finally cellular death. Future experiments aiming to determine TIGAR role in autophagy in human fibroblasts would need to be done in fibroblasts from patients

with sporadic, but also familial PD in order to fully address its role in autophagy PD-related mechanisms.

3.6 Conclusion

This is the first study to investigate TIGAR expression in human fibroblasts derived from patients with familial and sporadic PD. We did not find difference in TIGAR gene expression and protein level between controls and *parkin*-mutant fibroblasts. Although one patient showed TIGAR increased levels, which correlated with decreased parkin levels, it was only one patient.

Effective *TIGAR* knockdown was achieved in parkin deficient and *LRRK2*^{G2019S} fibroblasts, but the effect of TIGAR deficiency on mitochondrial function could not be tested due to masking effect of the transfection. Therefore, further investigations of the effect of TIGAR in cellular and neuronal models with PD-related mutations should be attempted by alternative methods such as stable transduction. TIGAR cellular localisation is not affected in *parkin* mutant fibroblasts in response to rotenone toxic exposure and cellular stress. No evidence of TIGAR involvement in autophagy was seen in sporadic patients with PD under the conditions tested in this study. Further experiments should be attempted in a stable cell line to determine effect of *TIGAR* knockdown in *PINK1* deficiency and confirm in dopaminergic neuronal cell lines.

4 Stable cell lines for PD research

4.1 Introduction

It is essential to fully understand the function of genes implicated in the development of the disease. Therefore, cellular and animal models with conditional gene expression and regulation need to be generated. The genetic function can be analysed by turning on or off the expression of mutated genes known to cause PD pathology, and therefore be able to recapitulate human health and disease. In the present, a wide variety of controlled gene expression systems are commercially available, including the tetracycline-inducible T-Rex™ Flp-IN™ cells from Thermo Fisher Scientific using common cell lines, such as HEK293T.

As previously stated, mutations in PD-related genes can cause autosomal or recessive forms of the disease. Knowing causal gene mutations enables researchers to generate cellular and animal models via genomic manipulation, in order to investigate potential disease leading mechanisms.

4.1.1 Gene silencing: molecular engineering

RNA interference (RNAi) methods allow the introduction of a double-stranded RNA (dsRNA) into a target cell. Small interfering RNAs (siRNAs), micro-RNAs (miRNAs) and short hairpin RNA (shRNAs) are some of the interfering RNA species used for gene silencing. MicroRNAs (miRNAs) are short transcripts encoded by endogenous genes, which activates repression at both, post-transcriptional and translational levels, of target genes. In mammalian cell lines, miRNA repression is fundamentally through translational repression (Guo et al., 2010; Wilczynska and

Bushell, 2014). miRNAs usually bind the 3'UTR in a partial but highly complementary manner. They are found in the nucleus, contained and transcribed in a cluster, known as long primary transcripts (pri-miRNAs), which are synthesised by the enzyme RNA polymerase II. Pri-miRNAs are subsequently cleaved by Drosha, a RNAse III protein located in the nucleus and important for miRNA processing. RNAse III proteins are specific endonucleases that cleave the RNA structure on each side. Drosha cleaves pri-miRNAs into small ~70 nucleotide hairpins known as pre-miRNAs. Pre-miRNAs are then exported from the nucleus through pores to the cytoplasm by Exportin-5. The pre-miRNAs are further processed into a 22-nucleotide mature RNA sequence (mRNA) by Dicer, another RNAse III protein located in the cytoplasm (Lee et al., 2003). The mRNA sequence binds the RNA-induced silencing complex (RISC), after which antisense strands align with the mRNA. The expression of the mRNA is repressed then by three mechanisms: a) preventing the translational initiation (repression), mRNA decay (decapping 5' and 3' ends) or direct RNA cleavage by RISC (Recasens et al., 2016). Plasmid and viral vectors usually contain small nuclear RNA pol III promoters, such as U6 and H1, widely used for shRNA and miRNAs construct design. Both are ubiquitously expressed promoters that promote efficient gene silencing effect, where U6 proved to be the most effective (Mäkinen et al., 2006; Zhou et al., 2007).

RNA interference (RNAi) is a powerful tool to gain insight into the biological and physiological function of specific genes. By controlling the environmental conditions and through genetic manipulation, protein levels can be regulated within the physiological margin. However, long-term gene repression might potentially cause non-physiological and undesired cellular effects. Generation of inducible RNAi

cellular regulation (e.g tetracycline) is a way to avoid these potential undesired effects. One disadvantage of this system is that in some particular cell lines background gene expression might still be high and detectable in the non-induced cells and affect the overall outcome (Gupta et al., 2004).

The Thermo Fisher Scientific engineered miRNAs, BLOCK-iT™ Pol II miR RNAi expression vector kit, is a new adapted method for expression of a specific designed miRNA sequence, which represent the target sequence of interest and RNAi research. This allows the generation of clones expressing double stranded (ds) oligos, encoding a pre-miRNA sequence generated by expression vector selection. These constructs can then be introduced into the cell of interest for transient or stable expression of the targeted miRNA sequence to study its effects within the cell (Werness and Anderson, 2010).

4.1.2   Site-specific recombinase systems

The site-specific recombinase systems (SSR) have been widely used to achieve gene knockout. SSR can be combined with and inducible gene expression system, such as tamoxifen and tetracycline, which enables the generation of cellular and animal models at a specific stage in the tissue of interest. This conditional knockout approach allows researchers to study the gene function at different cellular stages. There are several SSR developed systems, where Cre-loxP, Flp-FRT and ϕC31 are amongst the most commonly used.

4.1.3   Flp In-FRT

The Flp-In FRT system was derived from the yeast *Saccharomyces cerevisiae.* In this system, the recombinase Flp recognises a 34-base pair (bp) nucleotide sequence known as the FRT site. Within this site two 13bp palindromic

sequences are contained and separated by an 8 bp spacer. These palindromic sequences will give the orientation of the site, bind to the recombinase and the spacer. This region is where the DNA breaks and homologous recombination occurs between the *FRT* sites. The Flp system therefore allows DNA exchange between genomes, at the site of gene of interest, and the transfected plasmid (Golic and Lindquist, 1989). This homologous recombination occurs in a single targeted site, preventing from gaining or losing nucleotides as well as avoiding clonal variability (Shah et al., 2015; Zhang et al., 2012). This is important as it enables the generation of isogenic stable cell lines, in which control and disease cell lines are genetically identical, except for the expression of the disease-mutated gene (Liu et al., 2006).

4.1.4 Tetracycline system

The tetracycline systems are based on the *E. coli* tetracycline resistance operon, an operator sequence (TetO) contained within the operon, the efflux pump genes and a tetracycline-repressor protein (TetR). The regulation of this allows the gene expression in a spatiotemporal manner. Under normal conditions, the expression of the operon is inhibited when TetR binds the TetO. When tetracycline is added, the TetR binding is interrupted leading to the operon release, which promotes the gene expression. Two controlled systems were derived from this system:

• In the Tet-off (tTA) systems, the target gene is turned off after tetracycline is added, promoting TetR to bind the transcription activation domain VP6. Here, when tetracycline is absent, the tetracycline controlled transactivator protein (tTA), which is a repressor that binds the tTA responsive promoter (Ptet), enables the gene expression.

• In the Tet-ON system, the tTAT does not bind the Ptet. Once tetracycline is added, the tTA binds the Ptet, which subsequently leads to gene expression (Zhang et al., 2012).

Tet-off and Tet-On systems have been widely used for modelling neurodegenerative disorders, such as Alzheimer's Disease (AD) (Arif et al., 2014), PD (Bertolin et al., 2013; Carballo-Carbajal et al., 2010; Jiang et al., 2007; Kobayashi et al., 2006), Huntington's Disease (HD) (Igarashi et al., 2003; Waelter et al., 2001) using different cellular and animal models (Khlistunova et al., 2006; Sun et al., 2007).

4.1.5   FLP/FRT Inducible model

The combination of both techniques, tetracycline and Flp In systems, enabled the development and construction of improved conditional cell lines. The gene of interest (GOI) can be then targeted in a spatiotemporal manner by adding tetracycline or, the analogue, doxycycline (Spitzer et al., 2013; Yahata et al., 2005).

Thermo Fisher Scientific introduced the new Flp-In T-Rex Core Kit, for generation of stable cell lines with tetracycline-inducible expression. This system is controlled by the integration of the Flp Recombinase in a specific site, which mediates the expression of GOI in mammalian cell lines. This system follows three basic steps: generation of the Flp-In T-Rex™ host mammalian cell lines, followed by the integration of the vector expressing the GOI containing a tetracycline-controlled promoter and, gene induction by tetracycline addition (Spitzer et al., 2013) (Figure 4.1).

The Flp-In T-Rex System offers many advantages compared to many other cellular models. It is and efficient and rapid system for generation of Flp-In T-Rex cell

lines expressing the GOI after it has been integrated FRT site in the Flp-In T-Rex host cell line. Importantly, the generated inducible stable cell lines are isogenic (Yahata et al., 2005).

The Flp-In T-Rex host cell line is generated when two plasmids are co-transfected into the selected mammalian cell line:

• The pFRT/*lac*Zeo vector containing a SV40 promoter regulating the expression of the *lacZ*-Zeocin fusion gene. Downstream from the ATG initiation codon of the *lacZ*-Zeocin fusion gene, the FRT site is inserted. This is the recognition binding and excision site for the Flp endonuclease. The *lacZ*-Zeocin fusion gene encodes a fusion protein with a Zeocin resistance marker, which allows selection of stable cell lines by screening them for Zeocin sensitivity (Huang et al., 2007).

• The pcDNA6/TR plasmid expressing the TetR gene provides Tetracycline resistance (Møller et al., 2016) under the control of the human cytomegalovirus (CMV) promoter (Kim et al., 1995). The blasticidin resistance gene, which is under the control of the SV40 early polyadenylation signal, allows the expression of the blasticidin resistance gene for stable cell line selection (IzuMi et al., 1991).

Random independent genomic integration occurs when the pFRT/*lacZ*-Zeo and pcDNA6/TR plasmids are transfected and integrated into the mammalian cell line. Thus, the Flp-In™ T-Rex™ host cell line is then generated (Spitzer et al., 2013).

An expression vector containing the GOI is built by the operator that wishes to create a new inducible cell line and will then be integrated into the cells by the Flp recombinase. The expressing vector is co-transfected with a plasmid expressing the

Flp recombinase into the host cell line. This allows the expression of the Flp recombinase, which enables the integration of the expressing vector containing the GOI into the genome of the host cell. The Flp recombinase then mediates the homologous recombination between the two FRT sites. The *lacZ-Zeoc*in fusion gene is inactivated after the SV40 promoter and the ATG initiation codon are brought into frame with the hygromycin resistance gene. Stable cell lines can therefore be selected by screening them for blasticidin and hygromycin resitance and zeocin sensitivity. The expression of the GOI is then induced upon tetracycline addition (Figure 4.1).
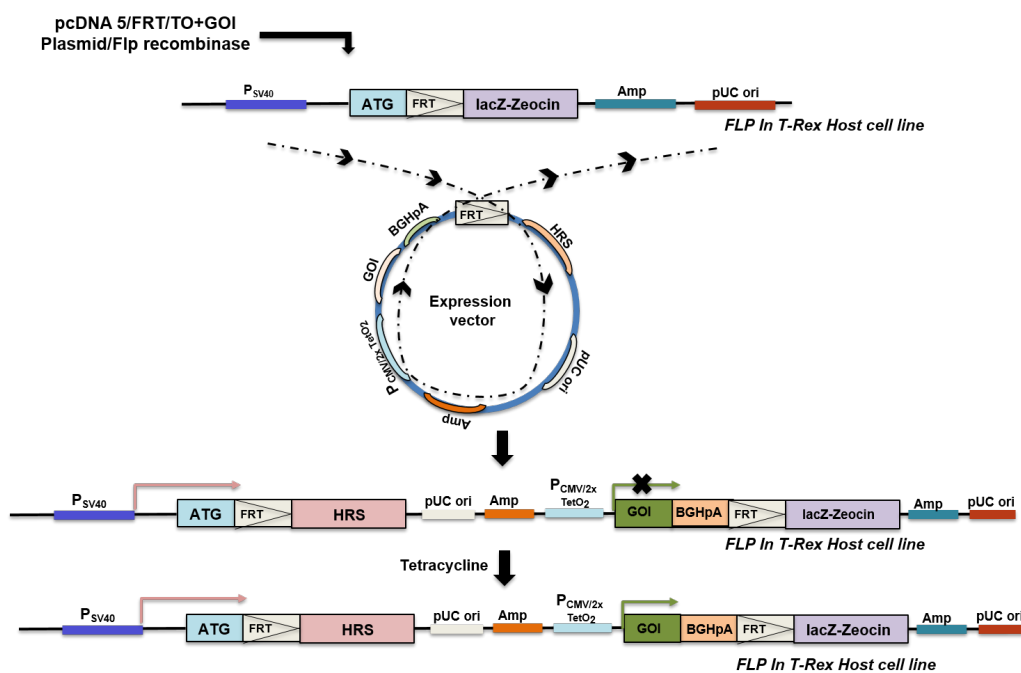
Figure 4.1. FLP-In T-Rex System Thermo Fisher Scientific. Schematic representation of the Flp-In T-Rex system. The pcDNA 5/FRT/TO construct genomic integration into the host cell line is performed by its cotransfection with the recombinase plasmid. Then, homologuos recombination occur between the FRT sites in the expression vector and the host cell line. The transcription of the Gene of interest (GOI) takes place once the expression is integrated. The host cell line is conferred with antibiotic resistance to Hygromycin and sensitivity to Zeocin. Tetracycline addition enables the expression and regulation of the inserted gene. Adapted from Flp-In™ T-REx™ Core Kit Manual, Thermo Fisher Scientific.

187

4.1.6 Inducible models in Parkinson's Disease

Autophagy has been suggested to be involved in the pathogenesis of many neurodegenerative diseases. Autophagy helps cellular clearance from misfolded proteins, its impairment could lead to accumulation and contribute to the pathogenesis in neurodegenerative diseases. When impaired, it could lead to accumulation of misfolded proteins within the cell. Stable doxycycline inducible PC12 cell lines expressing WT alpha-synuclein, A30P or A53T mutants were used as PD cellular model to study the neuroprotective effects of resveratrol. The resveratrol beneficial effects against aging, inflammation and cancer have been widely investigated; however, the involved mechanisms are still unknown. In this model, it was demonstrated that it acts as an autophagy and mitophagy inducer through modulation and activation of the silent regulator 2 (SIRT1) and AMP-activated protein kinase (AMPK) (Wu et al., 2011). Resveratrol is a potential drug for PD treatment due to its potential beneficial effects demonstrated in several models

The relation of alpha-synuclein and unfolded protein response (UPR) was studied in a PC12 alpha-synuclein overexpressing inducible cell line. Here, induced cells showed to have an impaired UPR, increased cellular vulnerability and death. An enhancement of cellular toxicity was correlated with cathecolamine, such as dopamine, function (Ito et al., 2010). The interaction between dopamine and alpha-synuclein in a PC12-Tet off (tetracycline inducible) system was studied. The stable inducible cell lines were expressing WT *alpha-synuclein*, mutants M116A, M127A and M116/M127A (in which the methionine residue was mutated), Y12D and S12A. It is suggested that the alpha-synuclein methionine residues are oxidized by dopamine, which induces oligomerization of alpha-synuclein with subsequent neurocytotoxicity. Here the dopamine-related M127A modification was reported to

play the main role in the oxidation process. It was suggested that the mechanism is via dopamine binding the C-terminal region of alpha-synuclein, where dopamine might be the main source of reactive oxygen species (ROS). Furthermore, an increase of the M127 modification might result under the presence of the pathogenic serine (S129) and tyrosine (Y12) alpha-synuclein forms (Nakaso et al., 2013). Moreover, the synergistic interaction between alpha-synuclein and dopamine was also demonstrated in a stable inducible cell line expressing WT *alpha-synuclein* and the PD-related *alpha-synuclein* mutant A53T. An increase of aggregates within the cytoplasm was observed in cells with *alpha-synuclein* overexpression, whereas mutant A53T showed increased dopamine induced cytotoxicity and vesicular formation. Alpha-synucein is mainly expressed in cells with high levels of dopamine, where it is suggested to be regulating its release in the synaptic terminals. At long term, the cumulative effect of defective dopamine compartmentalization, instability and ROS generation might lead to alpha-synuclein aggregation, aggregates formation and neuronal death (Tabrizi et al., 2000).

The pathophysiological cellular mechanisms of LRRK2 proteins remain poorly understood at the molecular, biochemical and biological levels. Thus, generation of reliable and robust cellular and animal models are valuable tools to study these mechanisms. Inducible dopaminergic MN9D cell lines (a fusion of embryonic ventral mesencephalic and neuroblastoma cells) expressing either WT *LRRK2* or mutant *LRRK2*^{G2019S}, were generated to serve for drug screening, testing therapeutic role of *LRRK2*^{G2019S} RNAi mediated gene knockdown and its kinase inhibitors. It was found that the *G2019S* cells had lower metabolic activity, which was increased in the presence of WT *LRRK2*. The *G2019S* displayed also shortened neurite extension

without cytotoxicity, which was rescued by kinase inhibitors and by *G2019S* RNAi mediated knockdown (Huang et al., 2013). Previous research in a *Drosophila* model, suggested that the eukaryotic initiation factor 4E (eIF4E)-binding protein) (4E-BP), important in protein synthesis and translation, had role as a LRRK2 substrate. This *Drosophila* model showed that LRRK2 phosphorylated the 4E-BP, impairing translation of proteins and altered cellular homeostasis, which could lead to neurodegeneration (Imai et al., 2008). To investigate the suspected interaction between LRRK2 and 4E-BP, as well as the involved mechanisms, a tetracycline inducible HEK 293FT FLP-In cells with WT *LRRK2* and mutant *G2019S* or *R1441C* were studied. Here, they showed that the 4E-BP was a weak substrate of *LRRK2 in vitro.* Its suspected role involved with LRRK2 functionality in human cellular models remain to be demonstrated (Kumar et al., 2010). The LRRK2 related cellular response to oxidative stress was studied in a lymphoblastoid LRRK2 inducible cell line. Here, cells were exposed to two oxidative stressors, namely arsenite and hydrogen peroxide (H_2O_2) and their effect in LRRK2 phosphorylation status. Both oxidative stressors induced the loss of phosphorylation at specific sites in LRRK2, which affected the GTP binding and kinase activity. This proposed LRRK2 as a modulator of the oxidative stress response linked to PD pathogenesis (Mamais et al., 2014). Further suspected mechanisms between WT *LRRK2*, *LRRK2* PD-linked mutations and tubulin or microtubules dynamics have been investigated in non-neuronal inducible lines. Here *LRRK2* mutations showed to affect the tubulin phosphorylation status and lead to impaired microtubule function and stability, leading to cellular damage (Gillardon, 2009).

The PINK1/Parkin pathway function in mitophagy is crucial for the cell to maintain healthy mitochondria. Impaired mitophagy has been suggested to be associated to PD. Many mechanisms have been studied, where mutations in the PD-related, *PINK1* and *Parkin*, genes play a major role. Stable inducible cell lines expression WT human Parkin (FLP-In GFP Parkin) and two mutants, K161N and G430D (PD-linked mutations); were used to screen a number of deubiquitinase (DUBs) enzymes by mass spectrometry. In the overexpressing Parkin cell line induced by carbonyl cyanide 3-chlorophenylhydrazone CCCP, USP30 showed to have opposite effects to Parkin. By overexpressing USP30 in Parkin cell lines, it was found that USP30 inhibits mitophagy by removing the ubiquitin attached by Parkin. Mitophagy was rescued in the GFP-Parkin, mutant G430D and K161N when USP30 was knocked down *in vitro* and the *in vivo* model *Drosophila*. A protective effect against paraquat toxicity was also demonstrated in the flies (Bingol et al., 2014).

Parkin tetracycline-inducible SH-SY5Y cell lines have been reported useful to study the effect of WT and mutant forms of Parkin proteins (Arena et al., 2013; Geisler et al., 2010a, 2010b; Ozgul et al., 2014; Rothfuss et al., 2009). Some of the mechanisms studied using these models were:

• Mitophagy: the involvement of PINK1, Parkin, ubiquitin, VDAC1 and p62 in the mitophagy pathway in a chronological manner after mitochondrial depolarization to remove damaged mitochondria. This pathway impaired by PD-related mutations, Parkin and PINK1 loss of function affect their interaction and solubility, mitochondrial localization, stabilization and Parkin translocation. Their functional impairment lead to defective mitophagy, suspected to be a key mechanism leading to neurodegeneration (Geisler et al., 2010a, 2010b).

- PINK1 neuroprotection: one of the PINK1 neuroprotection mechanisms was demonstrated to occur by preventing cellular death via Bcl-cL (anti-apoptotic protein) interaction in depolarized mitochondria. In the SH-SY5Y Parkin inducible cells, Bcl-Xl was not involved in depolarized mitochondria and mitophagy after Parkin recruitment. This proposed a Parkin-independent PINK1-Bcl-Xl pathway for mitochondrial mitophagy (Arena et al., 2013).

- By using 2D-DIGE to study the proteomic profile of this cell lines, 22 proteins were identified to be regulated by Parkin, from which 13 of them were particularly regulated in the mutant forms (Q311R and A371T) assessed. Most of the hits for the mutant forms, were proteins involved in energy metabolism and protein folding. Here, UCHL-1, 14-3-3 and heterogeneous nuclear ribonucleoprotein (hnRNP) was the most affected. Functional analysis with WT and mutant cell lines showed that one of the main differences is post-translational modifications in which mutant forms display lower molecular weight. However, protein stability, ubiquitylation activity and cellular localisation were not affected in the mutant forms. Further studies are required to confirm and correlate the relation of the Parkin substrates identified and the mechanisms related to PD and neurodegeneration (Ozgul et al., 2014).

PD cellular and animal models to study *DJ-1* role in neurodegeneration, showed that its main function is by providing neuroprotection against ROS and by regulating gene transcription. In the SH-SY5Y inducible cell model where *DJ-1* is silenced, microarray analysis showed that 166 genes were altered, where the rearranged during transfection (*RET*) gene showed the highest reduction of mRNA and protein levels. A direct correlation between *RET* and *DJ-1* expression was found

in this cellular model. Further functional analysis in this *DJ-1* deficient model showed that RET is acting as a ligand of the glial cell line-derived neurotrophic factor (GDNF), which is involved in the regulation of cellular death during early development and its vital for postnatal cellular survival and innervation. In addition to this, *DJ-1* deficiency produced increased ROS levels, which stabilises the hypoxia inducible factor 1α (HIF-1α). Increased HIF-1a levels induced cellular hypoxia and apoptosis. This study suggested a neuroprotection role of *DJ-1* via the *GDNF* pathway against hypoxia and ROS damaged in PD pathology (Foti et al., 2010).

Cell lines in which PD-related genes and mutations have been induced, have been a valuable source to study PD-related mechanisms and unknown biochemical, physiological and molecular pathways involved.

4.1.7   CRISPR/Cas9

Modern techniques have allowed us to use a wide range of molecular engineering methods in which a diversity of molecular, biological, biochemical pathways can be studied. CRISPR/Cas9 is a new identified genome editing technique, which depends on the bacterial Cas9 endonuclease activity. The *C*lustered *R*egularly *I*nterspaced *S*hort *P*alindromic *R*epeats (CRISPR)/Cas9 (CRISPR-associated endonuclease) is a system, in which the Cas9 endonuclease targets and cleaves specific DNA sequences directed by a small guide RNA (sgRNA). The system requires the target recognition by Cas9, via a seed sequence in the sgRNA and the adjacent GG-dinucleotide PAM sequence (Garneau et al., 2010; Jinek et al., 2012; Ran et al., 2013). Blunt DNA cleavage generates a double-strand break (DSB) by two endonucleases domains, which cut the complementary strand (Cas9 HNH nuclease domain) and the complementary strand (Cas 9 RuvC-

like nuclease domain) (Jinek et al., 2012). Cas9 nickase cut only one DNA strand (single-strand break, SSB). DSBs and SSBs are then repaired via the homology-directed repair (HDR) or the Non-homologous end-joining (NHEJ) pathways (Rubio et al., 2016).

Insertions and/or deletions can be generated by the NHEJ pathway, which result in truncated proteins and premature stop codons (Su et al., 2016). Gene Knock-in is generated via the HDR, displaying point mutations, insertions and epitope tags (Zhang et al., 2017). Cas9 nickase and SSB repair avoids indels; to cut both strands a double-nicking approach is required and DSBs are generated. Thus, the off-target effect is highly reduced. This approach requires co-transfection of two plasmids, Cas9 nickase, sgRNAs and markers, which affect transfection efficiency and efficacy (Yoshioka et al., 2016). The All-in-One (AIO) plasmid approach tackles this obstacle by carrying the Cas9 coupled to the fluorescent marker and the two sgRNAs. The two cuts or "nicks" (double nicking) are in opposite strands close to each other. This approach achieves slightly less efficiency and efficacy but with very low off-target effects (Chiang et al., 2016).

Targeting a specific gene and its alteration mimics mutations in humans in cellular and animal models. Gene knock-in or knock-out allows to investigate the defects from a particular disease and recapitulate pathology.

CRISPR/Cas9 has been used as a therapeutic tool for different conditions and diseases. Recombinant adeno-associated viral vectors (AVV) are currently used in some cellular (Kennedy and Cullen, 2015) and animal disease models (Ohmori et al.,

2017) as well as some clinical trials in gene therapy with promising outcomes (Rincon et al., 2015). However, the continue need of re-dosing due to loss of gene function and potential toxic effect in peripheral organs remain a problem secondary to viral sequestration. The combination of CRISPR/Cas9 and AAV genome modification, has successfully engineered an effective aav2G9 chimeric aav strain. The modified engineered strain possesses the ability to enter the cell by anchoring either the heparan sulphate or galactose receptors. This new strain promises an effective and specific cellular delivery in the central nervous system (CNS), avoiding off-target effects and with lower transgene expression (Murlidharan et al., 2016).

4.1.7.1   CRISPR/Cas9 and PD models

The anatomy, physiology and genome of pigs are very similar to the human, making them suitable as an animal model for a diversity of human pathologies. Moreover, their cerebral cortical folding is highly similar to the human brain, making them an ideal model to study neurodegenerative diseases. Recently, PD pig model has been generated via CRISPR/Cas9, in which *Parkin*, *DJ-1* and *PINK1* are simultaneously targeted. This new reliable, robust and promising animal model for PD was generated by introducing the multiplexing sgRNA into the pronuclear embryos via Cas9 mRNA injection. Despite the high possibility of antagonistic, off-target effects and mutagenesis due to multiple sgRNAs introduction; whole-genome sequencing showed no off-target effects and no mosaic mutations (Wang et al., 2016d).

Risk variants of PD-related genes have been associated with the sporadic form of PD. *Alpha-synuclein* was identified by Genome Wide Association Studies (GWAS) as the strongest risk loci for sporadic PD (Simón-Sánchez et al., 2009).

Isogenic human pluripotent stem cell lines with genetically modified PD-associated regulatory elements were generated via CRISPR/Cas9 system. Heterozygous deletion or exchange of associated elements in the risk and protective alleles were analysed in the progenitor cells and derived neurons. Here, the binding efficiency of the transcription factors was modified having a modulation effect in the enhancer activity. The cis-acting effect of the protective A allele at rs356168 in the genomic sequence showed lower expression of *alpha-synuclein,* reducing the risk for PD. Contrary, the risk G allele at rs356168 showed increased *alpha-synuclein* expression and higher risk for PD. This system showed to be a reliable and robust cellular model to study human disease and the effect of gene variations disease-related (Soldner et al., 2016).

It remains unclear the mechanism of the vacuolar protein sorting 35 gene (*VPS35*) in PD. A question of whether its pathology mechanism is due to a gain or loss of function has motivated researchers to create models to elucidate the cause. Recently, a knock-in mice model was generated via CRISPR/Cas9, in which endogenous expression patterns with Vps35 deletion 1 (Del1) are expressed alongside the mutant protein (Vps35 D620N KI). The Vps35 D620N KI was able to rescue the Vps35 del1 mice from lethality during embryonic stages, but with less survival rates. Therefore, the normal functionality of the wild-type protein was never achieved. Dopaminergic neurotransmission in the caudate putamen was impaired, but without evidence of neurodegeneration in the homozygous mice (Vps35 D620N KI). Due to these effects in the mice models, it has been proposed that VPS35 causal PD-related mechanisms are due to loss of function. However, further

functional mechanisms are required to confirm and identify the actual biological process implicated in the pathogenesis (Ishizu et al., 2016).

CRISPR/Cas9 offers the opportunity to generate cellular and animal models to simulate human diseases, alongside the opportunity to be use as a therapeutic tool to target specific genes and correct the genetic defect. Recently, a CRISPR-based genetic screen was designed in induced pluripotent stem cells (iPSC) derived neurons. This CRISPR-iPSC derived neuronal models offers a new platform, in which neurodegeneration and vulnerability of a specific neuron can be studied by manipulating a range of associated disease risk factors. This approach offers a new cellular model to study pathogenesis and related mechanisms, alongside the opportunity test new therapeutic techniques and drugs (Kampmann, 2017).

Despite all the advantages CRISPR tools offer, the system is still in early stages, where undesired effects hinder its utility. Some of the major disadvantages remain the off-target effects and chromosomal rearrangements, which in some instances can be difficult to detect (Mohr et al., 2014). This is due to mismatches occurring within the short 20 nucleotide sequence that are tolerated within the protospacer region (Ran et al., 2013). Furthermore, the larger size of the Cas9 protein makes it difficult as a delivery method via either viral vectors or as RNA molecule. CNS delivery techniques need to cross the blood-brain barrier, making it particularly difficult for use as a therapeutic tool in Neurological disorders. Moreover, the HDR requires an effective DNA damage repair, which is particularly less active and efficient in the post-mitotic neurons, where the likelihood of mutagenesis is enhanced (Yan et al., 2017). Current research is working to tackle this problem by

sequencing and looking into more prokaryotes genomes, new CRISPR or CRISPR-like systems, Cas9 modifications and designing algorithms in order to improve the DNA cleavage specificity and effectors (Haeussler et al., 2016; Yoshioka et al., 2016).

4.2   Aims and objectives

Assess the effect of *TIGAR* knockdown in a stable inducible human cellular model with *PINK1* deficiency. HEK 293 and HEK Flp In cells were chosen as the cellular model and expression system for this study. These cells are easy, inexpensive to grow and maintain, with rapid reproduction, easy to transfect, efficient protein production, ideal for viral vector production and gene therapy, amenable for recombinant protein production, express exogenous proteins and commercially available. They offer a robust and reliable cellular model. Furthermore, transfection procedures are easy and fast, achieving high efficiency and efficacy.

In this study we aimed to:

• Design RNAi methods for *TIGAR* and *PINK1* knockdown in mammalian cells.

• Achieve a consistent effective and efficient knockdown of *TIGAR* and *PINK1* in HEK 293 cells.

• Build isogenic stable inducible human cell models with *TIGAR* and *PINK1* deficiency to assess mitochondrial function by measuring ATP cellular production and the mitochondrial morphology.

• Compare two different molecular engineering techniques to assess gene silencing effect and function.

4.3   Materials and methods

4.3.1   Stable inducible cell line

4.3.1.1   HEK293T Flp In

Oligonucleotides design: microRNAs

In order to generate inducible knockdown lines, we used the BLOCK-iT™ Pol II miRNAi Expression kit (Invitrogen) to generate CMV promoter-based vectors that will allow genome-integration at the FRT site. The integration of the vectors enables the expression of miRNAs in the HEK293 Flp-IN host cell lines. miRNA are oligonucleotides that target a specific against a genomic region, namely *TIGAR* and *PINK1*. Such constructs are composed by:

• Single stranded oligonucleotide (ss oligos) for each gene were designed by using the online tool from Invitogen's RNAi Designer (http://rnaidesigner.lifetechnologies.com/rnaiexpress/) (Table 4.1 and Table 4.2). Pre-miRNA sequences for TIGAR (Table 4.1; Table 4.2) and PINK1 (Table 4.3 and Table 4.4) were designed for cloning into pcDNA™ 6.2-GW/+ EmGFP-miR vector. The Pre-miRNA (miR) sequences are inserted in the 3'UTR of the fluorescent GFP.

The designed ss oligos or pre-miRNA (miR) for TIGAR (Table 4.2) and PINK1 (Table 4.4) inserts have the following characteristics:

• Five derived-nucleotide (TGCTG) from endogenous miR-155. 5' overhang compatible with a four nucleotide overhang in the pcDNA 6.2-GW™/+ EmGFP-miR vector

• Reverse complement of the 21 nucleotide target sequence

• 19 nucleotide derived from miR-155 to form a terminal loop

No.	Start	Sequence(DNA)	GC%	Rank[1]
1	**334**	**GAAGAGTGCCCTGTGTTTACA**	**47.62**	★★★★★
2	563	GATTAGCAGCCAGTGTCTTAG	47.62	★★★★☆
3	567	AGCAGCCAGTGTCTTAGTTGT	47.62	★★★★★
4	**634**	**GACCTTAAGTGTTCCTTACCA**	**42.86**	★★★★★
5	677	TTATGTCAGTCACTCCCAATA	38.1	★★★★★
6	695	ATACAGGGATGAGTCTCTTTA	38.1	★★★★★
7	696	TACAGGGATGAGTCTCTTTAT	38.1	★★★★★
8	738	AGAAGTTAAACCAACGGTTCA	38.1	★★★★★
9	**743**	**TTAAACCAACGGTTCAGTGTA**	**38.1**	★★★★★
10	782	ATCATCTAAATGGACTGACTG	38.1	★★★★☆

Table 4.1. TIGAR (NM_020375.2) top 10 target sequences. [1]"Star scoring system" reflects the probability of knockdown, where the one with the highest probability is given 5 stars and the one with the lowest only 3 stars. Only duplexes that are most likely to be successful with higher quality are shown. Target sequences highlighted in yellow and were selected for miRNA design.

No.	Start	Oligo Type	Oligo Sequence
1	334	T S	5'- TGCTGTGTAAACACAGGGCACTCTTCGTTTTGGCCACTGACTGACGAAGAGTGCTGTGTTTACA -3'
		B S	5'- CCTGTGTAAACACAGCACTCTTCGTCAGTCAGTGGCCAAAACGAAGAGTGCCCTGTGTTTACAC -3'
2	634	T S	5'- TGCTGTGGTAAGGAACACTTAAGGTCGTTTTGGCCACTGACTGACGACCTTAAGTTCCTTACCA -3'
		B S	5'- CCTGTGGTAAGGAACTTAAGGTCGTCAGTCAGTGGCCAAAACGACCTTAAGTGTTCCTTACCAC -3'
3	743	T S	5'- TGCTGTACACTGAACCGTTGGTTTAAGTTTTGGCCACTGACTGACTTAAACCAGGTTCAGTGTA -3'
		B S	5'- CCTGTACACTGAACCTGGTTTAAGTCAGTCAGTGGCCAAAACTTAAACCAACGGTTCAGTGTAC -3'

Table 4.2. TIGAR oligonucleotide primers. 3 miRs (column 1) were designed against TIGAR. They target different regions within the gene (column 2). Top Strand, TS; Bottom Strand, BS.

No.	Start	Sequence(DNA)	GC%	Rank[1]
1	459	GGAGGAGTATCTGATAGGGCA	52.39	★★★★☆
2	**464**	**AGTATCTGATAGGGCAGTCCA**	**47.62**	★★★★★
3	465	GTATCTGATAGGGCAGTCCAT	47.62	★★★★☆
4	470	TGATAGGGCAGTCCATTGGTA	47.62	★★★★☆
5	496	TGCAGTGCTGCTGTGTATGAA	47.62	★★★★☆
6	**509**	**TGTATGAAGCCACCATGCCTA**	**47.62**	★★★★★
7	681	TTCCTCCAGCGAAGCCATCTT	52.39	★★★★☆
8	686	CCAGCGAAGCCATCTTGAACA	52.39	★★★★☆
9	690	CGAAGCCATCTTGAACACAAT	42.86	★★★★☆
10	**936**	**GACGCTGTTCCTCGTTATGAA**	**47.62**	★★★★★

Table 4.3. PINK1 (NM_032409.2) top 10 target sequences. [1]"Star scoring system" reflects the probability of knockdown, where the one with the highest probability is given 5 stars and the one with the lowest only 3 stars. Only duplexes that are most likely to be successful with higher quality are shown. Target sequence is highlighted in yellow and were selected for miRNA design.

No.	Start	Oligo Type	Oligo Sequence
1	464	TS	5'- TGCTG**TGGACTGCCCTATCAGATACT**GTTTTGGCCACTGACTGACAGTATCTGAGGGCAGTCCA -3'
		BS	5'- CCTGTGGACTGCCCTCAGATACTGTCAGTCAGTGGCCAAAAC**AGTATCTGATAGGGCAGTCCAC** -3'
2	509	TS	5'- TGCTG**TAGGCATGGTGGCTTCATACA**GTTTTGGCCACTGACTGACTGTATGAACACCATGCCTA -3'
		BS	5'- CCTGTAGGCATGGTGTTCATACAGTCAGTCAGTGGCCAAAAC**TGTATGAAGCCACCATGCCTAC** -3'
3	936	TS	5'- TGCTG**TTCATAACGAGGAACAGCGTC**GTTTTGGCCACTGACTGACGACGCTGTCTCGTTATGAA -3'
		BS	5'- CCTGTTCATAACGAGACAGCGTCGTCAGTCAGTGGCCAAAAC**GACGCTGTTCCTCGTTATGAAC** -3'

Table 4.4 PINK1 oligonucleotide primers. Three microRNAs (miRs) (column 1) were designed against PINK1. They target different regions within the gene (column 2). Top Strand, TS; Bottom Strand, BS.

4.3.2 Flag tagged TIGAR and pEFGPn1-PINK1

Flag-tagged TIGAR was designed and generated by PCR using the primers in Table 4.5. The pEGFPn1-PINK1 plasmid expressing PINK1 fused to a GFP tag was provided by Dr. Kurt de Vos.

Primer	Sequence
Sense / Forward	**GGCGGG**GG**ATCC**ATG*GCTCGCTTCGCTCTGACG*
Antisense / Reverse	*ACCTGACTGACTTTGAGCG*ATT**GAGCTCCCGCCC**

Table 4.5. Flag-tagged TIGAR plasmid design. Sequences rich in GC (green); BamHI restriction site (purple); start codon (dark blue); nucleotide target sequence (italics); stop codon (brown) and XhoI restriction site (light blue).

4.3.3 Agarose gel

Restriction digests or DNA fragments were resolved on 0.8-2% w/v agarose gels according to the DNA product size. Gels were run for 45 min - 1 hr at 80 V and visualised using a Generuler DNA ladder mix (Thermo Fisher Scientific).

4.3.4 Restriction digests

PCR products and plasmids were digested with the appropriate restriction enzymes. For this purpose, samples were digested using fast digestion restriction enzymes (Thermo Fisher Scientific) with 10x fast digest green restriction buffer (Thermo Fisher Scientific) diluted in dH$_2$O at 37° C for 2 hrs.

4.3.5 Vector preparation

The vector was digested with the appropriate restriction enzymes, which prevent non-compatible ends in order to prevent self-ligation. 5µg were digested and dephosphorylated with Calf Intestinal Phosphatase (CIP) and incubated at 37ºC for 5 min. Then, the vector was precipitated by using Phenol-chloroform and centrifuged at 15871 g for 3 min. Supernatant was discarded without disturbing the pellet. Pellet was air dried and diluted with 25 µl of dH$_2$O.

Plasmid	Description	Bacterial resistance	Source
pcDNA5 FRT/TO	FLP Recombination Target (FRT) site for Flp recombinase-mediated integration of the vector into the Flp-In™ T-REx™ host cell line	Ampicillin	Invitrogen
pPGKFLPobpA	Expression of recombinase	Ampicillin	Addgene
pcDNA™6.2-GW/EmGFP-miRs* TIGAR	Expression of miRs* against TIGAR	Spectinomycin	Invitrogen/ generated in this study
pcDNA5 FRT/3XFLAG TIGAR	Expression of 3XFLAG tagged TIGAR	Ampicillin	Generated in this study
PcDNA5 FRT/EmGFP miRs* PINK1	Expression of miRs* against PINK1	Spectinomycin	Generated in this study
pEGFPn1-PINK1	Expression of EGFP tagged PINK1	Kanamycin	Dr. Kurt de Vos

**Table 4.6. Plasmids for HEK FLP in construction. *For each gene, three microRNAs (miRs) were designed and tested for knockdown.

4.3.6 Annealing single stranded oligos

The synthesized complementary DNA oligos (Sigma Aldrich) were annealed to generate a double-stranded (ds) oligo. The annealing reaction was heated at 95ºC for 4 min and let cool down at RT for 10 min. The obtained sample was diluted 5,000 fold by serial dilutions to get a final concentration of 10nM. ds Oligos were cloned into the linearized vector.

4.3.7 Flagged TIGAR cloning

TIGAR DNA fragment was amplified by PCR. PCR samples consisted of 100 ng DNA obtained from human fibroblasts, 100ng forward primer, 100ng

reverse primer, 2.5nM dnTPs (Bioline) and 1 μl of TAQ enzyme. PCR samples were held at 94°C for 3 min, then 30 cycles consisting of 94 °C for 30 sec, 53°C for 30 sec and 72°C for 1 min 30 sec, followed by final step at 72°C for 10 min. Products were resolved in a 1% w/v agarose gel at 80V for 45min – 1 hr using a Generuler DNA ladder mix (Thermo Fisher Scientific). Observed DNA fragments were cut and extracted from the gel using QIAquick Gel Extraction Kit (Qiagen) and following the manufacturer´s protocol. Purified DNA was cloned into the dephosphorylated and restricted vector.

4.3.8 Ligation

The plasmids and DNA inserts were cloned by using a T4 DNA ligase (Roche) and 10X ligase Buffer (Roche). The ligation reaction was mixed and incubated for >16hrs at RT.

4.3.9 Plasmid Transformation

10 μl of the ligation reaction was combined with 100 μl of *E.coli* DH5α competent cells with gentle and swift movements. Then, samples were incubated on ice for 10 min and submitted to a heat-shock at 37º C for 5 mins. Samples were then taken out and 1 mL of sterile LB Buffer was added and further incubated at 37º C for 1 hr. After the incubation, samples were centrifuged at 17000 g for 1 min. and the supernatant was discarded. The obtained cell pellet was re-suspended in 100 μl of LB buffer and distributed in an agar plate with ampicillin or spectinomycin. Agar plates were then incubated at 37º C for >16 hrs.

Antibiotic resistant colonies were screened for suitable clone selection. Recombinant vectors were purified with QIAquick Gel Extraction Kit purification kit (Qiagen) and confirmed by sequencing.

4.3.10 Restriction

Restriction digest were performed by using the corresponding restriction fast digest enzymes (Thermo Fisher Scientific) with 10x fast digest restriction buffer (Thermo Fisher Scientific) at 37ºC for 2 hr.

4.3.11 DNA purification

Single bacterial colonies from the transformation step were collected and inoculated in 3ml of LB broth containing the corresponding selective antibiotic and grown at 37 ºC with vigorous shaking overnight. Successful DNA integration verification was carried out by using the Plasmid Mini Kit and following the manufacturer's instructions.

Bacterial cells were harvested by centrifugation at 17000 g for 1min at RT. Bacterial pellet was re-suspended in 200µl of Buffer P1 (Lysis buffer) followed by adding 200µl of Buffer P2. Samples were then inverted five times and incubated for 5 min at RT. 300 µl of Buffer P3 was then added and samples were mixed thoroughly by inverting ten times and centrifuged for 10 min at 17000 g. Supernatant was then transferred to a new collection tube. 700µl of Isosopropanol was added to the samples, mixed by inverting five times and further incubated for 10 min at RT. Samples were then centrifuged at 17000 g for 10 min, the obtained supernatant was then discarded without disturbing the pellet. Obtained pellets were air dried and re-suspended in 50 µl of dH$_2$O. Successful DNA inserts and vectors were verified by size of the restriction digests analysed in an agarose gel.

200 µl of the culture from the successful transformants were collected, grown in 5ml of LB containing the selective antibiotic and incubated at 37º C on a vigorous

shake overnight. Purification was performed using the Plasmid Plus Midi Kit according the manufacturer's instructions.

4.3.12 Chaining pre-miRNAs (miRs)

In order to express more than one miRNA in one primary transcript and ensure co-cistronic expression, TIGAR and PINK1 miRNAs were chained into a single vector. Restriction digestions were performed by: 1) the combination of two specific restriction enzymes to cut the pre-miRNA (miR) insert and; 2) the combination of two specific restriction enzymes to cut the expression vector. The obtained fragments from the restriction, were run on a 2% agarose gel; then backbone and inserts were cut from the gel and purified. The purified fragments and backbone were then ligated and transformed. The obtained clones were analysed by Sanger sequencing and tested for future experiments.

4.3.13 Removing EmGFP coding sequence from designed miRNAs to destination vector

To avoid EmGFP expression in functional analysis of *TIGAR* and *PINK1* knockdown, EmGFP sequence was removed from successful pcDNA6.2-GW/EmGFP-miR2 TIGAR 2, miR2 PINK1 and the chained miR2 TIGAR- miR2 PINK1 clones. EmGFP sequence was removed by DraI digestion for 2 hrs at 37ºC and run in a 0.8% agarose gel. The insert fragment was excised from the gel and purified. The purified fragment was ligated and inserted into the destination vector pcDNA5 FRT/TO. Competent cells were transformed and the obtained clones were selected and checked by DraI restriction digests, where the 750bp EmGFP fragment was not visible.

4.3.14 RNAi knockdown

Gene knockdown from the successful TIGAR and PINK1 constructs were verified by western blotting and qPCR.

4.3.14.1 Western blotting

To determine and compare gene knockdown performed by each miR constructs, transfected HEK cell pellets were dissolved with Lysis buffer containing RIPA (Radio-Immunoprecipitation Assay) buffer (Sigma Aldrich), diluted phosphatase inhibitors (1% v/v) (Sigma Aldrich) and protease inhibitors cocktail (1%v/v) (PIC). Cell lysates were incubated on ice and centrifuged for 30 min at 15871 g at 4°C. Supernatant was collected and the total protein was measured using the Bradford assay to select the appropriate amount of protein.

A standard curve was obtained and the sample protein concentration was calculated using the linear equation (See Chapter three). The volume of cell lysate was determined and equivalent amount of Laemmli buffer 2x was added. Samples were heated for 3 min. at 100°C and centrifuged for 1 min at 2347 g. Proteins equivalents from each sample were loaded on a 12% polyacrylamide gel (SDS-PAGE). Separating gels were run at low voltage (50 V) and running gel at a higher voltage (120 V). Proteins were transferred applying a wet electrophoretic transfer to a PVDF membrane for 1.5 hrs at 250 mA. The membranes were blocked with 5% non-fat dried milk diluted in TBS-T, after which, membranes were incubated overnight at 4ºC with primary antibodies against TIGAR (Santa Cruz) and GFP-PINK1 (Clonetech) (Table 4.7). Then, membranes were incubated with secondary antibody horseradish peroxidases (HRP) (Table 4.7) and bands were detected using chemiluminescence with ECL Western Blot detection kit. α-Tubulin and GAPDH

were used as loading controls (Table 4.7). Quantification was done by densitometry analysis using G-Box Syngene Image software.

Antibodies	Catalogue number	Company	Dilution	Molecular weight (kDa)	Host
Primary antibodies					
TIGAR antibody TIGAR(G2)	sc-74577	Santa Cruz Biotechnology	1:1000	30	M
Monoclonal anti-α-Tubulin	T9026	Sigma	1:10000	50	M
Anti-Actin antibody ACTN05 (C4)	ab3280	Abcam	1:1000	42	R
Anti-GADPH monoclonal antibody (6C5)	CB1001	Calbiochem	1:5000	36	M
Anti-GFP monoclonal antibody (JL-8)	632380	Clonetech	1:4000	/	M
Secondary antibodies					
Anti-rabbit HRP IgG	1706515	Biorad	1:5000	/	G
Anti-mouse HRP IgG	1706516	Biorad	1:10000	/	G

Table 4.7. Antibodies used for knockdown assessment. Goat (G), Mouse (R); Rabbit (R).

4.3.14.2 qPCR

Gene knockdown in HEK Flp-In successful clones was evaluated by Real-Time qPCR. Total RNA was extracted from cell pellets, using QIAGEN RNeasy kit (Qiagen) and cDNA was synthesised using SuperScript III cDNA first strand-synthesis Kit (Invitrogen), following the manufacturer's instructions. Target gene expression level was normalised using *U1 snRNA* as reference gene.

The gene quantitation was done relative to the reference genes by subtracting the cycle threshold (Ct) of *U1 snRNA*, from the Ct of *TIGAR* and *PINK1* ($\Delta\Delta$Ct=ΔCt sample - ΔCt reference gene). The resulting value of Ct (ΔCt) is the exponent of the base 2 ($2^{-\Delta\Delta Ct}$). This was represented as the fold difference of template for the genes (Table 4.8). Efficiency of the qPCR reactions of all gene primers were 95-99%. The normalised relative *TIGAR* and *PINK1* gene expression was calculated for each condition and normalised against the untreated control. Percent of knockdown was

calculated by subtracting the normalised $\Delta\Delta Ct$ expression of the control and multiplying by 100. The following formula was used in Excel for the calculation: $(\text{Power}(10,-((\Delta Ct_{target}-\Delta Ct_{reference})/3.333)))*100$.

GENE	SEQUENCE 5' > 3'	
TIGAR	F	CCAAAGCAGCCAGGGAAGAGTG
	R	CCGCTTCTTTCAGGATTAGTTGAC
PINK1	F	TGGACACCTCTGGGGCCATC
	R	GCCGGACGCTGTTCCTCGTT
U1 snRNA	F	CCATGATCACGAAGGTGGTT
	R	ATGCAGTCGAGTTTCCCACA

Table 4.8. Primers used for gene knockdown analysis. Primers used for *TIGAR* and *PINK1* gene expression by qPCR. F, Primer forward; R, Primer reverse. Efficiency of the qPCR reactions of all gene primers were 95-100%.

4.3.15 Sequencing

All miR constructs and overexpressing vectors were checked by Sanger sequencing using the Big Dye Terminator 3.1 (Applied Biosystems) protocol. Each sequencing reaction consisted of 1μg of DNA combined with the corresponding primer (Table 4.9), sequencing buffer and reaction mix diluted in dH$_2$O using the following PCR sequencing program: 1) 30s at 95ºC for 45 cycles, 2) 15s at 50ºC and, 3) 4 min at 60ºC.

The PCR products were precipitated and sent to Source Bioscience (Nottingham, UK) for analysis. Sequences in *abi* format were checked by using Finch TV software (Geopiza).

PRIMER	SEQUENCE
CMV (pcDNA5)	CGCAAATGGGCGGTAGGCGTG
BGH reverse	TAGAAGGCACAGTCGAGG
GFP seq forward	CGAGAAGCGCGATCACATGGTC

Table 4.9. Primers used for sequencing in this study.

4.3.16 Building Stable Inducible Cell Lines

4.3.16.1 HEK293T and HEK293T Flp-In

Cell culture and transfections

HEK 293T and HEK 293 FRT cell lines were grown in Dulbecco's modified Eagle's medium (DMEM, Sigma-Aldrich) supplemented with either 10% Fetal Bovine Serum or Tetracycline free fetal bovine serum (FBS), penicillin/streptomycin (100U/ml) at 37 C under 5% CO_2 atmosphere and a relative humidity of 95%. HEK293T FRT was maintained in media supplemented with Blasticidin S (Calbiochem) and Zeocin (Invitrogen) for mantainance. Stable cell line selection was performed by substituting Zeocin with Hygromycin B (Thermo Fisher Scientific) (Table 4.10).

For pcDNA6.2™6.2-GW/EmGFP-miRs TIGAR and PINK1 clones screening, HEK 293 cells were plated in a 24-well plate at 50,000 cells/well. Co-transfections of pcDNA6.2™-miRs and overexpressing vectors were carried out using polyethylenimine (PEI; Sigma) 1µg/ml and 500ng of total DNA and 50µl of OptiMEM® (Life Technologies). The mixture was added to each well with gently swirls and left for 48-96 hrs to assess knockdown.

For stable inducible cell line construction, the Flp-In T-Rex kit (Thermo Fisher Scientific) was used. After miRs contructs for both genes were checked and selected, they were transferred and cloned into the destination vector pcDNA5™/FRT/TO designed to be used with the Flp-In T-Rex system. The inducible expression vector contains:

- The hybrid human cytomegalovirus (CMV)/TetO2 promoter, with gene expression regulated by Tetracycline.

- Flp Recombination Target (FRT) site, for vector stable integration into the selected mammalian host cell line.

- Hygromycin resistant gene for cell line selection.

The integration and expression of the pcDNA 5/FRT/miRs TIGAR, PINK1 and chained TIGAR-PINK1 into the genome, occurs by intermolecular DNA recombination mediated by the Flp recombinase.

Stable inducible cell lines were generated for knockdown of the two genes *TIGAR* and *PINK1*, and the combination of both. Cells were seeded at 1 x 10^6 cells on a 10 cm dish in 15 ml culture medium containing Blasticidin to obtain a cellular confluency of $\geq$50%. 24 hrs after seeding, cells were co-transfected with the pPGKFLPobpA:pcDNA5FRT/TO DNA plasmid at a 6:4 ratio using 50 µg PEI (1 mL). 48hrs after transfection cells were harvested and split into 10 cm dish with 5 mL of conditioned medium (media from cells that have been in culture) and 5 mL of fresh culture medium without antibiotics. 24hrs after cells were plated, medium was supplemented with Hygromycin B and Blasticidin for selection. Cells were grown under selective growth conditions for seven days, after which, media was replaced with fresh selection medium until visible clones were identified. Hygromycin resistant clones were screened for Zeocin sensitivity to confirm pcDNA5/FRT/TO integration into the FRT site. Cells with successful recombination and stable integration will grow in selection medium with Hygromycin and Blasticidin. These cells do not grow in medium Zeocin and Blasticidin. Successful clones, where the cDNA construct had been recombined into the FRT site in the Flp-In-293 cells, were isolated, propagated and screened for gene knockdown by qRT-PCR for confirmation. Confirmation of

clones with the highest percentage of knockdown at 72 hrs after tetracycline induction were selected and expanded. All control cell lines were induced and assessed alongside HEK Flp In *CRNAi* negative control obtained from Dr. Guillaume Hautbergue.

Cell model stage	Antibiotic	Stock concentration	Working concentration
HEK FRT *Before transfection*	Blasticidin	10 mg/mL	15 µg/mL
	Zeocin	100 mg/mL	100 µg/mL
HEK Flp GOI *After transfection*	Blasticidin	10 mg/mL	15 µg/mL
	Hygromycin	50 mg/mL	100 µg/mL
HEK Flp In *Induction*	Tetracycline	10 mg/mL	1 µg/mL

Table 4.10. Antibiotic concentrations for HEK FRT and HEK Flp in.

4.3.17 Mitochondrial function and morphology assessment

4.3.17.1   ATP assays

ATP assays were performed to assess the effect of *TIGAR*, *PINK1* and double-knockdown in the mitochondrial function and whether there is a rescue effect in cells with *PINK1* deficiency when *TIGAR* is knockdown. Cultured cells generate their ATP mainly through glycolysis if grown in glucose-rich medium. Once the medium is replaced with galactose, they rely on the oxidative phosphorylation pathway to produce ATP (Mortiboys et al., 2008). The ATP assays were performed over three consecutive passages as biological triplicates of each cell line. Each cell line was maintained with selection medium containing Blasticidin and Hygromycin. Once cells were confluent, they were trypsinised and plated at 3×10^3 cells/well in a 96-well plate with glucose or galactose selection media with or without tetracycline. 48hrs after tetracycline addition, media was replaced with fresh selection media containing tetracycline. For each cell line, four conditions were tested:

- Glucose selection media: Not Induced and Induced with tetracycline.

- Galactose selection media: Not Induced and Induced with tetracycline.

ATP cellular level was measured using the ATPlite™ Luminescence Assay System (Perkin Elmer). In brief, reagents were warmed to RT before starting the assay. Cells were washed with 100 µl of PBS, after which 100µl of PBS was added with 50 µl of mammalian cell lysis solution per well and the plate was placed on a plate shaker at 700 rpm for 5 min. Then, 50 µl of substrate solution was added and plate was shaken for further 5 min at 700 rpm. The plate was then left to adapt to the dark for 10 min. and the luminescence was assessed using a FLUOstar Omega microplate reader (BMG LABTECH). Cell density was measured with CyQUANT Cell Proliferation Assay Kit (Life technologies). After ATP was measured, 50 µl were added per well and incubated for 1 hour at 37ºC. The fluorescence was measured at 530 nm using a FLUOstar Omega plate reader. The normalised data was obtained when the total ATP was divided by the CyQUANT measurement per well in triplicate. Averages from controls were taken as a 100% and the ratio corresponding to each condition per cell line was calculated.

4.3.17.2 Mitochondrial morphology

In order to assess the effect of *TIGAR, PINK1* and double-knockdown effect in mitochondrial morphology, HEK 293T Flp in cells and controls were stained with the mitochondrial marker Tom20 (Table 3.7). We assessed four different conditions of each cell line with selection media: glucose not induced, glucose/tetracycline induced, galactose not induced and galactose/tetracycline induced. Cells were seeded at a $5x10^4$ cells/well density in a 24-well plate containing a glass coverslip, in selection medium with or without tetracycline. After 48hrs, media was removed from wells and replaced with fresh medium with tetracycline. Cells were induced for 72 hrs and fixed for immunofluorescence. Briefly, cells were rinsed with PBS and permeabilised with 0.3% Triton-X followed by incubation with 5% bovine serum

albumin (BSA, Sigma) in PBS (Blocking buffer) for 1 hr at RT. Cells were then rinsed with PBS, mouse anti-Tom20 antibody (1:1000, BD Biosciences) in blocking buffer was applied to all the wells and incubated overnight at 4ºC. Cells were rinsed with PBS and incubated with secondary goat anti-mouse antibody Alexa Fluor 488 (1:1000; Life technologies) for 1 hr in the dark at RT. Images were captured with Opera Phenix Laser based Confocal High Throughput Cell Imaging System (Perkin Elmer). A total of nine Images per field per condition per cell line were captured and processed by high-content analysis using the Harmony PhenoLOGIC software (Perkin Elmer).

4.3.18 CRISPR/CAS9

Recently, new approaches in molecular biology towards genome editing continue to emerge with improved and promising results. The Clustered Regularly Interspaced Short Palindromic Repeats (CRISPR) Type II system is one of them. This is a bacterial immune system modified and designed for genome engineering. The system is composed of a "guide" RNA (gRNA) and a non-specific CRISPR-associated endonuclease (Cas9). The gRNA contains a scaffold sequence for Cas9-binding and an upstream PAM site conformed by a 20 nucleotide targeting sequence. The nuclease targets a precise target DNA sequence producing double-strand breaks (DSBs), which are repaired through non-homologous end-joining (NHEJ) or homology directed repair (HDR). The NHEJ is prone to error but highly efficient, whereas the DSB confers high fidelity but with low efficiency. Due to this, Cas9 can produce frame-shifts indels and gene loss of function, without modifying the genomic sequence.

4.3.18.1 Expression system

Plasmid based

> For this study, the plasmid expression system was selected. The All-in-One plasmid (AIO, #74630) contains two cloning sites that encode dual U6 promoter to express dual synthetic guide RNAs. The Cas9-D10A nickase is linked by a 2A peptide with the selectable puromycin resistant marker to enhance efficient and accurate genome editing (Figure 4.2).
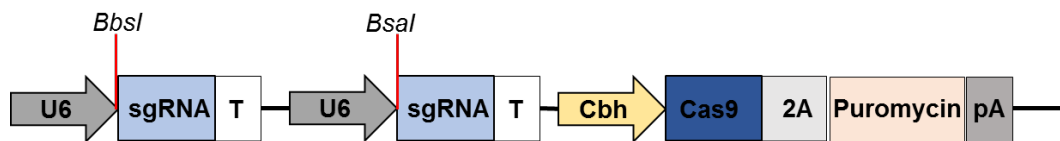
Figure 4.2. Plasmid expression system. AIO-Puro (#7430) nickase plasmid targeting each gene. BbsI and BsaI allow dual cloning of synthethic guides RNAs (sgRNA) and dual U6 promoter expression. Puromycin coupled to Cas9 via 2A peptide linker. Terminator (pA).

4.3.18.2 Target sequence selection and sgRNA design

> The complete sequence with isoforms for *TIGAR* and *PINK1* was obtained from NCBI. To select the most efficient 20-nucleotide sequences for nickase targeting, the online program (http://crispr.mit.edu/) was used (Table 4.11). It provides the nickase design and predicts its "off-target" sites and effects (Figure 4.15). To maximise gene disruption, we aimed for the first exons within each gene. However, for *TIGAR*, due to the first thee exons having a very short sequence (Figure 3.2), guides were only available for exons 4-6. For the nickase design, the PAM sequence lies upstream the target sequence and it was removed to leave only 20 nucleotide sequence. If target sequence did not begin with G, this was added in order to allow transcription by the U6 promoter. The space between the two gRNAs are variable and without exceeding 20 bp from each other (Table 4.11). The guides with the highest scores were selected and two paired gRNAs were chosen for each gene.

Gene	Exon	Guide Pair	Guide Sense	Sequence 5' > 3'
PINK1	1	1A	F	ACCGACCCTGCGAGGCTCCGCGCC
			R	AAACGGCGCGGAGCCTCGCAGGGT
		1B	F	ACCGTCTCCGCTTCTTCCGCCAGT
			R	AAACACTGGCGGAAGAAGCGGAGA
		2A	F	ACCGCCGCCTGTTTTTCCTCGATG
			R	AAACCATCGAGGAAAAACAGGCGG
		2B	F	ACCGGCGGGCGGTCTCGGCCTGTC
			R	AAACGACAGGCCGAGACCGCCCGC
TIGAR	4	1A	F	ACCGTCTCTCCAAAATTCCATGCA
			R	AAACTGCATGGAATTTTGGAGAGA
		1B	F	ACCGAAAGTATGACTCAAGACTTC
			R	AAACGAAGTCTTGAGTCATACTTT
	5	2A	F	ACCGTTCCCTGGCTGCTTTGGCCA
			R	AAACTGGCCAAAGCAGCCAGGGAA
		2B	F	ACCGCCTGTGTTTACACCGCCCGG
			R	AAACCCGGGCGGTGTAAACACAGG

Table 4.11. Designed primers for *TIGAR* and *PINK1*. Each paired guide are designed in opposite strands. Highlighted in green (F, forward) and yellow (R, reverse) are the cloning overhangs for *BbsI* or *BsaI* ligation. Pair guides are 1A and 1B, and 2A and 2B for each gene.

4.3.18.3 Molecular cloning

AIO-Puro vector was digested with BbsI, dephosphorylated and purified as previously described (Vector preparation). All the complimentary DNA oligos were annealed by heating at 90-95ºC for 4 min and allow slow cooling at RT. Then, the oligo pairs were individually phosphorylated with T4 Polynucleotide Kinase (PNK4). Each oligo pair was cloned into the BbsI digested vector using T4 Ligase. Each construct was transformed and purified using the Spin Miniprep Kit (QIAgen) and following the manufacturer's instructions. Resulting clones were checked and successful ones were selected and purified as previously described (See section 4.3.11).

4.3.18.4 Verification of inserts

Clones were screened by restriction digests using BamHI. Successful clones lose the BamHI recognition site and a linearised vector was then visualised.

4.3.18.5 Sequencing

All sgRNA cloned into *BbsI*-digested AIO-Puro plasmid were analysed by Sanger sequencing using the hU6 promoter primer (*F:TTTCCCATGATTCCTTCATATTTG*) and the Big Dye Terminator 3.1 (Applied Biosystems) protocol. Each sequencing reaction was performed as described previously (See section 4.3.18.5).

4.3.18.6 Cell culture and transfection

HEK 293T cell lines have been successfully used with CRISPR/Cas9 and optimised protocols have been already stablished. HEK293 were grown in Dulbecco's modified Eagle's medium supplemented with 10% FBS, penicillin/streptomycin (100U/ml) at 37° C under 5% CO_2 atmosphere and a relative humidity of 95%. The day before the transfection, $5x10^4$ cells/well were seeded in a 24 well plate. On the day, 70% confluent cells were transfected with 500ng of AIO-TIGAR and AIO-PINK1, each containing the respective paired dRNAs, using Lipofectamine 2000.

Then, 24 hrs after transfection, medium was replaced with fresh warm media and 3.5µg of Puromycin was added to each well. Cells were further incubated for 72hrs for selection. Cells that survived under the Puromycin condition, have maintained the plasmid expression, which integrates into the genome of the cell. Puromycin resistant cells were then harvested and cultured in regular medium for clonal selection.

4.3.18.7 Clonal selection

Clonal cell lines were isolated by limited dilution. Puromycin resistant cells were dissociated into single cells 72 hrs after transfection. Each transfected well with cells were counted and serially diluted in fresh medium. 60 cells per 10 mL in medium were obtained and plated for each 96-well plated, to obtain 0.5 cells/100 µL

media per well. Accurate dilution, calculation and single cell seeding is critical for single clone selection. Each transfected population for each paired gRNA for each gene was plated in duplicate. Cells were checked and inspected with media replacement for a period of 2-3 weeks, until clonal appearance with colonies were visualized. Cells were left growing in the incubator for a period of ~2 weeks for expansion. Clones from cells transfected with paired guides A and B for *TIGAR* knockdown were tested by WB to assess knockdown at the protein level. Clones from cells transfected with paired guides A and B for *PINK1* knockdown were tested by qPCR for gene expression.

4.3.19 Statistical Analysis

Statistical analysis was carried out with Prism 7 GraphPad software. *P* value significance was obtained using 2-way and one-way ANOVA with multiple comparisons with post hoc correction wherever it is indicated.

4.4 Results

4.4.1 Building the Flp In stable model

4.4.1.1 Flag tagged TIGAR

TIGAR was successfully cloned into pcDNA5 FRT/TO (Figure 4.3, a) and overexpressing vector verified in transfected HEK cells (Figure 4.3, b).
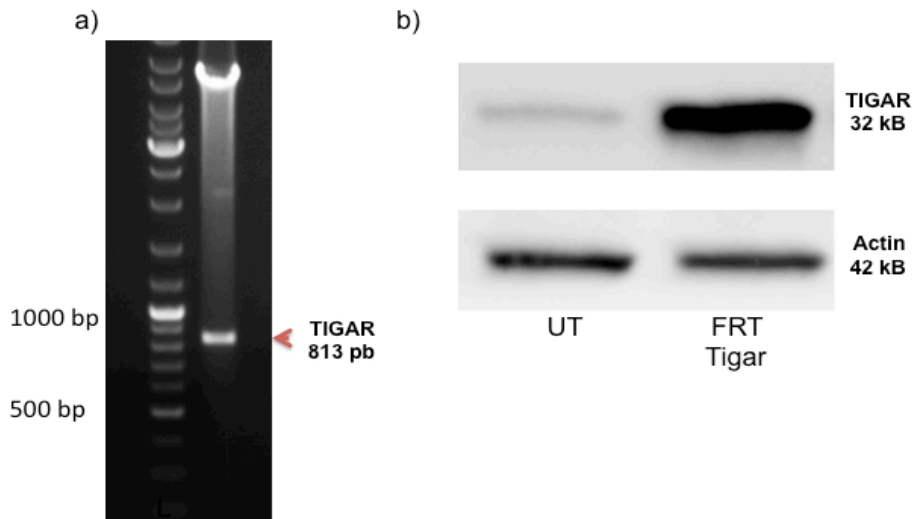
Figure 4.3. TIGAR cloning. a) *TIGAR* PCR product obtained from human fibroblasts; b) WB image of TIGAR in the Untreated (UT) and the overexpressing FRT-TIGAR construct in transfected HEK cells.

4.4.1.2 TIGAR and PINK1 miRNAs

miR constructs for *TIGAR* (Figure 4.4) and *PINK1* (Figure 4.5) were successfully synthethised and cloned into the pcDNA™6.2-GW/EmGFP vector, which allow the expression of the miR inserts against *TIGAR* (Figure 4.4) and *PINK1* (Figure 4.5). The cloned miRs size was expected to be ~200 bp. They were transfected into HEK cells for transient RNAi analysis. One miR construct for each gene, with the most effective and efficient knockdown, was selected for the generation of the HEK Flp In stable cell line.
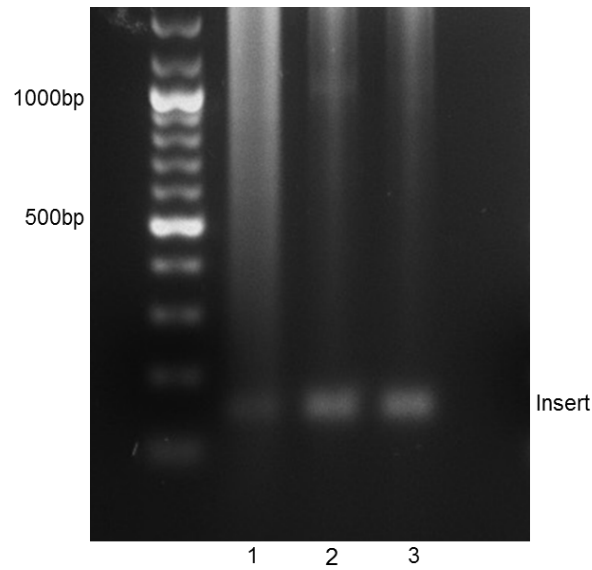
Figure 4.4. TIGAR miRs constructs. Agarose image of cloned TIGAR miR1, miR2 and miR3 inserts that were cloned into pcDNA™6.2-GW/EmGFP digested with BamHI and XhoI. Insert expected at ~200bp.
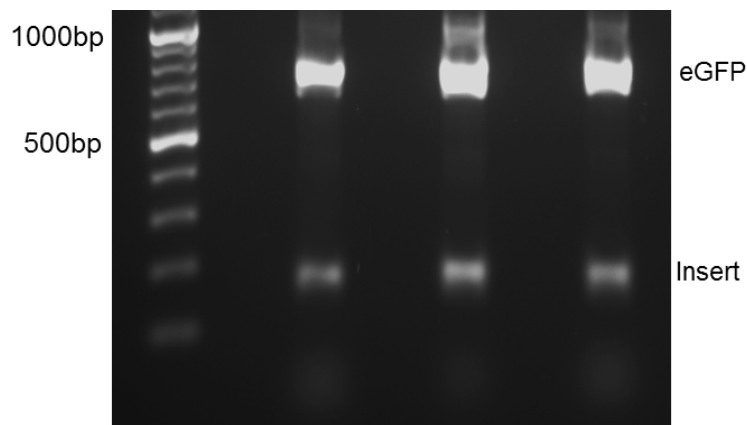
Figure 4.5. PINK1 miRs constructs. Agarose image of cloned TIGAR miR1, miR2 and miR3 inserts cloned into pcDNA™6.2-GW/EmGFP digested with DraI and XhoI. Insert expected at ~180pb.

4.4.1.3   miRNA mediated knockdown

TIGAR miR constructs screening

In order to assess TIGAR knockdown and to select the best miR construct for future assays, HEK cells were transfected with or without pcDNA5 FRT/FLAG TIGAR and the three cloned pcDNA™6.2-GW/EmGFP-miRs TIGAR knockdown

effect was assessed by by WB at 72hrs post-transfection (Figure 4.6). To see whether a combination of two miRs showed a higher knockdown, the three miRs were combined in two pairs and cloned into pcDNA™6.2-GW/EmGFP. The co-transfected cells with the overexpressing FLAG-TIGAR and the miR TIGAR constructs (Figure 4.6 a left panel) showed a reduction at the protein level of ectopic TIGAR, were miR2 TIGAR achieved the highest percentage of all (Figure 4.6 b). However, endogenous levels of TIGAR protein remained the same compared to the untransfected cells. When cells were transfected with single miR TIGAR constructs, TIGAR protein level was reduced in almost all of the transfected cells except for the cells transfected with chained miR2 and miR3 TIGAR. Overall, miR2 showed the highest knockdown percentage (~86%) (Figure 4.6). Constructs containing two miRs for TIGAR did not showed an increase in the knockdown effect, therefore miR2 TIGAR was selected for future assays and functional analysis.
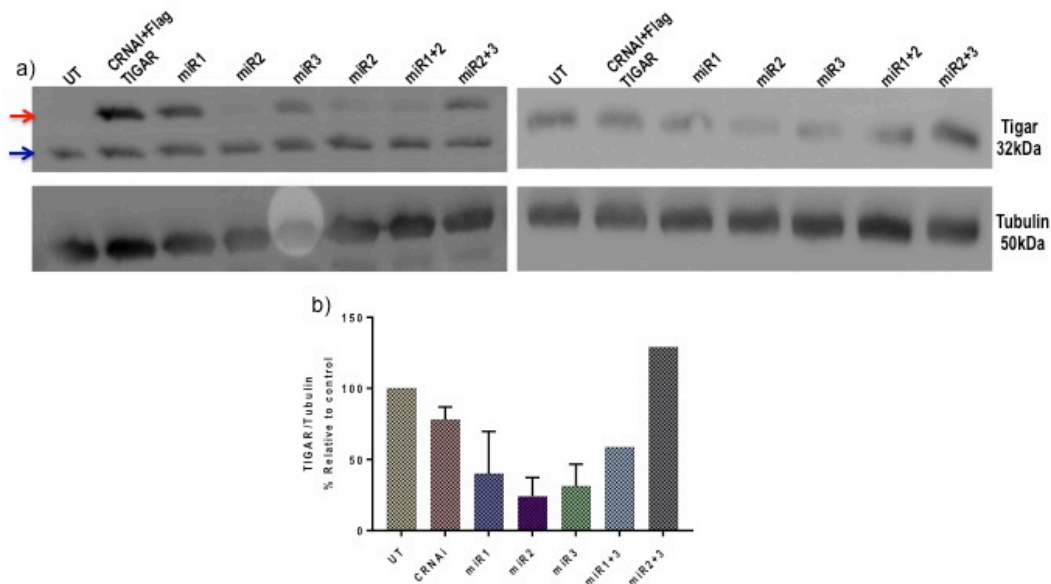
Figure 4.6. TIGAR knockdown in HEK 293T cells. a) Representative WB image of transfected HEK 293T with (left panel) or without (right panel) FLAG TIGAR and pcDNA6.2/miR1, miR2, miR3 and chained miRs TIGAR (left panel). A knockdown can be seen in all the single constructs and only in one chained. The highest knockdown (~86%) was obtained with miR2 against TIGAR. Ectopic (red arrow) and endogenous (blue arrow) TIGAR.

PINK1 miRs constructs screening

Cloned miRs for PINK1 were transfected in HEK and knockdown effect was assessed at the 48hrs. To asses PINK1 knockdown at the protein level, eGFP-PINK1 was co-transfected with the three pcDNA™6.2-GW/EmGFP-miRs PINK1. Since there are no reliable PINK1 antibodies, GFP-PINK1 knockdown was assessed at the 48hrs post-transfection. The three constructs showed high levels of knockdown, where miR2 PINK1 showed ~100% knockdown (Figure 4.7). Therefore, the construct containing miR2 PINK1was selected for stable inducible cell line generation and future functional analysis.
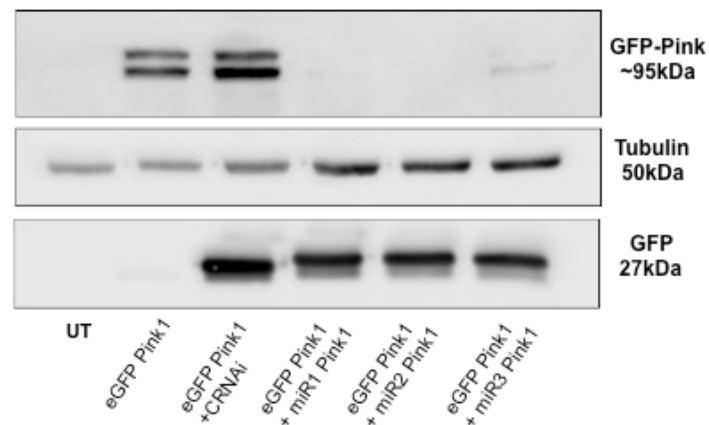
Figure 4.7. PINK1 knockdown in HEK cells. a) Representative Western Blot image of HEK cells co-transfected with eGFP-PINK1 and three pcDNA6.2/miR1, miR2 and miR3 against PINK1. Blots (upper panel) were probed with antibody against GFP, to detect eGFP-PINK1. The three miR2 PINK1 construct achieved the highest effect with ~100% knockdown.

4.4.1.4   GFP removal

Before the HEK FLP IN cellular model for each gene was established, the GFP 750bp sequence was removed from all miR constructs and transferred into the destination vector pcDNA5™/FRT/TO (Figure 4.8).
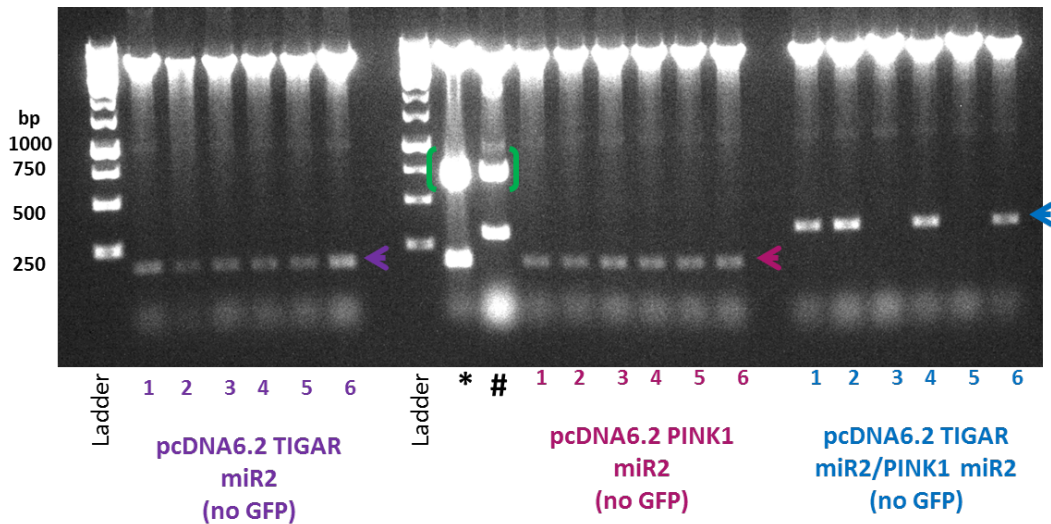
Figure 4.8. Restriction analysis of miRNAs after GFP removal. Image of digested miRNAs with DraI of the three miRNAs in pcDNA6.2 vector. First six lanes correspond to miR2 TIGAR. Lanes in the middle correspond to miR2 PINK1, where the first 2 lanes correspond to pcDNA6.2/EmGFP-miR2 TIGAR (asterix) and pcDNA6.2/EmGFP-miR2 TIGAR/miR2 Pink1 (dash), which were used as GFP controls respectively (single or chained inserts). Last six lanes correspond to chained miR2 TIGAR and miR2 PINK1.

Then, after GFP removal, miR2 TIGAR, miR2 PINK1 and miR2 TIGAR/miR2 PINK1 were successfully cloned into the pcDNA5/FRT/TO expression vector (Figure 4.8), TIGAR and GFP-PINK1 levels were assessed at the 48hrs by WB to verify knockdown effect (Figure 4.9). GFP-PINK1 continue to show ~100% knockdown in transfected cells with miR2 PINK1 (Figure 4.9) and miR2 TIGAR/miR2 PINK1. However, miR2 TIGAR showed a lower knockdown effect alone (Figure 4.9) (30%) and when co-transfected with eGFP-PINK1 and chained with miR2 PINK1 (Figure 4.9) (23%). When two miRs are co-transfected, it has been shown that percentage of knockdown might decrease (Werness and Anderson, 2010).
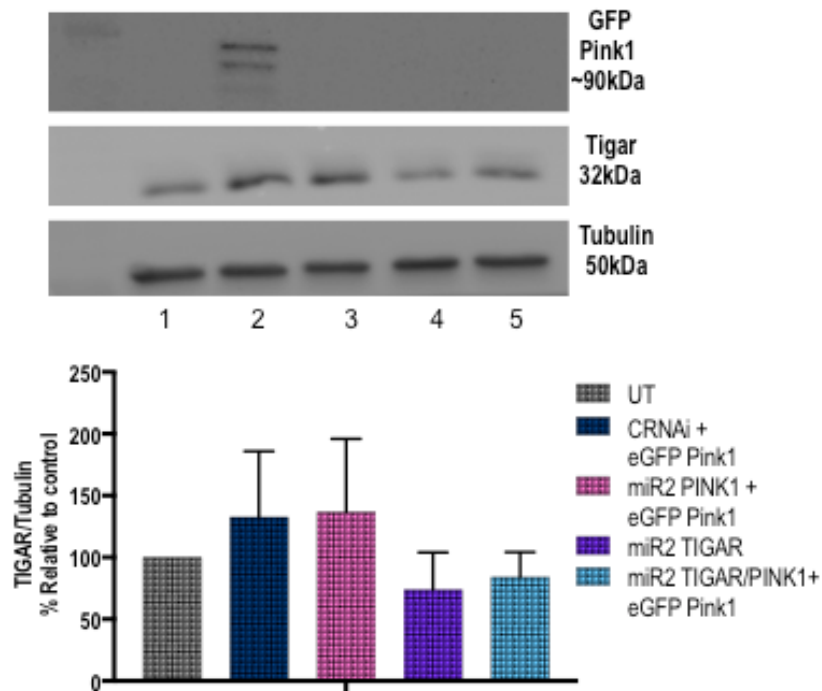
Figure 4.9. TIGAR Protein levels. a) Representative Western Blot image of HEK cells untransfected (lane 1), co-transfected with eGFP-PINK1 and pcDNA™5/FRT/miR2 TIGAR (lane 3), pcDNA™5/FRT/miR2 PINK1 (lane 4) and pcDNA™5/FRT/miR2 TIGAR/miR2 PINK1 (lane 5). Blots (upper panel) were probed with antibody against GFP, to detect eGFP-PINK1 The constructs showed a knockdown, in which miR2 PINK1 achieved a ~100% knockout; whereas TIGAR showed a knockdown of 30% alone and 23% when both inserts are expressed.

4.4.2 HEK Flp In TIGAR and PINK1 assessment

Once knockdown was achieved, the miR constructs were selected for further functional assays in the HEK Flp In cell lines. The miR constructs were transferred and cloned into the pcDNA™5/FRT/TO expression vector containing the hybrid human cytomegalovirus (CMV)/TetO2 promoter and Hygromycin resistance gene. This system allows inducible regulation after tetracycline addition and antibiotic selection.

Stable inducible cell lines for *TIGAR* and *PINK1* were generated after HEK FRT cells were transfected with the pcDNA5™/FRT/TO vector containing the pre-miRNA (miR) insert in the 3'UTR, directed against TIGAR, PINK1 or both, using the

Flp-In T-Rex kit. The integration of the vector is mediated by the Flp recombinase, which allows the DNA recombination at the FRT sites.

The HEK FRT host cell line contains the pFRT/lacZeo target site vector, containing the lac-Z-Zeocin fusion gene regulated by the SV40 promoter. The ATG initiation codon of the lac-Z-Zeocin fusion gene lies upstream the FRT site. HEK FRT cells express the lacZ-Zeocin resistance gene, which makes them Zeocin-resistant. The pcDNA5/FRT/TO constructs contain the hygromycin resistance gene within the 5' coding region, as well as a FRT site, which is lacking from the ATG initiation codon and a promoter. Once the constructs were co-transfected with pPGKFLPobpA plasmid, homologous recombination occurred between the FRT sites. Stable insertion into the genome of the pcDNA5/FRT/TO, the ATG initiation codon and the SV40 promoter are brought in frame within the hygromycin resistance gene, leading to lacZ-Zeocin fusion gene inactivation. Therefore, we were able to select the stable inducible cell lines via hygromycin and blasticidin resistance and Zeocin sensitivity. After the pcDNA5/FRT/TO vector containing the miR2 TIGAR, miR2 PINK1 and miR2 TIGAR/miR2 PINK1 is integrated, gene repression is achieved via tetracycline induction.

The pcDNA/FRT/TO vector contains the CMV/TetO$_2$ promoter, in which the miR inserts expression are regulated via tetracycline induction. The HEK FRT cells contained the blasticidin resistance gene and Tet repressor elements (TetR). This allowed blasticidin selection of cell lines expressing the tetracycline repressor protein. These cells are maintained under the regulation of the Tetracycline Operator 2, which inhibits the expression of the miR insert. Once tetracycline is added, it binds

the TetR, it changes it conformation and releases it from the Tet operator sequences. This leads to miRs transcription and expression.

After cells were transfected and single colonies were obtained, successful clones were selected for screening for each cellular model. Single visible colonies were picked and grown in a 24-well plate. Single colonies were then grown under the following selection conditions: a) medium with Hygromycin and Blasticidin.and b) medium with Zeocin and Hygromycin. Successful clones were grown in medium Hygromycin and Blasticidin, where cellular death occurred in medium containing Zeocin and Blasticidin. A total of three cell lines were selected from each cellular model. After tetracycline induction, knockdown was assessed by comparing the mRNA levels obtained by qPCR for each cell lines, (Figure 4.10, Figure 4.11 and Figure 4.12).

4.4.2.1   RNAi mediated knockdown

Three clones for screening from the HEK Flp In for each cell model were selected. Each cell line was harvested and plated into 10 cm dish with or without tetracycline addition. Next, the knockdown percentage was analysed for each of the clones by assessing the gene expression of *TIGAR* and *PINK1* at 48hrs post induction and using qPCR.

HEK Flp TIGAR cell lines.

All three Flp TIGAR cell lines were compared with the cells without tetracycline induction (control). Based on the obtained results from the 72 hrs post-induction, two of the three cell lines showed decreased TIGAR expression compared to their respective control (Figure 4.10 a). Flp TIGAR cell line T2 had a reduction of 55.3% (2-way ANOVA, ****$P<0.0001$) and A2 of ~30% (2-way ANOVA, ****$P<0.0001$), whereas T1 showed a 2-fold increased expression (2-way ANOVA,

****P<0.0001) (Figure 4.10 a). The T2 and A2 cell lines were then chosen to check for consistent decreased *TIGAR* expression after 72 hrs post induction. *TIGAR* expression showed was consistently knocked down after 48 hrs post induction in further assessments, where A2 showed a 65% decreased expression and T2 50% relative to their controls (2-way ANOVA, ****P <0.0001) (Figure 4.10 b and c). A2 demonstrated consistency with high reduction of *TIGAR* expression, therefore this cell line was selected for further functional analysis.
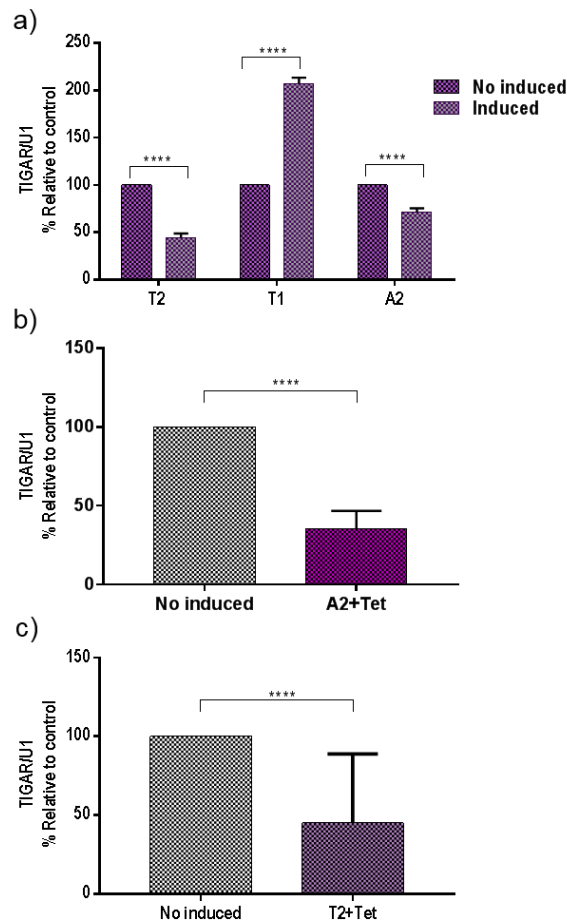
Figure 4.10. TIGAR Knockdown in HEK FLP IN cell lines. *TIGAR* mRNA level of HEK FLP TIGAR cell lines at 72 after of tetracycline induction. A) Three cell lines were selected for screening and selection for *TIGAR* knockdown, where a reduction of *TIGAR* expression was obtained for T2 (50%) (****P<0.0001) and A2 (30%) (****P<0.0001) and a 2-fold increased TIGAR expression was obtained for T1 (****P<0.0001). Two cell lines were selected for knockdown validation: A2 (b) and T2 (c), where a constant knockdown was achieved with both cell lines of 64.3 % (****P<0.0001) for A2 and 55% (****P<0.0001) for T2. 2-way ANOVA, Dunnett's test (n=3).

HEK Flp PINK1 cell lines

Initial assessment of HEK Flp PINK1 cell lines after 72 hrs of tetracycline induction, two from the three cell lines showed a reduction in *PINK1* expression when compared to their respective controls (Figure 4.11 a). Here, a decrease in *PINK1* expression of ~50 % (2-way ANOVA, ****$P<0.0001$) was observed in *PB11* and 40% (2-way ANOVA, ****$P<0.0001$) for *P2* and an increase of ~19% (2-way ANOVA, ****$P<0.0001$) in *P5* (Figure 4.11 a). Further analysis performed in *PB11* and *P2* demonstrated a consistent decrease of *PINK1* expression of 80% (2-way ANOVA, ****$P<0.0001$) and 50% respectively (2-way ANOVA, ****$P<0.0001$) relative to controls (Figure 4.11, b and c). *PB11* achieved the highest knockdown, therefore this cell line was selected for future functional analysis.
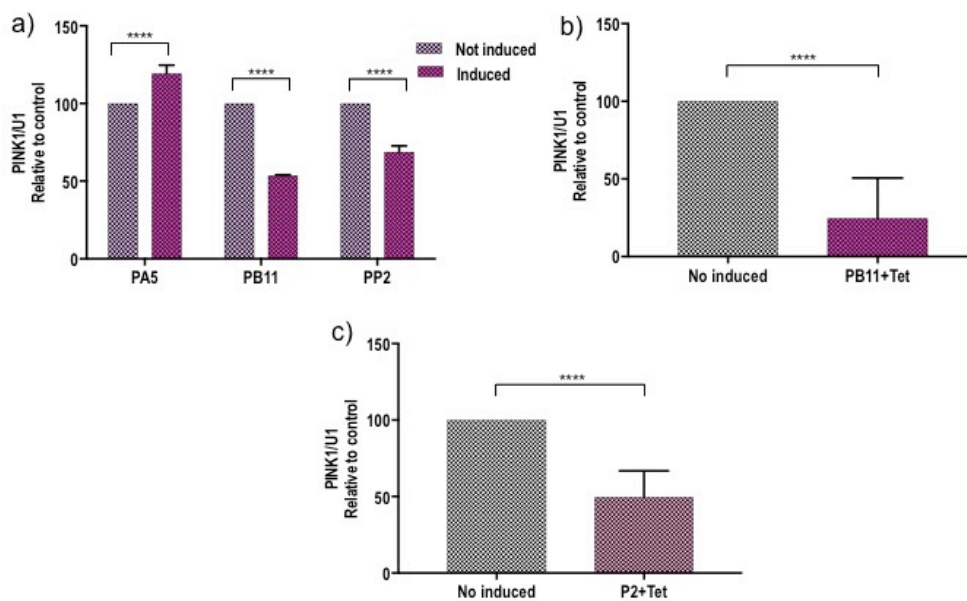
Figure 4.11. PINK1 knockdown in HEK FLP IN cell lines. *PINK1* mRNA level of HEK FLP PINK1 cell lines at 72 after tetracycline induction. A) Three cell lines were selected for screening for *PINK1* knockdown, where a reduction in *PINK1* expression was obtained for *PB11* (50%) (****$P<0.0001$) and *P2* (40%) (****$P<0.0001$) and a ~19% increase in PA5 (****$P<0.0001$). B11 (b) and A2 (c) were selected for further validation of knockdown, where a constant knockdown was seen with both cell lines of 80% in *PB11* for and 50% in *P2*. 2-way ANOVA Dunnett's test (n=3).

HEK Flp TIGAR/PINK1 cell lines

After 72 hrs of tetracycline induction, the three obtained cell lines showed a decreased expression in both genes of approximately 55% for *TIGAR* (2-way ANOVA, ****$P<0.0001$) and 72% for *PINK1* (TP8) (2-way ANOVA, ****$P<0.0001$); 63% for *TIGAR* and 78% for *PINK1* (TP9) (2-way ANOVA, ****$P<0.0001$); and 24% for *TIGAR* and 35% for *PINK1* (TP2) (2-way ANOVA, ****$P<0.0001$) (Figure 4.12 a). Two cell lines were selected for further confirmation, where TP8 showed consistent decrease expression of approximately ~94% in both genes (2-way ANOVA, ****$P<0.0001$) (Figure 4.12 b); and TP9 of ~53% in both genes (2-way ANOVA, ****$P<0.0001$) (Figure 4.12 c). TP8 achieved consistent high reduction for *TIGAR* and *PINK1* expression and was selected for functional analysis.
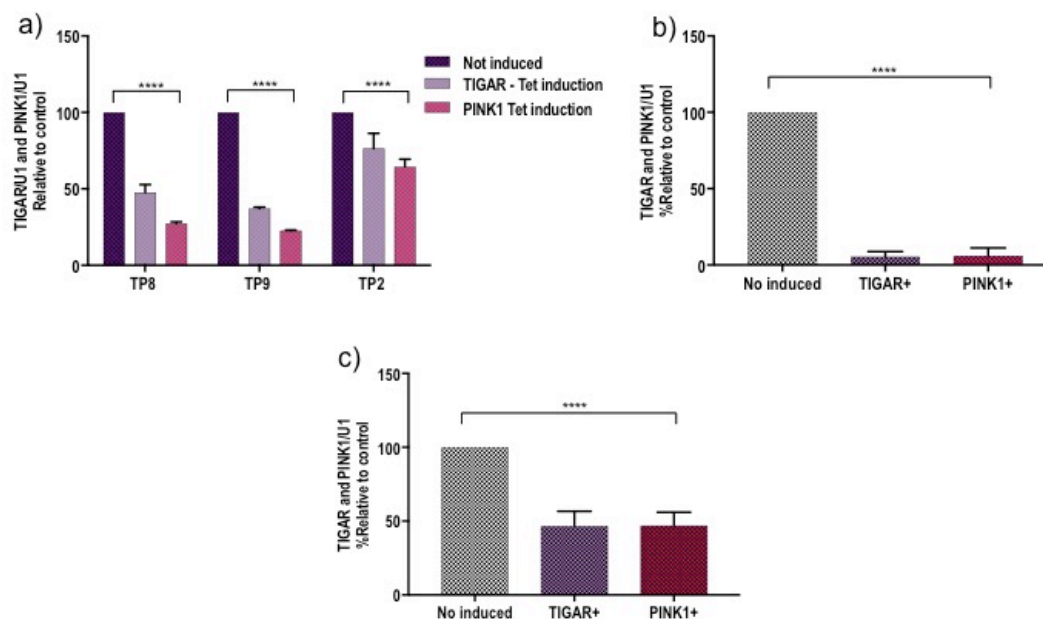
Figure 4.12. TIGAR and PINK1 knockdown in HEK FLP IN cell lines. *PINK1* knockdown in HEK FLP IN cell lines. *PINK1* and *TIGAR* mRNA level of HEK Flp TIGAR/PINK1 cell lines at 72 after tetracycline induction. a) Three cell lines were selected for screening for gene knockdown, where a reduction in *TIGAR* and *PINK1* expression was obtained for *TIGAR* of 55% (****$P<0.0001$) and 72% (****$P<0.0001$) for *PINK1* in TP8; 63% and 78% (****$P<0.0001$) in TP9 and 24% and 35% in (****$P<0.0001$) TP2 respectively. These two cell lines were selected for further validation of knockdown TP8 (b) and TP9 (c), where a constant knockdown for both genes of 94% (****$P <0.0001$) in TP8 and 53% (****$P <0.0001$) in TP9. 2-way ANOVA Dunnett's test (n=3).

4.4.2.2 HEK Flp In mitochondrial function

Since *tigarb* knockdown was demonstrated to have a mitochondrial rescue effect in *pink1* deficient zebrafish model (Flinn et al., 2013); we aimed to assess this effect in human cell lines.

Effect of TIGAR and PINK1 deficiency in ATP production

ATP production was assessed in the three selected cell lines for each cellular model (Figure 4.13). In the presence of glucose, after 48 hrs induction, we found a reduction of 58% (2-way ANOVA, $*P$=0.0309) in the HEK Flp TIGAR A2 induced cells compared to HEK Flp CRNAi induced cells (Figure 4.13 a). However, no statistical difference was found in HEK Flp TIGAR A2 compared to the not induced control (2-way ANOVA, P=0.703) (Figure 4.13a). ATP levels were increased in HEK Flp PINK1 B11 induced cells compared to not induced cells (20%), without reaching statistical difference (2-way ANOVA, P=0.52) (Figure 4.13a). ATP production was decreased in HEK Flp TIGAR A2 induced cells (58%) (2-way ANOVA, $*P$=0.0353) when compared to HEK Flp PINK1 B11 induced cells (Figure 4.13). ATP levels were reduced in TIGAR/PINK1 TP8 induced cells (~16%) compared to not induced controls, however they did not reach statistical significance (2-way ANOVA, P=0.95) (Figure 4.13 a).

In glucose-free medium at 48 hrs post tetracycline induction, HEK Flp TIGAR A2 and HEK Flp PINK1 PB11 induced cells showed an ATP reduction of 60% (2-way ANOVA, $*P$=0.0141) and 62% (2-way ANOVA, $*P$=0.0115) respectively, when compared to control HEK Flp CRNAi induced cells. HEK Flp TIGAR A2 and PINK1 BII showed a decrease of ATP levels ~20% (2-way ANOVA, P>0.05), without reaching statistical difference when compared to their respective not induced

controls. ATP levels showed a slight increase in HEK Flp TIGAR/PINK1 TP8 induced cells when compared to the not induced control (~5%) (2-way ANOVA, *P*>0.05), however this did not reach statistical difference (Figure 4.13 b). We demonstrated that *TIGAR* and *PINK1* deficiency produced a decrease in the ATP independently in the absence of glucose; whereas in glucose media TIGAR deficiency showed a decrease in ATP levels, opposite to an ATP increase when PINK1 is deficient. In glucose-free medium, although there was an increase in ATP production when both genes were deficient in the same cell line, it was minimal and no significant. Overall, there is a statistical difference in TIGAR and PINK1 cell lines when compared to negative control, but not to the respective not induced cell lines.
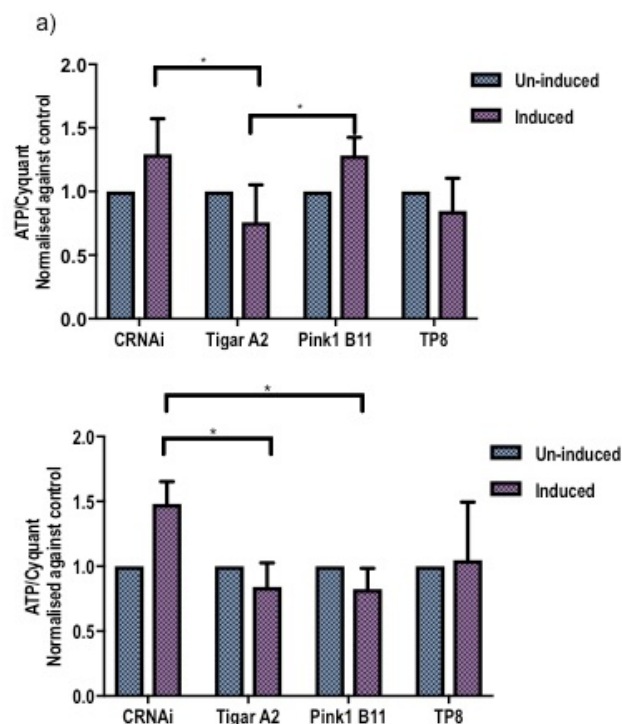
Figure 4.13. ATP assays in stable inducible cell lines for TIGAR and PINK1 knockdown. ATP assays were performed in HEK Flp In of each cellular model in two different medium conditions after 48 hrs of Tetracycline induction. a) In glucose medium, a reduction of ATP levels of induced cell lines of about 58% in HEK Flp TIGAR A2 relative to HEK Flp CRNAi induced cells (*P*=0.0309*).* An ATP reduction of ~58% in HEK Flp TIGAR A2 when compared to HEK Flp PINK1 B11 (*P* =0.0353); b) in glucose-free medium, induced cells showed an ATP reduction in HEK Flp TIGAR A2 (60%) (*P*=0.0141) and HEK Flp PINK1 B11 (62%) (*P*=0.0115) when compared to HEK Flp CRNAi induced cells. All cellular models showed no statistical difference in any of the conditions when compared to their respective not induced control. 2-way ANOVA, Turkey's test (n=3).

4.4.2.3   HEK Flp In mitochondrial morphology

Morphological changes have been reported in other cellular models linked to a defect in the ATP production in *PINK1* deficiency. We therefore investigated whether mitochondrial morphology was altered in the HEK Flp TIGAR, HEK Flp PINK1 and HEK Flp TIGAR/PINK1 induced cells. All cell lines were submitted to the same conditions as the ones assessed for ATP levels. Cells were stained with mitochondrial marker Tom 20 and visualised with the Opera Phoenix Laser based Confocal High Throuput Cell Imaging System. Nine Images per field per condition per cell line were captured and processed by high-content analysis using the Harmony PhenoLOGIC software to obtain mitochondrial length measurements. Qualitative analysis of individual cell lines was performed in the presence or absence of glucose. Overall, after 48 hrs of tetracycline induction, we did not find any significant difference in the mitochondrial length or branching in any of the conditions and any of the HEK Flp In cellular models. Overall, in our hands and under the conditions tested, these results suggested that *TIGAR* and *PINK1* deficiency does not alter the mitochondrial morphology in the HEK Flp In cellular model.
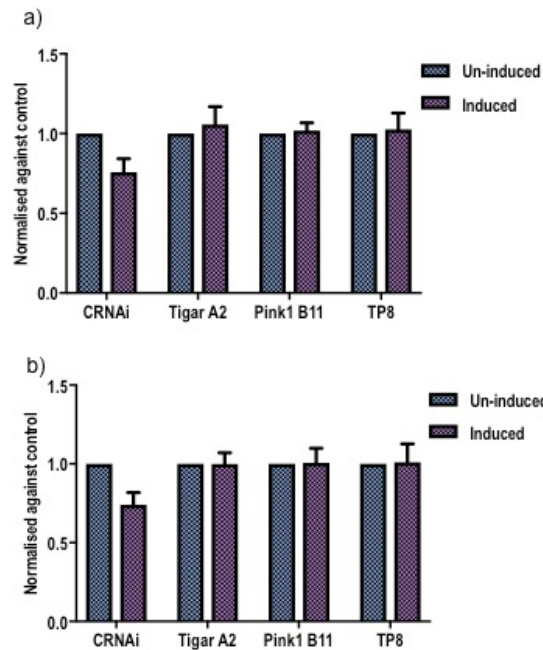
Figure 4.14. Mitochondrial morphology in stable inducible cell lines for *TIGAR* and *PINK1* knockdown. Cells were stained with the mitochondrial marker Tom20 and assessed at the 48hr after tetracycline induction in the presence (a) or absence (b) of glucose. Mitochondrial were visualised with the Opera Phoenix Laser based Confocal High Throughput Cell Imaging System. Mitochondrial length measurements were obtained by high-content analysis using the Harmony PhenoLOGIC software. No statistical difference was obtained in any of the cell lines in any of the conditions assessed (P>0.05). 2-way ANOVA multiple comparisons (n=3).

4.4.3 CRISPR/Cas9

The design for each gene using the CRISPR online tool (http://crispr.mit.edu/) produced 2 paired sgRNAs for *PINK1* in the exon 1, whereas for *TIGAR* one paired guide was design targeting the exon 4 and one within the exon 5, an example of the design is featured in Figure 4.15. The first three exon sequences of the *TIGAR* gene are too small, which result in no available suitable sgRNA for this regions due to their size (Table 4.11).
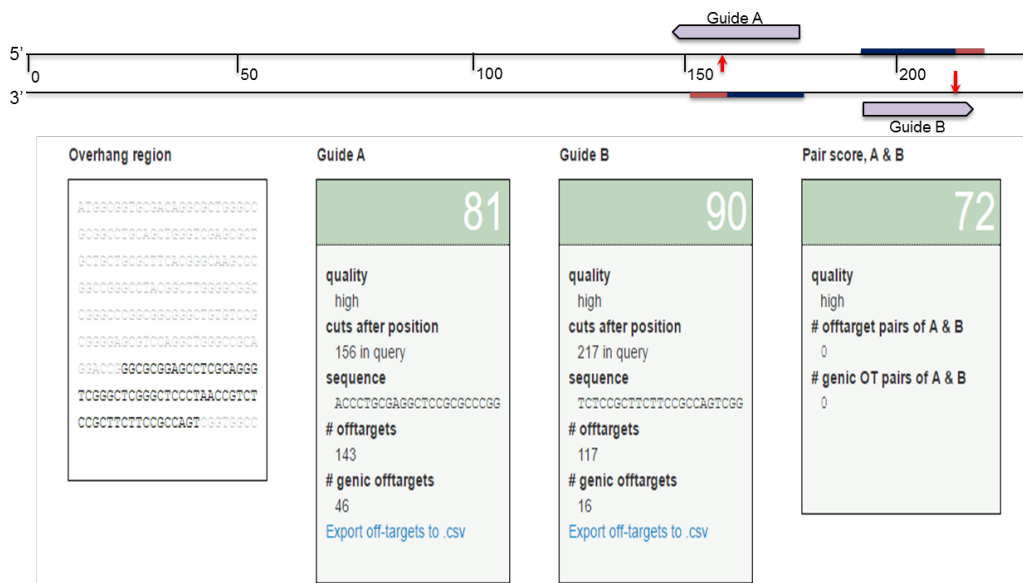
Figure 4.15. gRNA design and nicking strategy. Representative image of each paired guide gRNA designed in opposite strands, based on target sequences against human *TIGAR* and *PINK1*. gRNAs are separated from each other by 20 bp within the respective exon. When gRNAs are paired, the off-target effect is predicted to be null by the online CRISPR Design tool for all the paired guides against both genes (crispr.mit.edu). Each guide cuts after the PAM sequence (red arrow), creating the biallelic disruption.

4.4.3.1   *TIGAR* and *PINK1* colony screening

All gRNAs were cloned into *BbsI*-digested AIO-Puro vector. From the obtained transformants, 2-3 colonies were picked and checked by restriction digests with *BamHI* and *EcoRV*. Successful clones with the insert lose the *BamHI* site, from which the linearized vector was detected (Figure 4.16). Successful clones were selected and transformed. Afterwards, plasmids were purified, assessed and checked for right insertion without any mutations by Sanger sequencing. Four plasmid constructs, for the two paired guides corresponding to each gene, were selected for transfections.
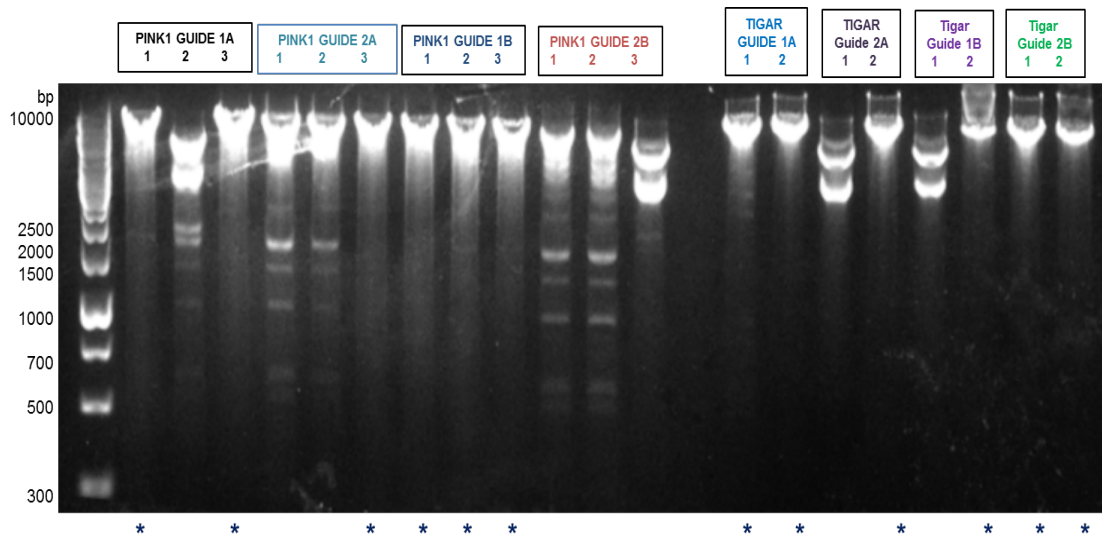
Figure 4.16. Colony screening for PINK1 and TIGAR. Restriction analysis of cloned gRNAs for *PINK1* and *TIGAR*. The oligonucleotide duplex was ligated into *BbsI*-digested AIO-Puro vector; restriction digests with *BamHI* and *EcoRV* of successful clones showed only the linearized vector (~10000bp) (asterix).

After cells were transfected with the correct paired guides for each gene and puromycin selected, successful clones were expanded and selected for knockdown or knock-out confirmation against *TIGAR* and *PINK1*.

TIGAR screening

TIGAR protein level was assessed by WB from the selected clones. A total of fourteen clones were obtained from each transfected gRNA pair, from which eight were selected for screening. Quantitative analysis from the blots showed a reduction in TIGAR protein level in five of the clones between 33-85% (Figure 4.17 a-b). Although clone 2A showed the highest reduction (One-way ANOVA, ***$P<0.001$), it was also the one with the least protein amount loaded, where Actin protein level was remarkably affected (Figure 4.17 a-b). Clones 5A, 6A and 11A showed an increase in TIGAR protein levels at almost 2-fold in one clone (Figure 4.17). The four clones 1B, 3B (33.5%) (ns $P>0.05$, n=2), 4B (58%) (*$P<0.05$, n=2) and 5B 52% (*$P<0.05$, n=2) demonstrated similar reduction of TIGAR protein levels (33-58%) (Figure 4.17

234

b). Since some of the clones were not assessed in triplicate, further verification of TIGAR knockdown is suggested in the remaining clones. In addition, quantifying mRNA levels would be an alternative method to assess if *TIGAR* was knocked down at the transcriptional level.
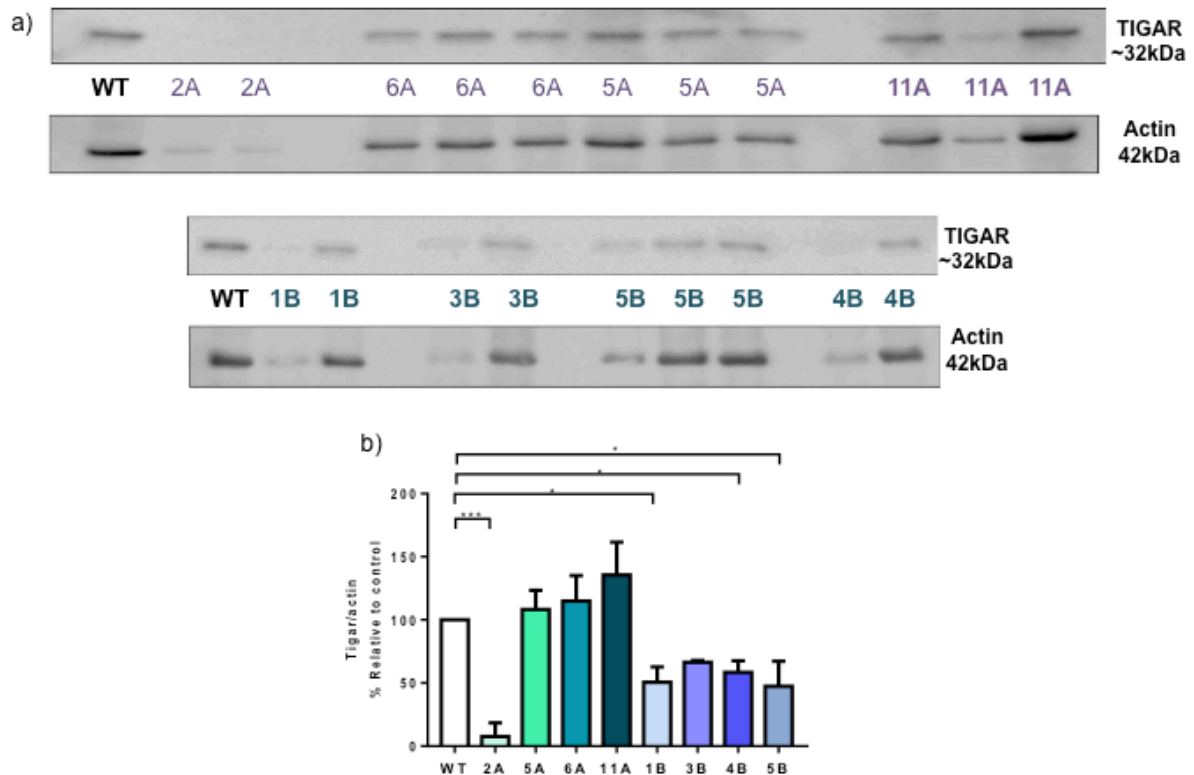
Figure 4.17. TIGAR CRISPR Cas9 screening. A) WB image of clones obtained from cells transfected with paired guides A and B; b) Densitometry analysis where protein level was quantified and normalised against the untransfected cells (WT). *TIGAR* knockdown was obtained for pair 2A of 85% (***$P<0.001$; n=2), pair 1B of ~50% (*$P<0.05$; n=2), pair 3B of 33.5% (ns $P>0.05$, n=2), pair 4B of 58% (*$P<0.05$, n=2) and for pair 5B of 52% (*$P<0.05$, n=2). One-way ANOVA Dunnett's test.

PINK1 screening

Since there is a lack of reliable antibodies against PINK1, we assessed *PINK1* mRNA levels by qPCR in five of the ten clones obtained for this cell model. From the results obtained, only two of the five clones assessed showed a reduction of *PINK1* mRNA levels. Clone 4B and 3B showed a reduction of 87% (One-way ANOVA,

235

**P<0.01, n=2) and 85% (One-way ANOVA, **P<0.01, n=3) respectively compared to WT cells. A non-significant reduction in *PINK1* mRNA levels was detected in 6B (33.7%) (One-way ANOVA, *ns p*>0.05, n=3) and 3A (One-way ANOVA, *P*>0.05, n=2) (Figure 4.18). Some of the clones were tested in duplicate, therefore further screening in triplicate and for the remaining clones should be performed in order to verify the knockdown effect in order to select a suitable cell line for functional analysis in *PINK1* deficient cells.
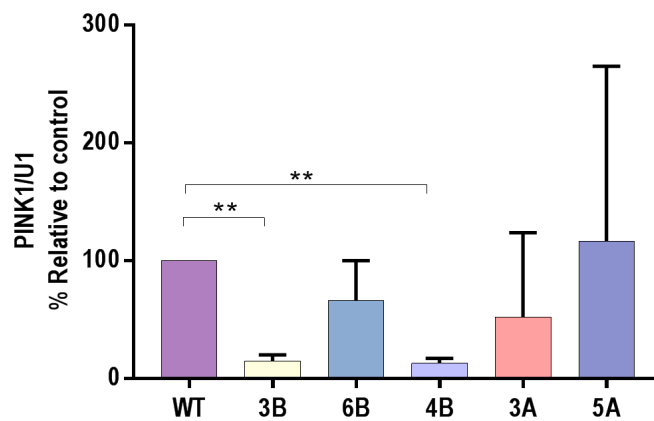
Figure 4.18. PINK1 CRISPR Cas9 screening. Quantification of the mRNA level of transfected cells with paired guides A and B for PINK1 knockdown, where level of expression was normalised against the untransfected cells (WT), where a significant knockdown was obtained for PINK1 3B (85%) (**P<0.01, n=3), and PINK1 4B (87%) (**P<0.01) (n=2) cell lines only. Although PINK1 6B and PINK1 3A cell lines showed a reduction, it was no statistical different. One-way ANOVA Dunnett's test.

All cell lines from both cellular models were only screened for knockdown or knockout efficacy and efficiency. Detection of indel mutations and polymorphism should be verified by functional testing and genotyping for fully validation of the system, detect mutations and off-target effects. Further functional testing assays should be performed by isolating the DNA of each cell model.

4.5 Discussion

Previous research performed in the zebrafish *pink1* deficient model from our group, suggested an unknown implication of TIGAR in PD neurodegenerative process (Flinn et al., 2013). The proper mechanisms related to the development of the disease were still elusive and needed to be validated in a human model. The aim of the current project was to confirm and verify TIGAR PD-related mechanisms in a reliable and robust cellular model with *PINK1* deficiency. Thanks to modern molecular engineering techniques, we achieved to build a stable inducible model, which allow us to study the implications and effects of *TIGAR* when *PINK1* is deficient.

4.5.1 Gene knockdown

Previous attempts to assess the effects of *TIGAR* knockdown in human fibroblasts were not successful and inconclusive. Although, they proved to be a very valuable model with potential promising results, effects of transient transfections and chemical reagents prevented us from assessing the knockdown effect. In order to overcome and tackle this problem, we build an isogenic stable inducible cell line, which allow us to study the functional effects in a *PINK1* deficient stable inducible model.

In our study, using RNAi by microRNAs, we achieved a 40-50% TIGAR knockdown at the protein and gene level consistently. *PINK1* showed to have almost a ~100% knockdown at the protein level, achieving almost a knock-out. The fact that TIGAR knockdown effect was lower in HEK transfected cells might be for a number of reasons. First, TIGAR protein levels have been reported to be higher in HEK cells (See chapter three), whereas mRNA levels has been shown to be lower

(http://www.proteinatlas.org). So, even when TIGAR is knockdown, it is a lower percentage due to its abundancy or a long protein half-life time in HEK cells. Second, even when transient transfections help to study the effect of a target gene and protein production, they do it in a limited temporal manner due to the fact that the genome is not integrated to the host cell line. For this, knockdown effect should be then assessed over a period of time from 24-96 hrs to see whether the maximum effect is achieved at shorter or longer period. Third, chemical and physical methods might interfere with the physiological response of the cell, produce chemical modifications of the microRNA (unlikely) and the overall outcome. The efficiency of the knockdown also depends on the targeted sequence site within the gene, which can result in a high variability. Although, there are no reported TIGAR isoforms, there is the probability that there are produced, not targeted by the miRNA (miR) and therefore detected by WB. A higher *TIGAR* knockdown was expected with chained microRNAs (miRs) targeting only one gene, but the results showed that the percentage was similar or lower than when using miR2 TIGAR alone. miR1 targets exon number 5, whereas miR2 and 3 target the middle and distal part of the exon number 6 of the gene (Table 4.1). These different sites explain the differences of the knockdown effect, suggesting that effective *TIGAR* knockdown occurs when miR are targeting the centre region of exon number 6, the largest of the gene. Contrary to this, the chaining of miRNAs targeting two or more different genes can usually result in lower knockdown effect of both genes, explaining the difference in the knockdown percentage between the two genes in the co-construct (Werness and Anderson, 2010).

Both, *TIGAR* and *PINK1*, protein products are present within the cell in the cytoplasm or the mitochondrial membrane. Current antibodies against all forms of endogenous PINK1 lack reliability, where many of them recognise different cleaved products or do not recognise them at all, displaying unspecific background bands that are likely to be detected at different molecular levels (Deas et al., 2009). PINK1 protein is processed and displayed in three different species within the cell: 1) as full length (~63 kDa), that upon mitochondrial depolarization it is cleaved by, 2) the mitochondrial processing peptidase into a 60-kDa intermediate form, and 3) a 52 kDa mature form processed by the presenilin-associated rhomboid-like protein (PARL) (Greene et al., 2012; Jin et al., 2010). Therefore, the PINK1 protein has a short half-life due to its rapid cellular turnover and modifications (Liu et al., 2017), which explains the higher protein reduction when it is knocked down and detected when tagged with the eGFP protein. PINK1 mRNA levels remain to be a more reliable source for PINK1 detection, since they are ubiquitously stably expressed within the cell (Blackinton et al., 2007; Duan et al., 2014).

TIGAR and PINK1 knockdown results by WB were both confirmed and verified in the stable inducible cell lines by detection of mRNA levels by qPCR. We were confident of our results and the silencing effect mediated by the miRNAs (miRs) to study the effect in the mitochondrial function and morphology in the cellular inducible models.

4.5.2 Stable inducible models

There are a wide variety of techniques for transient RNAi, such as: microinjection of the desired specific nucleotide sequence, viral and plasmid vectors carrying genes and probes that target specific cell. However, one shortcoming with

the microinjection is that only a very limited number of cells are transfected (Hsu and Uludağ, 2012). Viral vectors have the characteristic to be very useful for transfections in primary cells, which are difficult to transfect. Another advantage of viral and plasmid vectors is that they often carry a marker for cellular selection of cells successfully transduced. Viral vectors require the transcriptional machinery from the host to express integrated DNA material. Thus, the host is exposed to random integration of the DNA material alongside the bio-hazard risk implied when using a viral vector (Ramachandran and Ignacimuthu, 2013).

Stable inducible cell lines offer several advantages for investigating the biological and molecular processes not only for PD but for a number of human diseases (Falkenburger et al., 2016; Kappel et al., 2007). They can be grown for longer periods of time and be produced in larger quantities. The gene function can be assessed in a spatiotemporal manner, where gain or loss of function mutations are avoided. By turning on and off the gene expression, it helps to understand the involvement in the development and progression of the disease. Gene over-expression can be also studied through this approach and assess gene dose cellular effect and toxicity. More than one gene can be easily introduced by the carrying vector; allowing to assess protein levels as well as to investigate the clonal functionality when different genes are integrated in the same cell. The system also prevents the risk of random integration, undesired, not predictable and not reproducible gene and cellular effects are minimal (Yahata et al., 2005).

The Tetracycline-Inducible Flp In T-Rex System from Thermo Fisher Scientific provides the tools for generation of stable, isogenic and inducible cell lines

with a unique FRT integration site. All of which will contain identical backgrounds and cellular models can be generated to knockdown or introduce mutations of a particular gene of interest. By using this system, we were then able to generate three stable inducible cellular models: HEK Flp TIGAR, PINK1 and co-construct TIGAR-PINK1 for PD research. The generated cell lines from each model showed a good knockdown for both genes, particularly *PINK1*. The clones with the highest percentage reduction at the mRNA level were used to assess the mitochondrial function and morphology. However, for Flp TIGAR and the co-construct Flp TIGAR/PINK1 cell model, TIGAR silencing showed to be more variable and $\leq$ 50% at the mRNA and protein level. This could be due to the fact that it is a metabolic protein and any cellular insult may modify its expression, which is also highly dependent in the cellular type. Moreover, HEK cells have a higher TIGAR expression than PINK1, which also affects the knockdown effect.

4.5.3 Limitations

Opposed to neurons, where the pathology occurs, the HEK cellular model is continuously dividing. The ongoing division could be providing the cell the opportunity to repair and compensate the damage by alternative mechanisms. Stable HEK cells have shown similar physiological effects as neuronal cells, however stable expression and phenotype maintenance had been difficult in some cellular types, with irreproducible results subjected to different culture conditions. Moreover, HEKs are cells with a different phenotype and metabolism different to neurons (Stepanenko and Dmitrenko, 2015). To overcome this problem, inducible models could be transformed into dopaminergic neurons by converting them either into iPSC, or directly into induced human neuronal progenitor cells (iNPCs). Mitochondrial translation, glycolysis, mitochondrial functions, protein balance between

mitochondrial and nucleus, and molecular changes are suggested to occur in cells induced with doxycycline mainly and less likely with tetracycline. (Houtkooper, 2015).

4.5.4 Mitochondrial morphology and function

Mitochondrial function and morphology are impaired in *PINK1* deficiency. In this study we assessed the changes obtained in the mitochondrial morphology in the HEK Flp cells with either PINK1 and/or TIGAR and with TIGAR/PINK1 deficiency. Our current results suggested that they might not be affecting the mitochondrial morphology in HEK cells.

There are a number of reasons for our current results. First, HEK cells have a small particular size (20-30µm length). The detection by the high throughput microscopy analysis, OPERA Phoenix, provides better results in larger cells with flat morphology. This is explained by the fact the mitochondrial morphology 3D images are represented by the obtained 2D image. Moreover, some proteins that are constitutively highly expressed might be influencing the expression of the exogenous or introduced gene (Thomas and Smart, 2005). Since HEK Flp In are not neuronal cells, some genes and protein products might have different levels of expression and post-translational modifications. Their rapid growth, clusters or clumps formation and cell to cell variation might also contribute to obtained results

A link between mitochondrial function, mitochondrial complexes, mitochondrial complexes, ATP production and morphology has been demonstrated in a diversity of non-neuronal cellular models. This has been mainly reported in cell lines and tissue from patients with *PINK1*, *Parkin* and *LRRK2* (*G2019S*) mutations. The zebrafish study demonstrated a clear deficit in mitochondrial complex I and III, which

correlated with increased *tigarb* (zebrafish homologue) expression in *pink1* deficiency (Flinn et al., 2013). Here, we aimed to investigate whether the mitochondrial function and ATP production is affected in *TIGAR* and *PINK1* deficiency models, and if there is a rescue effect when both genes are silenced in the cell.

In this study, the three HEK Flp In cellular models showed that ATP cellular levels were different within the two growth medium conditions. In glucose presence, HEK Flp *TIGAR* and *TIGAR/PINK1* cells showed a drop in ATP levels, which was only significant when compared to the negative control (HEK Flp CRNAi) but not the not induced control cells. Interestingly, HEK Flp *PINK1* cells showed higher ATP cellular levels compared to its not induced control (Figure 4.13 a). This could be due to the fact that higher cellular ATP levels in cells in culture rely on glucose and glycolysis. Thus, in *PINK1* deficiency, cells still rely on glycolysis and generate ATP, whereas cells with *TIGAR* deficiency produce ATP via OXPHOS which is less active but more productive. *PINK1* deficient cells in glucose free media had slightly lower ATP, whereas ATP in *TIGAR* deficient cells remained lower. Although cells have to switch to OXPHOS metabolism, cells with lower ATP production have been shown to have severe defects of the mitochondrial respiratory chain complexes. Therefore, *TIGAR* deficient cells continued to generate energy through OXPHOS. *PINK1* deficient had a tendency to produce lower levels of ATP, which could be due to remaining active mechanisms for energy production. Furthermore, cells with *TIGAR/PINK1* deficiency, had lower ATP levels in glucose presence, but not significant, whereas a tendency for an increase was seen in glucose free media. The overall results showed that ATP levels had a tendency to be affected in all three

cellular models, although we were expecting a higher effect in all of them. One of the most likely explanations for the obtained results is a relation between the knockdown percent in each cell line. *TIGAR* knockdown was achieved at ~50% and ~80% for PINK1, with similar results in the cell line with TIGAR/PINK1 deficiency. The fact that there are still cells able to express either TIGAR or PINK1, explains the impact on the ATP levels obtained for each model. Furthermore, not induced cells could be also expressing the miRNA and repressing the targeted genes, thus interfering with the outcome. Moreover, since cells were induced, split and plated 24 hrs for the assay, acute compensatory mechanisms could be triggered within the cells. Therefore, a still active glycolytic pathway and other sources of energy (eg. Glutamine) that could be triggered by the cell as a compensatory mechanism might increase the ATP production levels in the cells.

Recently, *PINK1* levels have been directly correlated with ATP cellular levels dependent in glucose as a source. Low levels of *PINK1* expression were found in cultures with low levels of glucose, likely due to impaired translation. Furthermore, *PINK1* expression levels were found to depend in an active glycolytic pathway rather than the glucose content. A link between glucose metabolism, *PINK1* mitochondrial damage sensing mechanisms and PINK1/Parkin mitophagy pathway have been suggested (Lee et al., 2014b) and with opposed results in other some lines (Yao et al., 2011) . TIGAR role in neuronal metabolism is still unclear, it has been suggested only to be a neuroprotector only after ischemia-reperfusion events (Cao et al., 2015; Li et al., 2014; Sun et al., 2015; Zhou et al., 2016). The suspected role of *TIGAR* in *PINK1* deficiency related mechanisms in PD still remain unclear. Interestingly, in glioblastoma cells *TIGAR* and *PINK1* have opposed effects, in which the linked

mechanisms are by their effect in cellular growth and survival. Both genes are regulators of the Warburg effect, in which cellular main source of energy is through glycolysis. *TIGAR* positive regulator provides cellular survival (Peña-Rico et al., 2011; Sinha et al., 2013; Wanka et al., 2012) , whereas *PINK1* negative regulation impairs cellular growth (Agnihotri et al., 2016). However, both act as ROS scavengers preventing cellular death (Agnihotri et al., 2016; Peña-Rico et al., 2011; Sinha et al., 2013; Wanka et al., 2012). These mechanisms could be the link between *TIGAR* and *PINK1*-related PD pathology. However, it is still unknown how exactly TIGAR is involved in PD PINK1 related pathology.

The present study remains to be confirmed and further optimised to detect significant changes in the mitochondrial function and morphology, as well as further related mechanisms such as autophagy/mitophagy, which have been both related to TIGAR and PINK1. Moreover, higher knockdown needs to be achieved for both models, which could be performed by optimising the protocol and studied the effect at different time-points. ATP defects are highly correlated to defects in the mitochondrial respiratory chain. The mitochondrial chain complexes should also be assessed since the original zebrafish *pink1* deficient model showed complex I and III defect. Energy demands and metabolism are different depending on the cellular type, which has been also demonstrated true for the function of TIGAR and PINK1. Therefore, the link between both genes need to be studied in a dopaminergic neuronal model, which could be achieved by converting the cells into induced human neuronal progenitor cells (iNPCs).

4.5.5 CRISPR/Cas 9: *TIGAR* and *PINK1*

The new era in genomic engineering brought the CRISPR/Cas9 approach for genome editing. This new method offers many advantages compared to previous systems like zinc-finger nucleases (ZFN) and transcription activator-like effector nucleases (TALENs), which are highly complex and expensive. With CRISPR/Cas9 a specific gene sequence is targeted, yielding a higher efficiency. Moreover, it allows the introduction of two or more sgRNAs targeting different sites in the genome.

One of the main limitations of this technique is the possible occurrence of off-target effects. Random integration and repair can also result in different cellular mosaic mutations. One of the recent developed approaches to avoid those effects is by the "double nicking" method using nickase endonucleases. In this study, we used the combination of an All-In One vector and Nickase approach to generate CRISPR/Cas9 cell lines with *TIGAR* and *PINK1* deficiency. Generation and selection of the clones were done without any FACS and only by antibiotic selection and clone isolation. This could explain the variability obtained in the TIGAR protein level and the *PINK1* expression between and within the same clones. As previous results with the FLP-In T-Rex system from Invitrogen, TIGAR showed to have less effective knockdown in HEK cells (Figure 4.10 and Figure 4.17), whereas almost a complete knockout of *PINK1* (~80-90%) (Figure 4.11 and Figure 4.18) was achieved by using both methods. One of the main caveats is that without FACS sorting and any assay for checking the correct integration and screening for mutations (eg. Surveyor or T731 assays) before clonal expansion. However, recently a study by Manikoth Ayyathan et al., 2017; showed that the main difference obtained in knockout efficiency is due to the cell line rather than the method approached (Manikoth Ayyathan et al., 2017).

CRISPR/Cas 9 TIGAR tested clones also showed an effect in Actin protein level, which could be due to an off-target effect within the clones. Another main limitation with CRISPR/Cas9 is that the cell lines are not isogenic, compared to the FLP-In cells, and mosaic mutations within the different cell lines might still occur. Although CRISPR/Cas9 PINK1 cell lines showed higher knockdown, some clones were only tested in two biological replicates. Further confirmation awaits by assessing the protein level and gene expression in three biological replicates for both genes to confirm effective gene knockdown/knockout, from all the obtained clones to select the best one. Before any functional analysis, sequence the full genome looking also for candidate off-target sites occurring within either TIGAR or PINK1 clones.

In order to study the mechanisms involved in PD-related pathogenesis in the main affected region of the disease, the generated isogenic cell lines should be converted directly into induced neural stem cells or neural precursor cells to generate dopaminergic neurons.

4.6   Conclusions

Comparing both systems in the current study, it is clear that here the best approach for gene knockdown is by the FLP-In T-Rex system. Limited time for the generation of the CRISPR/Cas9 cell models for TIGAR and PINK1 is one of the reasons of the lower efficiency and efficacy of this system in this approach. Optimisation of the method should be performed in a suitable cell model in which a knockout for both genes could be successfully achieved. The dopaminergic neurons,

in the SN, are the main site affected in PD, where the pathology results in neuronal death and disease phenotype.

To fully understand the underlying mechanisms leading to PD and related to *TIGAR* and *PINK1*, studies need to be conducted in a dopaminergic neuronal model and *in vivo*. Overexpression of *TIGAR* in *PINK1* deficient neurons could help to understand if *TIGAR* has a toxic effect within the cells. It would be interesting and valuable to understand the role of *PINK1* overexpression in dopaminergic neurons with *TIGAR* deficiency. Overall, we were able to establish a stable inducible cell model for *TIGAR* and *PINK1*. We showed a tendency to an effect on mitochondrial function, but this was not significant. These results require to be optimised over different time points and be studied together with the mitochondrial respiratory complexes.

5 General Discussion and Conclusions

5.1 TIGAR expression in different cellular models

TIGAR is a multifunctional protein with a number different binding regulators and targets. Its expression is tightly regulated and depends on the cell type and the nature of the stimuli. In our study, there was widespread TIGAR expression in the different brain regions studied, as well as in human fibroblasts, HEK293, LUHMES and SHSY-5Y cells. This supports the proposed role of TIGAR to maintain cellular homeostasis across different cell types and tissues. The main function of TIGAR is to inhibit glycolysis and promote the metabolic shunt to the Pentose Phosphate Pathway (PPP). The function of TIGAR as a pro-survival protein is reflected by its capacity to provide antioxidant defence against ROS, cellular stress and hypoxia, and nucleotides for DNA synthesis (Bensaad et al., 2006).

How TIGAR-related pathways might be contributing to PD and neurodegeneration are still unclear. Since it is a glycolysis inhibitor, in cells that are highly depending on energy production from the glycolytic pathway, such as neurons, this function might be deleterious for them. *PINK1* deficiency causes OXPHOS impairment, making the cell rely on ATP production by other sources different from the mitochondria, but from glycolysis. *TIGAR* overexpression impact on glycolysis might therefore have a particularly marked effect in *PINK1* mutant tissue.

However, TIGAR expression similar in the sporadic PD brains as well as in fibroblasts from patients with *parkin* mutations compared to controls. PINK1 and Parkin share many cellular functions. However, there is also evidence of them acting in independent pathways (Kageyama et al., 2014; Lazarou et al., 2015; Murakawa et

al., 2015). This suggests that *TIGAR* up-regulation may be a specific feature of *PINK1*-related disease. Unlike in familial cases, a complex interplay between environmental and genetic factors will contribute to the development of the disease in patients with sporadic PD. Thus, different genes and pathways might explain the wide variation of TIGAR levels in our study. Unfortunately, we did not have access to *PINK1* mutant PD patient tissue.

TIGAR was found to co-localise with alpha-synuclein in the Lewy bodies, which could be due to a synergetic interaction, altering their conformation and leading to further aggregation. The interaction between alpha-synuclein and TIGAR, alongside the previous finding of TIGAR overexpression in the *pink1* deficient model, suggests new shared mechanisms in sporadic and familial PD. However, proof of interaction awaits further investigation, using co-immunoprecipitation assays in the PD and DLB brain extracts, stable cell lines overexpressing *alpha-synuclein* with and without additional stressors such as oxidative stress. Since oxidative stress has been suggested to be one of the mechanisms in PD and demonstrated to be related to alpha-synuclein, TIGAR and PINK1, it would be interesting to study TIGAR and alpha-synuclein interaction in the generated stable cell lines, as well as in induced neurons under oxidative stress conditions. Many proteins including the PD-related LRRK2, PINK1 and Parkin proteins showed impaired conjugation under oxidative stress and have also been detected in Lewy bodies (Brudek et al., 2016b; Murakami et al., 2007; Volpicelli-Daley et al., 2016). Notably, only antibodies against the C-terminal did recognise TIGAR in the neuronal bodies and Lewy bodies, which suggests that the protein might be fragmented or has undergone a conformational change. This could result in misfolding, reduced solubility and aggregation of TIGAR

protein in the inclusions.

5.2 *The suspected role of TIGAR in PD*

The zebrafish *pink1* deficient model showed a defect in the mitochondrial complex I and III, with a slight defect in the mitochondrial morphology but no ATP assays were carried out (Flinn et al., 2013).

In this study, we assessed the effect of TIGAR and PINK1 knockdown in a stable inducible cell culture model, where we did not see a mitochondrial defect. We found some promising results carried out in the human fibroblasts with TIGAR knockdown, but overall the results were inconclusive due to the transfection affecting the mitochondrial function. Therefore, our results obtained in fibroblasts and HEK cells suggest that mitochondrial function and morphology might not be affected by TIGAR levels. However, these results are inconclusive and require further optimisation. Fibroblasts and HEK cells are not neuronal cells and their metabolic demands differ from neurons. Neuronal metabolisms and energetic demands have been demonstrated to depend on glucose metabolism, where the Pentose phosphate pathway (PPP) was suggested to be essential. Continue damage in neurons has been reported to occur from oxidative stress. TIGAR has been demonstrated to function as a pro-survival (Bensaad et al., 2006; Cheung et al., 2013b; Ma et al., 2017; Martinez-Outschoorn et al., 2010; Peña-Rico et al., 2011; Wanka et al., 2012; Yin et al., 2012b), as well as an apoptotic mediator in different cell types (Hoshino et al., 2012; Kimata et al., 2010). Moreover, a dual function in autophagy and apoptosis has been demonstrated in cancer cell lines (Cheung et al., 2015; Xie et al., 2014). So, TIGAR might be acting as a neuroprotector by dampening the ROS levels and maintaining NADPH and glutathione levels to

prevent further damage (Bolaños and Heales, 2010; Herrero-Mendez et al., 2009). As a glycolysis inhibitor, TIGAR might also promote cellular death by inhibiting glycolysis, leading vulnerable cells and unable to meet energetic demands. Furthermore, TIGAR has been demonstrated to protect neurons and other cell types, by preventing damage from ischemic injury (Al-Maghrebi and Renno, 2016; Cao et al., 2015; Hoshino et al., 2012; Li et al., 2014; Sun et al., 2015; Zhou et al., 2016). However, several studies have suggested a dysregulation of the PPP pathway and glucose metabolism as one of the earliest events occurring in the pathogenesis of neurodegeneration (Bouzier-Sore and Bolaños, 2015; Dunn et al., 2013; Hilker et al., 2012) providing a tentative but largely hypothetical link with TIGAR.

TIGAR was only detected in Lewy bodies but not in other intracellular inclusion bodies, which further reinforces the hypothesis of its disease specificity. Therefore, since we TIGAR was present in pathological inclusions of PD and DLB patients, it will be interesting to study the effect of its overexpression in induced neurons (iN) from fibroblasts with familial and sporadic PD as well as in the generated stable cell lines (Hek Flp In) with *PINK1* deficiency. TIGAR was found to co-localise with alpha-synuclein, therefore, we propose to study the effect of alpha-synuclein overexpression when TIGAR is either absent or overexpressed in cultured neuronal models.

TIGAR is one of the target proteins of p53, but we did not find evidence of p53 upregulation in in the post-mortem tissue of the PD and DLB brains. A number of p53-independent TIGAR mechanisms have been demonstrated in several cellular models under different physiological and stress conditions, which could explain this

finding (Sinha et al., 2013; Venkatanarayan et al., 2016; Zou et al., 2012, 2013). The p53-independent pathways might provide insight into the suspected role of TIGAR in PD. However, p53 was not investigated in the generated stable cell lines and in the PD patient fibroblasts.

Reduced ROS levels have been suggested to be associated to autophagy inhibition (Bensaad et al., 2009; Ye et al., 2013), where TIGAR opposes autophagy (Bensaad et al., 2009). Autophagy has also been suggested to play an important role for the development of PD. Therefore, defects in the autophagy pathway, have been suggested in PD and other neurodegenerative diseases (Rahman and Rhim, 2017). Lewy body pathology may be a consequence of cellular self-defence for clearance of cytotoxic proteins (Fecchio et al., 2013) TIGAR presence in Lewy bodies could be the result of the same cellular mechanism and suggests an acquired cytotoxic property of TIGAR. Both TIGAR and alpha-synuclein have been suggested to have a role in autophagy impairment, so increased production of both proteins may lead to impaired autophagy and promote protein aggregation. The role of TIGAR in autophagy was demonstrated in unstressed cells and independent from mTOR pathway. In this study we also investigated the role in TIGAR for autophagy in sporadic PD fibroblasts. In our hands, we did not find any impairment in autophagy in the patient tissue. However, the study was performed in only two patient cell lines. Moreover, unlike familial PD, the evidence of impaired autophagy in sporadic PD still remains inconclusive (Ryan et al., 2015).

Further experiments in neuronal cellular models are required to study this hypothesis.

TIGAR pathways involving HK-I and HK-II were investigated in the brains of PD patients in the SN. We found a slight increase in HK-I expression but the difference did not reach statistical significance. TIGAR was reported to translocate to the mitochondria and interact with HK-II in cells upon hypoxic conditions and metabolic stress, providing survival to the cells (Cheung et al., 2012). No difference in the HK-II expression was found in our experiments, which might be explained by the fact that it has low levels of expression in the human brain. Moreover, we did not observe TIGAR translocation to the mitochondria after rotenone exposure. Furthermore, we only study the effect of rotenone exposure in one PD patient fibroblast cell line and did not study the association of TIGAR with HK-II in the stable cell lines. In order to verify TIGAR association with HK-II, further experiments need to be performed in a larger cohort of fibroblasts, in the stable cell lines and preferably in induced dopaminergic neurons. Furthermore, microarrays in post-mortem tissue, stable inducible cell lines, human fibroblasts, derived neurons, exposed to metabolic stress would also provide insight into the disease pathomechanisms related to TIGAR.

5.3 PD models: from zebrafish to post-mortem tissue and cellular models

In this study we used different cellular models to investigate TIGAR suspected role in PD. They help to unravel TIGAR-related mechanisms leading to the disease, with their own advantages and disadvantages. Combining them provided us with a good insight of the suspected role of TIGAR in PD.

Zebrafish models are a valuable model to study human disease because they are in vivo models that are transparent, small size and with fast development. Moreover, they are a robust platform for genetic manipulation and drug screening, as well as to study development during embryogenesis and at different stages. Contrary to fly models, zebrafish are vertebrate animals, where many genes are highly conserved, and their findings can be translated into humans (Matsui, 2017). However, zebrafish also have some limitations. For example, they do not completely resemble the human brain. Morpholino antisense (MO) and TILLING approaches can sometimes lead to off-target effects (MO); depending on the size and sequence of the coding exons (Sood et al., 2013).

In this study, we aimed to translate the findings in *pink1* deficient zebrafish into human PD tissue. Post-mortem tissue offers great advantages over other models, and help us to gain insight into the pathogenesis of the disease. Their correct processing and handling help their preservation and provides an invaluable model for DNA, RNA and protein studies. Fibroblast cultures are also derived from patient tissue. However, fibroblasts mirror the biochemical defect occurring in the neurons only partially., Investigations in post-mortem brain tissue can nevertheless be complemented by performing functional and enzymatic assays in living cells with or without a PD gene mutation. Confirmation of their function and interaction can be further investigated in a generated stable cell line, which is isogenic and genetically manipulated to study the gene/protein function of interest. Although post-mortem brain tissue studies are important for research in neurodegeneration, it has some limitations.

In vitro cellular models allow us to study the process and dynamics leading to impaired cellular function and cell death. Fibroblasts and HEK are both, cheap, commercially available, easy to handle and maintain, and well established models for disease research. HEK cell lines are easy to transfect, whereas fibroblasts are slightly more difficult to transfect cells. These cell lines were used when attempting *TIGAR* knockdown, showing different efficiency and efficacy due to their different behaviour. We found that TIGAR expression was higher in HEK cells compared to human fibroblasts, which resulted in a lower knockdown effect in HEK cells when compared to the fibroblasts. Moreover, the siRNA smart pool targets four regions in the gene, whereas the miRs target only one region of the gene. This suggests that due to the diversity amongst the cell lines and methods, to achieve the desired knockdown, an optimised general protocol had to be established for each cellular model.

5.4   Concluding remarks

TIGAR was found to be present in Lewy bodies in the SN of PD and DLB patients. Notably, TIGAR co-localises with alpha-synuclein. These findings suggest TIGAR role in neurodegeneration and Lewy body formation. TIGAR-positive pathological inclusions were only found in the SN. TIGAR-positive inclusions were not found in spinal cords of MND, or in the glial cytoplasmic inclusions of MSA cases. This suggests TIGAR specificity for Lewy-type pathology. p53 localization and expression was not found when comparing PD cases to controls. TIGAR is translated in human fibroblasts derived from patients with familial and sporadic PD. TIGAR gene expression and protein level was not significantly different in *parkin*-mutant fibroblasts when compared to controls.

TIGAR knockdown was successful in *parkin*-deficient and *LRRK2^{G2019S}* fibroblasts, however its effect could not be assessed due the transfection secondary effects. TIGAR cellular localisation is not affected in *parkin*-mutant fibroblasts exposed to rotenone toxicity and cellular stress. No evidence of TIGAR involvement after autophagy/mitophagy induction in sporadic PD patients in this particular study.

A stable inducible cell model for *TIGAR* and *PINK1* deficiency was established to investigate TIGAR-pathology in PD. An effect on mitochondrial function was seen, but without statistical difference. These results require further optimisation and to be studied together with the mitochondrial respiratory complexes.

5.5   Future studies

Further cellular and post-mortem tissue studies need to be conducted to elucidate the TIGAR-related pathological mechanisms and pathways leading to neurodegeneration. These studies should be performed in more controls and PD patients with *Parkin* and/or *PINK1* mutations. Moreover, further TIGAR up and downregulators (i.e., SP-1, CREB, mTOR, ATM) should be assessed to elucidate TIGAR related mechanisms. Further assays, such as co-immunoprecipitation assays, are needed in the PD and DLB brain extracts, stable cell lines overexpressing *alpha-synuclein* and neuronal cellular models*,* with and without additional stressors such as oxidative stress and severe hypoxia. Future experiments aiming to determine TIGAR role in autophagy in human fibroblasts would need to be done in more patients with sporadic and familial PD, ideally with *PINK1* mutations, in order to fully address its role in mitochondrial function and autophagy/mitophagy PD-related mechanisms.

TIGAR effect and mechanisms need to be performed in cellular and neuronal, *in vitro* and *in vivo* models, with PD-related mutations should be attempted by alternative methods such as stable transduction. Neuronal models with TIGAR and/or alpha-synuclein overexpression are required to study its effect in the mitochondrial function, autophagy/mitophagy and cellular survival.

Although CRISPR/Cas9 achieved good knockdown, mainly for *PINK1*, a small limited number of clones were tested. Further confirmation needs to be done by assessing the protein level and gene expression in three biological replicates for both genes to confirm effective gene knockdown/knockout. Before any functional analysis, sequence the full genome looking also for candidate off-target sites occurring within either TIGAR or PINK1 clones. Once achieved, this new promising technique will be ideal to develop and establish stable neuronal lines to verify and investigate further TIGAR-PD related mechanisms and pathways.

References

Abramov, A.Y., Gegg, M., Grunewald, A., Wood, N.W., Klein, C., and Schapira, A.H.V. (2011). Bioenergetic consequences of PINK1 mutations in Parkinson disease. PLoS One *6*, e25622.

Agnihotri, S., Golbourn, B., Huang, X., Remke, M., Younger, S., Cairns, R.A., Chalil, A., Smith, C.A., Krumholtz, S.L., Mackenzie, D., et al. (2016). PINK1 is a negative regulator of growth and the warburg effect in glioblastoma. Cancer Res. *76*, 4708–4719.

Aguirre, J.D., Dunkerley, K.M., Mercier, P., and Shaw, G.S. (2017). Structure of phosphorylated UBL domain and insights into PINK1-orchestrated parkin activation. Proc. Natl. Acad. Sci. U. S. A. *114*, 298–303.

Aharon-Peretz, J., Rosenbaum, H., and Gershoni-Baruch, R. (2004). Mutations in the glucocerebrosidase gene and Parkinson's disease in Ashkenazi Jews. N. Engl. J. Med. *351*, 1972–1977.

Ahmad, F., Ghosh, S., Sinha, S., Joshi, S.D., Mehta, V.S., and Sen, E. (2015). TGF-β-induced hCG-β regulates redox homeostasis in glioma cells. Mol. Cell. Biochem. *399*, 105–112.

Ahmad, R., Alam, M., Hasegawa, M., Uchida, Y., Al-Obaid, O., Kharbanda, S., and Kufe, D. (2017). Targeting MUC1-C inhibits the AKT-S6K1-elF4A pathway regulating TIGAR translation in colorectal cancer. Mol. Cancer *16*, 33.

Al-Khayal, K., Abdulla, M., Al-Obeed, O., Al Kattan, W., Zubaidi, A., Vaali-Mohammed, M.-A., Alsheikh, A., and Ahmad, R. (2015). Identification of the TP53-induced glycolysis and apoptosis regulator in various stages of colorectal cancer patients. Oncol. Rep. *7805*, 1–6.

Al-Maghrebi, M., and Renno, W.M. (2016). Altered expression profile of glycolytic enzymes during testicular ischemia reperfusion injury is associated with the p53/TIGAR pathway: effect of fructose 1,6-diphosphate. PeerJ *4*, e2195.

Alcalay, R.N., Caccappolo, E., Mejia-Santana, H., Tang, M.X., Rosado, L., Ross, B.M., Verbitsky, M., Kisselev, S., Louis, E.D., Comella, C., et al. (2010). Frequency of Known Mutations in Early-Onset Parkinson Disease. Arch. Neurol. *67*, 213–223.

Aleshin, A.E., Zeng, C., Bourenkov, G.P., Bartunik, H.D., Fromm, H.J., and Honzatko, R.B. (1998). The mechanism of regulation of hexokinase: new insights from the crystal structure of recombinant human brain hexokinase complexed with glucose and glucose-6-phosphate. Structure *6*, 39–50.

Alves, C., Duplan, E., and Checler, F. (2016). A-Synuclein and P53 Functional Interplay in Physiopathological Contexts. 1–2.
Alves da Costa, C., and Checler, F. (2010). A novel parkin-mediated transcriptional function links p53 to familial Parkinson's disease. Cell Cycle *9*, 16–17.

Ambrosi, G., Ghezzi, C., Sepe, S., Milanese, C., Payan-Gomez, C., Bombardieri, C.R., Armentero, M.-T., Zangaglia, R., Pacchetti, C., Mastroberardino, P.G., et al. (2014). Bioenergetic and proteolytic defects in fibroblasts from patients with sporadic Parkinson's disease. Biochim. Biophys. Acta.

Ando, M., Fiesel, F.C., Hudec, R., Caulfield, T.R., Ogaki, K., Górka-Skoczylas, P., Koziorowski, D., Friedman, A., Chen, L., Dawson, V.L., et al. (2017). The PINK1 p.I368N mutation affects protein stability and ubiquitin kinase activity. Mol. Neurodegener. *12*, 32.

Anichtchik, O., Diekmann, H., Fleming, A., Roach, A., Goldsmith, P., and Rubinsztein, D.C. (2008). Loss of PINK1 function affects development and results in neurodegeneration in zebrafish. J. Neurosci. *28*, 8199–8207.

Arai, T., Hasegawa, M., Akiyama, H., Ikeda, K., Nonaka, T., Mori, H., Mann, D., Tsuchiya, K., Yoshida, M., Hashizume, Y., et al. (2006). TDP-43 is a component of ubiquitin-positive tau-negative inclusions in frontotemporal lobar degeneration and amyotrophic lateral sclerosis. Biochem. Biophys. Res. Commun. *351*, 602–611.

Arena, G., Gelmetti, V., Torosantucci, L., Vignone, D., Lamorte, G., Rosa, P. De, Cilia, E., Jonas, E.A., Valente, E.M., De Rosa, P., et al. (2013). PINK1 protects against cell death induced by mitochondrial depolarization, by phosphorylating Bcl-xL and impairing its pro-apoptotic cleavage. Cell Death Differ. *20*, 920–930.

Arif, M., Wei, J., Zhang, Q., Liu, F., Basurto-Islas, G., Grundke-Iqbal, I., and Iqbal, K. (2014). Cytoplasmic Retention of Protein Phosphatase 2A Inhibitor 2 (I 2 PP2A) Induces Alzheimer-like Abnormal Hyperphosphorylation of Tau. J. Biol. Chem. *289*, 27677–27691.

Asakawa, S., Tsunematsu Ki, Takayanagi, A., Sasaki, T., Shimizu, A., Shintani, A., Kawasaki, K., Mungall, A.J., Beck, S., Minoshima, S., et al. (2001). The genomic structure and promoter region of the human parkin gene. Biochem. Biophys. Res. Commun. *286*, 863–868.

Auburger, G., Klinkenberg, M., Drost, J., Marcus, K., Morales-Gordo, B., Kunz, W.S., Brandt, U., Broccoli, V., Reichmann, H., Gispert, S., et al. (2012). Primary skin fibroblasts as a model of Parkinson's disease. Mol. Neurobiol. *46*, 20–27.

Austin, S.A., Rojanathammanee, L., Golovko, M.Y., Murphy, E.J., and Combs, C.K. (2011). Lack of alpha-synuclein modulates microglial phenotype in vitro. Neurochem. Res. *36*, 994–1004.

Azkona, G., López de Maturana, R., del Rio, P., Sousa, A., Vazquez, N., Zubiarrain, A., Jimenez-Blasco, D., Bolaños, J.P., Morales, B., Auburger, G., et al. (2016). LRRK2 Expression Is Deregulated in Fibroblasts and Neurons from Parkinson Patients with Mutations in PINK1. Mol. Neurobiol.

Baba, M., Nakajo, S., Tu, P.-H., Tomita, T., Nakaya, K., Lee, V.M., Trojanowski, J.Q., and Iwatsubo, T. (1998). Aggregation of alpha-synuclein in Lewy bodies of sporadic Parkinson's disease and dementia with Lewy bodies. Am. J. Pathol. *152*, 879–884.
Badger, J.L., Cordero-Llana, O., Hartfield, E.M., and Wade-Martins, R. (2014). Parkinson's disease in a dish - Using stem cells as a molecular tool. Neuropharmacology *76 Pt A*, 88–96.

Bandopadhyay, R., Kingsbury, A.E., Cookson, M.R., Reid, A.R., Evans, I.M., Hope, A.D., Pittman, A.M., Lashley, T., Canet-Aviles, R., Miller, D.W., et al. (2004). The expression of DJ-1 (PARK7) in normal human CNS and idiopathic Parkinson's disease. Brain *127*, 420–430.

Bang, Y., Kim, K.S., Seol, W., and Choi, H.J. (2016). LRRK2 interferes with aggresome formation for autophagic clearance. Mol. Cell. Neurosci. *75*, 71–80.

Bayreuther, K., Francz, P.I., Gogol, J., Hapke, C., Maier, M., and Meinrath, H.-G. (1991). Differentiation of primary and secondary fibroblasts in cell culture systems. Mutat. Res. *256*, 233–242.

Beilina, A., and Cookson, M.R. (2015). Genes associated with Parkinson's disease: Regulation of autophagy and beyond. J. Neurochem. *139*, 1–17.

Beishline, K., and Azizkhan-Clifford, J. (2015). Sp1 and the "hallmarks of cancer." FEBS J. *282*, 224–258.

Bensaad, K., Tsuruta, A., Selak, M. a, Vidal, M.N.C., Nakano, K., Bartrons, R., Gottlieb, E., and Vousden, K.H. (2006). TIGAR, a p53-inducible regulator of glycolysis and apoptosis. Cell *126*, 107–120.

Bensaad, K., Cheung, E.C., and Vousden, K.H. (2009). Modulation of intracellular ROS levels by TIGAR controls autophagy. EMBO J. *28*, 3015–3026.

Béraud, D., Twomey, M., Bloom, B., Mittereder, A., Ton, V., Neitzke, K., Chasovskikh, S., Mhyre, T.R., and Maguire-Zeiss, K.A. (2011). α-Synuclein Alters Toll-Like Receptor Expression. Front. Neurosci. *5*, 1–11.

Bertolin, G., Ferrando-Miguel, R., Jacoupy, M., Traver, S., Grenier, K., Greene, A.W., Dauphin, A., Waharte, F., Bayot, A., Salamero, J., et al. (2013). The TOMM machinery is a molecular switch in PINK1 and PARK2/PARKIN-dependent mitochondrial clearance. Autophagy *9*, 1801–1817.

Bezard, E., Yue, Z., Kirik, D., and Spillantini, M.G. (2013). Animal models of Parkinson's disease: limits and relevance to neuroprotection studies. Mov. Disord. *28*, 61–70.

Bingol, B., Tea, J.S., Phu, L., Reichelt, M., Bakalarski, C.E., Song, Q., Foreman, O., Kirkpatrick, D.S., and Sheng, M. (2014). The mitochondrial deubiquitinase USP30 opposes parkin-mediated mitophagy. Nature *510*, 370–375.

Blackinton, J.G., Anvret, A., Beilina, A., Olson, L., Cookson, M.R., and Galter, D. (2007). Expression of PINK1 mRNA in human and rodent brain and in Parkinson's disease. Brain Res. *1184*, 10–16.

Blesa, J., Trigo‑Damas, I., Quiroga‑Varela, A., and Rey, N.L. del (2016). Animal Models of Parkinson's Disease. J. Dorszewska, and W.B.T.-C. in P.D. Kozubski, eds. (Rijeka: InTech), p. Ch. 10.

Bolaños, J.P., and Heales, S.J.R. (2010). Persistent mitochondrial damage by nitric oxide and its derivatives: neuropathological implications. Front. Neuroenergetics *2*, 1.

BOLTE, S., and CORDELIÈRES, F.P. (2006). A guided tour into subcellular colocalization analysis in light microscopy. J. Microsc. *224*, 213–232.

Bonifati, V. (2014). Genetics of Parkinson's disease - state of the art, 2013. Parkinsonism Relat. Disord. *20 Suppl 1*, S23-8.
Bonifati, V., Oostra, B.A., and Heutink, P. (2004). Linking DJ-1 to neurodegeneration offers novel insights for understanding the pathogenesis of Parkinson's disease. J. Mol. Med. (Berl). *82*, 163–174.

Bouzier-Sore, A.K., and Bolaños, J.P. (2015). Uncertainties in pentose-phosphate pathway flux assessment underestimate its contribution to neuronal glucose consumption: Relevance for neurodegeneration and aging. Front. Aging Neurosci. *7*, 1–5.

Braak, H., Tredici, K. Del, Rüb, U., de Vos, R. a . ., Jansen Steur, E.N.., and Braak, E. (2003). Staging of brain pathology related to sporadic Parkinson's disease. Neurobiol. Aging *24*, 197–211.

Braidy, N., Gai, W.-P., Xu, Y.H., Sachdev, P., Guillemin, G.J., Jiang, X.-M., Ballard, J.W.O., Horan, M.P., Fang, Z.M., Chong, B.H., et al. (2013). Uptake and mitochondrial dysfunction of alpha-synuclein in human astrocytes, cortical neurons and fibroblasts. Transl. Neurodegener. *2*, 20.

Bravo-San Pedro, J.M., Gómez-Sánchez, R., Niso-Santano, M., Pizarro-Estrella, E., Aiastui-Pujana, A., Gorostidi, A., Climent, V., López de Maturana, R., Sanchez-Pernaute, R., López de Munain, A., et al. (2012). The MAPK1/3 pathway is essential for the deregulation of autophagy observed in G2019S LRRK2 mutant fibroblasts. Autophagy *8*, 1537–1539.

Bravo-San Pedro, J.M., Niso-Santano, M., Gómez-Sánchez, R., Pizarro-Estrella, E., Aiastui-Pujana, A., Gorostidi, A., Climent, V., López de Maturana, R., Sanchez-Pernaute, R., López de Munain, A., et al. (2013). The LRRK2 G2019S mutant exacerbates basal autophagy through activation of the MEK/ERK pathway. Cell. Mol. Life Sci. *70*, 121–136.

Brudek, T., Winge, K., Rasmussen, N.B., Bahl, J.M.C., Tanassi, J., Agander, T.K., Hyde, T.M., and Pakkenberg, B. (2016a). Altered ??-synuclein, parkin, and synphilin isoform levels in multiple system atrophy brains. J. Neurochem. *136*, 172–185.

Caesar, M., Felk, S., Aasly, J.O., and Gillardon, F. (2015). Changes in actin dynamics and F-actin structure both in synaptoneurosomes of LRRK2(R1441G) mutant mice and in primary human fibroblasts of LRRK2(G2019S) mutation carriers. Neuroscience *284*, 311–324.

Campos, F.L., Carvalho, M.M., Cristovão, A.C., Je, G., Baltazar, G., Salgado, A.J., Kim, Y.-S., and Sousa, N. (2013). Rodent models of Parkinson's disease: beyond the motor symptomatology. Front. Behav. Neurosci. *7*, 175.

Cao, L., Chen, J., Li, M., Qin, Y.-Y., Sun, M., Sheng, R., Han, F., Wang, G., and Qin, Z.-H. (2015). Endogenous level of TIGAR in brain is associated with vulnerability of neurons to ischemic injury. Neurosci. Bull. 1–14.

Carballo-Carbajal, I., Weber-Endress, S., Rovelli, G., Chan, D., Wolozin, B., Klein, C.L., Patenge, N., Gasser, T., and Kahle, P.J. (2010). Leucine-rich repeat kinase 2 induces alpha-synuclein expression via the extracellular signal-regulated kinase pathway. Cell. Signal. *22*, 821–827.

Caviness, J.N., Adler, C.H., Hentz, J.G., Shill, H.A., Evidente, V.G.H., Driver-Dunckley, E.D., Sabbagh, M.N., Sue, L., and Beach, T.G. (2011). Incidental Lewy body disease: Electrophysiological findings suggesting pre-clinical Lewy body disorders. Clin. Neurophysiol. *122*, 2426–2432.

Cheung, E.C., Ludwig, R.L., and Vousden, K.H. (2012). Mitochondrial localization of TIGAR under hypoxia stimulates HK2 and lowers ROS and cell death. Proc. Natl. Acad. Sci. U. S. A. *109*, 20491–20496.

Cheung, E.C., Athineos, D., Lee, P., Ridgway, R. a Lambie, W., Nixon, C., Strathdee, D., Blyth, K., Sansom, O.J., and

Vousden, K.H. (2013a). TIGAR is required for efficient intestinal regeneration and tumorigenesis. Dev. Cell *25*, 463–477.

Cheung, E.C., Lee, P., Ceteci, F., Nixon, C., Blyth, K., Sansom, O.J., and Vousden, K.H. (2015). Opposing effects of TIGAR- and RAC1-derived ROS on Wnt-driven proliferation in the mouse intestine. Genes Dev. 52–63.

Chiang, T.-W.W., le Sage, C., Larrieu, D., Demir, M., and Jackson, S.P. (2016). CRISPR-Cas9D10A nickase-based genotypic and phenotypic screening to enhance genome editing. Sci. Rep. *6*, 24356.

Chinta, S.J., Mallajosyula, J.K., Rane, A., and Andersen, J.K. (2010). Mitochondrial alpha-synuclein accumulation impairs complex I function in dopaminergic neurons and results in increased mitophagy in vivo. Neurosci. Lett. *486*, 235–239.

Choubey, V., Safiulina, D., Vaarmann, A., Cagalinec, M., Wareski, P., Kuum, M., Zharkovsky, A., and Kaasik, A. (2011). Mutant A53T α-Synuclein induces neuronal death by increasing mitochondrial autophagy. J. Biol. Chem. *286*, 10814–10824.

Chung, S.J., Armasu, S.M., Biernacka, J.M., Lesnick, T.G., Rider, D.N., Lincoln, S.J., Ortolaza, A.I., Farrer, M.J., Cunningham, J.M., Rocca, W.A., et al. (2011). Common Variants in PARK Loci and Related Genes and Parkinson ' s Disease. *26*, 280–288.

Chung, S.Y., Kishinevsky, S., Mazzulli, J.R., Graziotto, J., Mrejeru, A., Mosharov, E. V., Puspita, L., Valiulahi, P., Sulzer, D., Milner, T.A., et al. (2016). Parkin and PINK1 Patient iPSC-Derived Midbrain Dopamine Neurons Exhibit Mitochondrial Dysfunction and α-Synuclein Accumulation. Stem Cell Reports *7*, 664–677.

Ciryam, P., Lambert-Smith, I.A., Bean, D.M., Freer, R., Cid, F., Tartaglia, G.G., Saunders, D.N., Wilson, M.R., Oliver, S.G., Morimoto, R.I., et al. (2017). Spinal motor neuron protein supersaturation patterns are associated with inclusion body formation in ALS. Proc. Natl. Acad. Sci. *114*, E3935–E3943.

Cochemé, H.M., and Murphy, M.P. (2008). Complex I is the major site of mitochondrial superoxide production by paraquat. J. Biol. Chem. *283*, 1786–1798.

Cornejo-Olivas, M.R., Torres, L., Mata, I.F., Mazzetti, P., Rivas, D., Cosentino, C., Inca-Martinez, M., Cuba, J.M., Zabetian, C.P., and Leverenz, J.B. (2015). A Peruvian family with a novel PARK2 mutation: Clinical and pathological characteristics. Parkinsonism Relat. Disord. *21*, 444–448.

Cornelissen, T., Haddad, D., Wauters, F., Van Humbeeck, C., Mandemakers, W., Koentjoro, B., Sue, C., Gevaert, K., De Strooper, B., Verstreken, P., et al. (2014). The deubiquitinase USP15 antagonizes Parkin-mediated mitochondrial ubiquitination and mitophagy. Hum. Mol. Genet. *23*, 5227–5242.

Corona, J.C., Gimenez-Cassina, A., Lim, F., and Díaz-Nido, J. (2010). Hexokinase II gene transfer protects against neurodegeneration in the rotenone and MPTP mouse models of Parkinson's disease. J. Neurosci. Res. *88*, 1943–1950.

da Costa, C.A., Sunyach, C., Giaime, E., West, A., Corti, O., Brice, A., Safe, S., Abou-Sleiman, P.M., Wood, N.W., Takahashi, H., et al. (2009). Transcriptional repression of p53 by parkin and impairment by mutations associated with autosomal recessive juvenile Parkinson's disease. Nat. Cell Biol. *11*, 1370–1375.

Covy, J.P., Yuan, W., Waxman, E.A., Hurtig, H.I., Van Deerlin, V.M., and Giasson, B.I. (2009). Clinical and pathological characteristics of patients with leucine-rich repeat kinase-2 mutations. Mov. Disord. *24*, 32–39.

Dachsel, J.C., Ross, O.A., Mata, I.F., Kachergus, J., Toft, M., Cannon, A., Baker, M., Adamson, J., Hutton, M., Dickson, D.W., et al. (2007). Lrrk2 G2019S substitution in frontotemporal lobar degeneration with ubiquitin-immunoreactive neuronal inclusions. Acta Neuropathol. *113*, 601–606.

Dalfó, E., Portero-Otín, M., Ayala, V., Martínez, A., Pamplona, R., and Ferrer, I. (2005). Evidence of Oxidative Stress in the Neocortex in Incidental Lewy Body Disease. J. Neuropathol. Exp. Neurol. *64*, 816–830.

Deas, E., Plun-Favreau, H., and Wood, N.W. (2009). PINK1 function in health and disease. EMBO Mol. Med. *1*, 152–165.
Decressac, M., Mattsson, B., and Björklund, a (2012). Comparison of the behavioural and histological characteristics of the 6-OHDA and α-synuclein rat models of Parkinson's disease. Exp. Neurol. *235*, 306–315.

DelleDonne, A., Klos, K.J., Fujishiro, H., Ahmed, Z., Parisi, J.E., Josephs, K.A., Frigerio, R., Burnett, M., Wszolek, Z.K., Uitti, R.J., et al. (2008). Incidental Lewy Body Disease and Preclinical Parkinson Disease. Arch. Neurol. *65*, 1074–1080.

Devi, L., Raghavendran, V., Prabhu, B.M., Avadhani, N.G., and Anandatheerthavarada, H.K. (2008). Mitochondrial import and accumulation of alpha-synuclein impair complex I in human dopaminergic neuronal cultures and Parkinson disease brain. J. Biol. Chem. *283*, 9089–9100.

Dias, V., Junn, E., and Mouradian, M.M. (2013). The role of oxidative stress in parkinson's disease. J. Parkinsons. Dis. *3*, 461–491.

Dimant, H., Kalia, S.K., Kalia, L. V, Zhu, L.N., Kibuuka, L., Ebrahimi-Fakhari, D., McFarland, N.R., Fan, Z., Hyman, B.T., and McLean, P.J. (2013). Direct detection of alpha synuclein oligomers in vivo. Acta Neuropathol. Commun. *1*, 6.

Du, Y., Yang, D., Li, A., Luo, G., Li, T., Fan, X., Wang, Q., Zhang, X., Wang, Y., and Le, W. (2009). An insight into the mechanistic role of p53-mediated autophagy induction in response to proteasomal inhibition-induced neurotoxicity. Autophagy *5*, 663–675.

Duan, X., Tong, J., Xu, Q., Wu, Y., Cai, F., Li, T., and Song, W. (2014). Upregulation of human PINK1 gene expression by NFκB signalling. Mol. Brain *7*, 57.

Dunn, K.W., Kamocka, M.M., and McDonald, J.H. (2011). A practical guide to evaluating colocalization in biological microscopy. Am. J. Physiol. - Cell Physiol. *300*, C723–C742.

Dunn, L., Allen, G.F., Mamais, A., Ling, H., Li, A., Duberley, K.E., Hargreaves, I.P., Pope, S., Holton, J.L., Lees, A., et al. (2013). Dysregulation of glucose metabolism is an early event in sporadic Parkinson's disease. Neurobiol. Aging 1–5.

Duplan, E., Giordano, C., Checler, F., and Alves da Costa, C. (2016). Direct α-synuclein promoter transactivation by the tumor suppressor p53. Mol. Neurodegener. *11*, 13.

Elder, G.J., Mactier, K., Colloby, S.J., Watson, R., Blamire, A.M., O'Brien, J.T., and Taylor, J.P. (2017). The influence of hippocampal atrophy on the cognitive phenotype of dementia with Lewy bodies. Int. J. Geriatr. Psychiatry 1–8.

Emre, M., Aarsland, D., Brown, R., Burn, D.J., Duyckaerts, C., Mizuno, Y., Broe, G.A., Cummings, J., Dickson, D.W., Gauthier, S., et al. (2007). Clinical diagnostic criteria for dementia associated with Parkinson's disease. Mov. Disord. *22*, 1689–707; quiz 1837.

Engelender, S., Kaminsky, Z., Guo, X., Sharp, A.H., Amaravi, R.K., Kleiderlein, J.J., Margolis, R.L., Troncoso, J.C., Lanahan, A.A., Worley, P.F., et al. (1999). Synphilin-1 associates with alpha-synuclein and promotes the formation of cytosolic inclusions. Nat. Genet. *22*, 110–114.

Exner, N., Treske, B., Paquet, D., Holmström, K., Schiesling, C., Gispert, S., Carballo-Carbajal, I., Berg, D., Hoepken, H.-H., Gasser, T., et al. (2007). Loss-of-function of human PINK1 results in mitochondrial pathology and can be rescued by parkin. J. Neurosci. *27*, 12413–12418.

Exner, N., Lutz, A.K., Haass, C., and Winklhofer, K.F. (2012). Mitochondrial dysfunction in Parkinson's disease: molecular mechanisms and pathophysiological consequences. EMBO J. *31*, 3038–3062.

Falkenburger, B.H., Saridaki, T., and Dinter, E. (2016). Cellular models for Parkinson's disease. J. Neurochem. *139*, 121–130.
Farrer, M., Gwinn-Hardy, K., Muenter, M., DeVrieze, F.W., Crook, R., Perez-Tur, J., Lincoln, S., Maraganore, D., Adler, C., Newman, S., et al. (1999). A chromosome 4p haplotype segregating with Parkinson's disease and postural tremor. Hum. Mol. Genet. *8*, 81–85.

Farrer, M., Chan, P., Chen, R., Tan, L., Lincoln, S., Hernandez, D., Forno, L., Gwinn-Hardy, K., Petrucelli, L., Hussey, J., et al. (2001). Lewy bodies and parkinsonism in families with parkin mutations. Ann. Neurol. *50*, 293–300.

Fecchio, C., De Franceschi, G., Relini, A., Greggio, E., Dalla Serra, M., Bubacco, L., and Polverino de Laureto, P. (2013). α-Synuclein Oligomers Induced by Docosahexaenoic Acid Affect Membrane Integrity. PLoS One *8*, e82732.

Ferreira, M., and Massano, J. (2017). An updated review of Parkinson's disease genetics and clinicopathological correlations. Acta Neurol. Scand. *135*, 273–284.

Ferretta, A., Gaballo, A., Tanzarella, P., Piccoli, C., Capitanio, N., Nico, B., Annese, T., Di Paola, M., Dell'aquila, C., De Mari, M., et al. (2014). Effect of resveratrol on mitochondrial function: implications in parkin-associated familiar Parkinson's disease. Biochim. Biophys. Acta *1842*, 902–915.

Fiesel, F.C., Ando, M., Hudec, R., Hill, A.R., Castanedes-Casey, M., Caulfield, T.R., Moussaud-Lamodiere, E.L., Stankowski, J.N., Bauer, P.O., Lorenzo-Betancor, O., et al. (2015). (Patho-)physiological relevance of PINK1-dependent ubiquitin phosphorylation. EMBO Rep. *16*, 1114–1130.

Fitzmaurice, P.S., Ang, L., Guttman, M., Rajput, A.H., Furukawa, Y., and Kish, S.J. (2003). Nigral glutathione deficiency is not specific for idiopathic Parkinson's disease. Mov. Disord. *18*, 969–976.

Fleming, S. (2017). Mechanisms of Gene-Environment Interactions in Parkinson's Disease. Curr. Environ. Heal. Reports *4*, 192–199.

Flinn, L., Mortiboys, H., Volkmann, K., Köster, R.W., Ingham, P.W., and Bandmann, O. (2009). Complex I deficiency and dopaminergic neuronal cell loss in parkin-deficient zebrafish (Danio rerio). Brain *132*, 1613–1623.

Flinn, L.J., Keatinge, M., Bretaud, S., Mortiboys, H., Matsui, H., De Felice, E., Woodroof, H.I., Brown, L., McTighe, A., Soellner, R., et al. (2013). TigarB causes mitochondrial dysfunction and neuronal loss in PINK1 deficiency. Ann. Neurol. *74*, 837–847.

Foo, H., Mak, E., Chander, R.J., Ng, A., Au, W.L., Sitoh, Y.Y., Tan, L.C.S., and Kandiah, N. (2016). Associations of hippocampal subfields in the progression of cognitive decline related to Parkinson's disease. NeuroImage Clin. *14*, 37–42.

Foti, R., Zucchelli, S., Biagioli, M., Roncaglia, P., Vilotti, S., Calligaris, R., Krmac, H., Girardini, J.E., Del Sal, G., and Gustincich, S. (2010). Parkinson's disease-associated DJ-1 is required for the expression of the Glial cell line-derived neurotrophic factor receptor RET in human neuroblastoma cells. J. Biol. Chem. *285*, jbc.M109.088294.

De Franceschi, G., Fecchio, C., Sharon, R., Schapira, A.H.V., Proukakis, C., Bellotti, V., and De Laureto, P.P. (2017). α-Synuclein structural features inhibit harmful polyunsaturated fatty acid oxidation, suggesting roles in neuroprotection. J. Biol. Chem. *292*, 6927–6937.

Freundt, E.C., Maynard, N., Clancy, E.K., Roy, S., Bousset, L., Sourigues, Y., Covert, M., Melki, R., Kirkegaard, K., and Brahic, M. (2012). Neuron-to-neuron transmission of α-synuclein fibrils through axonal transport. Ann. Neurol. *72*, 517–524.

Fujioka, S., Ogaki, K., Tacik, P.M., Uitti, R.J., Ross, O. a, and Wszolek, Z.K. (2014). Update on novel familial forms of Parkinson's disease and multiple system atrophy. Parkinsonism Relat. Disord. *20 Suppl 1*, S29-34.

Fujishiro, H., Imamura, A.Y., Lin, W., Uchikado, H., Mark, M.H., Golbe, L.I., Markopoulou, K., Wszolek, Z.K., and Dickson, D.W. (2013). Diversity of pathological features other than Lewy bodies in familial Parkinson's disease due to SNCA mutations. Am. J. Neurodegener. Dis. *2*, 266–275.

Gaig, C., Martí, M.J., Ezquerra, M., Rey, M.J., Cardozo, A., and Tolosa, E. (2007). G2019S LRRK2 mutation causing Parkinson's disease without Lewy bodies. J. Neurol. Neurosurg. Psychiatry *78*, 626–628.

Gaig, C., Ezquerra, M., Martí, M.J., Valldeoriola, F., Muñoz, E., Lladó, A., Rey, M.J., Cardozo, A., Molinuevo, J.L., and Tolosa, E. (2008). Screening for the LRRK2 G2019S and codon-1441 mutations in a pathological series of parkinsonian syndromes and frontotemporal lobar degeneration. J. Neurol. Sci. *270*, 94–98.

Galvin, J.E., Uryu, K., Lee, V.M., and Trojanowski, J.Q. (1999). Axon pathology in Parkinson's disease and Lewy body dementia hippocampus contains alpha-, beta-, and gamma-synuclein. Proc. Natl. Acad. Sci. U. S. A. *96*, 13450–13455.
Gámez-Valero, A., Prada-Dacasa, P., Santos, C., Adame-Castillo, C., Campdelacreu, J., Reñé, R., Gascón-Bayarri, J., Ispierto, L., Álvarez, R., Ariza, A., et al. (2016). GBA Mutations Are Associated With Earlier Onset and Male Sex in Dementia With Lewy Bodies. Mov. Disord. *31*, 1066–1070.

Gan-Or, Z., Dion, P.A., and Rouleau, G.A. (2015). Genetic perspective on the role of the autophagy-lysosome pathway in Parkinson disease. Autophagy *11*, 1443–1457.

Gandhi, S. (2006). PINK1 protein in normal human brain and Parkinson's disease. Brain *129*, 1720–1731.

Garcia-Miralles, M., Coomaraswamy, J., Häbig, K., Herzig, M.C., Funk, N., Gillardon, F., Maisel, M., Jucker, M., Gasser, T., Galter, D., et al. (2015). No dopamine cell loss or changes in cytoskeleton function in transgenic mice expressing physiological levels of wild type or G2019S mutant LRRK2 and in human fibroblasts. PLoS One *10*, e0118947.

Garneau, J.E., Dupuis, M.-È., Villion, M., Romero, D.A., Barrangou, R., Boyaval, P., Fremaux, C., Horvath, P., Magadán, A.H., and Moineau, S. (2010). The CRISPR/Cas bacterial immune system cleaves bacteriophage and plasmid DNA. Nature *468*, 67–71.

Gazzina, S., Premi, E., Turrone, R., Acosta-Cabronero, J., Rizzetti, M.C., Cotelli, M.S., Gasparotti, R., Padovani, A., and Borroni, B. (2016). Subcortical matter in the ?-synucleinopathies spectrum: an MRI pilot study. J. Neurol. *263*, 1575–1582.

Geisler, S., Holmström, K.M., Treis, A., Skujat, D., Weber, S.S., Fiesel, F.C., Kahle, P.J., and Springer, W. (2010a). The PINK1/Parkin-mediated mitophagy is compromised by PD-associated mutations. Autophagy *6*, 871–878.

Geisler, S., Holmström, K.M., Skujat, D., Fiesel, F.C., Rothfuss, O.C., Kahle, P.J., and Springer, W. (2010b). PINK1/Parkin-mediated mitophagy is dependent on VDAC1 and p62/SQSTM1. Nat. Cell Biol. *12*, 119–131.

Gerin, I., Noël, G., Bolsée, J., Haumont, O., Van Schaftingen, E., and Bommer, G.T. (2014). Identification of TP53-induced glycolysis and apoptosis regulator (TIGAR) as the phosphoglycolate-independent 2,3-bisphosphoglycerate phosphatase. Biochem. J. *458*, 439–448.

Gerlach, M., and Riederer, P. (1996). Animal models of Parkinson's disease: An empirical comparison with the phenomenology of the disease in man. J. Neural Transm. *103*, 987–1041.

Giasson, B.I., Covy, J.P., Bonini, N.M., Hurtig, H.I., Farrer, M.J., Trojanowski, J.Q., and Van Deerlin, V.M. (2006). Biochemical and pathological characterization of Lrrk2. Ann. Neurol. *59*, 315–322.

Gibb, W.R., and Lees, A.J. (1988). The relevance of the Lewy body to the pathogenesis of idiopathic Parkinson's disease. J. Neurol. Neurosurg. Psychiatry *51*, 745–752.

Gilks, W.P., Abou-Sleiman, P.M., Gandhi, S., Jain, S., Singleton, A., Lees, A.J., Shaw, K., Bhatia, K.P., Bonifati, V., Quinn, N.P., et al. (2005). A common LRRK2 mutation in idiopathic Parkinson's disease. Lancet (London, England) *365*, 415–416.

Gillardon, F. (2009). Leucine-rich repeat kinase 2 phosphorylates brain tubulin-beta isoforms and modulates microtubule stability - A point of convergence in Parkinsonian neurodegeneration? J. Neurochem. *110*, 1514–1522.

Gille, G., Hung, S.-T., Reichmann, H., and Rausch, W.-D. (2004). Oxidative stress to dopaminergic neurons as models of Parkinson's disease. Ann. N. Y. Acad. Sci. *1018*, 533–540.

Gimenez-Cassina, A., Lim, F., Cerrato, T., Palomo, G.M., and Diaz-Nido, J. (2009). Mitochondrial Hexokinase II Promotes Neuronal Survival and Acts Downstream of Glycogen Synthase Kinase-3. J. Biol. Chem. *284*, 3001–3011.

Giordana, M.T., D'Agostino, C., Albani, G., Mauro, A., Di Fonzo, A., Antonini, A., and Bonifati, V. (2007). Neuropathology of Parkinson's disease associated with the LRRK2 Ile1371Val mutation. Mov. Disord. *22*, 275–278.

Goker-Alpan, O., Stubblefield, B.K., Giasson, B.I., and Sidransky, E. (2010). Glucocerebrosidase is present in alpha-synuclein inclusions in Lewy body disorders. Acta Neuropathol. *120*, 641–649.

Golic, K.G., and Lindquist, S. (1989). The FLP recombinase of yeast catalyzes site-specific recombination in the drosophila genome. Cell *59*, 499–509.

Gomez, A., and Ferrer, I. (2010). Involvement of the cerebral cortex in Parkinson disease linked with G2019S LRRK2 mutation without cognitive impairment. Acta Neuropathol. *120*, 155–167.

Gomez-Nicola, D., and Perry, V.H. (2014). Microglial Dynamics and Role in the Healthy and Diseased Brain. Neurosci. *21*, 169–184.

Gomperts, S.N., Rentz, D.M., Moran, E., Becker, J.A., Locascio, J.J., Klunk, W.E., Mathis, C.A., Elmaleh, D.R., Shoup, T., Fischman, A.J., et al. (2008). Imaging amyloid deposition in lewy body diseases. Neurology *71*, 903–910.

Gopalakrishnan, S., Hor, P., and Ichida, J.K. (2017). New approaches for direct conversion of patient fibroblasts into neural cells. Brain Res. *1656*, 2–13.

Gouider-Khouja, N., Larnaout, A., Amouri, R., Sfar, S., Belal, S., Ben Hamida, C., Ben Hamida, M., Hattori, N., Mizuno, Y., and Hentati, F. (2003). Autosomal recessive parkinsonism linked to parkin gene in a Tunisian family. Clinical, genetic and pathological study. Park. Relat. Disord. *9*, 247–251.

Greene, A.W., Grenier, K., Aguileta, M.A., Muise, S., Farazifard, R., Haque, M.E., McBride, H.M., Park, D.S., and Fon, E.A. (2012). Mitochondrial processing peptidase regulates PINK1 processing, import and Parkin recruitment. EMBO Rep. *13*, 378–385.

Grunewald, A., Arns, B., Meier, B., Brockmann, K., Tadic, V., and Klein, C. (2014). Does uncoupling protein 2 expression qualify as marker of disease status in LRRK2-associated Parkinson's disease? Antioxid. Redox Signal. *20*, 1955–1960.

Grünewald, A., Voges, L., Rakovic, A., Kasten, M., Vandebona, H., Hemmelmann, C., Lohmann, K., Orolicki, S., Ramirez, A., Schapira, A.H. V, et al. (2010). Mutant Parkin impairs mitochondrial function and morphology in human fibroblasts. PLoS One *5*, e12962.

Grünewald, a, Gegg, M.E., Taanman, J.-W., King, R.H., Kock, N., Klein, C., and Schapira, a H. V (2009). Differential effects of PINK1 nonsense and missense mutations on mitochondrial function and morphology. Exp. Neurol. *219*, 266–273.

Guerreiro, P.S., Huang, Y., Gysbers, A., Cheng, D., Gai, W.P., Outeiro, T.F., and Halliday, G.M. (2013). LRRK2 interactions with α-synuclein in Parkinson's disease brains and in cell models. J. Mol. Med. (Berl). *91*, 513–522.

Guhathakurta, S., Bok, E., Evangelista, B.A., and Kim, Y.S. (2017). Deregulation of α-synuclein in Parkinson's disease: Insight from epigenetic structure and transcriptional regulation of SNCA. Prog. Neurobiol. *154*, 21–36.

Guo, H., Ingolia, N.T., Weissman, J.S., and Bartel, D.P. (2010). Mammalian microRNAs predominantly act to decrease target mRNA levels. Nature *466*, 835–840.

Gupta, S., Schoer, R.A., Egan, J.E., Hannon, G.J., and Mittal, V. (2004). Inducible, reversible, and stable RNA interference in mammalian cells. Proc. Natl. Acad. Sci. U. S. A. *101*.

Gustot, A., Gallea, J.I., Sarroukh, R., Celej, M.S., Ruysschaert, J.-M., and Raussens, V. (2015). Amyloid fibrils are the molecular trigger of inflammation in Parkinson's disease. Biochem. J. *471*, 323 LP-333.

Haeussler, M., Schönig, K., Eckert, H., Eschstruth, A., Mianné, J., Renaud, J.-B., Schneider-Maunoury, S., Shkumatava, A., Teboul, L., Kent, J., et al. (2016). Evaluation of off-target and on-target scoring algorithms and integration into the guide RNA selection tool CRISPR. Genome Biol. *17*, 148.

Hayashi, S., Wakabayashi, K., Ishikawa, A., Nagai, H., Saito, M., Maruyama, M., Takahashi, T., Ozawa, T., Tsuji, S., and Takahashi, H. (2000). An autopsy case of autosomal-recessive juvenile parkinsonism with a homozygous exon 4 deletion in the parkin gene. Mov. Disord. *15*, 884–888.

Haylett, W., Swart, C., van der Westhuizen, F., van Dyk, H., van der Merwe, L., van der Merwe, C., Loos, B., Carr, J., Kinnear, C., and Bardien, S. (2016). Altered Mitochondrial Respiration and Other Features of Mitochondrial Function in *Parkin* -Mutant Fibroblasts from Parkinson's Disease Patients. Parkinsons. Dis. *2016*, 1–11.

Henson, J., Saffer, J., and Furneaux, H. (1992). The transcription factor Sp1 binds to the JC virus promoter and is selectively expressed in glial cells in human brain. Ann. Neurol. *32*, 72–77.

Hernán, M.A., Takkouche, B., Caamaño-Isorna, F., and Gestal-Otero, J.J. (2002). A meta-analysis of coffee drinking, cigarette smoking, and the risk of Parkinson's disease. Ann. Neurol. *52*, 276–284.

Herrero-Mendez, A., Almeida, A., Fernández, E., Maestre, C., Moncada, S., and Bolaños, J.P. (2009). The bioenergetic and antioxidant status of neurons is controlled by continuous degradation of a key glycolytic enzyme by APC/C-Cdh1. Nat. Cell Biol. *11*, 747–752.

Higashi, S., Biskup, S., West, A.B., Trinkaus, D., Dawson, V.L., Faull, R.L.M., Waldvogel, H.J., Arai, H., Dawson, T.M., Moore, D.J., et al. (2007). Localization of Parkinson's disease-associated LRRK2 in normal and pathological human brain. Brain Res. *1155*, 208–219.

Highley, J.R., Kirby, J., Jansweijer, J.A., Webb, P.S., Hewamadduma, C.A., Heath, P.R., Higginbottom, A., Raman, R., Ferraiuolo, L., Cooper-Knock, J., et al. (2014). Loss of nuclear TDP-43 in amyotrophic lateral sclerosis (ALS) causes altered expression of splicing machinery and widespread dysregulation of RNA splicing in motor neurones. Neuropathol. Appl. Neurobiol. *40*, 670–685.

Hilker, R., Pilatus, U., Eggers, C., Hagenah, J., Roggendorf, J., Baudrexel, S., Klein, J.C., Neumaier, B., Fink, G.R., Steinmetz, H., et al. (2012). The bioenergetic status relates to dopamine neuron loss in familial PD with PINK1 mutations. PLoS One *7*, e51308.

Hockey, L.N., Kilpatrick, B.S., Eden, E.R., Lin-Moshier, Y., Brailoiu, G.C., Brailoiu, E., Futter, C.E., Schapira, A.H., Marchant, J.S., and Patel, S. (2015). Dysregulation of lysosomal morphology by pathogenic LRRK2 is corrected by TPC2 inhibition. J. Cell Sci. *128*, 232–238.

Hoffman-Zacharska, D., Koziorowski, D., Ross, O.A., Milewski, M., Poznański, J., Jurek, M., Wszolek, Z.K., Soto-Ortolaza, A., Sławek, J., Janik, P., et al. (2013). Novel A18T and pA29S substitutions in α-synuclein may be associated with sporadic Parkinson's disease. Parkinsonism Relat. Disord. *19*, 1057–1060.

Hoshino, A., Matoba, S., Iwai-Kanai, E., Nakamura, H., Kimata, M., Nakaoka, M., Katamura, M., Okawa, Y., Ariyoshi, M., Mita, Y., et al. (2012). p53-TIGAR axis attenuates mitophagy to exacerbate cardiac damage after ischemia. J. Mol. Cell. Cardiol. *52*, 175–184.

Hoshino, A., Mita, Y., Okawa, Y., Ariyoshi, M., Iwai-Kanai, E., Ueyama, T., Ikeda, K., Ogata, T., and Matoba, S. (2013). Cytosolic p53 inhibits Parkin-mediated mitophagy and promotes mitochondrial dysfunction in the mouse heart. Nat. Commun. *4*, 2308.

Houtkooper, R.H. (2015). Tetracycline Antibiotics Impair Mitochondrial Function and Its Experimental Use Confounds. 1–5.

Hsieh, S.-L., Chen, C.-T., Wang, J.-J., Kuo, Y.-H., Li, C.-C., Hsieh, L.-C., and Wu, C.-C. (2015). Sedanolide induces autophagy through the PI3K, p53 and NF-κB signaling pathways in human liver cancer cells. Int. J. Oncol.

Hsu, C.Y.M., and Uludağ, H. (2012). A simple and rapid nonviral approach to efficiently transfect primary tissue-derived cells using polyethylenimine. Nat. Protoc. *7*, 935–945.

Hsu, L.J., Sagara, Y., Arroyo, A., Rockenstein, E., Sisk, A., Mallory, M., Wong, J., Takenouchi, T., Hashimoto, M., and Masliah, E. (2000). α-Synuclein Promotes Mitochondrial Deficit and Oxidative Stress. Am. J. Pathol. *157*, 401–410.

Huang, L., Shimoji, M., Wang, J., Shah, S., Kamila, S., Biehl, E.R., Lim, S., Chang, A., Maguire-Zeiss, K.A., Su, X., et al. (2013). Development of Inducible Leucine-rich Repeat Kinase 2 (LRRK2) Cell Lines for Therapeutics Development in Parkinson's Disease. Neurotherapeutics *10*, 840–851.

Huang, Y., Li, Y., Wang, Y.G., Gu, X., Wang, Y., and Shen, B.F. (2007). An efficient and targeted gene integration system for high-level antibody expression. J. Immunol. Methods *322*, 28–39.

Igarashi, S., Morita, H., Bennett, K.M., Tanaka, Y., Engelender, S., Peters, M.F., Cooper, J.K., Wood, J.D., Sawa, A., and Ross, C. a (2003). Inducible PC12 cell model of Huntington's disease shows toxicity and decreased histone acetylation. Neuroreport *14*, 565–568.

Imai, Y., Gehrke, S., Wang, H.-Q., Takahashi, R., Hasegawa, K., Oota, E., and Lu, B. (2008). Phosphorylation of 4E-BP by LRRK2 affects the maintenance of dopaminergic neurons in Drosophila. EMBO J. *27*, 2432–2443.

Ingelsson, M. (2016). Alpha-synuclein oligomers-neurotoxic molecules in Parkinson's disease and other lewy body disorders. Front. Neurosci. *10*, 1–10.

Irwin, I., and William Langston, J. (1985). II. Selective accumulation of MPP+ in the substantia nigra: A key to neurotoxicity? Life Sci. *36*, 207–212.

Irwin, D.J., Grossman, M., Weintraub, D., Hurtig, H.I., Duda, J.E., Xie, S.X., Lee, E.B., Van Deerlin, V.M., Lopez, O.L., Kofler, J.K., et al. (2017). Neuropathological and genetic correlates of survival and dementia onset in synucleinopathies: a retrospective analysis. Lancet Neurol. *16*, 55–65.

Ishizu, N., Yui, D., Hebisawa, A., Aizawa, H., Cui, W., Fujita, Y., Hashimoto, K., Ajioka, I., Mizusawa, H., Yokota, T., et al. (2016). Impaired striatal dopamine release in homozygous Vps35 D620N knock-in mice. Hum. Mol. Genet. ddw279.

Ito, S., Nakaso, K., Imamura, K., Takeshima, T., and Nakashima, K. (2010). Endogenous catecholamine enhances the dysfunction of unfolded protein response and α-synuclein oligomerization in PC12 cells overexpressing human α-synuclein. Neurosci. Res. *66*, 124–130.

Iwai, A., Masliah, E., Yoshimoto, M., Ge, N., Flanagan, L., Rohan de Silva, H.A., Kittel, A., and Saitoh, T. (1995). The precursor protein of non-Aβ component of Alzheimer's disease amyloid is a presynaptic protein of the central nervous system. Neuron *14*, 467–475.

IzuMi, M., Miyazawa, H., Kamakura, T., Yamaguchi, I., Endo, T., and Hanaoka, F. (1991). Blasticidin S-resistance gene (bsr): A novel selectable marker for mammalian cells. Exp. Cell Res. *197*, 229–233.

Jellinger, K.A. (2003). Neuropathological spectrum of synucleinopathies. Mov. Disord. *18 Suppl 6*, S2-12.

Jellinger, K.A., Seppi, K., Wenning, G.K., Hishikawa, N., Hashizume, Y., Yoshida, M., and Sobue, G. (2003). Clinical and neuropathological correlates of Lewy body disease (multiple letters). Acta Neuropathol. *106*, 341–350.

Jiang, H., Wu, Y.C., Nakamura, M., Liang, Y., Tanaka, Y., Holmes, S., Dawson, V.L., Dawson, T.M., Ross, C.A., and Smith, W.W. (2007). Parkinson's disease genetic mutations increase cell susceptibility to stress: Mutant ??-synuclein enhances H2O2- and Sin-1-induced cell death. Neurobiol. Aging *28*, 1709–1717.

Jin, S.M., Lazarou, M., Wang, C., Kane, L.A., Narendra, D.P., and Youle, R.J. (2010). Mitochondrial membrane potential regulates PINK1 import and proteolytic destabilization by PARL. J. Cell Biol. *191*, 933–942.

Jinek, M., Chylinski, K., Fonfara, I., Hauer, M., Doudna, J.A., and Charpentier, E. (2012). A programmable dual-RNA-guided DNA endonuclease in adaptive bacterial immunity. Science *337*, 816–821.

John, S., Weiss, J.N., and Ribalet, B. (2011). Subcellular localization of hexokinases I and II directs the metabolic fate of glucose. PLoS One *6*.

Kaestner, L., Scholz, A., and Lipp, P. (2015). Conceptual and technical aspects of transfection and gene delivery. Bioorganic Med. Chem. Lett. *25*, 1171–1176.

Kageyama, Y., Hoshijima, M., Seo, K., Bedja, D., Sysa-Shah, P., Andrabi, S.A., Chen, W., Höke, A., Dawson, V.L., Dawson, T.M., et al. (2014). Parkin-independent mitophagy requires Drp1 and maintains the integrity of mammalian heart and brain. EMBO J. *33*, 2798 LP-2813.

Kalia, L. V, Lang, A.E., Hazrati, L.-N., Fujioka, S., Wszolek, Z.K., Dickson, D.W., Ross, O.A., Van Deerlin, V.M., Trojanowski, J.Q., Hurtig, H.I., et al. (2015). Clinical correlations with Lewy body pathology in LRRK2-related Parkinson disease. JAMA Neurol. *72*, 100–105.

Kamp, F., Exner, N., Lutz, A.K., Wender, N., Hegermann, J., Brunner, B., Nuscher, B., Bartels, T., Giese, A., Beyer, K., et al. (2010). Inhibition of mitochondrial fusion by α-synuclein is rescued by PINK1, Parkin and DJ-1. EMBO J. *29*, 3571 LP-3589.
Kampmann, M. (2017). A CRISPR Approach to Neurodegenerative Diseases. Trends Mol. Med. *23*, 483–485.

Kappel, S., Matthess, Y., Kaufmann, M., and Strebhardt, K. (2007). Silencing of mammalian genes by tetracycline-inducible shRNA expression. Nat. Protoc. *2*, 3257–3269.

Katsel, P., Tan, W., Fam, P., Purohit, D.P., and Haroutunian, V. (2013). Cycle checkpoint abnormalities during dementia: a plausible association with the loss of protection against oxidative stress in Alzheimer's disease. PLoS One *8*, e68361.

Kawano, T., Ahmad, R., Nogi, H., Agata, N., Anderson, K., and Kufe, D. (2008). MUC1 oncoprotein promotes growth and survival of human multiple myeloma cells. Int J Oncol *33*, 153–159.

Kennedy, E.M., and Cullen, B.R. (2015). Bacterial CRISPR/Cas DNA endonucleases: A revolutionary technology that could dramatically impact viral research and treatment. Virology *479–480*, 213–220.

Khan, N.L., Jain, S., Lynch, J.M., Pavese, N., Abou-Sleiman, P., Holton, J.L., Healy, D.G., Gilks, W.P., Sweeney, M.G., Ganguly, M., et al. (2005). Mutations in the gene LRRK2 encoding dardarin (PARK8) cause familial Parkinson's disease: clinical, pathological, olfactory and functional imaging and genetic data. Brain *128*, 2786–2796.

Khlistunova, I., Biernat, J., Wang, Y., Pickhardt, M., Bergen, M. Von, Gazova, Z., Mandelkow, E., and Mandelkow, E. (2006). Inducible Expression of Tau Repeat Domain in Cell Models of Tauopathy. J. Biol. Chem. *281*, 1205–1214.

Kim, H.J., Gatz, C., Hillen, W., and Jones, T.R. (1995). Tetracycline repressor-regulated gene repression in recombinant human cytomegalovirus. J. Virol. *69*, 2565–2573.

Kimata, M., Matoba, S., Iwai-Kanai, E., Nakamura, H., Hoshino, A., Nakaoka, M., Katamura, M., Okawa, Y., Mita, Y., Okigaki, M., et al. (2010). p53 and TIGAR regulate cardiac myocyte energy homeostasis under hypoxic stress. Am. J. Physiol. Heart Circ. Physiol. *299*, H1908-16.

Kitada, T., Asakawa, S., Hattori, N., Matsumine, H., Yamamura, Y., Minoshima, S., Yokochi, M., Mizuno, Y., and Shimizu, N. (1998). Mutations in the parkin gene cause autosomal recessive juvenile parkinsonism. Nature *392*, 605–608.

Klinkenberg, M., Thurow, N., Gispert, S., Ricciardi, F., Eich, F., Prehn, J.H.M., Auburger, G., and Kögel, D. (2010). Enhanced vulnerability of PARK6 patient skin fibroblasts to apoptosis induced by proteasomal stress. Neuroscience *166*, 422–434.

Klos, K.J., Ahlskog, J.E., Josephs, K.A., Apaydin, H., Parisi, J.E., Boeve, B.F., DeLucia, M.W., and Dickson, D.W. (2006). -Synuclein pathology in the spinal cords of neurologically asymptomatic aged individuals. Neurology *66*, 1100–1102.

Kobayashi, K., Yasuhara, T., Agari, T., Muraoka, K., Kameda, M., Ji Yuan, wen, Hayase, H., Matsui, T., Miyoshi, Y., Shingo, T., et al. (2006). Control of dopamine-secretion by Tet-Off system in an in vivo model of parkinsonian rat. Brain Res. *1102*, 1–11.

Koga, S., Parks, A., Uitti, R.J., and Gerpen, J.A. Van (2016). Profile of Cognitive Impairment and Underlying Pathology in Multiple System Atrophy. *0*, 1–9.

Konno, T., Ross, O.A., Puschmann, A., Dickson, D.W., and Wszolek, Z.K. (2016). Autosomal dominant Parkinson's disease caused by SNCA duplications. Park. Relat. Disord. *22*, S1–S6.

Krige, D., Carroll, M.T., Cooper, J.M., Marsden, C.D., and Schapira, A.H. V (1992). Platelet Mitochondrial-Function in Parkinsons-Disease. Ann. Neurol. *32*, 782–788.

Kumar, A., Greggio, E., Beilina, A., Kaganovich, A., Chan, D., Taymans, J.M., Wolozin, B., and Cookson, M.R. (2010). The Parkinson's disease associated LRRK2 exhibits weaker in vitro phosphorylation of 4E-BP compared to autophosphorylation. PLoS One *5*.

Kumar, B., Iqbal, M.A., Singh, R.K., and Bamezai, R.N.K. (2015). Resveratrol inhibits TIGAR to promote ROS induced apoptosis and autophagy. Biochimie *118*, 26–35.

Kwakye, F.G., Paoliello, M.M., Mukhopadhyay, S., Bowman, B.A., and Aschner, M. (2015). Manganese-Induced Parkinsonism and Parkinson's Disease: Shared and Distinguishable Features. Int. J. Environ. Res. Public Heal. *12*.

de la Monte, S.M., Sohn, Y.K., and Wands, J.R. (1997). Correlates of p53- and Fas (CD95)-mediated apoptosis in Alzheimer's disease. J. Neurol. Sci. *152*, 73–83.

Langston, J.W., Ballard, P., Tetrud, J.W., and Irwin, I. (1983). Chronic Parkinsonism in humans due to a product of meperidine-analog synthesis. Science *219*, 979–980.

Langston, J.W., Forno, L.S., Rebert, C.S., and Irwin, I.A.N. (1984). Selective nigral toxicity after systemic administration of 1-methyl-4-phenyl-1 , 2 , 5 , 6- tetrahydropyrine (MPTP) in the squirrel monkey. *292*, 390–394.

Lautenschläger, J., Kaminski, C.F., and Kaminski Schierle, G.S. (2017). α-Synuclein – Regulator of Exocytosis, Endocytosis, or Both? Trends Cell Biol. *27*, 468–479.

Lazarou, M., Sliter, D.A., Kane, L.A., Sarraf, S.A., Wang, C., Burman, J.L., Sideris, D.P., Fogel, A.I., and Youle, R.J. (2015). The ubiquitin kinase PINK1 recruits autophagy receptors to induce mitophagy. Nature *524*, 309–314.

Lee, J.M., Derkinderen, P., Kordower, J.H., Freeman, R., Munoz, D.G., Kremer, T., Zago, W., Hutten, S.J., Adler, C.H., Serrano, G.E., et al. (2017). The search for a peripheral biopsy indicator of a-synuclein pathology for Parkinson disease. J. Neuropathol. Exp. Neurol. *76*, 2–15.

Lee, P., Vousden, K.H., and Cheung, E.C. (2014a). TIGAR, TIGAR, burning bright. Cancer Metab. *2*, 1.

Lee, P., Hock, a K., Vousden, K.H., and Cheung, E.C. (2015). p53- and p73-independent activation of TIGAR expression in vivo. Cell Death Dis. *6*, e1842.

Lee, S., Zhang, C., and Liu, X. (2014b). Role of Glucose Metabolism and ATP in Maintaining PINK1 Levels During Parkin-mediated Mitochondrial Damage Responses. J. Biol. Chem. *290*, 904–917.

Lee, Y., Ahn, C., Han, J., Choi, H., Kim, J., Yim, J., Lee, J., Provost, P., Rådmark, O., Kim, S., et al. (2003). The nuclear RNase III Drosha initiates microRNA processing. Nature *425*, 415–419.

Lesage, S., Anheim, M., Condroyer, C., Pollak, P., Durif, F., Dupuits, C., Viallet, F., Lohmann, E., Corvol, J.-C., Honoré, A., et al. (2011). Large-scale screening of the Gaucher's disease-related glucocerebrosidase gene in Europeans with Parkinson's disease. Hum. Mol. Genet. *20*, 202–210.

Leverenz, J.B., Umar, I., Wang, Q., Montine, T.J., McMillan, P.J., Tsuang, D.W., Jin, J., Pan, C., Shin, J., Zhu, D., et al. (2007). Proteomic identification of novel proteins in cortical Lewy bodies. Brain Pathol. *17*, 139–145.

Li, H., and Jogl, G. (2009). Structural and biochemical studies of TIGAR (TP53-induced glycolysis and apoptosis regulator). J. Biol. Chem. *284*, 1748–1754.

Li, M., Sun, M., Cao, L., Gu, J. -h., Ge, J., Chen, J., Han, R., Qin, Y.-Y., Zhou, Z.-P., Ding, Y., et al. (2014). A TIGAR-Regulated Metabolic Pathway Is Critical for Protection of Brain Ischemia. J. Neurosci. *34*, 7458–7471.

Li, Y., Sekine, T., Funayama, M., Li, L., Yoshino, H., Nishioka, K., Tomiyama, H., and Hattori, N. (2013). Clinicogenetic study of GBA mutations in patients with familial Parkinson's disease. Neurobiol. Aging 1–6.

Liu, W., Xiong, Y., and Gossen, M. (2006). Stability and homogeneity of transgene expression in isogenic cells. J. Mol. Med. *84*, 57–64.

Liu, Y., Guardia-Laguarta, C., Yin, J., Erdjument-Bromage, H., Martin, B., James, M., Jiang, X., and Przedborski, S. (2017). The Ubiquitination of PINK1 Is Restricted to Its Mature 52-kDa Form. Cell Rep. *20*, 30–39.

Lobasso, S., Tanzarella, P., Vergara, D., Maffia, M., Cocco, T., and Corcelli, A. (2017). Lipid profiling of parkin -mutant human skin fibroblasts. J. Cell. Physiol.

Lohmann, K., and Klein, C. (2008). Genetics of Parkinson disease. Contin. Lifelong Learn. Neurol. *14*, 90–113.

Lohmann, E., Periquet, M., Bonifati, V., Wood, N.W., De Michele, G., Bonnet, A.M., Fraix, V., Broussolle, E., Horstink, M.W.I.M., Vidailhet, M., et al. (2003). How much phenotypic variation can be attributed to parkin genotype? Ann. Neurol. *54*, 176–185.

Lonskaya, I., Desforges, N.M., Hebron, M.L., and Moussa, C.E.-H. (2013a). Ubiquitination Increases Parkin Activity to Promote Autophagic α-Synuclein Clearance. PLoS One *8*, e83914.

Lonskaya, I., Hebron, M.L., Algarzae, N.K., Desforges, N., and Moussa, C.E.-H. (2013b). Decreased parkin solubility is associated with impairment of autophagy in the nigrostriatum of sporadic Parkinson's disease. Neuroscience *232*, 90–105.

Lopez-Fabuel, I., Martin-Martin, L., Resch-Beusher, M., Azkona, G., Sanchez-Pernaute, R., and Bola, J.P. (2017). Mitochondrial respiratory chain disorganization in Parkinson's disease-relevant PINK1 and DJ1 mutants.

López-Guerra, M., Trigueros-Motos, L., Molina-Arcas, M., Villamor, N., Casado, F.J., Montserrat, E., Campo, E., Colomer, D., and Pastor-Anglada, M. (2008). Identification of TIGAR in the equilibrative nucleoside transporter 2-mediated response to

fludarabine in chronic lymphocytic leukemia cells. Haematologica *93*, 1843–1851.

Loureiro, C., and Silva, R.H. (2017). Genetic Variants in SNCA and the Risk of Sporadic Parkinson ' s Disease and Clinical Outcomes : A Review. *2017*.

Lücking, C.B., Dürr, A., Bonifati, V., Vaughan, J., De Michele, G., Gasser, T., Harhangi, B.S., Meco, G., Denèfle, P., Wood, N.W., et al. (2000). Association between early-onset Parkinson's disease and mutations in the parkin gene. N. Engl. J. Med. *342*, 1560–1567.

Lui, V.W.Y., Lau, C.P.Y., Cheung, C.S.F., Ho, K., Ng, M.H.L., Cheng, S.H., Hong, B., Tsao, S.-W., Tsang, C.M., Lei, K.I.K., et al. (2010). An RNA-directed nucleoside anti-metabolite, 1-(3-C-ethynyl-beta-d-ribo-pentofuranosyl)cytosine (ECyd), elicits antitumor effect via TP53-induced Glycolysis and Apoptosis Regulator (TIGAR) downregulation. Biochem. Pharmacol. *79*, 1772–1780.

Lui, V.W.Y., Wong, E.Y.L., Ho, K., Ng, P.K.S., Lau, C.P.Y., Tsui, S.K.W., Tsang, C.-M., Tsao, S.-W., Cheng, S.H., Ng, M.H.L., et al. (2011). Inhibition of c-Met downregulates TIGAR expression and reduces NADPH production leading to cell death. Oncogene *30*, 1127–1134.

Luk, K.C., and Lee, V.M.-Y. (2014). Modeling Lewy pathology propagation in Parkinson's disease. Parkinsonism Relat. Disord. *20 Suppl 1*, S85-7.

Luth, E.S., Stavrovskaya, I.G., Bartels, T., Kristal, B.S., and Selkoe, D.J. (2014). Soluble, prefibrillar α-synuclein oligomers promote complex I-dependent, Ca2+-induced mitochondrial dysfunction. J. Biol. Chem. *289*, 21490–21507.

Lutz, a K., Exner, N., Fett, M.E., Schlehe, J.S., Kloos, K., Lämmermann, K., Brunner, B., Kurz-Drexler, A., Vogel, F., Reichert, A.S., et al. (2009). Loss of parkin or PINK1 function increases Drp1-dependent mitochondrial fragmentation. J. Biol. Chem. *284*, 22938–22951.

Ma, L., Tao, Y., Duran, A., Llado, V., Galvez, A., Barger, J.F., Castilla, E. a, Chen, J., Yajima, T., Porollo, A., et al. (2013). Control of Nutrient Stress-Induced Metabolic Reprogramming by PKCζ in Tumorigenesis. Cell *152*, 599–611.

Ma, T., Zhang, Y., Zhang, C., Luo, J.-G., and Kong, L.-Y. (2017). Downregulation of TIGAR sensitizes the antitumor effect of physapubenolide through increasing intracellular ROS levels to trigger apoptosis and autophagosome formation in human breast carcinoma cells. Biochem. Pharmacol.

Madan, E., Gogna, R., Kuppusamy, P., Bhatt, M., Pati, U., and Mahdi, a a (2012). TIGAR induces p53-mediated cell-cycle arrest by regulation of RB-E2F1 complex. Br. J. Cancer *107*, 516–526.

Maddocks, O.D.K., and Vousden, K.H. (2011). Metabolic regulation by p53. J. Mol. Med. (Berl). *89*, 237–245.

Magrì, A., Belfiore, R., Reina, S., Tomasello, M.F., Di Rosa, M.C., Guarino, F., Leggio, L., De Pinto, V., and Messina, A. (2016). Hexokinase I N-terminal based peptide prevents the VDAC1-SOD1 G93A interaction and re-establishes ALS cell viability. Sci. Rep. *6*, 34802.

Mäkinen, P.I., Koponen, J.K., Kärkkäinen, A.-M., Malm, T.M., Pulkkinen, K.H., Koistinaho, J., Turunen, M.P., and Ylä-Herttuala, S. (2006). Stable RNA interference: comparison of U6 and H1 promoters in endothelial cells and in mouse brain. J. Gene Med. *8*, 433–441.

Mamais, A., Raja, M., Manzoni, C., Dihanich, S., Lees, A., Moore, D., Lewis, P.A., and Bandopadhyay, R. (2013). Divergent α-synuclein solubility and aggregation properties in G2019S LRRK2 Parkinson's disease brains with Lewy Body pathology compared to idiopathic cases. Neurobiol. Dis. *58*, 183–190.

Mamais, A., Chia, R., Beilina, A., Hauser, D.N., Hall, C., Lewis, P. a, Cookson, M.R., and Bandopadhyay, R. (2014). Arsenite stress down-regulates phosphorylation and 14-3-3 binding of leucine-rich repeat kinase 2 (LRRK2), promoting self-association and cellular redistribution. J. Biol. Chem. *289*, 21386–21400.

Manikoth Ayyathan, D., Ilić, N., Gil-Henn, H., and Blank, M. (2017). Generation of SMURF2 knockout human cells using the CRISPR/Cas9 system. Anal. Biochem. *531*, 56–59.

Mann, V.M., Cooper, J.M., Krige, D., Daniel, S.E., Schapira, A.H. V, and Marsden, C.D. (1992). Brain, skeletal muscle and platelet homogenate mitochondrial function in parkinson's disease. Brain *115*, 333–342.

Manzoni, C., Mamais, A., Dihanich, S., McGoldrick, P., Devine, M.J., Zerle, J., Kara, E., Taanman, J.-W., Healy, D.G., Marti-Masso, J.-F., et al. (2013a). Pathogenic Parkinson's disease mutations across the functional domains of LRRK2 alter the autophagic/lysosomal response to starvation. Biochem. Biophys. Res. Commun. *441*, 862–866.

Manzoni, C., Mamais, A., Dihanich, S., McGoldrick, P., Devine, M.J., Zerle, J., Kara, E., Taanman, J.-W., Healy, D.G., Marti-Masso, J.-F., et al. (2013b). Pathogenic Parkinson's disease mutations across the functional domains of LRRK2 alter the autophagic/lysosomal response to starvation. Biochem. Biophys. Res. Commun. *441*, 862–866.

Markopoulou, K., Dickson, D.W., McComb, R.D., Wszolek, Z.K., Katechalidou, L., Avery, L., Stansbury, M.S., and Chase, B.A. (2008). Clinical, neuropathological and genotypic variability in SNCA A53T familial Parkinson's disease. Acta Neuropathol. *116*, 25–35.

Marti-Masso, J.-F., Ruiz-Martinez, J., Bolano, M.J., Ruiz, I., Gorostidi, A., Moreno, F., Ferrer, I., and Lopez de Munain, A. (2009). Neuropathology of Parkinson's disease with the R1441G mutation in LRRK2. Mov. Disord. *24*, 1998–2001.

Martinez-Outschoorn, U.E., Goldberg, A., Lin, Z., Ko, Y., Flomenberg, N., Wang, C., Pavlides, S., Pestell, R.G., Howell, A., Sotgia, F., et al. (2010). Anti-estrogen resistance in breast cancer is induced by the tumor microenvironment and can be overcome by inhibiting mitochondrial function in epithelial cancer cells. Cancer Biol. Ther. *9*, 924–938.

Matsui, H. (2017). The use of fish models to study human neurological disorders. Neurosci. Res.

Mazzulli, J.R., Zunke, F., Isacson, O., Studer, L., and Krainc, D. (2016). α-Synuclein–induced lysosomal dysfunction occurs through disruptions in protein trafficking in human midbrain synucleinopathy models. Proc. Natl. Acad. Sci. *113*, 1931–1936.

McCann, H., Stevens, C.H., Cartwright, H., and Halliday, G.M. (2014). α-Synucleinopathy phenotypes. Park. Relat. Disord. *20*,

S62–S67.

van der Merwe, C., Loos, B., Swart, C., Kinnear, C., Henning, F., van der Merwe, L., Pillay, K., Muller, N., Zaharie, D., Engelbrecht, L., et al. (2014). Mitochondrial impairment observed in fibroblasts from South African Parkinson's disease patients with parkin mutations. Biochem. Biophys. Res. Commun. *447*, 334–340.

Miklossy, J., Arai, T., Guo, J.P., Klegeris, a, Yu, S., McGeer, E.G., and McGeer, P.L. (2006). LRRK2 expression in normal and pathologic human brain and in human cell lines. J. Neuropathol. Exp. Neurol. *65*, 953–963.

Miraglia, F., Betti, L., Palego, L., and Giannaccini, G. (2015). Parkinson ' s Disease and Alpha-Synucleinopathies : from Arising Pathways to Therapeutic Challenge. 109–116.

Mitsui, J., Matsukawa, T., Sasaki, H., Yabe, I., Matsushima, M., Dürr, A., Brice, A., Takashima, H., Kikuchi, A., Aoki, M., et al. (2015). Variants associated with Gaucher disease in multiple system atrophy. Ann. Clin. Transl. Neurol. *2*, 417–426.

Mizuno, Y., Ohta, S., Tanaka, M., Takamiya, S., Suzuki, K., Sato, T., Oya, H., Ozawa, T., and Kagawa, Y. (1989). Deficiencies in Complex I subunits of the respiratory chain in Parkinson's disease. Biochem. Biophys. Res. Commun. *163*, 1450–1455.

Mohr, S.E., Smith, J. a, Shamu, C.E., and Neumüller, R. a (2014). RNAi screening comes of age : improved techniques and complementary approaches. Nat. Publ. Gr. *15*, 591–600.

Møller, T.S.B., Overgaard, M., Nielsen, S.S., Bortolaia, V., Sommer, M.O.A., Guardabassi, L., and Olsen, J.E. (2016). Relation between tetR and tetA expression in tetracycline resistant Escherichia coli. BMC Microbiol. *16*, 39.

Momcilovic, O., Sivapatham, R., Oron, T.R., Meyer, M., Mooney, S., Rao, M.S., and Zeng, X. (2016). Derivation, characterization, and neural differentiation of integration-free induced pluripotent stem cell lines from Parkinson's disease patients carrying SNCA, LRRK2, PARK2, and GBA mutations. PLoS One *11*.

Morais, V.A., Haddad, D., Craessaerts, K., De Bock, P.-J., Swerts, J., Vilain, S., Aerts, L., Overbergh, L., Grünewald, A., Seibler, P., et al. (2014). PINK1 Loss-of-Function Mutations Affect Mitochondrial Complex I Activity via NdufA10 Ubiquinone Uncoupling. Science (80-.). *344*, 203 LP-207.

Morales, B., Martinez, A., Gonzalo, I., Vidal, L., Ros, R., Gomez-Tortosa, E., Rabano, A., Ampuero, I., Sanchez, M., Hoenicka, J., et al. (2002). Steele-Richardson-Olszewski syndrome in a patient with a single C212Y mutation in the parkin protein. Mov. Disord. *17*, 1374–1380.

Mori, H., Hattori, N., and Mizuno, Y. (2003). Genotype-phenotype correlation: Familial Parkinson disease. Neuropathology *23*, 90–94.

Mortiboys, H., Thomas, K.J., Koopman, W.J.H., Klaffke, S., Abou-Sleiman, P., Olpin, S., Wood, N.W., Willems, P.H.G.M., Smeitink, J. a M., Cookson, M.R., et al. (2008). Mitochondrial function and morphology are impaired in parkin-mutant fibroblasts. Ann. Neurol. *64*, 555–565.

Mortiboys, H., Johansen, K.K., Aasly, J.O., and Bandmann, O. (2010a). Mitochondrial impairment in patients with Parkinson disease with the G2019S mutation in LRRK2. Neurology *75*, 2017–2020.

Mortiboys, H., Aasly, J., and Bandmann, O. (2013). Ursocholanic acid rescues mitochondrial function in common forms of familial Parkinson's disease. Brain *136*, 3038–3050.

Mortiboys, H., Furmston, R., Bronstad, G., Aasly, J., Elliott, C., and Bandmann, O. (2015). UDCA exerts beneficial effect on mitochondrial dysfunction in LRRK2 G2019S carriers and in vivo. Neurology *85*, 846–852.

Müftüoglu, M., Elibol, B., Dalmizrak, Ö., Ercan, A., Kulaksiz, G., Ögüs, H., Dalkara, T., and Özer, N. (2004). Mitochondrial complex I and IV activities in leukocytes from patients with parkin mutations. Mov. Disord. *19*, 544–548.

Murakami, T., Moriwaki, Y., Kawarabayashi, T., Nagai, M., Ohta, Y., Deguchi, K., Kurata, T., Morimoto, N., Takehisa, Y., Matsubara, E., et al. (2007). PINK1, a gene product of PARK6, accumulates in -synucleinopathy brains. J. Neurol. Neurosurg. Psychiatry *78*, 653–654.

Murakawa, T., Yamaguchi, O., Hashimoto, A., Hikoso, S., Takeda, T., Oka, T., Yasui, H., Ueda, H., Akazawa, Y., Nakayama, H., et al. (2015). Bcl-2-like protein 13 is a mammalian Atg32 homologue that mediates mitophagy and mitochondrial fragmentation. Nat. Commun. *6*, 7527.

Murlidharan, G., Sakamoto, K., Rao, L., Corriher, T., Wang, D., Gao, G., Sullivan, P., and Asokan, A. (2016). CNS-restricted Transduction and CRISPR/Cas9-mediated Gene Deletion with an Engineered AAV Vector. Mol. Ther. - Nucleic Acids *5*, e338.

Murphy, D.D., Rueter, S.M., Trojanowski, J.Q., and Lee, V.M. (2000). Synucleins are developmentally expressed, and alpha-synuclein regulates the size of the presynaptic vesicular pool in primary hippocampal neurons. J. Neurosci. *20*, 3214–3220.

Nakaso, K., Tajima, N., Ito, S., Teraoka, M., Yamashita, A., Horikoshi, Y., Kikuchi, D., Mochida, S., Nakashima, K., and Matsura, T. (2013). Dopamine-Mediated Oxidation of Methionine 127 in ??-Synuclein Causes Cytotoxicity and Oligomerization of ??-Synuclein. PLoS One *8*.

Nakata, Y., Yasuda, T., Fukaya, M., Yamamori, S., Itakura, M., Nihira, T., Hayakawa, H., Kawanami, A., Kataoka, M., Nagai, M., et al. (2012). Accumulation of α-synuclein triggered by presynaptic dysfunction. J. Neurosci. *32*, 17186–17196.

Nalls, M.A. (2014). Large-scale meta-analysis of genome-wide association data identifies six new risk loci for Parkinson's disease. Nat. Genet. *46*, 989–993.

Navarro, A., Boveris, A., Bández, M.J., Sánchez-Pino, M.J., Gómez, C., Muntané, G., and Ferrer, I. (2009). Human brain cortex: mitochondrial oxidative damage and adaptive response in Parkinson disease and in dementia with Lewy bodies. Free Radic. Biol. Med. *46*, 1574–1580.

Neumann, J., Bras, J., Deas, E., O'Sullivan, S.S., Parkkinen, L., Lachmann, R.H., Li, A., Holton, J., Guerreiro, R., Paudel, R., et al. (2009). Glucocerebrosidase mutations in clinical and pathologically proven Parkinson's disease. Brain *132*, 1783–1794.
Niv, Y. (2008). MUC1 and colorectal cancer pathophysiology considerations. World J. Gastroenterol. *14*, 2139–2141.

Ohmori, T., Nagao, Y., Mizukami, H., Sakata, A., Muramatsu, S., Ozawa, K., Tominaga, S., Hanazono, Y., Nishimura, S.,

Nureki, O., et al. (2017). CRISPR/Cas9-mediated genome editing via postnatal administration of AAV vector cures haemophilia B mice. Sci. Rep. *7*, 4159.

Orth, M., and Schapira, a H. (2001). Mitochondria and degenerative disorders. Am. J. Med. Genet. *106*, 27–36.

Ozgul, S., Kasap, M., Akpinar, G., Kanli, A., Güzel, N., Karaosmanoglu, K., Baykal, A.T., and Iseri, P. (2014). Linking a compound-heterozygous Parkin mutant (Q311R and A371T) to Parkinson's disease by using proteomic and molecular approaches. Neurochem. Int. *85–86*, 1–13.

Pacelli, C., De Rasmo, D., Signorile, A., Grattagliano, I., di Tullio, G., D'Orazio, A., Nico, B., Comi, G. Pietro, Ronchi, D., Ferranini, E., et al. (2011). Mitochondrial defect and PGC-1α dysfunction in parkin-associated familial Parkinson's disease. Biochim. Biophys. Acta *1812*, 1041–1053.

Paisán-Ruíz, C., Jain, S., Evans, E.W., Gilks, W.P., Simón, J., van der Brug, M., López de Munain, A., Aparicio, S., Gil, A.M., Khan, N., et al. (2004). Cloning of the gene containing mutations that cause PARK8-linked Parkinson's disease. Neuron *44*, 595–600.

Palacino, J.J., Sagi, D., Goldberg, M.S., Krauss, S., Motz, C., Wacker, M., Klose, J., and Shen, J. (2004). Mitochondrial Dysfunction and Oxidative Damage in parkin-deficient Mice. J. Biol. Chem. *279*, 18614–18622.

Palma, J.-A., and Kaufmann, H. (2014). Autonomic disorders predicting Parkinson's disease. Parkinsonism Relat. Disord. *20 Suppl 1*, S94-8.

Pan, P.-Y., and Yue, Z. (2014). Genetic causes of Parkinson's disease and their links to autophagy regulation. Parkinsonism Relat. Disord. *20 Suppl 1*, S154-7.

Panicker, N., Dawson, V.L., and Dawson, T.M. (2017). Activation mechanisms of the E3 ubiquitin ligase parkin. Biochem. J. *474*, 3075 LP-3086.

Papkovskaia, T.D., Chau, K.-Y., Inesta-Vaquera, F., Papkovsky, D.B., Healy, D.G., Nishio, K., Staddon, J., Duchen, M.R., Hardy, J., Schapira, A.H. V, et al. (2012). G2019S leucine-rich repeat kinase 2 causes uncoupling protein-mediated mitochondrial depolarization. Hum. Mol. Genet. *21*, 4201–4213.

Park, J., Lee, S.B., Lee, S., Kim, Y., Song, S., Kim, S., Bae, E., Kim, J., Shong, M., Kim, J.-M., et al. (2006). Mitochondrial dysfunction in Drosophila PINK1 mutants is complemented by parkin. Nature *441*, 1157–1161.

Parker, W.D., Boyson, S.J., and Parks, J.K. (1989). Abnormalities of the electron transport chain in idiopathic Parkinson's disease. Ann. Neurol. *26*, 719–723.

Parker, W.D., Parks, J.K., and Swerdlow, R.H. (2008). Complex I deficiency in Parkinson's disease frontal cortex. Brain Res. *1189*, 215–218.

Pascale, E., Di Battista, M.E., Rubino, A., Purcaro, C., Valente, M., Fattapposta, F., Ferraguti, G., and Meco, G. (2016). Genetic Architecture of MAPT Gene Region in Parkinson Disease Subtypes. Front. Cell. Neurosci. *10*, 96.

Peerally, T., and Tan, E.K. (2012). Genetic variants in sporadic Parkinson's disease: East vs West. Parkinsonism Relat. Disord. *18 Suppl 1*, S63-5.

Pelkonen, A., Kallunki, P., and Yavich, L. (2013). Effects of exogenous alpha-synuclein on stimulated dopamine overflow in dorsal striatum. Neurosci. Lett. *554*, 141–145.

Peña-Rico, M. a, Calvo-Vidal, M.N., Villalonga-Planells, R., Martínez-Soler, F., Giménez-Bonafé, P., Navarro-Sabaté, À., Tortosa, A., Bartrons, R., and Manzano, A. (2011). TP53 induced glycolysis and apoptosis regulator (TIGAR) knockdown results in radiosensitization of glioma cells. Radiother. Oncol. *101*, 132–139.

Perry, T.L., Godin, D. V., and Hansen, S. (1982). Parkinson's disease: A disorder due to nigral glutathione deficiency? Neurosci. Lett. *33*, 305–310.

Pickrell, A.M., and Youle, R.J. (2017). The Roles of PINK1, Parkin, and Mitochondrial Fidelity in Parkinson’s Disease. Neuron *85*, 257–273.

Playne, R., and Connor, B. (2017). Understanding Parkinsons Disease through the Use of Cell Reprogramming. Stem Cell Rev. Reports *13*, 151–169.

Poewe, W., and Wenning, G. (2002). The differential diagnosis of Parkinson's disease. Eur. J. Neurol. *9*, 23–30.

Polymeropoulos, M.H. (1997). Mutation in the -Synuclein Gene Identified in Families with Parkinson's Disease. Science (80-.). *276*, 2045–2047.

Polymeropoulos, M.H., Higgins, J.J., Golbe, L.I., Johnson, W.G., Ide, S.E., Di Iorio, G., Sanges, G., Stenroos, E.S., Pho, L.T., Schaffer, A.A., et al. (1996). Mapping of a gene for Parkinson's disease to chromosome 4q21-q23. Science *274*, 1197–1199.

Pramstaller, P.P., Schlossmacher, M.G., Jacques, T.S., Scaravilli, F., Eskelson, C., Pepivani, I., Hedrich, K., Adel, S., Gonzales-McNeal, M., Hilker, R., et al. (2005). Lewy body Parkinson's disease in a large pedigree with 77 Parkin mutation carriers. Ann. Neurol. *58*, 411–422.

Priyadarshini, M., Tuimala, J., Chen, Y.C., and Panula, P. (2013). A zebrafish model of PINK1 deficiency reveals key pathway dysfunction including HIF signaling. Neurobiol. Dis. *54*, 127–138.

Puschmann, A., Englund, E., Ross, O.A., Vilarino-Guell, C., Lincoln, S.J., Kachergus, J.M., Cobb, S.A., Tornqvist, A.-L., Rehncrona, S., Widner, H., et al. (2012). First neuropathological description of a patient with Parkinson's disease and LRRK2 p.N1437H mutation. Parkinsonism Relat. Disord. *18*, 332–338.

Puschmann, A., Fiesel, F.C., Caulfield, T.R., Hudec, R., Ando, M., Truban, D., Hou, X., Ogaki, K., Heckman, M.G., James, E.D., et al. (2016). Heterozygous PINK1 p.G411S increases risk of Parkinson's disease via a dominant-negative mechanism. Brain 1–20.

Qing, H., Zhang, Y., Deng, Y., McGeer, E.G., and McGeer, P.L. (2009). Lrrk2 interaction with ??-synuclein in diffuse Lewy body disease. Biochem. Biophys. Res. Commun. *390*, 1229–1234.

Qiu, Z., Norflus, F., Singh, B., Swindell, M.K., Buzescu, R., Bejarano, M., Chopra, R., Zucker, B., Benn, C.L., DiRocco, D.P., et al. (2006). Sp1 is up-regulated in cellular and transgenic models of huntington disease, and its reduction is neuroprotective. J. Biol. Chem. *281*, 16672–16680.

Qureshi, H.Y., and Paudel, H.K. (2011). Parkinsonian neurotoxin 1-methyl-4-phenyl-1,2,3,6-tetrahydropyridine (MPTP) and alpha-synuclein mutations promote Tau protein phosphorylation at Ser262 and destabilize microtubule cytoskeleton in vitro. J. Biol. Chem. *286*, 5055–5068.

Rahman, M.A., and Rhim, H. (2017). Therapeutic implication of autophagy in neurodegenerative diseases. BMB Rep. *50*, 345–354.

Rajput, A., Dickson, D.W., Robinson, C.A., Ross, O.A., Dachsel, J.C., Lincoln, S.J., Cobb, S.A., Rajput, M.L., and Farrer, M.J. (2006). Parkinsonism, Lrrk2 G2019S, and tau neuropathology. Neurology *67*, 1506–1508.

Rakovic, A., Grünewald, A., Seibler, P., Ramirez, A., Kock, N., Orolicki, S., Lohmann, K., and Klein, C. (2010). Effect of endogenous mutant and wild-type PINK1 on Parkin in fibroblasts from Parkinson disease patients. Hum. Mol. Genet. *19*, 3124–3137.

Rakovic, A., Grünewald, A., Kottwitz, J., Brüggemann, N., Pramstaller, P.P., Lohmann, K., and Klein, C. (2011). Mutations in PINK1 and Parkin impair ubiquitination of Mitofusins in human fibroblasts. PLoS One *6*, e16746.

Rakovic, A., Shurkewitsch, K., Seibler, P., Grunewald, A., Zanon, A., Hagenah, J., Krainc, D., and Klein, C. (2013). Phosphatase and Tensin Homolog (PTEN)-induced Putative Kinase 1 (PINK1)-dependent Ubiquitination of Endogenous Parkin Attenuates Mitophagy: STUDY IN HUMAN PRIMARY FIBROBLASTS AND INDUCED PLURIPOTENT STEM CELL-DERIVED NEURONS. J. Biol. Chem. *288*, 2223–2237.

Ramachandran, P.V., and Ignacimuthu, S. (2013). RNA interference--a silent but an efficient therapeutic tool. Appl. Biochem. Biotechnol. *169*, 1774–1789.

Ramos-Martinez, J.I. (2017). The regulation of the pentose phosphate pathway: Remember Krebs. Arch. Biochem. Biophys. *614*, 50–52.

Ran, F.A., Hsu, P.D., Wright, J., Agarwala, V., Scott, D.A., and Zhang, F. (2013). Genome engineering using the CRISPR-Cas9 system. Nat Protoc *8*, 2281–2308.

Ransom, B.R., Kunis, D.M., Irwin, I., and Langston, J.W. (1987). Astrocytes convert the parkinsonism inducing neurotoxin, MPTP, to its active metabolite, MPP+. Neurosci. Lett. *75*, 323–328.

Recasens, A., Perier, C., and Sue, C.M. (2016). Role of microRNAs in the Regulation of α-Synuclein Expression: A Systematic Review. Front. Mol. Neurosci. *9*, 128.

Redenšek, S., Trošt, M., and Dolžan, V. (2017). Genetic determinants of Parkinson's disease: Can they help to stratify the patients based on the underlying molecular defect? Front. Aging Neurosci. *9*, 1–17.

Reeve, A.K., Ludtmann, M.H., Angelova, P.R., Simcox, E.M., Horrocks, M.H., Klenerman, D., Gandhi, S., Turnbull, D.M., and Abramov, A.Y. (2015). Aggregated α-synuclein and complex I deficiency: exploration of their relationship in differentiated neurons. Cell Death Dis. *6*, e1820.

Rh, H., Nasirian, F., Nakano, K., Ward, D., Pay, M., Hill, R., and Cw, S. (1995). Low platelet mitochondrial complex I and complex II / III activity in early untreated Parkinson ' s disease . *37*, 7778844.

Riganti, C., Gazzano, E., Polimeni, M., Aldieri, E., and Ghigo, D. (2012). The pentose phosphate pathway: an antioxidant defense and a crossroad in tumor cell fate. Free Radic. Biol. Med. *53*, 421–436.

Rincon, M.Y., VandenDriessche, T., and Chuah, M.K. (2015). Gene therapy for cardiovascular disease: Advances in vector development, targeting, and delivery for clinical translation. Cardiovasc. Res. *108*, 4–20.

Rohan, Z., Rahimi, J., Weis, S., Kapas, I., Auff, E., Mitrovic, N., Liberski, P.P., Sikorska, B., Matej, R., and Kovacs, G.G. (2015). Screening for α-synuclein immunoreactive neuronal inclusions in the hippocampus allows identification of atypical MSA (FTLD-synuclein). Acta Neuropathol. *130*, 299–301.

Rothfuss, O., Fischer, H., Hasegawa, T., Maisel, M., Leitner, P., Miesel, F., Sharma, M., Bornemann, A., Berg, D., Gasser, T., et al. (2009). Parkin protects mitochondrial genome integrity and supports mitochondrial DNA repair. Hum. Mol. Genet. *18*, 3832–3850.

Rubio, A., Luoni, M., Giannelli, S.G., Radice, I., Iannielli, A., Cancellieri, C., Di Berardino, C., Regalia, G., Lazzari, G., Menegon, A., et al. (2016). Rapid and efficient CRISPR/Cas9 gene inactivation in human neurons during human pluripotent stem cell differentiation and direct reprogramming. Sci. Rep. *6*, 37540.

Ryan, B.J., Hoek, S., Fon, E.A., and Wade-Martins, R. (2015). Mitochondrial dysfunction and mitophagy in Parkinson's: From familial to sporadic disease. Trends Biochem. Sci. *40*, 200–210.

Sallinen, V., Kolehmainen, J., Priyadarshini, M., Toleikyte, G., Chen, Y.-C., and Panula, P. (2010). Dopaminergic cell damage and vulnerability to MPTP in Pink1 knockdown zebrafish. Neurobiol. Dis. *40*, 93–101.

Salvesen, L., Winge, K., Brudek, T., Agander, T.K., Lokkegaard, A., and Pakkenberg, B. (2015). Neocortical Neuronal Loss in Patients with Multiple System Atrophy: A Stereological Study. Cereb. Cortex.

Samaranch, L., Lorenzo-Betancor, O., Arbelo, J.M., Ferrer, I., Lorenzo, E., Irigoyen, J., Pastor, M. a, Marrero, C., Isla, C., Herrera-Henriquez, J., et al. (2010). PINK1-linked parkinsonism is associated with Lewy body pathology. Brain *133*, 1128–1142.

Sanchez-Martinez, A., Beavan, M., Gegg, M.E., Chau, K.-Y., Whitworth, A.J., and Schapira, A.H. V (2016). Parkinson disease-linked GBA mutation effects reversed by molecular chaperones in human cell and fly models. Sci. Rep. *6*, 31380.

Santpere, G., Nieto, M., Puig, B., and Ferrer, I. (2006). Abnormal Sp1 transcription factor expression in Alzheimer disease and tauopathies. Neurosci. Lett. *397*, 30–34.

Sasaki, S., Shirata, A., Yamane, K., and Iwata, M. (2004). Parkin-positive autosomal recessive juvenile Parkinsonism with

alpha-synuclein-positive inclusions. Neurology *63*, 678–682.

Sasaki, S., Shirata, A., Yamane, K., and Iwata, M. (2008). Involvement of spinal motor neurons in parkin-positive autosomal recessive juvenile parkinsonism. Neuropathology *28*, 74–80.

Schapira, a H., Cooper, J.M., Dexter, D., Jenner, P., Clark, J.B., and Marsden, C.D. (1989). Mitochondrial complex I deficiency in Parkinson's disease. Lancet *1*, 1269.

Schlossmacher, M.G., Frosch, M.P., Gai, W.P., Medina, M., Sharma, N., Forno, L., Ochiishi, T., Shimura, H., Sharon, R., Hattori, N., et al. (2002). Parkin localizes to the Lewy bodies of Parkinson disease and dementia with Lewy bodies. Am. J. Pathol. *160*, 1655–1667.

Schrepfer, E., and Scorrano, L. (2016). Mitofusins, from Mitochondria to Metabolism. Mol. Cell *61*, 683–694.

Schubert, A.F., Gladkova, C., Pardon, E., Wagstaff, J.L., Freund, S.M. V., Steyaert, J., Maslen, S.L., and Komander, D. (2017). Structure of PINK1 in complex with its substrate ubiquitin. Nature 1–28.

Seibler, P., Graziotto, J., Jeong, H., Simunovic, F., Klein, C., and Krainc, D. (2011). Mitochondrial Parkin recruitment is impaired in neurons derived from mutant PINK1 induced pluripotent stem cells. J. Neurosci. *31*, 5970–5976.

Seidel, K., Schöls, L., Nuber, S., Petrasch-Parwez, E., Gierga, K., Wszolek, Z., Dickson, D., Gai, W.P., Bornemann, A., Riess, O., et al. (2010). First appraisal of brain pathology owing to A30P mutant alpha-synuclein. Ann. Neurol. *67*, 684–689.

Sekigawa, A., Takamatsu, Y., Sekiyama, K., and Hashimoto, M. (2015). Role of α- and β-Synucleins in the Axonal Pathology of Parkinson's Disease and Related Synucleinopathies. Biomolecules *5*, 1000–1011.

Sengupta, U., Guerrero-Muñoz, M.J., Castillo-Carranza, D.L., Lasagna-Reeves, C.A., Gerson, J.E., Paulucci-Holthauzen, A.A., Krishnamurthy, S., Farhed, M., Jackson, G.R., and Kayed, R. (2015). Pathological Interface between Oligomeric Alpha-Synuclein and Tau in Synucleinopathies. Biol. Psychiatry *78*, 672–683.

Sethi, N., and Kang, Y. (2011). Unravelling the complexity of metastasis - molecular understanding and targeted therapies. Nat. Rev. Cancer *11*, 735–748.

Shah, R., Li, F., Voziyanova, E., and Voziyanov, Y. (2015). Target-specific variants of Flp recombinase mediate genome engineering reactions in mammalian cells. FEBS J. *282*, 3323–3333.

Shanbhag, A.G. (1994). Utilization of Information Measure as a Means of Image Thresholding. CVGIP Graph. Model. Image Process. *56*, 414–419.

Sharma, N., and Nehru, B. (2013). Beneficial Effect of Vitamin E in Rotenone Induced Model of PD: Behavioural, Neurochemical and Biochemical Study. Exp. Neurobiol. *22*, 214–223.

Sharp, M.E., Marder, K.S., Côté, L., Clark, L.N., Nichols, W.C., Vonsattel, J.-P., and Alcalay, R.N. (2013). Parkinson's disease with Lewy bodies associated with a heterozygous PARKIN dosage mutation. Mov. Disord.

Shi, X.-Y., Xiong, L.-X., Xiao, L., Meng, C., Qi, G.-Y., and Li, W.-L. (2016). Downregulation of caveolin‑1 upregulates the expression of growth factors and regulators in co‑culture of fibroblasts with cancer cells. Mol. Med. Rep. *13*, 744–752.

Sidransky, E., Nalls, M. a, Aasly, J.O., Aharon-Peretz, J., Annesi, G., Barbosa, E.R., Bar-Shira, a, Berg, D., Bras, J., Brice, a, et al. (2009). Multicenter analysis of glucocerebrosidase mutations in Parkinson's disease. N. Engl. J. Med. *361*, 1651–1661.

Simón-Sánchez, J., Schulte, C., Bras, J.M., Sharma, M., Gibbs, J.R., Berg, D., Paisan-Ruiz, C., Lichtner, P., Scholz, S.W., Hernandez, D.G., et al. (2009). Genome-wide association study reveals genetic risk underlying Parkinson's disease. Nat. Genet. *41*, 1308–1312.

Singleton, A.B., Farrer, M., Johnson, J., Singleton, A., Hague, S., Kachergus, J., Hulihan, M., Peuralinna, T., Dutra, A., Nussbaum, R., et al. (2003a). alpha-Synuclein locus triplication causes Parkinson's disease. Science *302*, 841.

Sinha, S., Ghildiyal, R., Mehta, V.S., and Sen, E. (2013). ATM-NFκB axis-driven TIGAR regulates sensitivity of glioma cells to radiomimetics in the presence of TNFα. Cell Death Dis. *4*, e615.

Siuda, J., Jasinska-Myga, B., Boczarska-Jedynak, M., Opala, G., Fiesel, F.C., Moussaud-Lamodière, E.L., Scarffe, L. a, Dawson, V.L., Ross, O. a, Springer, W., et al. (2014). Early-onset Parkinson's disease due to PINK1 p.Q456X mutation - Clinical and functional study. Parkinsonism Relat. Disord. *20*, 1274–1278.

Smith, G.A., Jansson, J., Rocha, E.M., Osborn, T., Hallett, P.J., and Isacson, O. (2016). Fibroblast Biomarkers of Sporadic Parkinsons Disease and LRRK2 Kinase Inhibition. Mol. Neurobiol. *53*, 5161–5177.

Sofic, E., Lange, K.W., Jellinger, K., and Riederer, P. (1992). Reduced and oxidized glutathione in the substantia nigra of patients with Parkinson's disease. Neurosci. Lett. *142*, 128–130.

Soldner, F., Stelzer, Y., Shivalila, C.S., Abraham, B.J., Latourelle, J.C., Barrasa, M.I., Goldmann, J., Myers, R.H., Young, R.A., and Jaenisch, R. (2016). Parkinson-associated risk variant in distal enhancer of α-synuclein modulates target gene expression. Nature *533*, 95–99.

Sood, R., Carrington, B., Bishop, K., Jones, M., Rissone, A., Candotti, F., Chandrasekharappa, S.C., and Liu, P. (2013). Efficient Methods for Targeted Mutagenesis in Zebrafish Using Zinc-Finger Nucleases: Data from Targeting of Nine Genes Using CompoZr or CoDA ZFNs. PLoS One *8*.

Soto-ortolaza, A.I., Heckman, M.G., Labbé, C., Serie, D.J., Rayaprolu, S., Strongosky, A., Boczarska-jedynak, M., Opala, G., Krygowska-wajs, A., Barcikowska, M., et al. (2013). Original Article GWAS risk factors in Parkinson ' s disease : LRRK2 coding variation and genetic interaction with PARK16. *2*, 287–299.

Spillantini, M.G., Schmidt, M.L., Lee, V.M.-Y., Trojanowski, J.Q., Jakes, R., and Goedert, M. (1997). a-Synuclein in Lewy bodies. Nature *388*, 839–840.

Spitzer, J., Landthaler, M., and Tuschl, T. (2013). Rapid creation of stable mammalian cell lines for regulated expression of proteins using the Gateway® recombination cloning technology and Flp-In T-REx® lines (Elsevier Inc.).

Stepanenko, A.A., and Dmitrenko, V. V. (2015). HEK293 in cell biology and cancer research: Phenotype, karyotype, tumorigenicity, and stress-induced genome-phenotype evolution. Gene *569*, 182–190.

Su, Y.-C., and Qi, X. (2013). Inhibition of excessive mitochondrial fission reduced aberrant autophagy and neuronal damage caused by LRRK2 G2019S mutation. Hum. Mol. Genet. *22*, 4545–4561.

Su, T., Liu, F., Gu, P., Jin, H., Chang, Y., Wang, Q., Liang, Q., and Qi, Q. (2016). A CRISPR-Cas9 assisted non-homologous end-joining strategy for one-step engineering of bacterial genome. Sci. Rep. *6*, 37895.

Sun, M., Li, M., Huang, Q., Han, F., Gu, J.-H., Xie, J., Han, R., Qin, Z.-H., and Zhou, Z. (2015). Ischemia/reperfusion-induced upregulation of TIGAR in brain is mediated by SP1 and modulated by ROS and hormones involved in glucose metabolism. Neurochem. Int. *80*, 99–109.

Sun, Y., Chen, X., and Xiao, D. (2007). Tetracycline-inducible expression systems: new strategies and practices in the transgenic mouse modeling. Acta Biochim Biophys Sin *39*, 235–246.

Tabrizi, S.J., Orth, M., Wilkinson, J.M., Taanman, J.W., Warner, T.T., Cooper, J.M., and Schapira, a H. (2000). Expression of mutant α-synuclein causes increased susceptibility to dopamine toxicity. Hum. Mol. Genet. *9*, 2683–2689.

Tai, G., Zhang, H., Du, J., Chen, G., Huang, J., Yu, J., Cai, J., and Liu, F. (2015). TIGAR overexpression diminishes radiosensitivity of parotid gland fibroblast cells and inhibits IR-induced cell autophagy. Int. J. Clin. Exp. Pathol. *8*, 4823–4829.

Taipa, R., Pereira, C., Reis, I., Alonso, I., Bastos-Lima, A., Melo-Pires, M., and Magalhães, M. (2016). DJ-1 linked parkinsonism (PARK7) is associated with Lewy body pathology. Brain *139*, 1680–1687.

Tam, C.W.C., Burton, E.J., McKeith, I.G., Burn, D.J., and O'Brien, J.T. (2005). Temporal lobe atrophy on MRI in Parkinson disease with dementia: a comparison with Alzheimer disease and dementia with Lewy bodies. Neurology *64*, 861–865.

Tan, V.P., and Miyamoto, S. (2015). HK2/hexokinase-II integrates glycolysis and autophagy to confer cellular protection. Autophagy *11*, 963–964.

Tanner, C.M., Kame, F., Ross, G.W., Hoppin, J.A., Goldman, S.M., Korell, M., Marras, C., Bhudhikanok, G.S., Kasten, M., Chade, A.R., et al. (2011). Rotenone, paraquat, and Parkinson's disease. Environ. Health Perspect. *119*, 866–872.

Tanner, J.J., McFarland, N.R., and Price, C.C. (2017). Striatal and hippocampal atrophy in idiopathic Parkinson's disease patients without dementia: A morphometric analysis. Front. Neurol. *8*, 1–10.

Tayebi, N., Walker, J., Stubblefield, B., Orvisky, E., LaMarca, M.E., Wong, K., Rosenbaum, H., Schiffmann, R., Bembi, B., and Sidransky, E. (2003). Gaucher disease with parkinsonian manifestations: does glucocerebrosidase deficiency contribute to a vulnerability to parkinsonism? Mol. Genet. Metab. *79*, 104–109.

Thomas, P., and Smart, T.G. (2005). HEK293 cell line: a vehicle for the expression of recombinant proteins. J. Pharmacol. Toxicol. Methods *51*, 187–200.

Tolosa, E., and Vilas, D. (2015). Peripheral synuclein tissue markers: A step closer to Parkinson's disease diagnosis. Brain *138*, 2120–2122.

Trojanowski, J.Q., and Revesz, T. (2007). Proposed neuropathological criteria for the post mortem diagnosis of multiple system atrophy. Neuropathol. Appl. Neurobiol. *33*, 615–620.

Valente, E.M., Bentivoglio, a R., Dixon, P.H., Ferraris, a, Ialongo, T., Frontali, M., Albanese, a, and Wood, N.W. (2001). Localization of a novel locus for autosomal recessive early-onset parkinsonism, PARK6, on human chromosome 1p35-p36. Am. J. Hum. Genet. *68*, 895–900.

Valente, E.M., Salvi, S., Ialongo, T., Marongiu, R., Elia, A.E., Caputo, V., Romito, L., Albanese, A., Dallapiccola, B., and Bentivoglio, A.R. (2004). PINK1 mutations are associated with sporadic early-onset parkinsonism. Ann. Neurol. *56*, 336–341.

Velayati, A., Yu, W.H., and Sidransky, E. (2010). The role of glucocerebrosidase mutations in Parkinson disease and Lewy body disorders. Curr. Neurol. Neurosci. Rep. *10*, 190–198.

Venda, L.L., Cragg, S.J., Buchman, V.L., and Wade-Martins, R. (2017). α-Synuclein and dopamine at the crossroads of Parkinson's disease. Trends Neurosci. *33*, 559–568.

Venkatanarayan, A., Raulji, P., Norton, W., and Flores, E.R. (2016). Novel therapeutic interventions for p53-altered tumors through manipulation of its family members, p63 and p73. Cell Cycle *15*, 164–171.

Vergara, D., Ferraro, M.M., Cascione, M., Del Mercato, L.L., Leporatti, S., Ferretta, A., Tanzarella, P., Pacelli, C., Santino, A., Maffia, M., et al. (2014). Cytoskeletal Alterations and Biomechanical Properties of parkin-Mutant Human Primary Fibroblasts. Cell Biochem. Biophys.

Visanji, N.P., Brooks, P.L., Hazrati, L.-N., and Lang, A.E. (2013). The prion hypothesis in Parkinson's disease: Braak to the future. Acta Neuropathol. Commun. *1*, 2.

Vitte, J., Traver, S., Maués De Paula, A., Lesage, S., Rovelli, G., Corti, O., Duyckaerts, C., and Brice, A. (2010). Leucine-rich repeat kinase 2 is associated with the endoplasmic reticulum in dopaminergic neurons and accumulates in the core of Lewy bodies in Parkinson disease. J. Neuropathol. Exp. Neurol. *69*, 959–972.

Volpicelli-Daley, L.A., Abdelmotilib, H., Liu, Z., Stoyka, L., Daher, J.P.L., Milnerwood, A.J., Unni, V.K., Hirst, W.D., Yue, Z., Zhao, H.T., et al. (2016). G2019S-LRRK2 Expression Augments α-Synuclein Sequestration into Inclusions in Neurons. J. Neurosci. *36*, 7415–7427.

Waelter, S., Boeddrich, A., Lurz, R., Scherzinger, E., Lueder, G., Lehrach, H., and Wanker, E.E. (2001). Accumulation of mutant huntingtin fragments in aggresome-like inclusion bodies as a result of insufficient protein degradation. Mol. Biol. Cell *12*, 1393–1407.

Wakabayashi, K., Tanji, K., Odagiri, S., Miki, Y., Mori, F., and Takahashi, H. (2012). The Lewy Body in Parkinson's Disease

and Related Neurodegenerative Disorders. Mol. Neurobiol. 1–14.

Wakabayashi, K., Tanji, K., Odagiri, S., Miki, Y., Mori, F., and Takahashi, H. (2013). The Lewy body in Parkinson's disease and related neurodegenerative disorders. Mol Neurobiol 47, 495–508.

Wallings, R., Manzoni, C., and Bandopadhyay, R. (2015). Cellular processes associated with LRRK2 function and dysfunction. FEBS J. 282, 2806–2826.

Wang, X. (2017). Destructive Cellular Paths Underlying Familial and Sporadic Parkinson Disease Converge on Mitophagy. Autophagy 8627, 00–00.

Wang, B., Abraham, N., Gao, G., and Yang, Q. (2016a). Dysregulation of autophagy and mitochondrial function in Parkinson's disease. Transl. Neurodegener. 5, 19.

Wang, J., Duan, Z., Nugent, Z., Zou, J.X., Borowsky, A.D., Zhang, Y., Tepper, C.G., Li, J.J., Fiehn, O., Xu, J., et al. (2016b). Reprogramming metabolism by histone methyltransferase NSD2 drives endocrine resistance via coordinated activation of pentose phosphate pathway enzymes. Cancer Lett. 378, 69–79.

Wang, J.-Y., Zhuang, Q.-Q., Zhu, L.-B., Zhu, H., Li, T., Li, R., Chen, S.-F., Huang, C.-P., Zhang, X., and Zhu, J.-H. (2016c). Meta-analysis of brain iron levels of Parkinson's disease patients determined by postmortem and MRI measurements. 6, 36669.

Wang, L., Das, U., Scott, D.A., Tang, Y., McLean, P.J., and Roy, S. (2014). α-Synuclein multimers cluster synaptic vesicles and attenuate recycling. Curr. Biol. 24, 2319–2326.

Wang, X., Cao, C., Huang, J., Yao, J., Hai, T., Zheng, Q., Wang, X., Zhang, H., Qin, G., Cheng, J., et al. (2016d). One-step generation of triple gene- targeted pigs using CRISPR/Cas9 system. Sci. Rep. 1–7.

Wang, Y.W., Chen, X., Ma, R., and Gao, P. (2016e). Understanding the CREB1-miRNA feedback loop in human malignancies. Tumor Biol. 37, 8487–8502.

Wanka, C., Steinbach, J.P., and Rieger, J. (2012). Tp53-induced glycolysis and apoptosis regulator (TIGAR) protects glioma cells from starvation-induced cell death by up-regulating respiration and improving cellular redox homeostasis. J. Biol. Chem. 287, 33436–33446.

van de Warrenburg, B.P., Lammens, M., Lucking, C.B., Denefle, P., Wesseling, P., Booij, J., Praamstra, P., Quinn, N., Brice, A., and Horstink, M.W. (2001). Clinical and pathologic abnormalities in a family with parkinsonism and parkin gene mutations. Neurology 56, 555–557.

Werness, S. a, and Anderson, D.J. (2010). Block-IT miRNA manual. Comput. Programs Biomed. 18, 99–108.

Wider, C., Foroud, T., and Wszolek, Z.K. (2010). Clinical implications of gene discovery in Parkinson's disease and parkinsonism. Mov. Disord. 25 Suppl 1, S15-20.

WIEDEMANN, F.R., WINKLER, K., LINS, H., WALLESCH, C.-W., and KUNZ, W.S. (1999). Detection of Respiratory Chain Defects in Cultivated Skin Fibroblasts and Skeletal Muscle of Patients with Parkinson's Disease. Ann. N. Y. Acad. Sci. 893, 426–429.

Wilczynska, A., and Bushell, M. (2014). The complexity of miRNA-mediated repression. Cell Death Differ. 22, 22–33.
Wild, P., and Dikic, I. (2010). Mitochondria get a Parkin' ticket. Nat. Cell Biol. 12, 104–106.

Winkler-Stuck, K., Wiedemann, F.R., Wallesch, C.-W., and Kunz, W.S. (2004). Effect of coenzyme Q10 on the mitochondrial function of skin fibroblasts from Parkinson patients. J. Neurol. Sci. 220, 41–48.

Won, K.Y., Lim, S.-J., Kim, G.Y., Kim, Y.W., Han, S.-A., Song, J.Y., and Lee, D.-K. (2012). Regulatory role of p53 in cancer metabolism via SCO2 and TIGAR in human breast cancer. Hum. Pathol. 43, 221–228.

Wong, K., Sidransky, E., Verma, A., Mixon, T., Sandberg, G.D., Wakefield, L.K., Morrison, A., Lwin, A., Colegial, C., Allman, J.M., et al. (2004). Neuropathology provides clues to the pathophysiology of Gaucher disease. Mol. Genet. Metab. 82, 192–207.
Wray, S., Self, M., Lewis, P.A., Taanman, J.W., Ryan, N.S., Mahoney, C.J., Liang, Y., Devine, M.J., Sheerin, U.M., Houlden, H., et al. (2012). Creation of an open-access, mutation-defined fibroblast resource for neurological disease research. PLoS One 7.

Wu, Y., Li, X., Zhu, J.X., Xie, W., Le, W., Fan, Z., Jankovic, J., and Pan, T. (2011). Resveratrol-activated AMPK/SIRT1/autophagy in cellular models of Parkinson's disease. Neurosignals 19, 163–174.

Xie, J.-M., Li, B., Yu, H.-P., Gao, Q.-G., Li, W., Wu, H.-R., and Qin, Z.-H. (2014). TIGAR Has a Dual Role in Cancer Cell Survival through Regulating Apoptosis and Autophagy. Cancer Res. 74, 5127–5138.

Xie, Y.-Y., Zhou, C.-J., Zhou, Z.-R., Hong, J., Che, M.-X., Fu, Q.-S., Song, A.-X., Lin, D.-H., and Hu, H.-Y. (2010). Interaction with synphilin-1 promotes inclusion formation of alpha-synuclein: mechanistic insights and pathological implication. FASEB J. 24, 196–205.

Xilouri, M., Brekk, O.R., Polissidis, A., Chrysanthou-Piterou, M., Kloukina, I., and Stefanis, L. (2016). Impairment of chaperone-mediated autophagy induces dopaminergic neurodegeneration in rats. Autophagy 12, 2230–2247.

Xu, Z., Chu, X., Jiang, H., Schilling, H., Chen, S., and Feng, J. (2017). Induced dopaminergic neurons: A new promise for Parkinson's disease. Redox Biol. 11, 606–612.

Yahata, K., Kishine, H., Sone, T., Sasaki, Y., Hotta, J., Chesnut, J.D., Okabe, M., and Imamoto, F. (2005). Multi-gene Gateway clone design for expression of multiple heterologous genes in living cells: Conditional gene expression at near physiological levels. J. Biotechnol. 118, 123–134.

Yakhine-Diop, S.M.S., Bravo-San Pedro, J.M., Gómez-Sánchez, R., Pizarro-Estrella, E., Rodríguez-Arribas, M., Climent, V., Aiastui, A., de Munain, A.L., Fuentes, J.M., and González-Polo, R. a (2014). G2019S LRRK2 mutant fibroblasts from Parkinson's disease patients show increased sensitivity to neurotoxin 1-methyl-4-phenylpyridinium dependent of autophagy. Toxicology 324, 1–9.

Yamamura, Y., Kuzuhara, S., Kondo, K., Yanagi, T., Uchida, M., Matsumine, H., and Mizuno, Y. (1998). Clinical, pathologic and genetic studies on autosomal recessive early-onset parkinsonism with diurnal fluctuation. Parkinsonism Relat. Disord. 4, 65–72.

Yan, S., Tu, Z., Li, S., and Li, X.-J. (2017). Use of CRISPR/Cas9 to model brain diseases. Prog. Neuro-Psychopharmacology Biol. Psychiatry.

Yang, W., and Yu, S. (2017). Synucleinopathies: common features and hippocampal manifestations. Cell. Mol. Life Sci. *74*, 1485–1501.

Yao, Z., Gandhi, S., Burchell, V.S., Plun-Favreau, H., Wood, N.W., and Abramov, A.Y. (2011). Cell metabolism affects selective vulnerability in PINK1-associated Parkinson's disease. J. Cell Sci. *124*, 4194–4202.

Ye, L., Zhao, X., Lu, J., Qian, G., Zheng, J.C., and Ge, S. (2013). Knockdown of TIGAR by RNA interference induces apoptosis and autophagy in HepG2 hepatocellular carcinoma cells. Biochem. Biophys. Res. Commun. *437*, 300–306.

Yin, L., Kosugi, M., and Kufe, D. (2012a). Inhibition of the MUC1-C oncoprotein induces multiple myeloma cell death by down-regulating TIGAR expression and depleting NADPH. Blood *119*, 810–816.

Yin, L., Kosugi, M., and Kufe, D. (2012b). Inhibition of the MUC1-C oncoprotein induces multiple myeloma cell death by down-regulating TIGAR expression and depleting NADPH. Blood *119*, 810–816.

Yin, L., Kufe, T., Avigan, D., and Kufe, D. (2014). Targeting MUC1-C is synergistic with bortezomib in downregulating TIGAR and inducing ROS-mediated myeloma cell death. Blood *123*, 2997–3006.

Yong-Kee, C.J., Sidorova, E., Hanif, A., Perera, G., and Nash, J.E. (2012). Mitochondrial dysfunction precedes other sub-cellular abnormalities in an in vitro model linked with cell death in Parkinson's disease. Neurotox. Res. *21*, 185–194.

Yoshii, S.R., and Mizushima, N. (2017). Monitoring and Measuring Autophagy. Int. J. Mol. Sci. *18*.

Yoshino, H., Nakagawa-Hattori, Y., Kondo, T., and Mizuno, Y. (1992). Mitochondrial complex I and II activities of lymphocytes and platelets in Parkinson's disease. J. Neural Transm. - Park. Dis. Dement. Sect. *4*, 27–34.

Yoshioka, S., Fujii, W., Ogawa, T., Sugiura, K., and Naito, K. (2016). Development of a mono-promoter-driven CRISPR/Cas9 system in mammalian cells. Sci. Rep. *5*, 18341.

Yu, H.-P., Xie, J.-M., Li, B., Sun, Y.-H., Gao, Q.-G., Ding, Z.-H., Wu, H.-R., and Qin, Z.-H. (2015). TIGAR regulates DNA damage and repair through pentosephosphate pathway and Cdk5-ATM pathway. Sci. Rep. *5*, 9853.

Zanellati, M.C., Monti, V., Barzaghi, C., Reale, C., Nardocci, N., Albanese, A., Valente, E.M., Ghezzi, D., and Garavaglia, B. (2015). Mitochondrial dysfunction in Parkinson disease: evidence in mutant PARK2 fibroblasts. Front. Genet. *6*, 78.

Zarranz, J.J., Alegre, J., Gómez-Esteban, J.C., Lezcano, E., Ros, R., Ampuero, I., Vidal, L., Hoenicka, J., Rodriguez, O., Atarés, B., et al. (2004). The New Mutation, E46K, of α-Synuclein Causes Parkinson and Lewy Body Dementia. Ann. Neurol. *55*, 164–173.

Zhang, C., Lin, M., Wu, R., Wang, X., Yang, B., Levine, A.J., Hu, W., and Feng, Z. (2011). Parkin, a p53 target gene, mediates the role of p53 in glucose metabolism and the Warburg effect. Proc. Natl. Acad. Sci. U. S. A. *108*, 16259–16264.

Zhang, H., Gu, C., Yu, J., Wang, Z., Yuan, X., Yang, L., Wang, J., Jia, Y., Liu, J., and Liu, F. (2014). Radiosensitization of glioma cells by TP53-induced glycolysis and apoptosis regulator knockdown is dependent on thioredoxin-1 nuclear translocation. Free Radic. Biol. Med. *69*, 238–248.

Zhang, J., Zhao, J., Jiang, W., Shan, X., Yang, X., and Gao, J. (2012). Conditional gene manipulation: Cre-ating a new biological era. J. Zhejiang Univ. Sci. B *13*, 511–524.

Zhang, J.-P., Li, X.-L., Li, G.-H., Chen, W., Arakaki, C., Botimer, G.D., Baylink, D., Zhang, L., Wen, W., Fu, Y.-W., et al. (2017). Efficient precise knockin with a double cut HDR donor after CRISPR/Cas9-mediated double-stranded DNA cleavage. Genome Biol. *18*, 35.

Zhou, H., Falkenburger, B.H., Schulz, J.B., Tieu, K., Xu, Z., and Xu, G.X. (2007). Silencing of the Pink1 gene expression by conditional RNAi does not induce dopaminergic neuron death in mice. Int. J. Biol. Sci. *3*, 242–250.

Zhou, J.-H., Zhang, T.-T., Song, D.-D., Xia, Y.-F., Qin, Z.-H., and Sheng, R. (2016). TIGAR contributes to ischemic tolerance induced by cerebral preconditioning through scavenging of reactive oxygen species and inhibition of apoptosis. Sci. Rep. *6*, 27096.

Zhou, X., Xie, W., Li, Q., Zhang, Y., Zhang, J., Zhao, X., Liu, J., and Huang, G. (2013). TIGAR is correlated with maximal standardized uptake value on FDG-PET and survival in non-small cell lung cancer. PLoS One *8*, e80576.

Zimprich, A., Biskup, S., Leitner, P., Lichtner, P., Farrer, M., Lincoln, S., Kachergus, J., Hulihan, M., Uitti, R.J., Calne, D.B., et al. (2004). Mutations in LRRK2 cause autosomal-dominant parkinsonism with pleomorphic pathology. Neuron *44*, 601–607.

Zou, S., Gu, Z., Ni, P., Liu, X., Wang, J., and Fan, Q. (2012). SP1 plays a pivotal role for basal activity of TIGAR promoter in liver cancer cell lines. Mol. Cell. Biochem. *359*, 17–23.

Zou, S., Wang, X., Deng, L., Wang, Y., Huang, B., Zhang, N., Fan, Q., and Luo, J. (2013). CREB, another culprit for TIGAR promoter activity and expression. Biochem. Biophys. Res. Commun. *439*, 481–486.

Zuo, L., and Motherwell, M.S. (2013). The impact of reactive oxygen species and genetic mitochondrial mutations in Parkinson's disease. Gene *532*, 18–23.